

TCC training seminar (Nov 12, 2018)

Introduction to Climate

Tomoaki Ose

Climate Research Department
Meteorological Research Institute (MRI), JMA

■ Outline of the lecture

1. Climate System (60 min. + α)

1.1 Introduction

1.2 Radiative Balance

1.3 Horizontal Radiative Imbalance and Circulations

1.4 Seasonal Change

1.5 Role of Orography on Climate

2. Climate Variability (90 min. + α)

2.1 Introduction

2.2 Intraseasonal Variability: Quasi-stationary Rossby wave, MJO and equatorial waves

2.3 Interannual Variability: ENSO, El Nino Modoki, IOD

2.4 Decadal Variability: PDO, ENSO-Monsoon relation

3. Climate change due to anthropogenic forcing (30 min. + α)

■ Outline of the lecture

1. Climate System (60 min. + α)

1.1 Introduction

1.2 Radiative Balance

1.3 Horizontal Radiative Imbalance and Circulations

1.4 Seasonal Change

1.5 Role of Orography on Climate

2. Climate Variability (90 min. + α)

2.1 Introduction

2.2 Intraseasonal Variability: Quasi-stationary Rossby wave, MJO and equatorial waves

2.3 Interannual Variability: ENSO, El Nino Modoki, IOD

2.4 Decadal Variability: PDO, ENSO-Monsoon relation

3. Climate change due to anthropogenic forcing (30 min. + α)

■ 1.1 Introduction

■ Climate and Climate System

From WMO HP

What is Climate?

Climate, sometimes understood as the "average weather," is defined as the measurement of the mean and variability of relevant quantities of certain variables (such as temperature, precipitation or wind) over a period of time, ranging from months to thousands or millions of years.

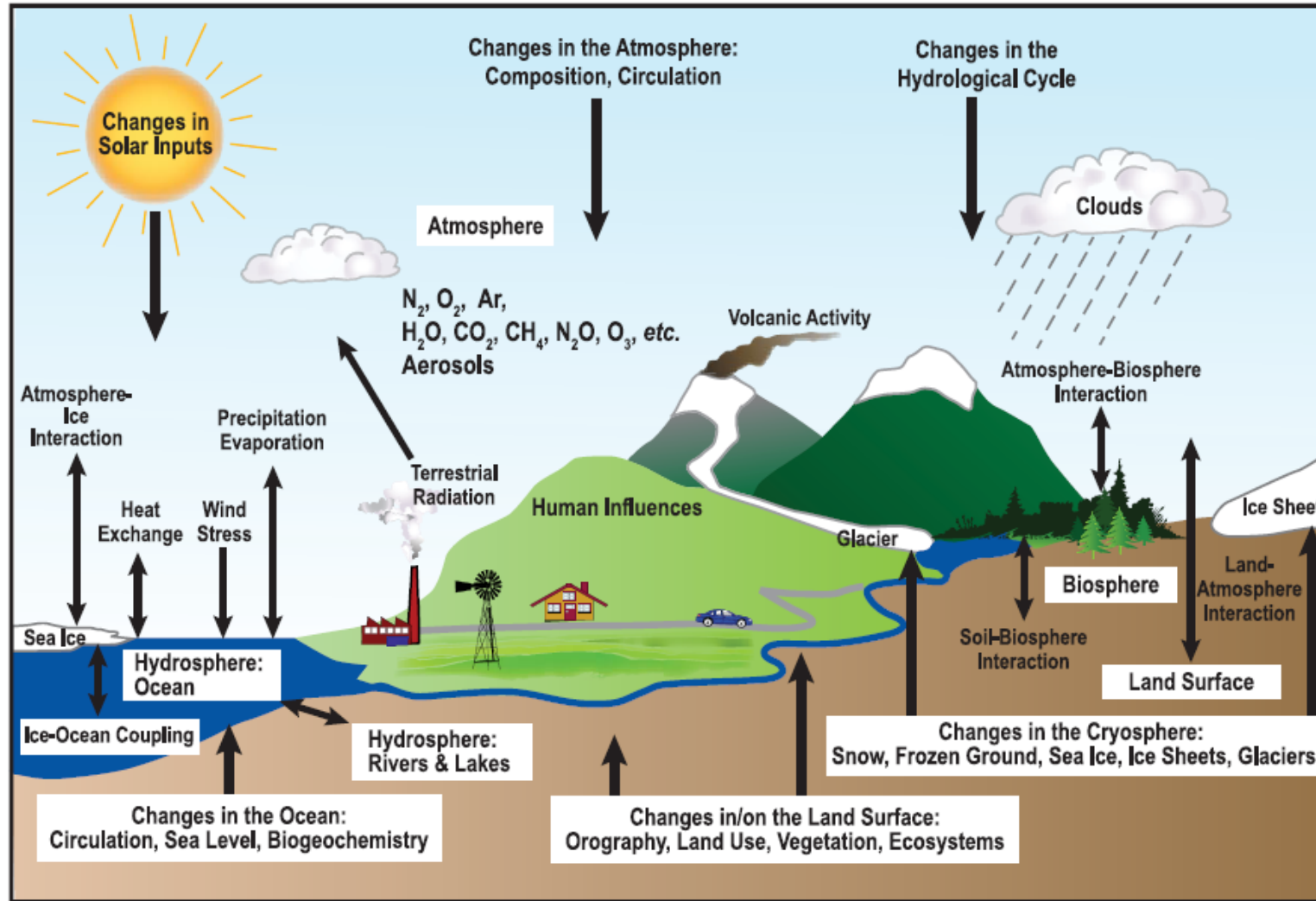
Climate in a wider sense is the state, including a statistical description, of **the climate system.**

What is the Climate System?

The climate system consists of five major components: the atmosphere, the hydrosphere, the cryosphere, land surface, and the biosphere.

The climate system is continually changing due to the interactions between the components as well as external factors such as volcanic eruptions or solar variations and human-induced factors such as changes to the atmosphere and changes in land use.

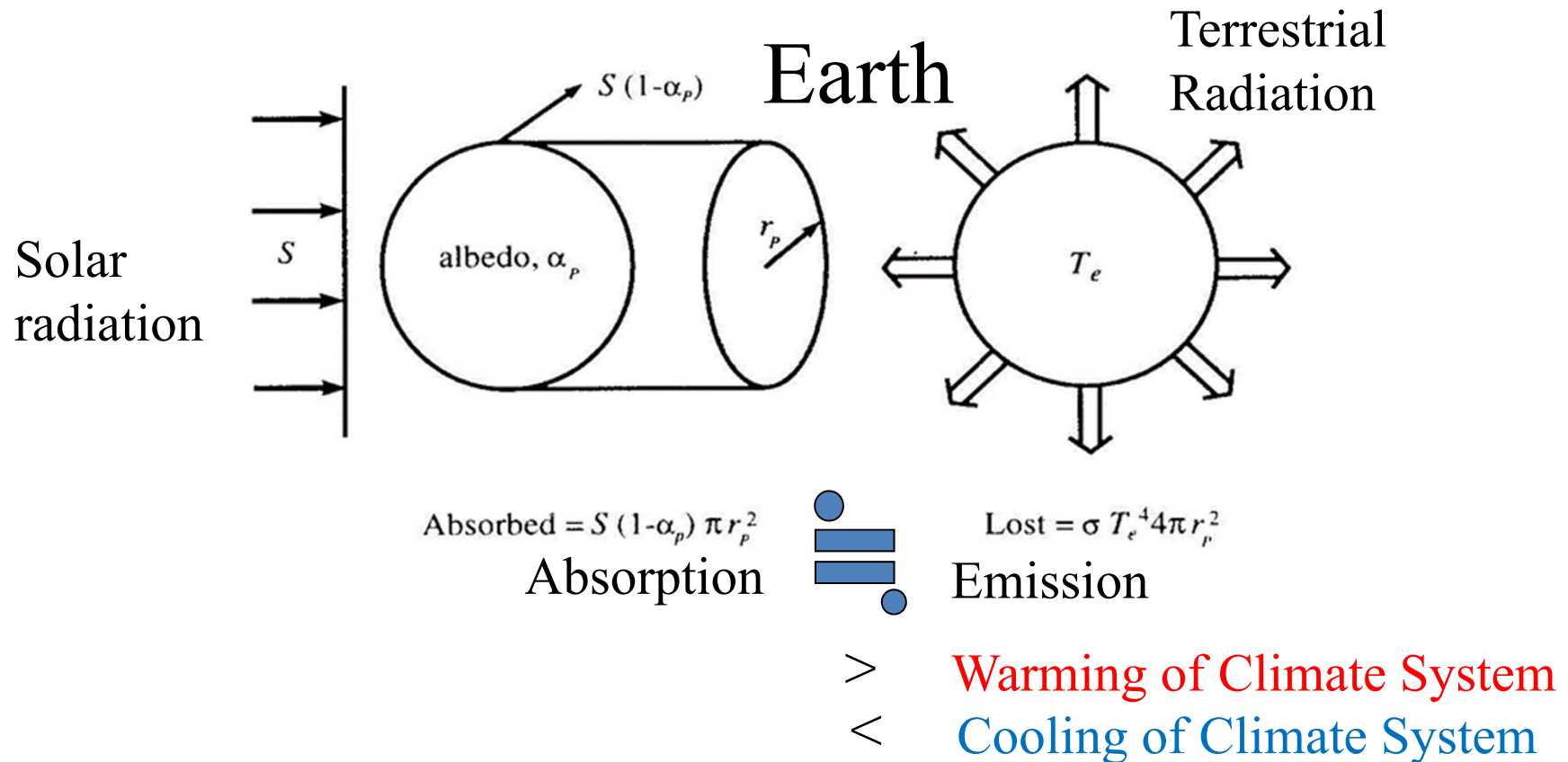
■ The climate system is complicated!



FAQ 1.2, Figure 1. Schematic view of the components of the climate system, their processes and interactions.

(IPCC AR4)

■ 1.2 Radiative Balance



■ Radiative Balance between Earth and Space

■ Solar Radiation

■ Solar constant : $S \approx 1370 \text{ Wm}^{-2}$

■ insolation : $\frac{S}{4} \approx 342 \text{ Wm}^{-2}$

■ planetary albedo : $\alpha_p \approx 0.31$

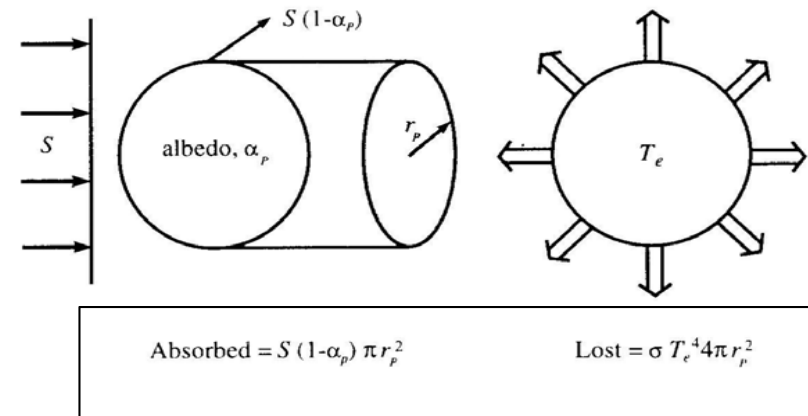
■ absorption : $\frac{S}{4}(1 - \alpha_p) \approx 235 \text{ Wm}^{-2}$

■ Terrestrial Radiation

■ equilibrium radiative temperature : T_e^*

■ emission : σT_e^{*4}

Earth's temperature observed from the cosmic space



■ Radiation Balance

■ Balance between absorbed solar radiation and terrestrial emission

$$T_e^* = \sqrt[4]{\frac{S(1 - \alpha_p)}{4\sigma}} \approx 254 \text{ K} \approx -19^\circ\text{C}$$

Surface Temperature = 15°C

Absorption of Radiation from 6000K (Sun) and 255K (Earth) Blackbodies

Solar radiation

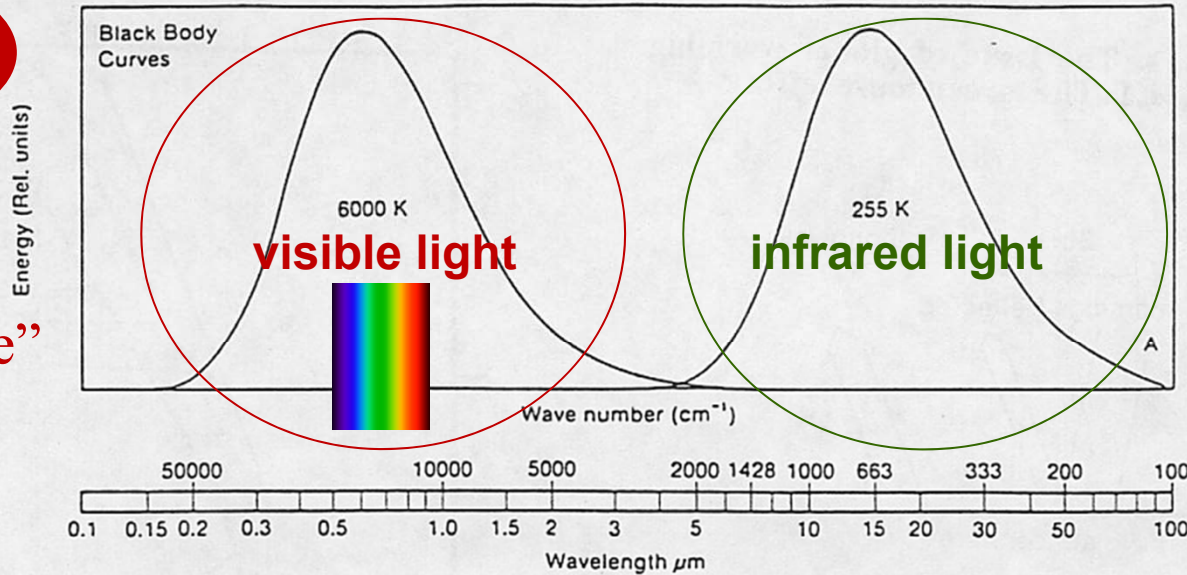


“Short Wave”

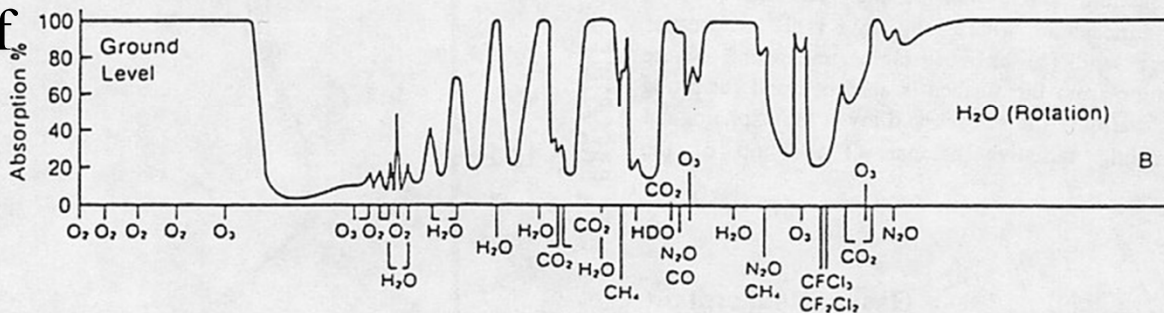
Terrestrial radiation



“Long Wave”



Percentage of atmospheric absorption

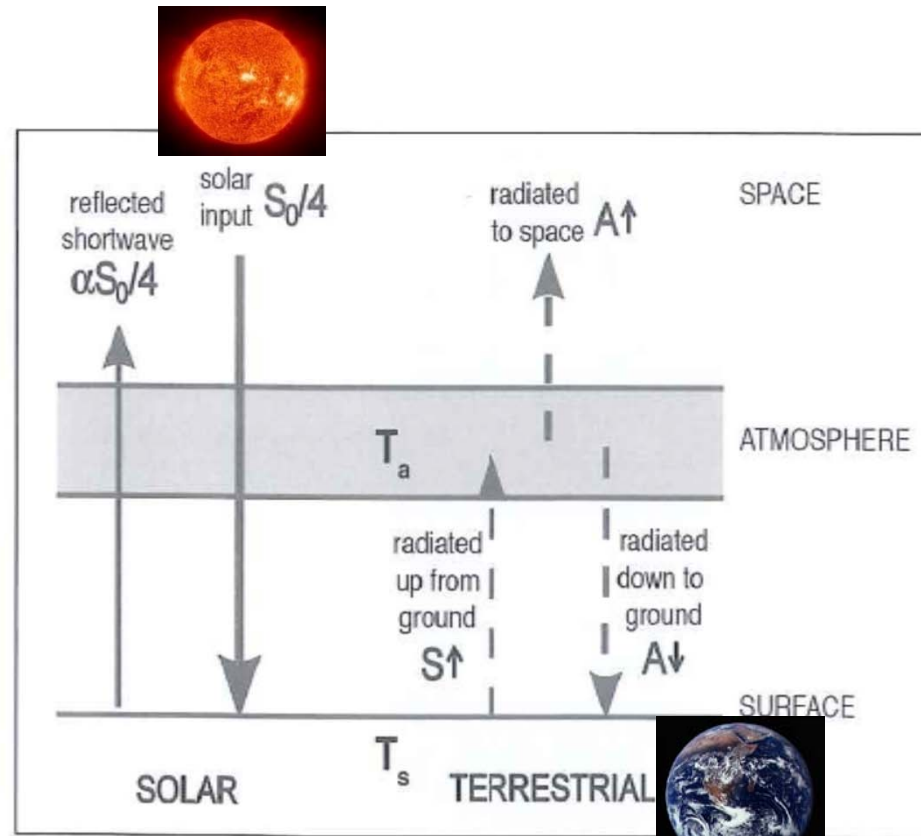


(a) Spectral distribution of long-wave emission from blackbodies at 6000 K and 255 K, corresponding to the mean emitting temperatures of the Sun and Earth, respectively, and (b) percentage of atmospheric absorption for radiation passing from

the top of the atmosphere to the surface. Notice the comparatively weak absorption of the solar spectrum and the region of weak absorption from 8 to 12 μm in the long-wave spectrum [from MacCracken and Luther, 1985].

■ The simplest greenhouse model

1-layer atmosphere is placed between space and surface



$$S\uparrow = (1-\alpha)S_0/4 + A\downarrow$$

$$= 2A\downarrow$$

$$S\uparrow \propto T_s^4$$

$$A\uparrow \propto T_a^4$$



$$T_s = 2^{1/4} T_a > T_a$$

$$T_s = 2^{1/4} \times 255\text{K}$$

$$= 303\text{K} ??$$

FIGURE 2.7. The simplest greenhouse model, comprising a surface at temperature T_s , and an atmospheric layer at temperature T_a , subject to incoming solar radiation $S_0/4$. The terrestrial radiation upwelling from the ground is assumed to be completely absorbed by the atmospheric layer.

From Marshall J., and R. A. Plumb, 2008: Atmosphere, Ocean, and Climate Dynamics, Academic Press, 319pp.

Pictures are from NASA web-sites

■ Atmosphere at Various Planets

■ Venus

- Solar constant : 2600 W/m²
- planetary albedo : 0.77
- Equilibrium radiative temperature : - 46° C

■ Earth

- Solar constant : $S \approx 1370 \text{ Wm}^{-2}$
- planetary albedo : $\alpha_p \approx 0.31$
- Equilibrium radiative temperature

$$T_e^* = \sqrt[4]{\frac{S(1 - \alpha_p)}{4\sigma}} \approx 254 \text{ K} \approx -19^\circ\text{C}$$

■ Mars

- Solar constant : 590 W/m²
- planetary albedo : 0.15
- Equilibrium radiative temperature : -56° C

Surface Temperature

457° C

Surface Pressure

90,000hPa



Surface Temperature

15° C

Surface Pressure

1,000hPa



Surface Temperature

-55° C

Surface Pressure

10hPa



Pictures are from NASA web-sites

■ Radiative Equilibrium and Radiative-Convective Equilibrium

Radiative heating tends to create vertical instability between heated ground and cooled atmosphere

One-Dimensional Vertical Profile Model

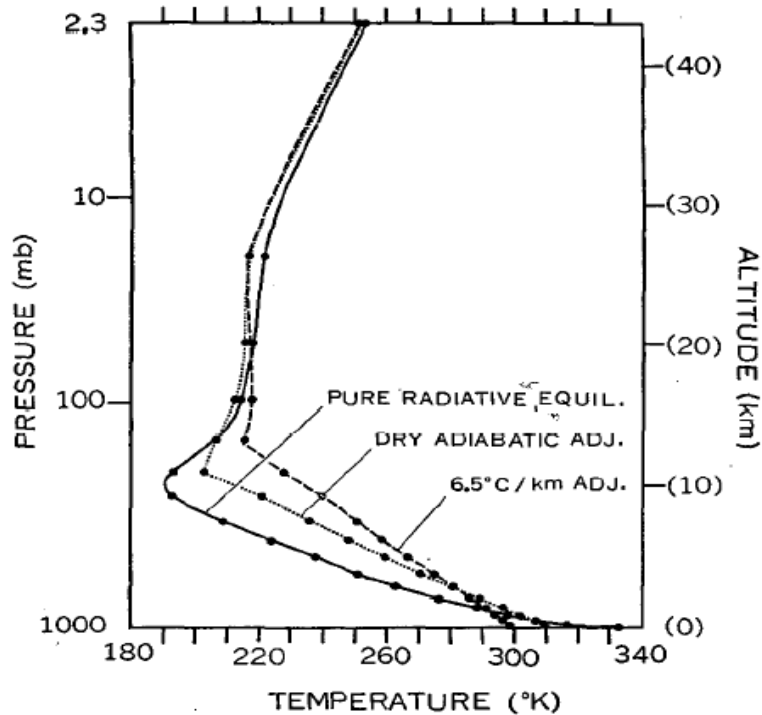


FIG. 4. The dashed, dotted, and solid lines show the thermal equilibrium with a critical lapse rate of 6.5 deg km^{-1} , a dry-adiabatic critical lapse rate (10 deg km^{-1}), and pure radiative equilibrium.

Thermal Equilibrium of the Atmosphere with a Convective Adjustment

SYUKURO MANABE AND ROBERT F. STRICKLER

General Circulation Research Laboratory, U. S. Weather Bureau, Washington, D. C.

(Manuscript received 19 December 1963, in revised form 13 April 1964)

Typical condition at 35N in April

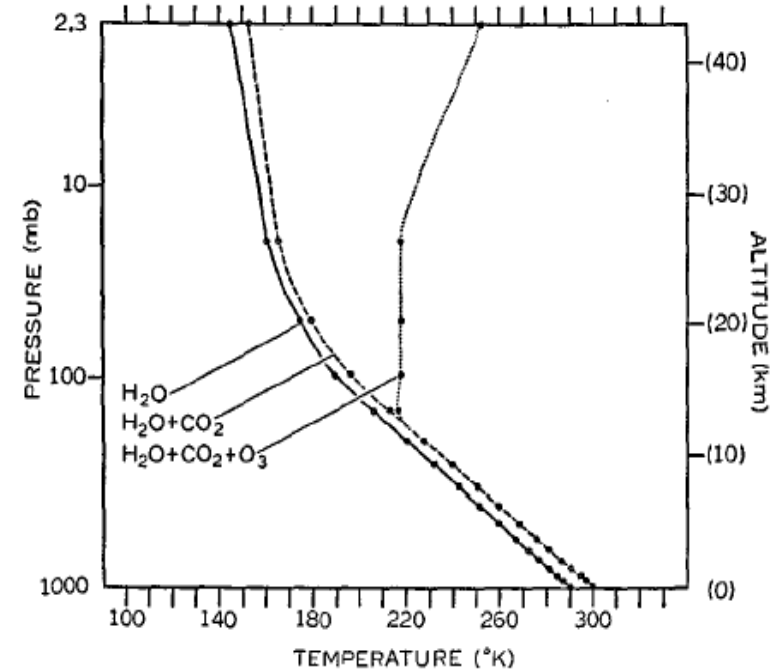


FIG. 6c. Thermal equilibrium of various atmospheres which have a critical lapse rate of 6.5 deg km^{-1} . Vertical distributions of gaseous absorbers at 35N, April, were used. $S_c = 2 \text{ ly min}^{-1}$, $\cos \bar{\tau} = 0.5$, $r = 0.5$, no clouds.

Energy Budget

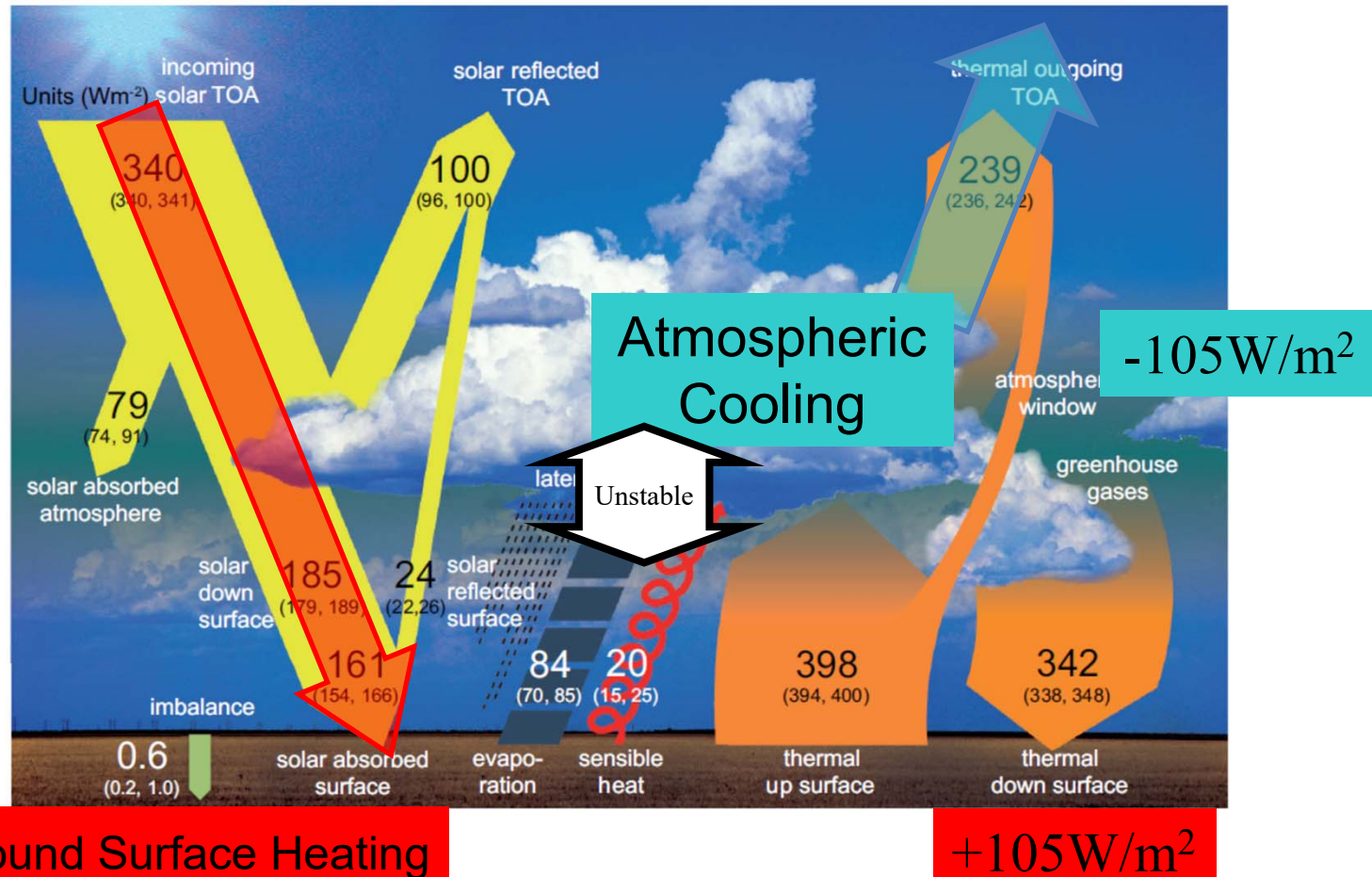


Fig. 2 Schematic diagram of the global mean energy balance of the Earth. Numbers indicate best estimates for the magnitudes of the globally averaged energy balance components together with their uncertainty ranges, representing present day climate conditions at the beginning of the twenty first century. Units Wm^{-2} . Source: Wild et al.(2013.)

1-D model is not perfect

What process is lacked in 1-D model?

Observed Temperature

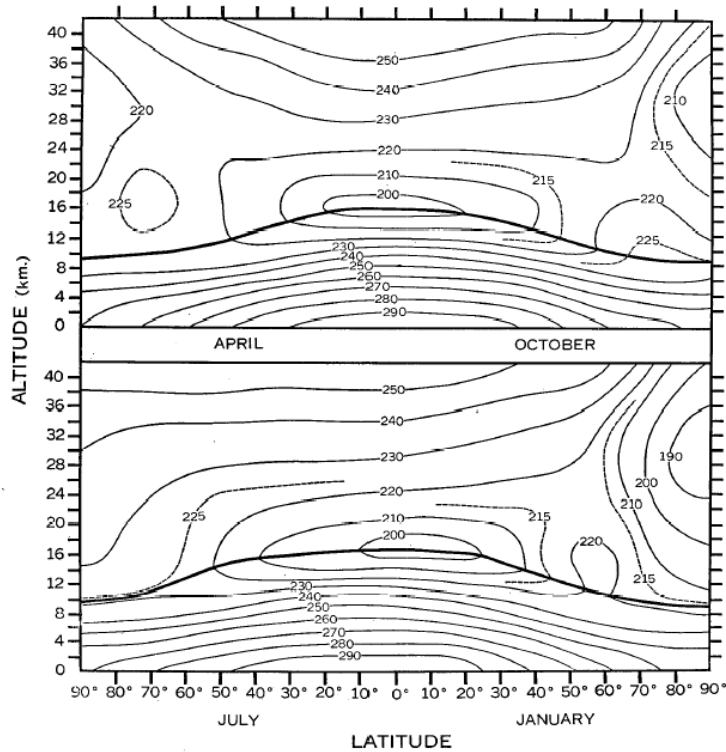


FIG. 12. Distribution of the observed temperature (deg k) in the northern hemisphere for different seasons. From J. London (1956).

Thermal Equilibrium of the Atmosphere with a Convective Adjustment

SYUKURO MANABE AND ROBERT F. STRICKLER

General Circulation Research Laboratory, U. S. Weather Bureau, Washington, D. C.
(Manuscript received 19 December 1963, in revised form 13 April 1964)

One-Dimensional Vertical Profile Model

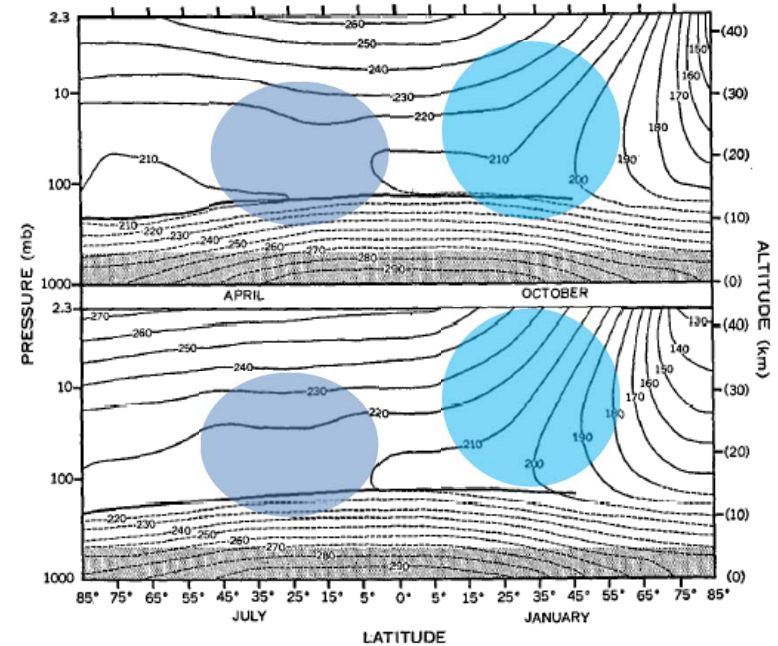
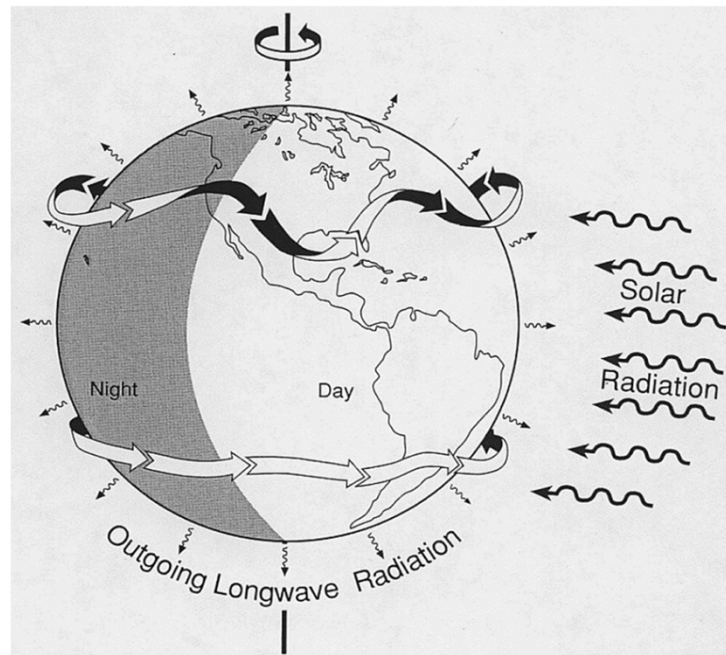
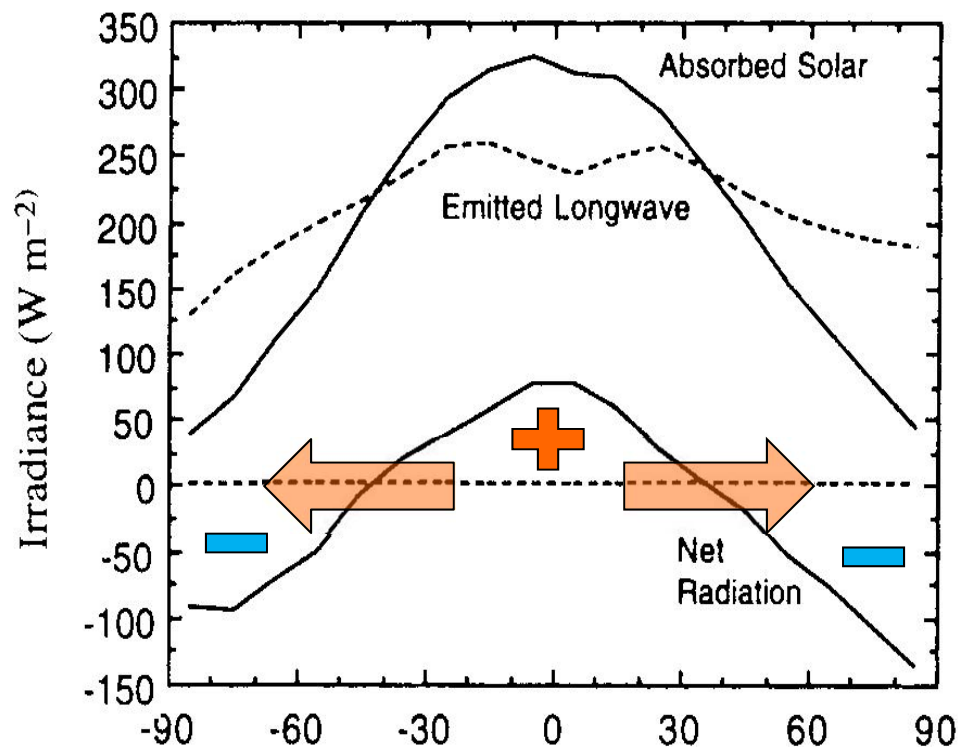


FIG. 13. The local radiative equilibrium temperature of the stratosphere. The shaded area is the region where the temperature was fixed at the observed value. Above the shaded area the state of the convective equilibrium, whose critical lapse rate for convective adjustment is deg km^{-1} , is shown. The region covered by solid lines is in local radiative equilibrium.

■ 1.3 Horizontal Radiative Imbalance and Circulations



Meridional distribution of Annual mean radiation balance

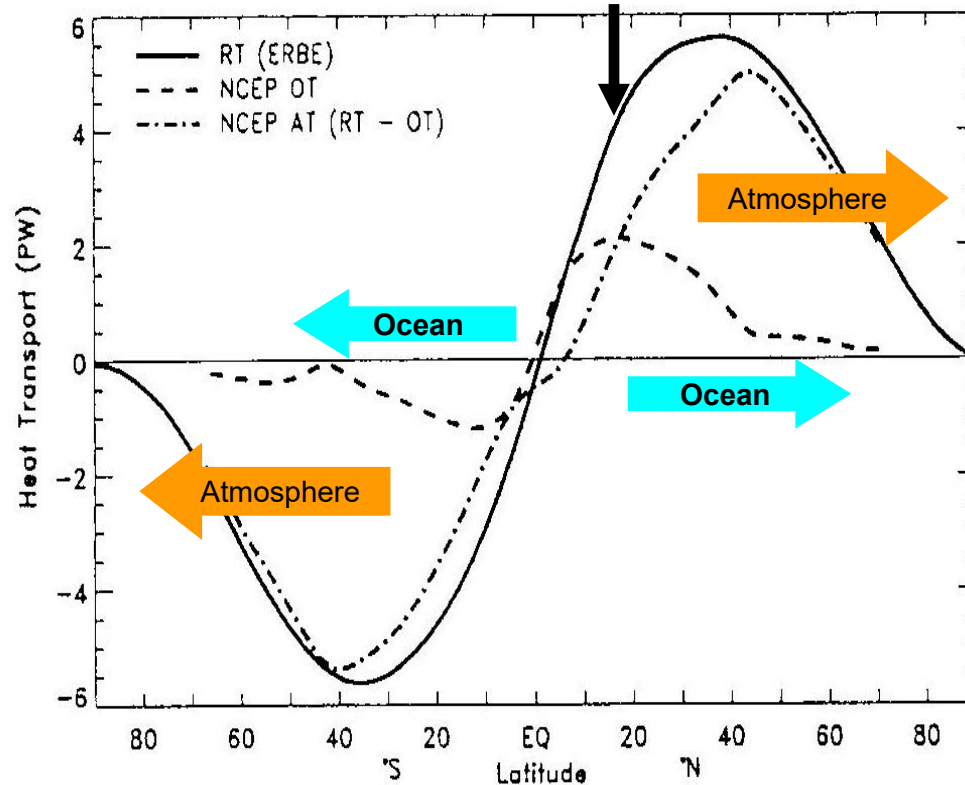


Hartmann (1994)

- Solar radiation
 - Global mean : 235 Wm^{-2}
 - Low latitude : over 300 Wm^{-2}
 - Poles : about 50 Wm^{-2}
- Terrestrial radiation
 - Global mean : 235 Wm^{-2}
 - Less gradient between low latitudes and poles compared to that in solar radiation
- Net radiation
 - Global mean : 0 Wm^{-2}
 - Positive in low latitudes, negative in high latitudes
- ◆ Poleward heat transport by the atmosphere and ocean balances this meridional heat imbalance

Energy transport by the atmosphere and ocean

Integration from the South Pole of Net radiation absorbed in the Earth



Trenberth and Caron (2001)

- Both the atmosphere and ocean are responsible for energy transport
- Atmospheric transport is larger, particularly in the mid and high latitudes
- Oceanic transport is large in low-latitudes

■ General atmospheric circulation from a state of rest in a climate model

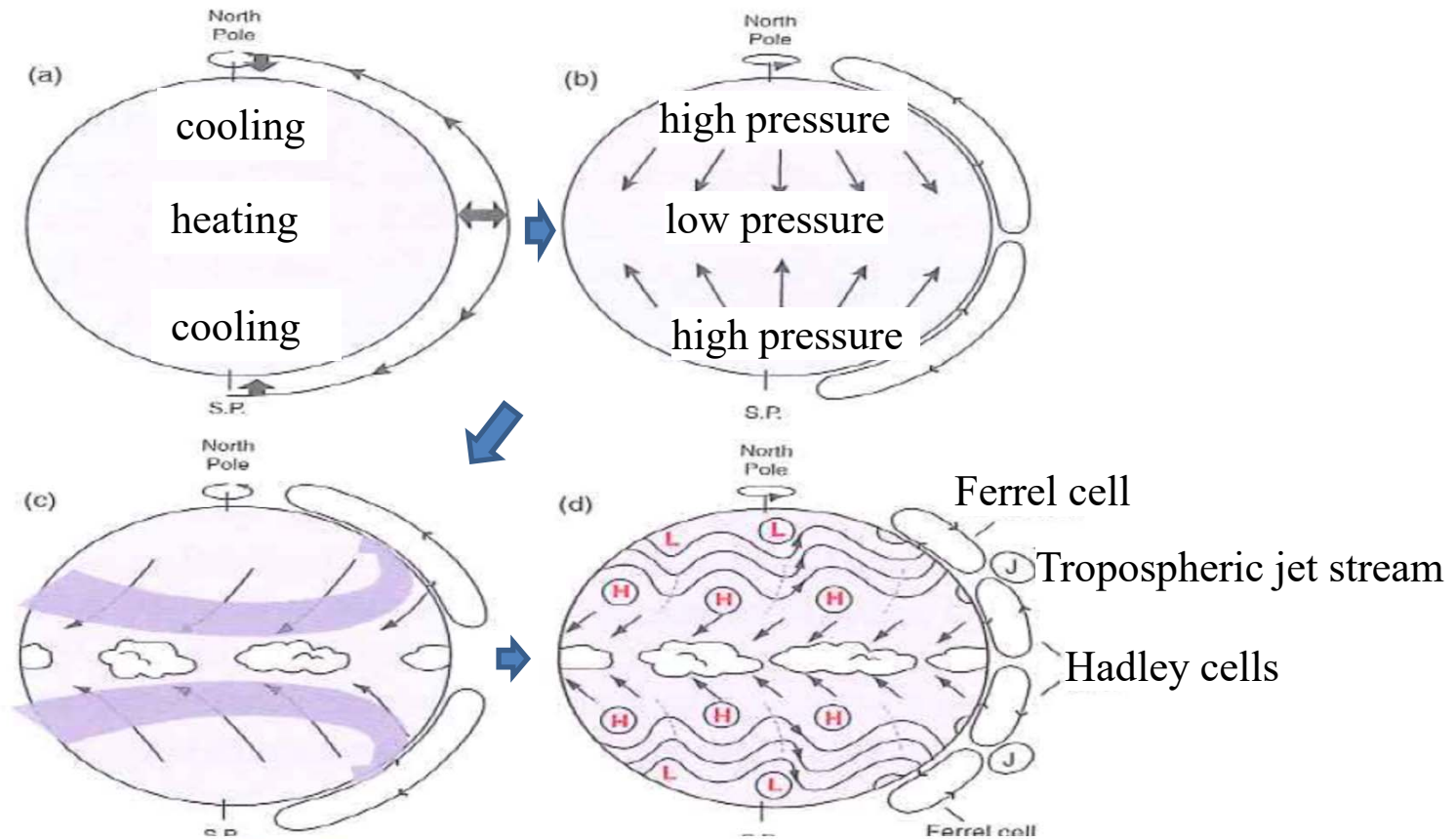


Fig. 7.21 Schematic depiction of the general circulation as it develops from a state of rest in a climate model for equinox conditions in the absence of land-sea contrasts. See text for further explanation.

■ Observed atmospheric general circulation

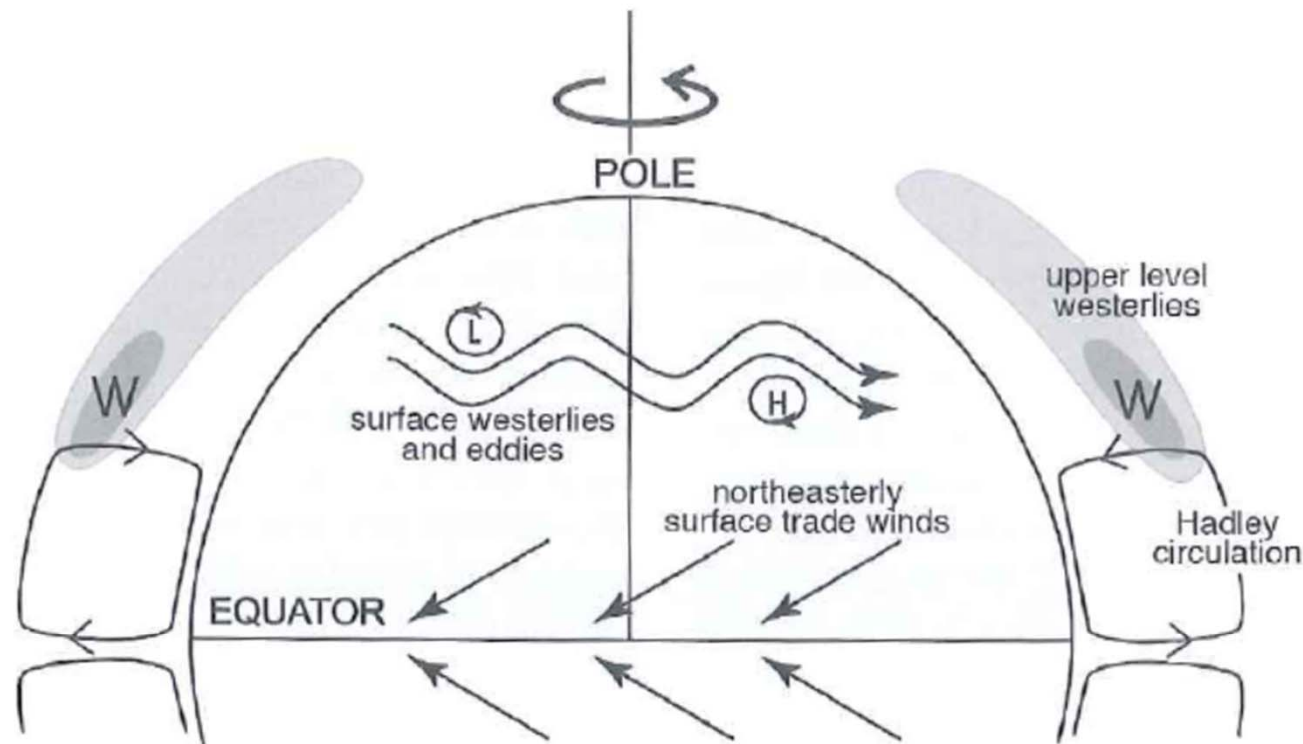


FIGURE 8.2. Schematic of the observed atmospheric general circulation for annual-averaged conditions. The upper level westerlies are shaded to reveal the core of the subtropical jet stream on the poleward flank of the Hadley circulation. The surface westerlies and surface trade winds are also marked, as are the highs and lows of middle latitudes. Only the northern hemisphere is shown. The vertical scale is greatly exaggerated.

Energy Transport by Atmospheric Circulation in the tropics

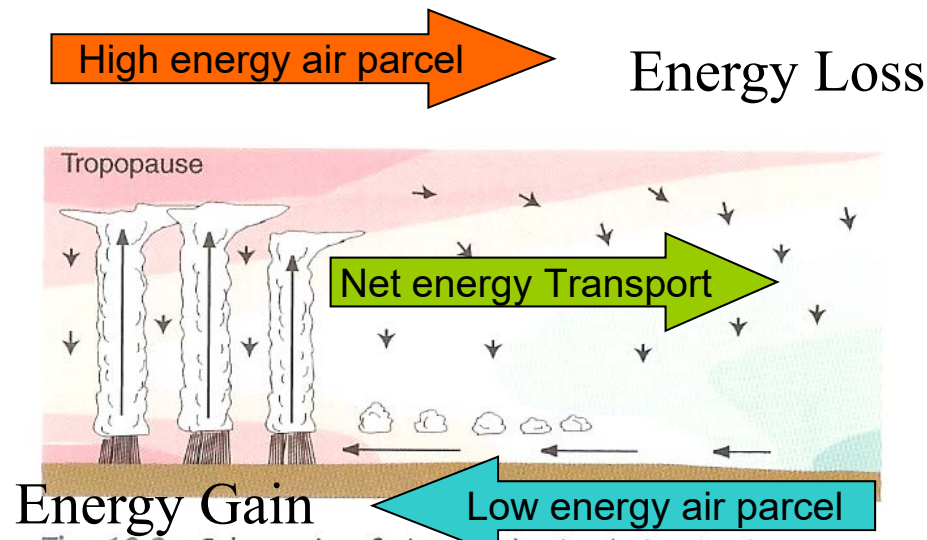


Fig. 10.3 Schematic of air parcels circulating in the atmosphere. The Colored shading represents potential temperature or moist static energy, with pink indicating higher values and blue lower values. Air parcels acquire latent and sensible heat during the time that they reside within the boundary layer, raising their moist static energy. They conserve moist static energy as they ascend rapidly in updrafts in clouds, and they cool by radiative transfer as they descend much more slowly in clear air.

□ Moist Static Energy
 $H = C_p T + gZ + Lq$

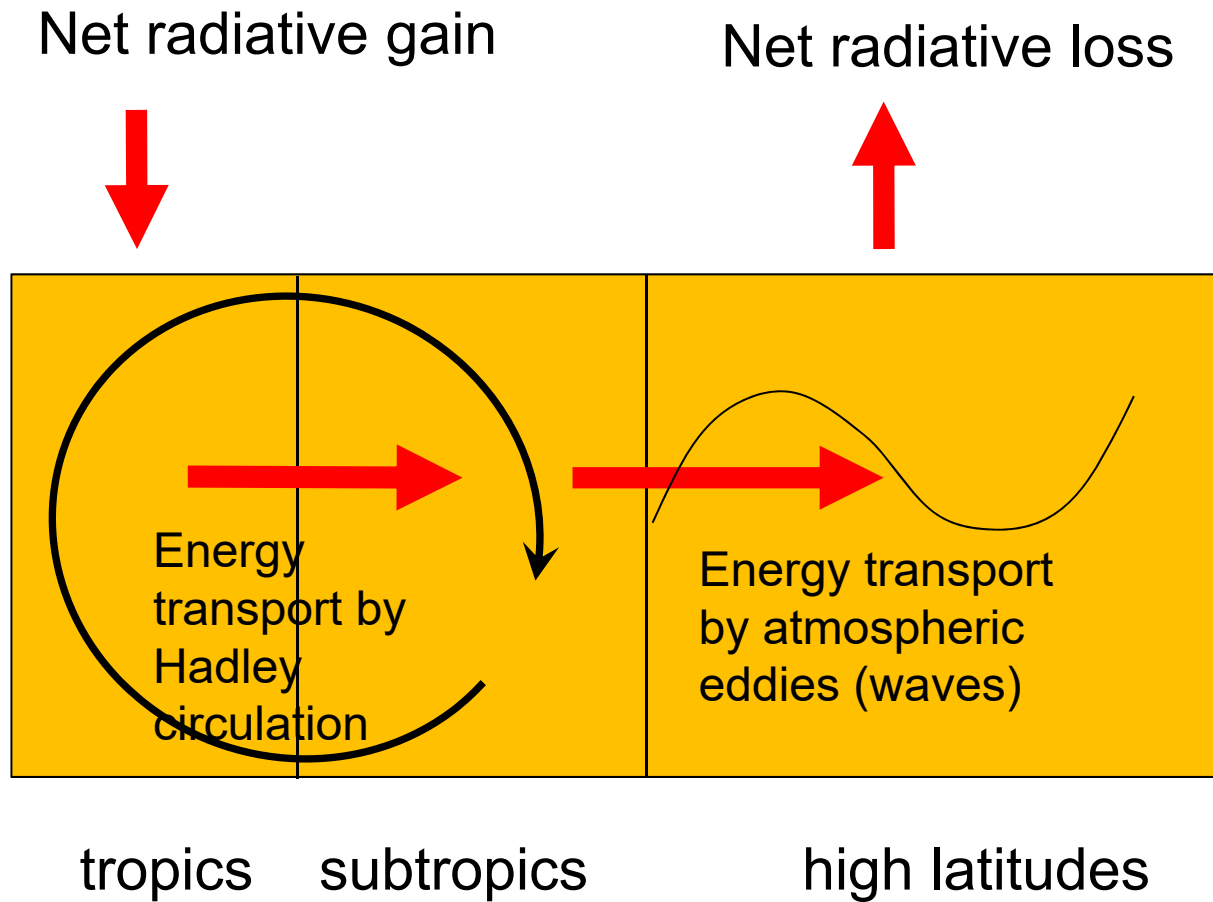
T: Temperature

Z: Height

q: Specific Humidity

H of air parcels is conserved even through adiabatic process and/or condensation process, but, not conserved through the processes of radiation, heat and moisture supply from ground surface.

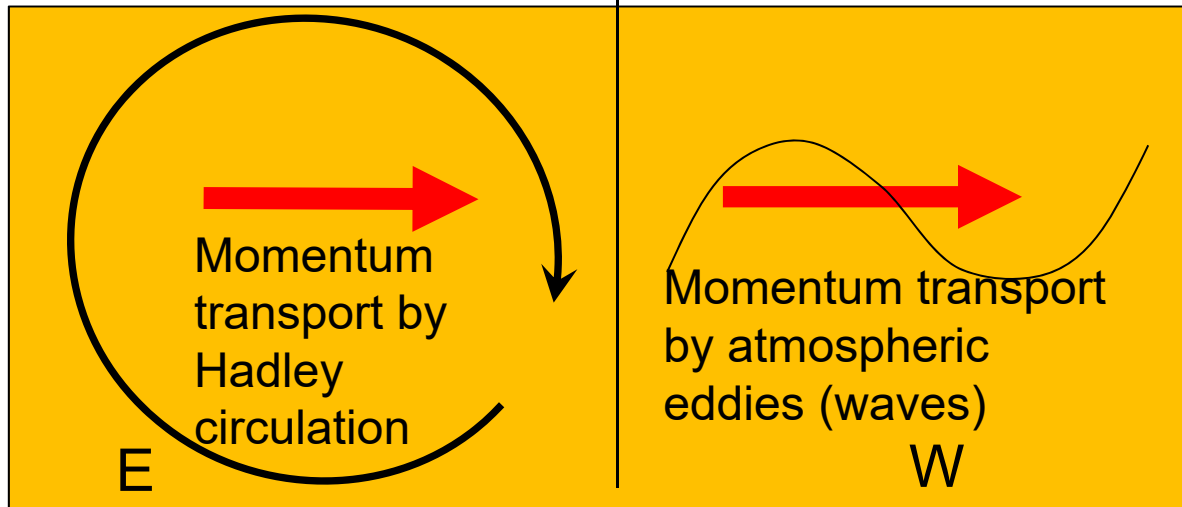
■ Energy transport by atmospheric general circulation



■ Momentum transport by atmospheric general circulation

tropics

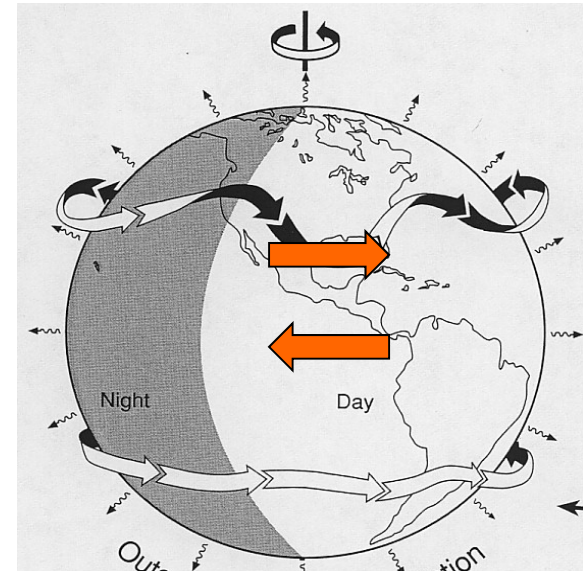
middle latitudes



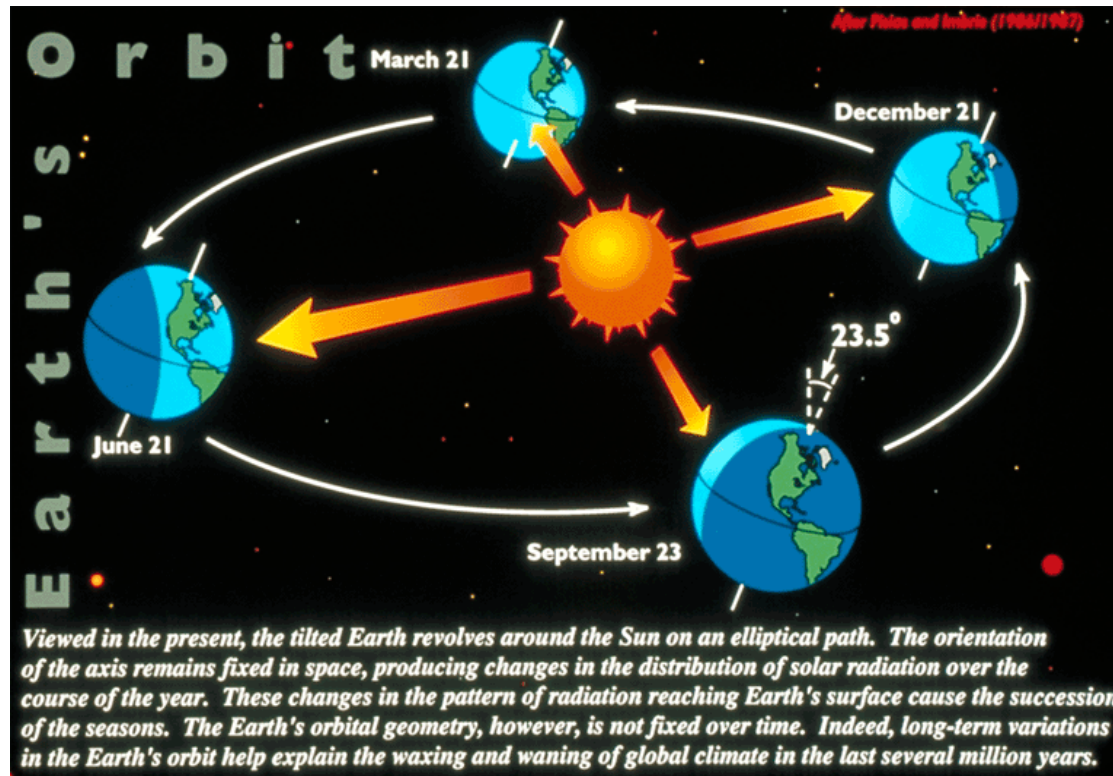
momentum gain



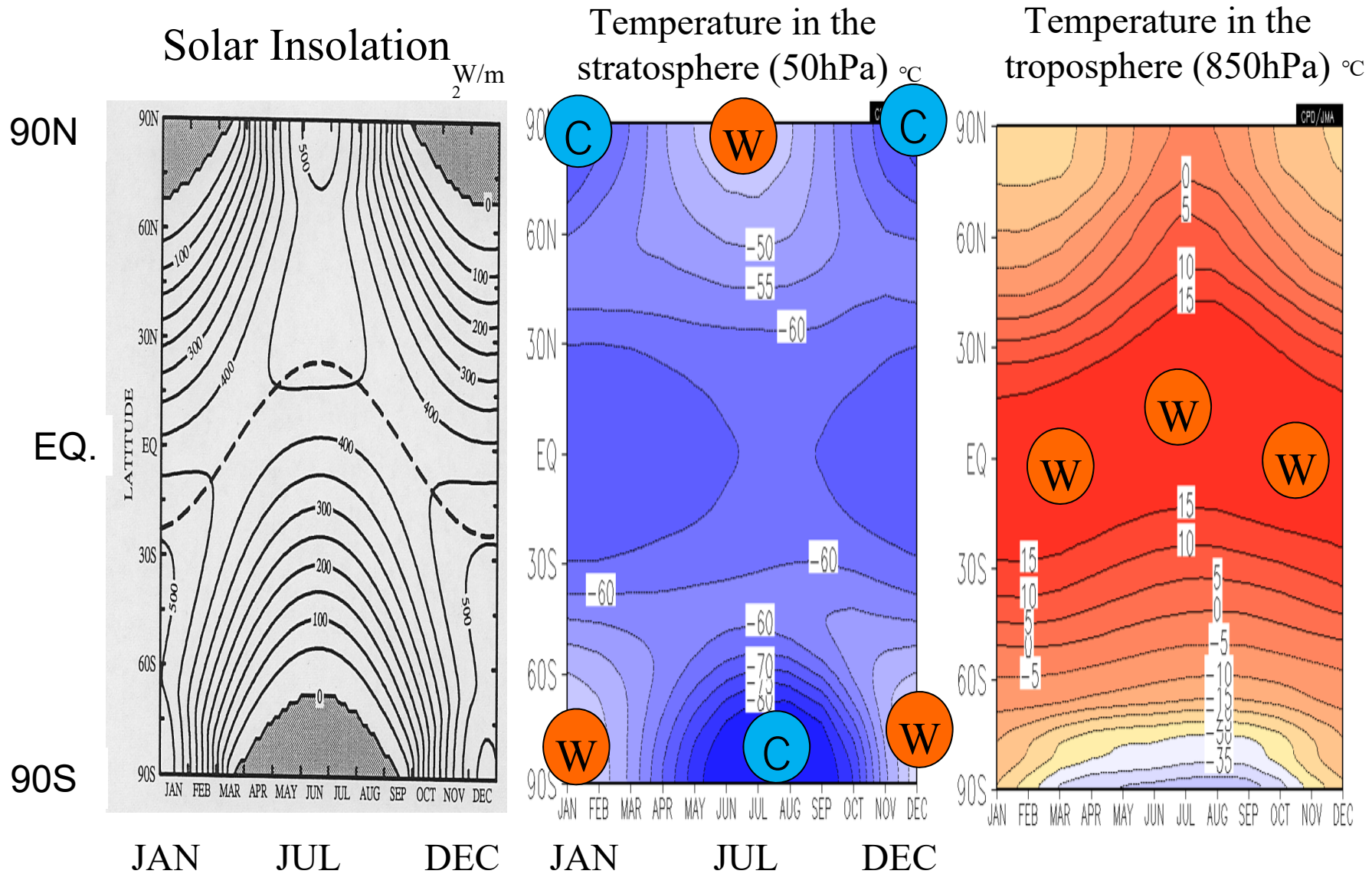
momentum loss



■ 1.4 Seasonal Change



Seasonal Change of Solar Insolation and Temperature

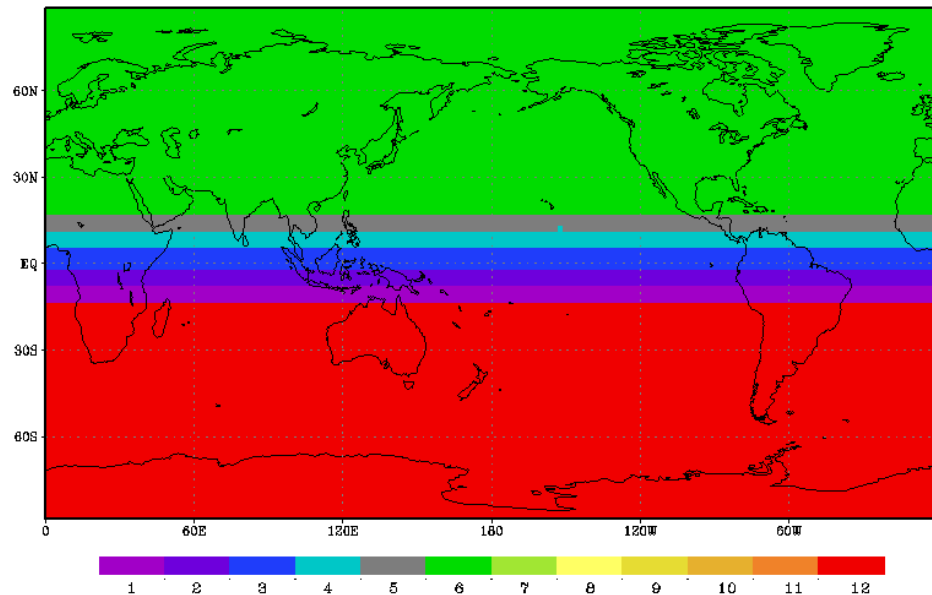


Month of maximum monthly mean temperature

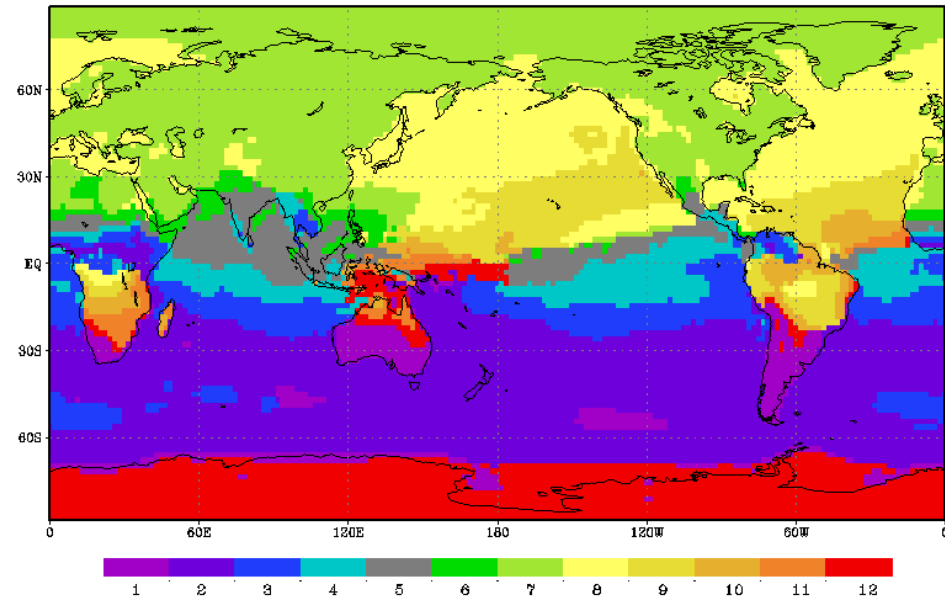
Solar max/min = Dec/Jan

Temperature max/min = Jan, Feb/Jul, Aug

Month of Maximum Downward Solar Radiation Flux at top



Month of Maximum T2m NCEP(1949–2000)

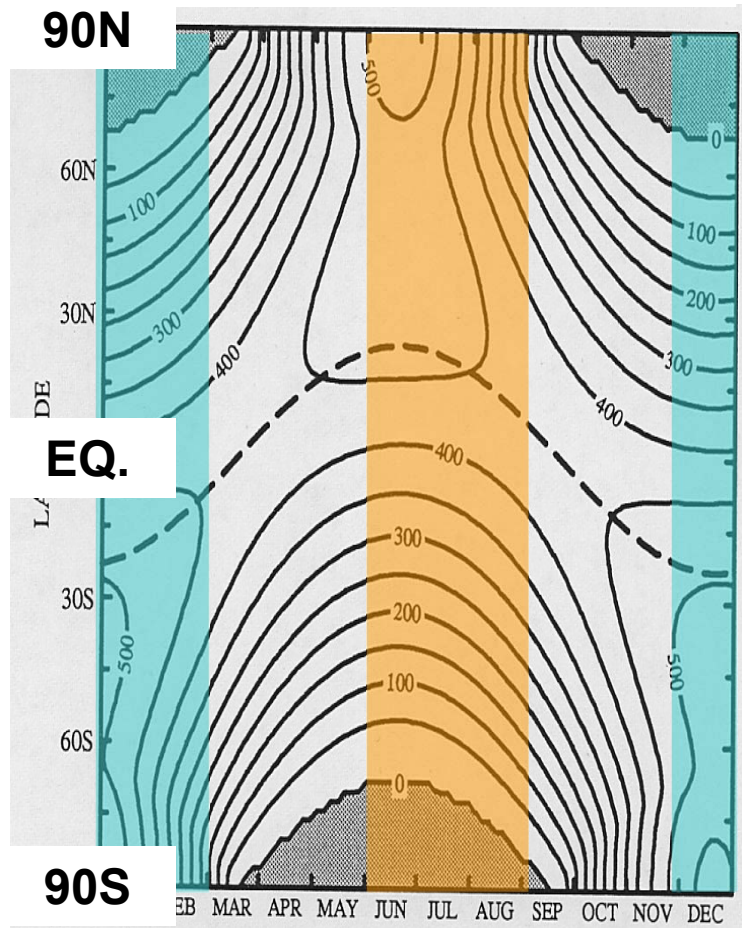


(Left) Downward solar radiation at the top of the atmosphere is maximum in June (December) poleward of about 15° latitude in the NH (SH). In the tropics, it is January, February, March, April and May at 10° S, 4° S, 2° N, 8° N and 14° N, respectively.

(Right) Actual month of maximum monthly mean temperature is quite different due to inertia of atmosphere, land and ocean. It is July over the continents and August over the oceans in the NH, but its distribution is not simple.

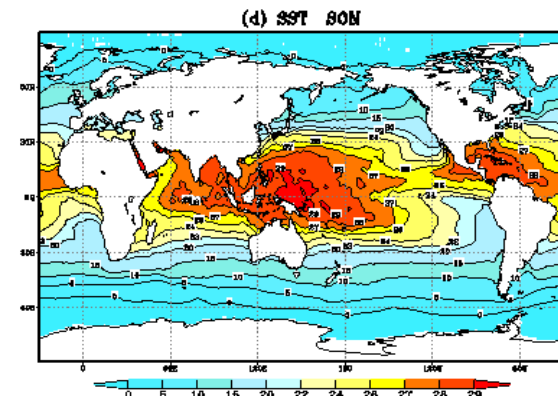
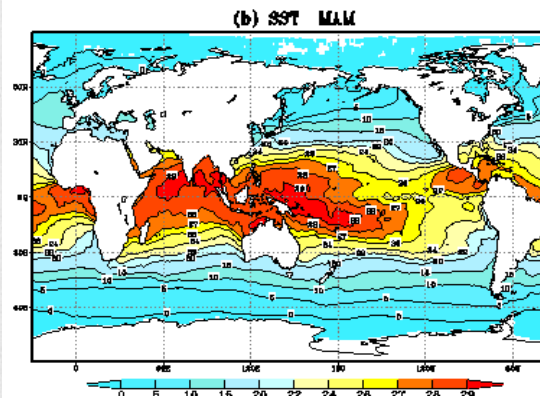
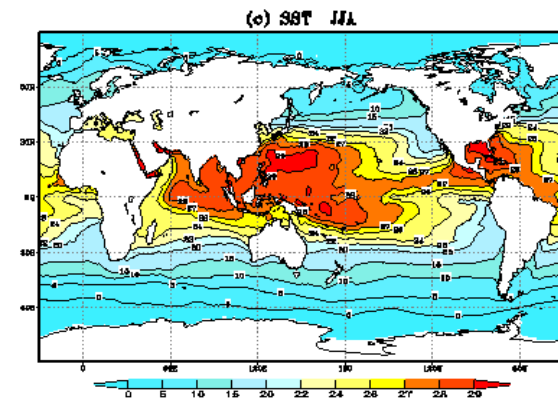
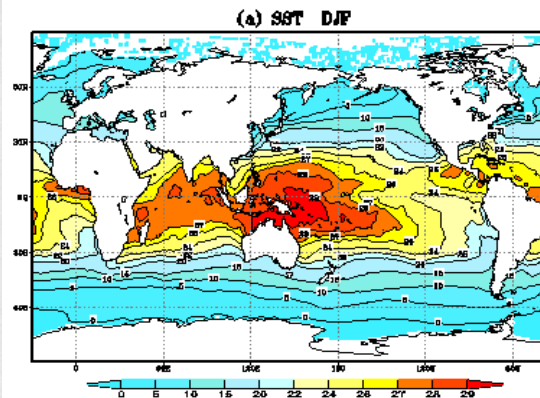
Seasonal Change of Sea Surface Temperature (SST)

Solar Insolation



Dec.-Jan.-Feb.

Jun-July-August



Mar.-Apr.-May

Sep.-Oct.-Nov.

■ Heat Capacity of atmosphere and ocean

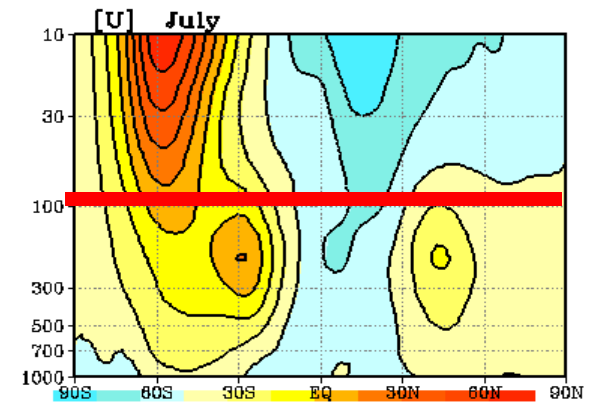
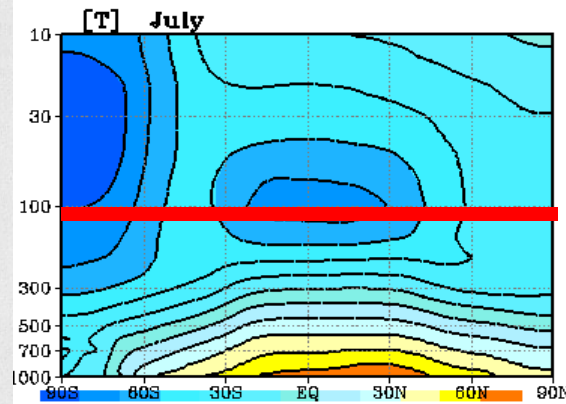
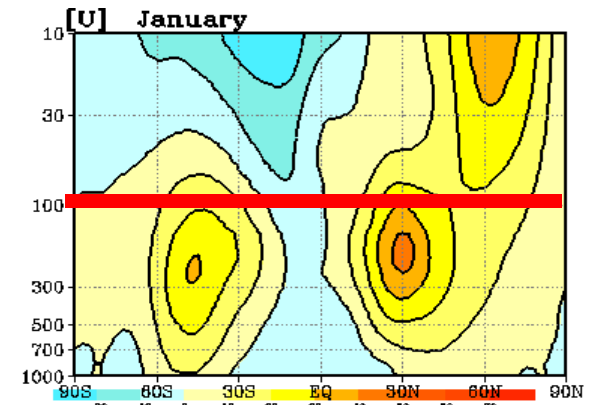
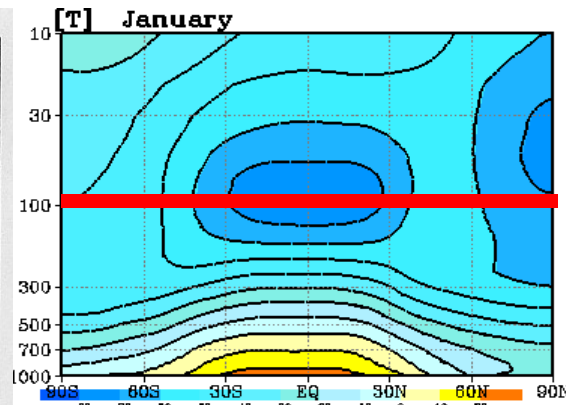
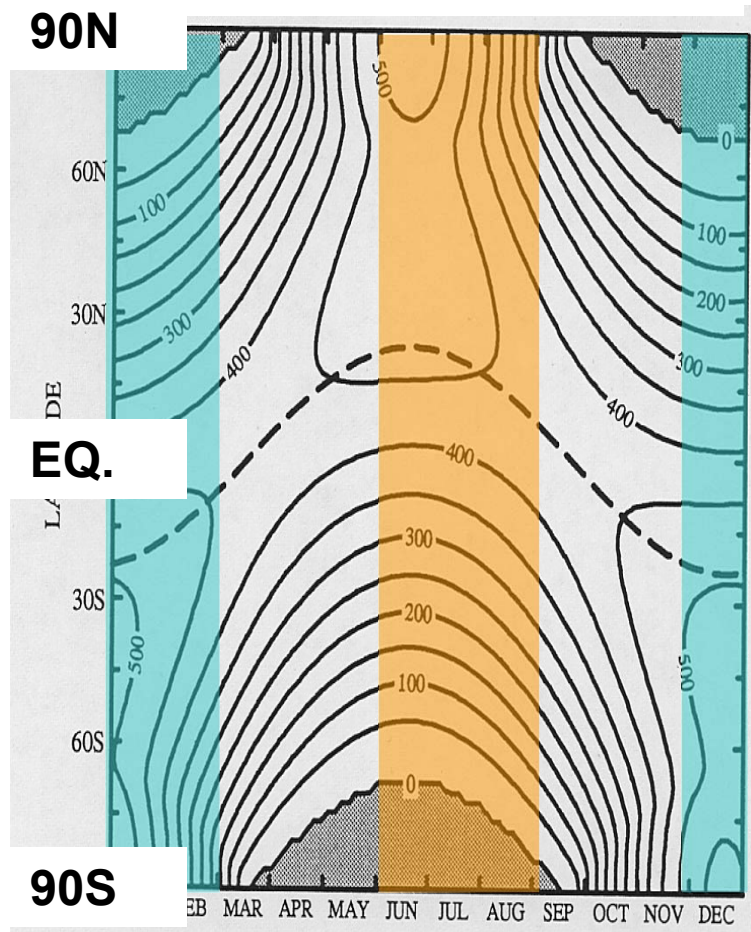
	Atmosphere	Ocean
Density	1.2-1.3kgm ⁻³	10 ³ kgm ⁻³ : atom. X 800
Mass(per 1 m ²)	(Top ~ Surface) 10 ⁴ kgm ⁻²	(Surface ~ 10m depth) 10 ⁴ kgm ⁻² : Mass of the atmosphere is the same as that of ocean with 10m depth
Specific heat	10 ³ Jkg ⁻¹ K ⁻¹	4 × 10 ³ Jkg ⁻¹ K ⁻¹ : atom. X 4
Heat capacity (per 1 m ²)	(Top ~ Surface) 10 ⁷ JK ⁻¹ m ⁻²	(Surface ~ 2.5m depth) 10 ⁷ JK ⁻¹ m ⁻² : Heat capacity of the atmosphere is the same as that of ocean with 2.5m depth

“1K in 250m depth ocean” is near equal to “100K in the atmosphere”

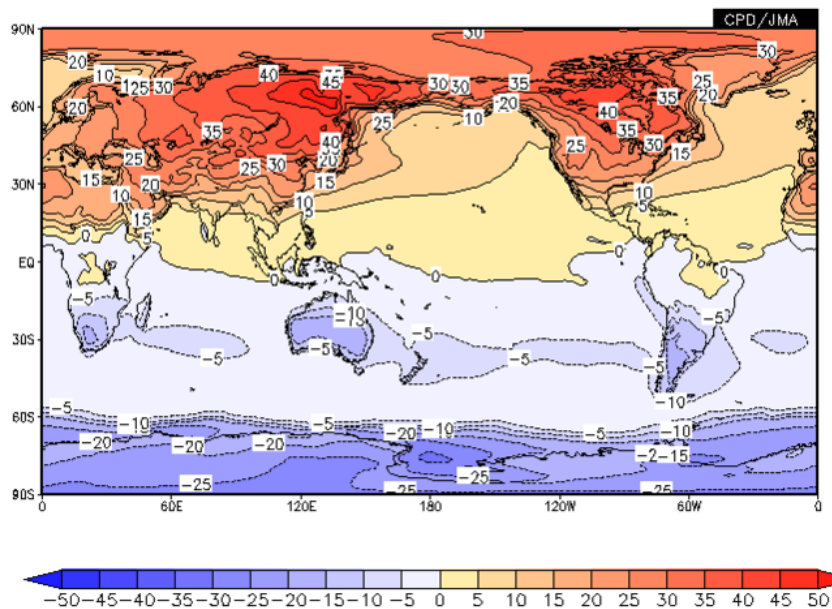
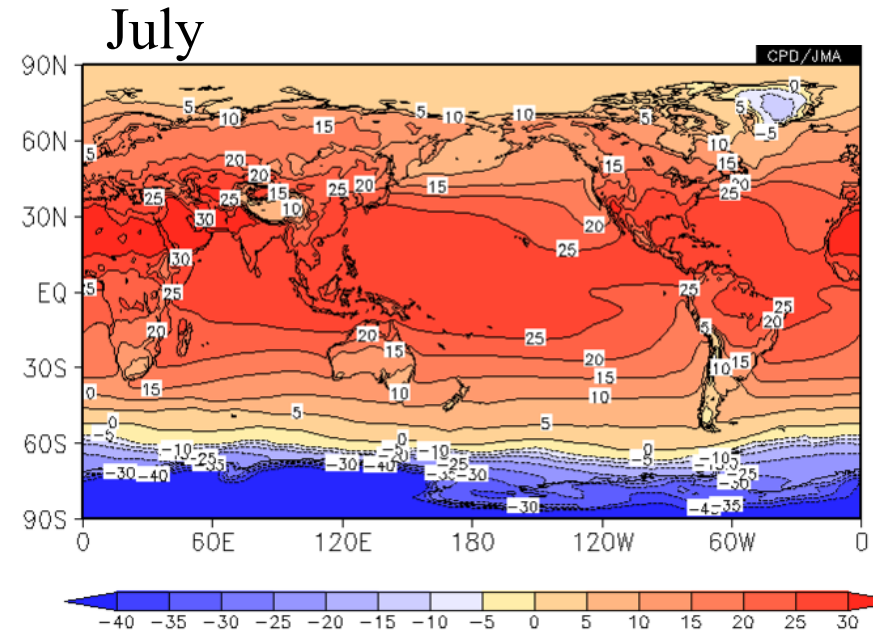
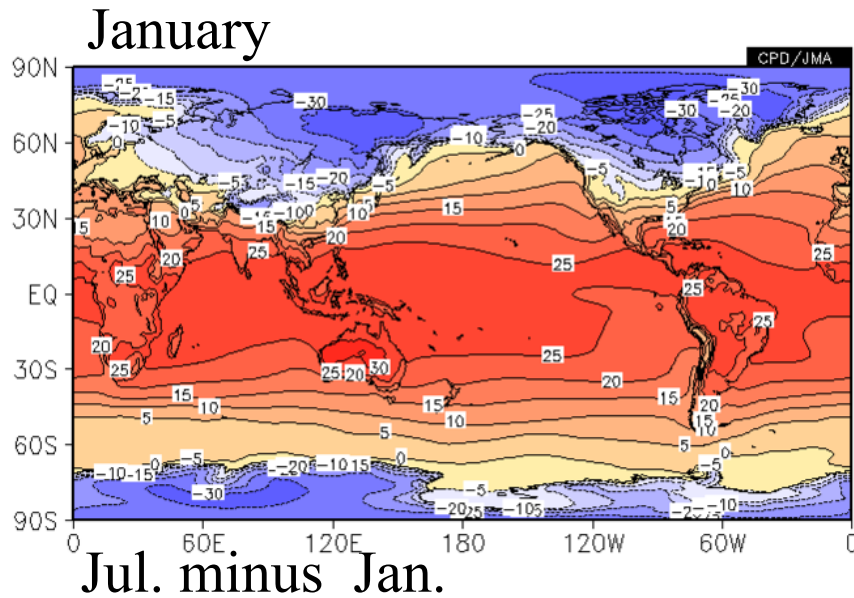
* from Gill 1982

Seasonal Change of Temperature and Zonal Wind

Solar Insolation



Jan-Jul contrast of surface temperature (°C)



Larger temperature contrast over lands

Winter: land temp. < ocean temp.

Summer: land temp. > ocean temp.

■ Monsoon circulation

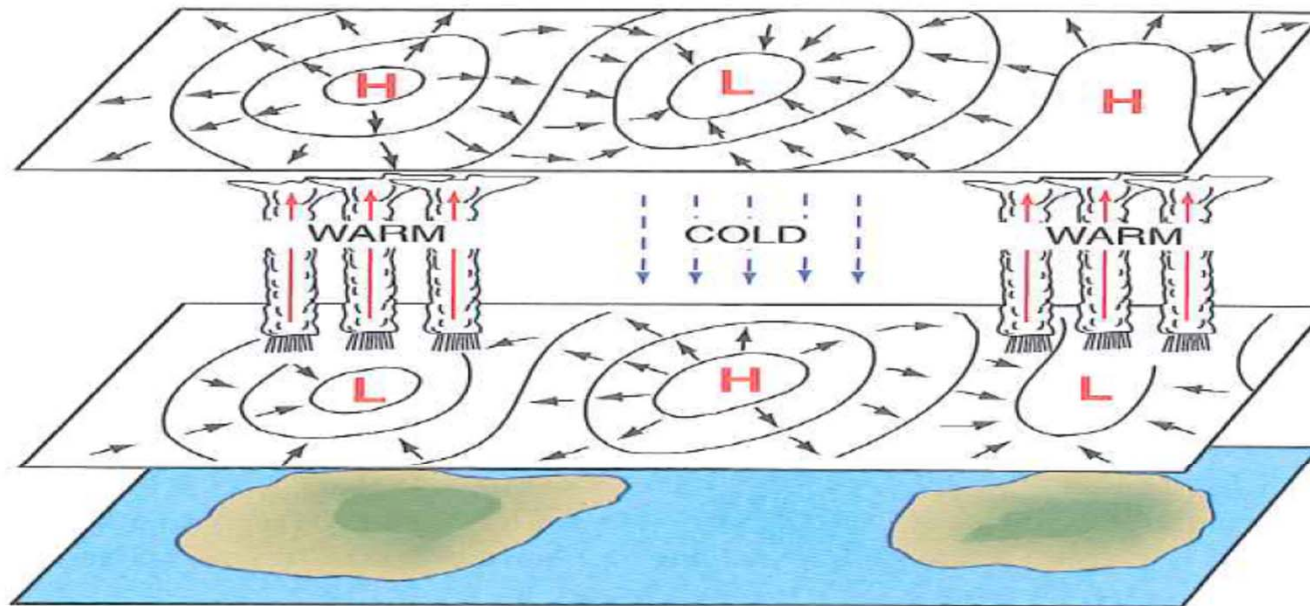
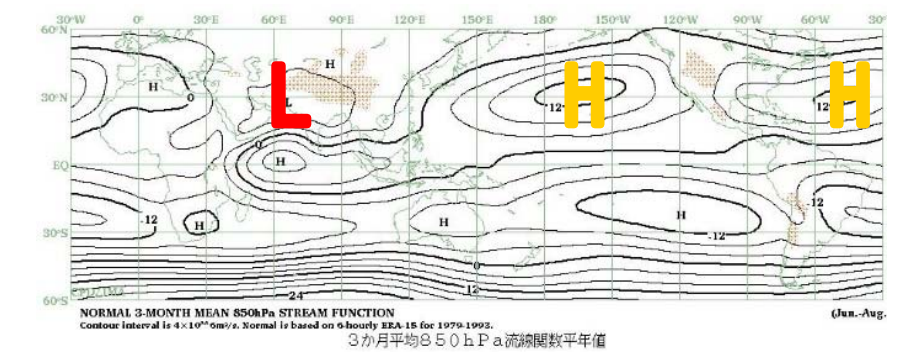
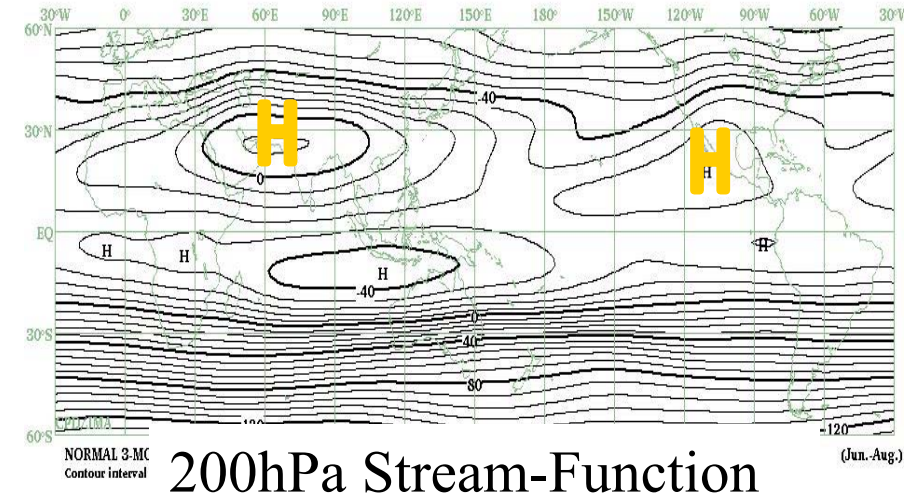
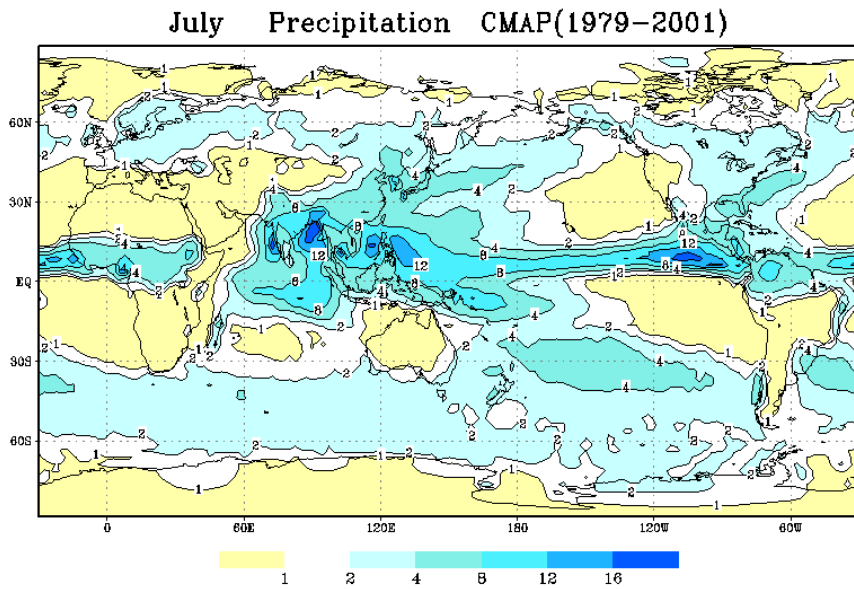


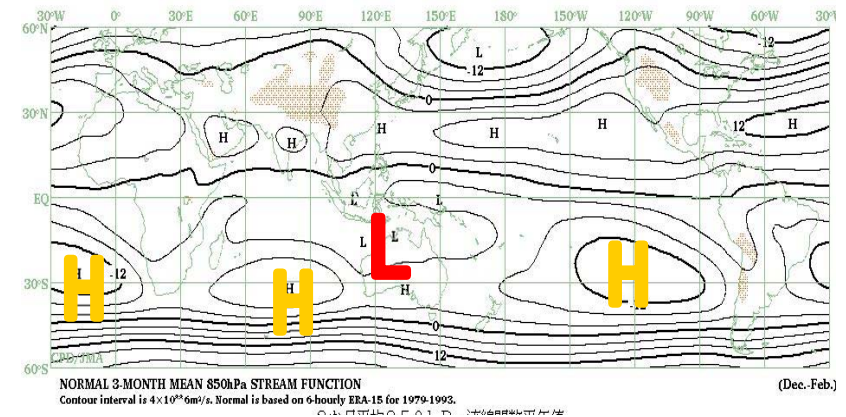
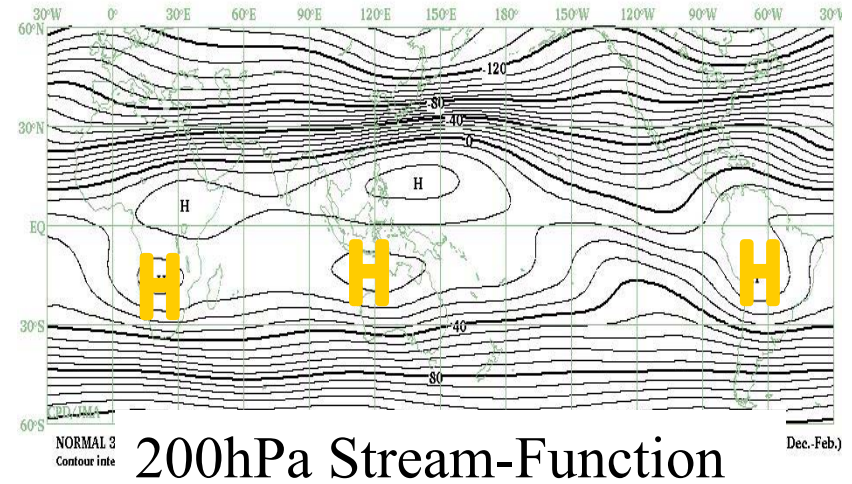
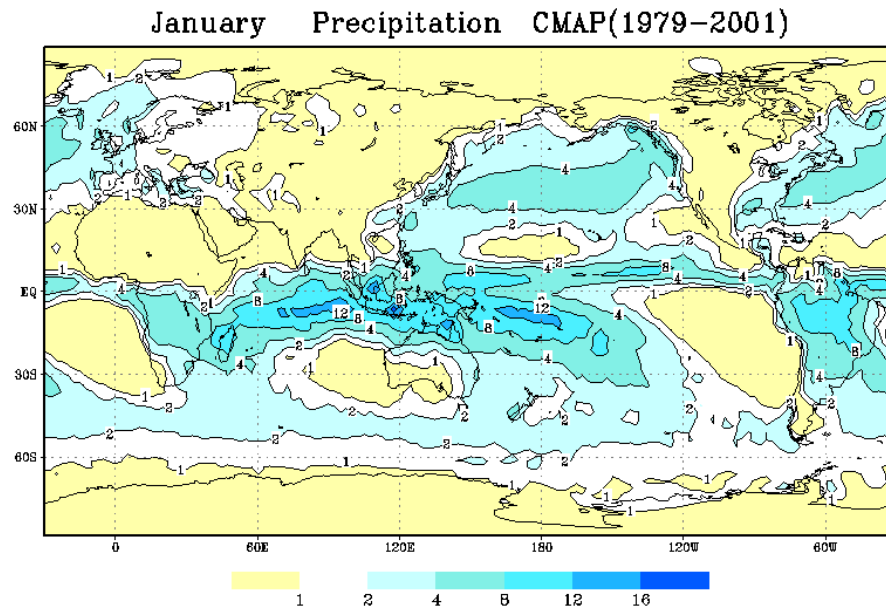
Fig. 10.9 Idealized representation of the monsoon circulations. The islands represent the subtropical continents in the summer hemisphere. Solid lines represent isobars or height contours near sea level (lower plane) and near 14 km or 150 hPa (upper plane). Short solid arrows indicate the sense of the cross-isobar flow. Vertical arrows indicate the sense of the vertical motions in the middle troposphere. Regions that experience of summer monsoon rainfall are also indicated.

Northern Summer Monsoon



850hPa Stream-Function

Southern Summer Monsoon



850hPa Stream-Function

Local heating in the tropics forces stationary waves

Diabatic heating in Jan.

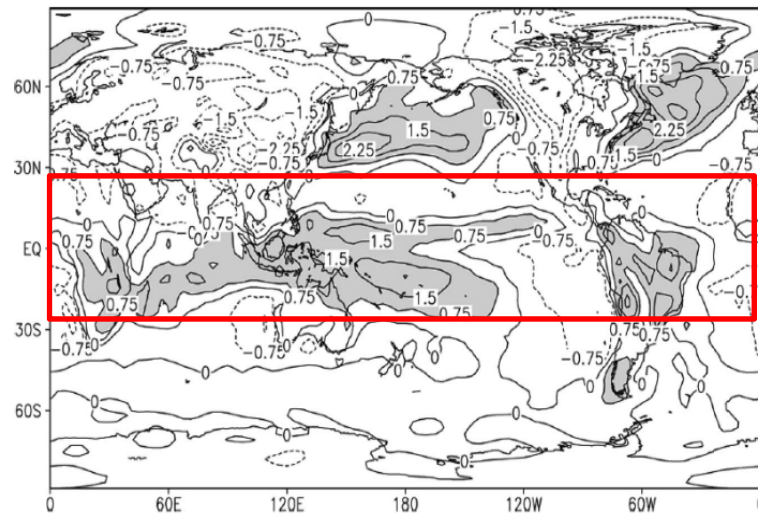
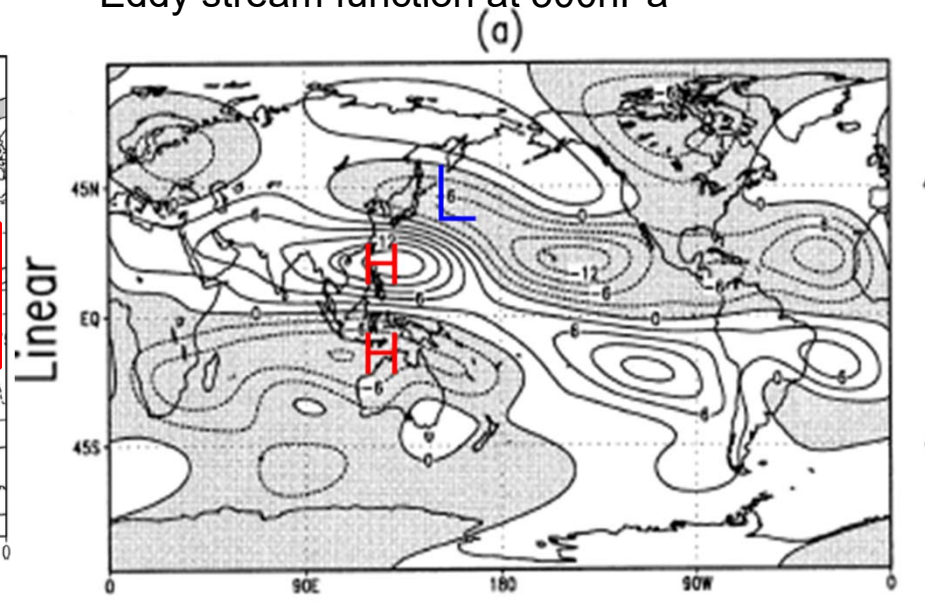


FIG. 8. The column-averaged diabatic heating field in Jan obtained from the NCEP-NCAR reanalysis as described in the appendix. The contour interval is 0.5 K day⁻¹.

Linear response to the heating in the left panel
Eddy stream function at 300hPa

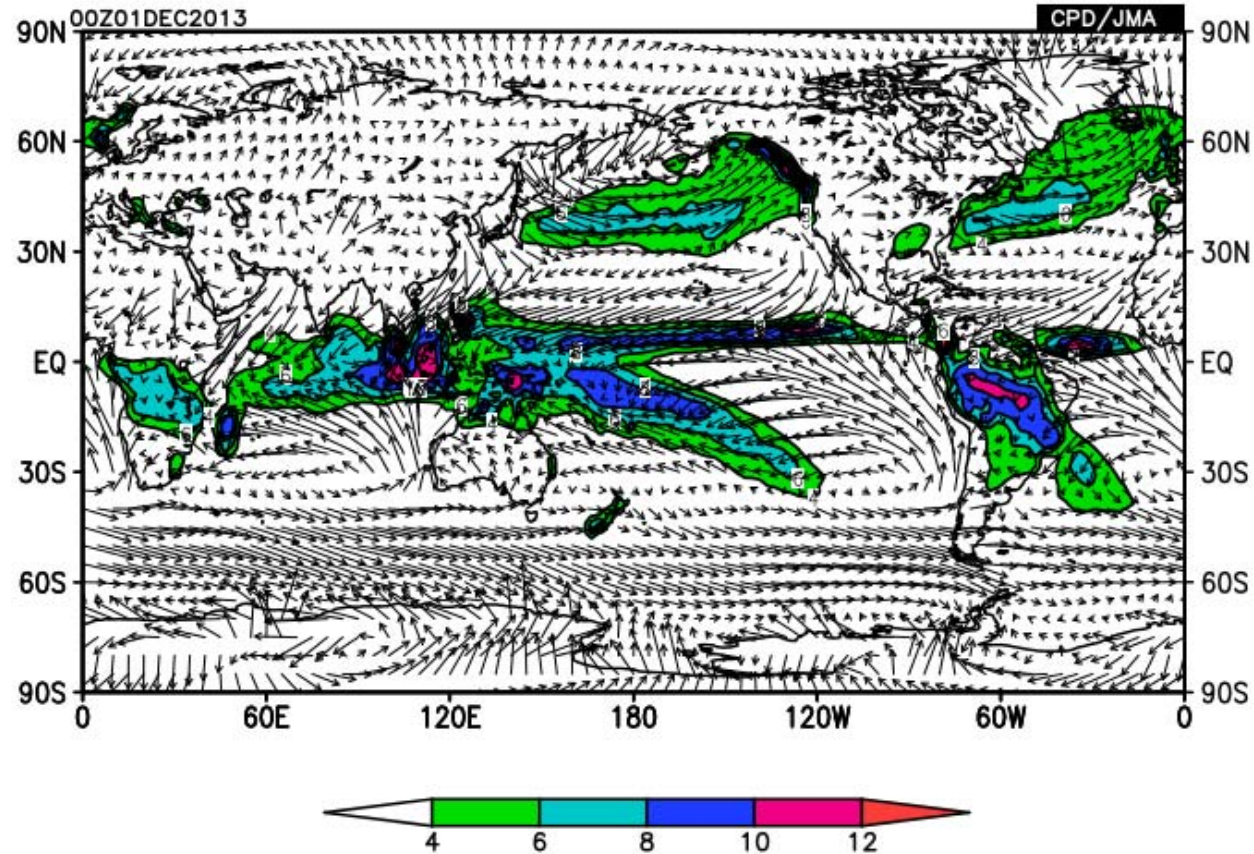


Held et al. (2002)

Seasonal change of precipitation and surface wind

DATA1 JRA-55 u10m,v10m NORM lat = -90:90 lon = 0:360 level = 1:1
time = 2013010100:2013120100 ave = 1MO

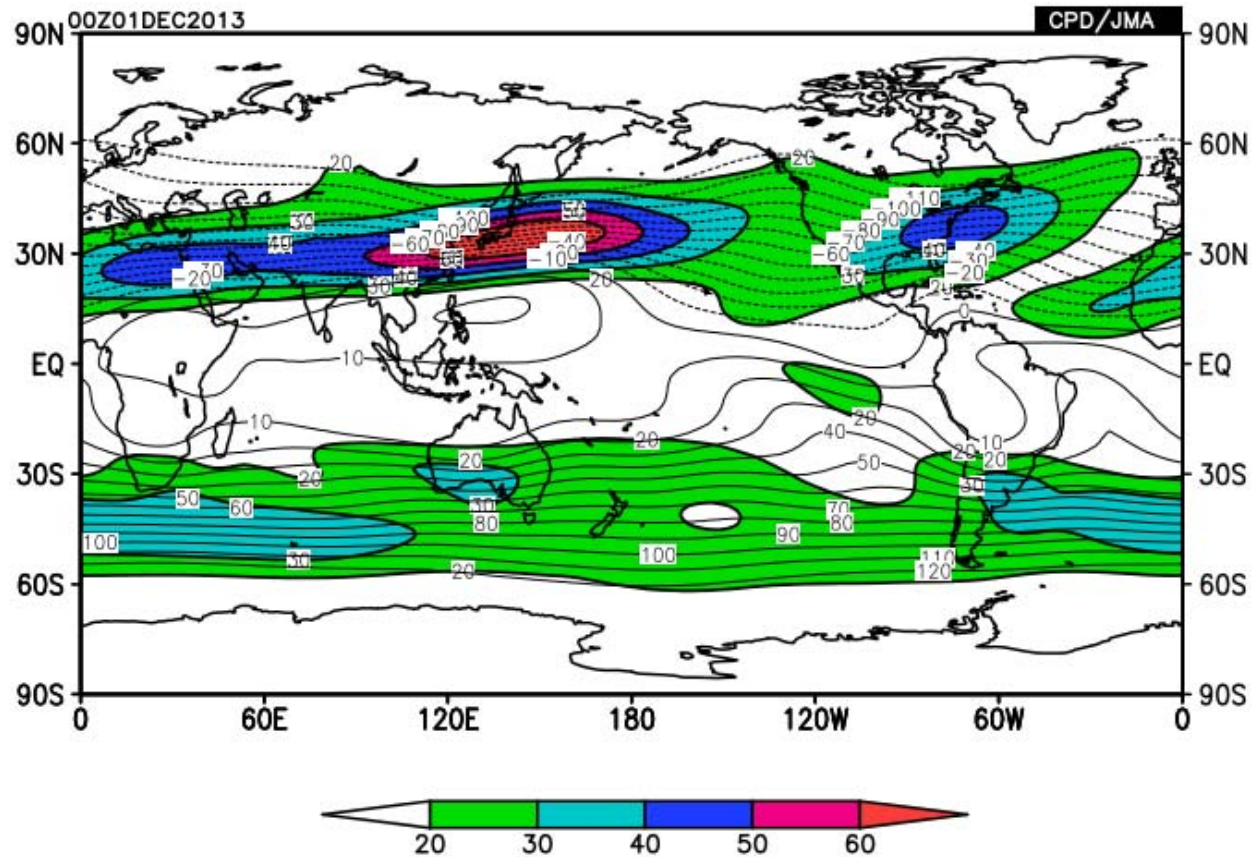
DATA2 x_GPCP gpcp NORM lat = -90:90 lon = 0:360 level = 1:1
time = 2013010100:2013120100 ave = 1MO analysis method = DATA1_DATA2



Seasonal change of zonal wind and stream function at 200hPa

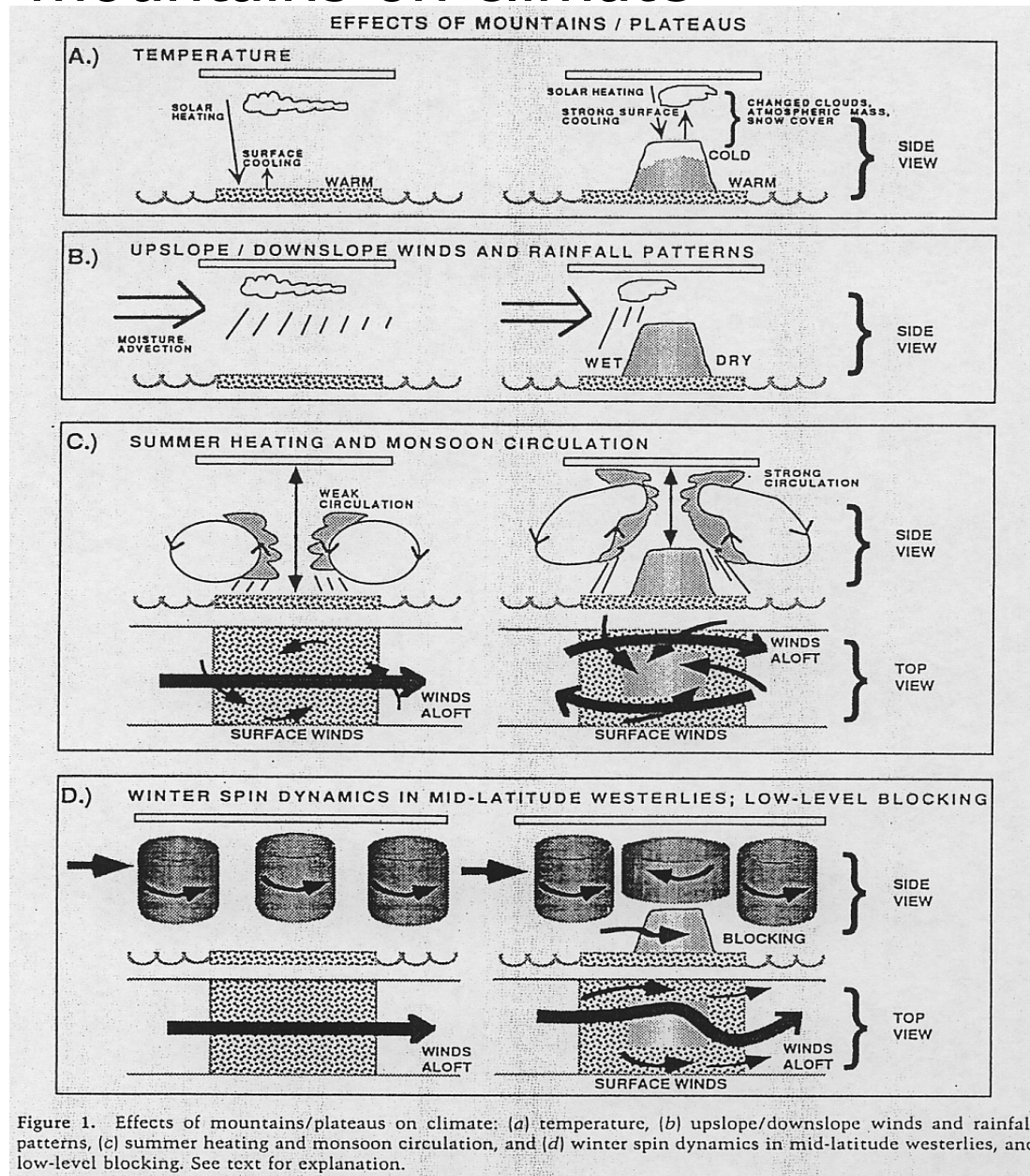
DATA1 JRA-55 u37 NORM lat = -90:90 lon = 0:360 level = 23:23
time = 2013010100:2013120100 ave = 1MO

DATA2 JRA-55 psi37 NORM lat = -90:90 lon = 0:360 level = 23:23
time = 2013010100:2013120100 ave = 1MO analysis method = DATA1_DATA2



■ 1.5 Role of orography on climate

Effect of mountains on climate

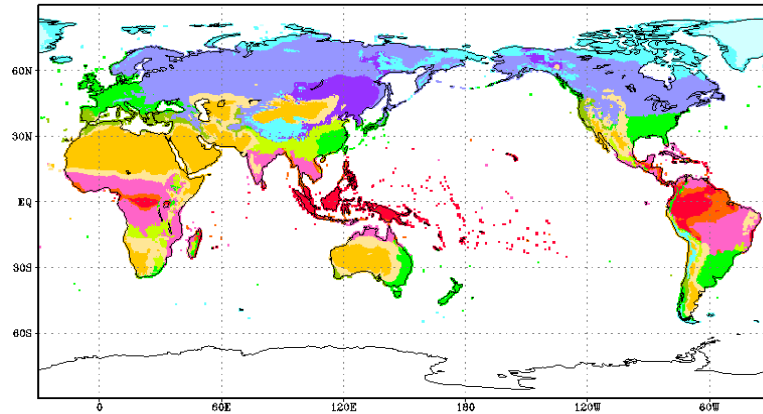


Kutzbach et al.
(1993) J.Geology

Effect of mountain: Koppen climate

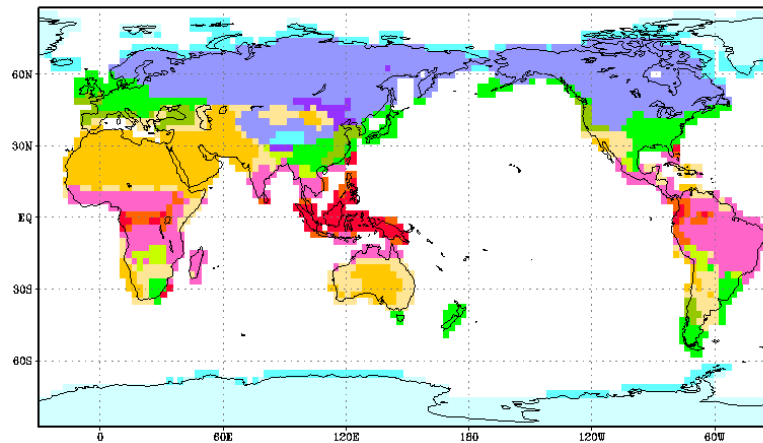
OBS.

Observation



Af Am Aw BS BW Ca Cw Cf Df Dw ET EF

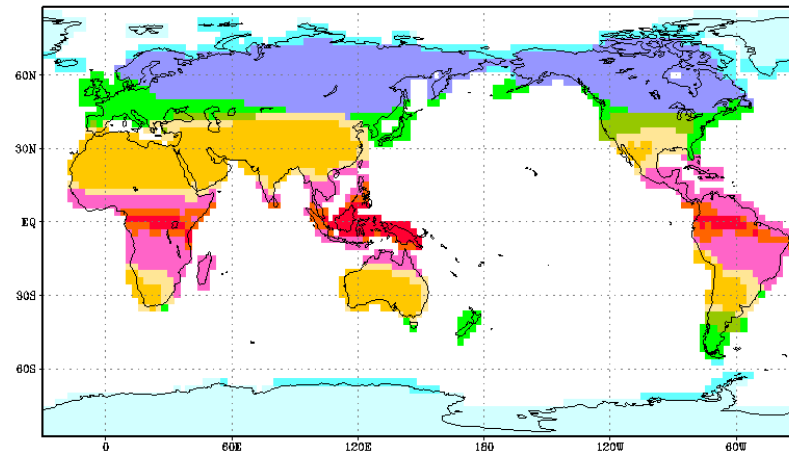
Simulation by Climate Model
MRI-CGCM2.2 control



Af Am Aw BS BW Ca Cw Cf Df Dw ET EF

Simulation by Climate Model
without mountain

MRI-CGCM2.2 no-mountain



Af Am Aw BS BW Ca Cw Cf Df Dw ET EF

■ Outline of the lecture

1. Climate System (60 min. + α)

1.1 Introduction

1.2 Radiative Balance

1.3 Horizontal Radiative Imbalance and Circulations

1.4 Seasonal Change

1.5 Role of Orography on Climate

2. Climate Variability (90 min. + α)

2.1 Introduction

2.2 Intraseasonal Variability: Quasi-stationary Rossby wave, MJO and equatorial waves

2.3 Interannual Variability: ENSO, El Nino Modoki, IOD

2.4 Decadal Variability: PDO, ENSO-Monsoon relation

3. Climate change due to anthropogenic forcing (30 min. + α)

■ 2.1 Introduction

■ Causes of Climate Variability

- Natural origin

external: land-sea distribution, orography

solar constant, orbital variations, volcano

internal variability of the climate system

(e.g., air-sea interaction,,)

- Anthropogenic origin

emission of greenhouse gases, destruction of ozone layer, land surface modification,, (= climate change)

■ Various time scales of climate variability

- days to intraseasonal variability
Blocking, Quasi-stationary Rossby wave
Madden-Julian Oscillation (MJO)
- seasonal to interannual climate variability
El Nino/Southern Oscillation (ENSO)
monsoon variability
modes of variability (NAO, PNA, WP patterns)
- decadal to interdecadal climate variability
- ocean thermohaline circulation
- glacial and interglacial

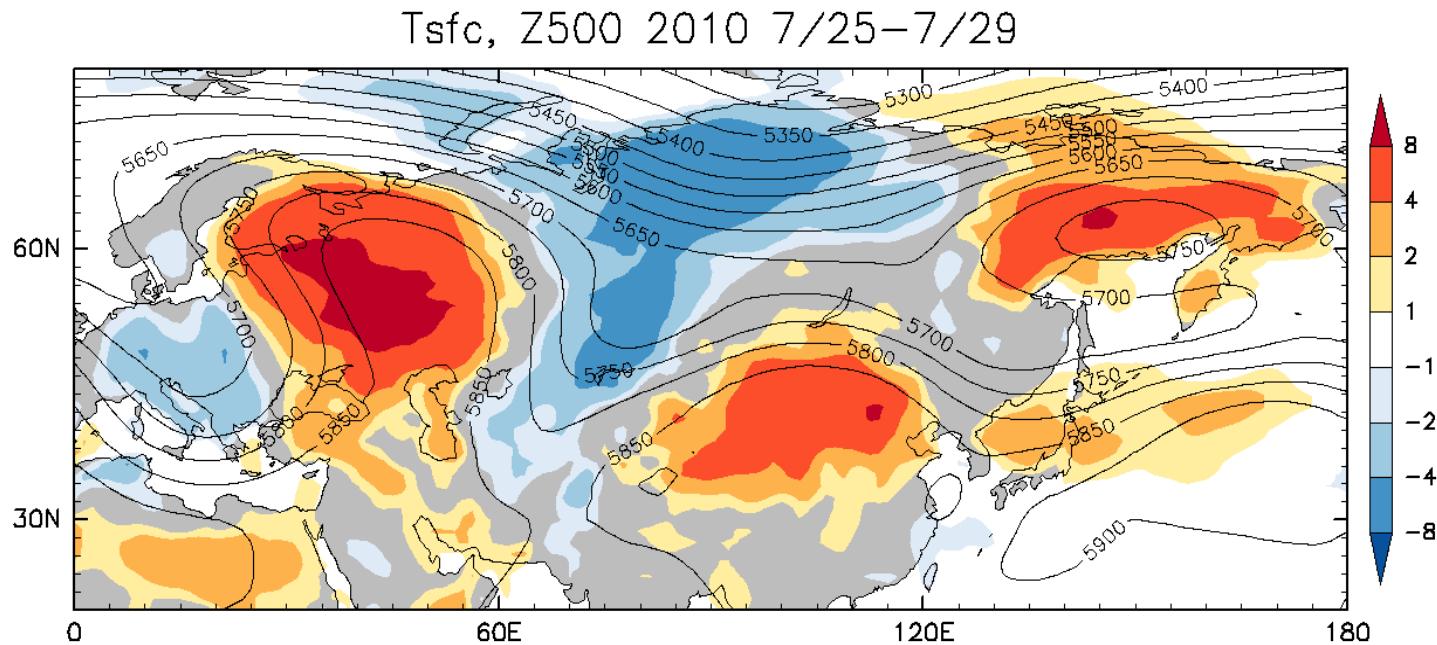
N.B. climate system is not in equilibrium

■ 2.2 Intraseasonal Variability

Blocking and Rossby wave,
MJO and equatorial waves

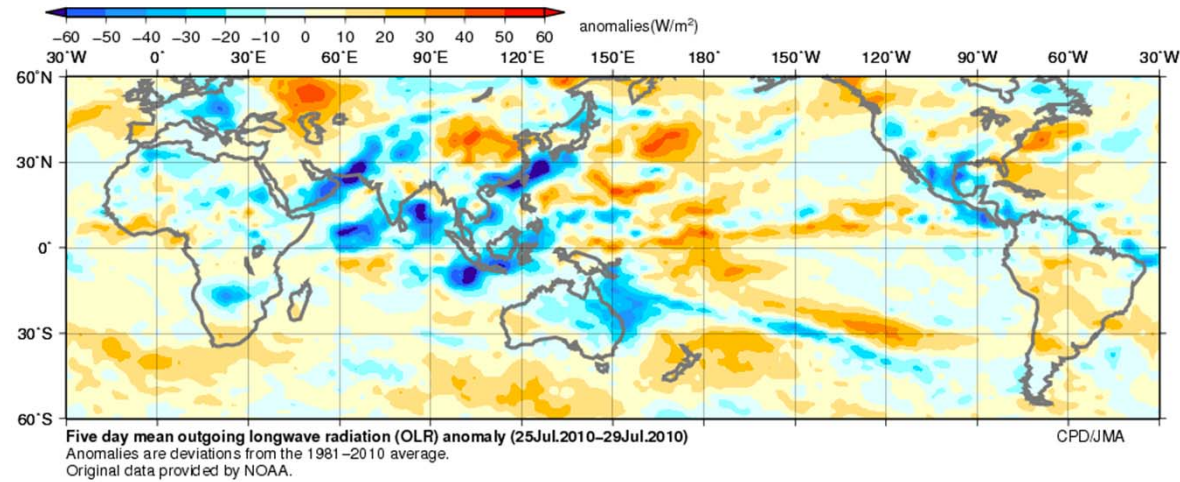
■ Blocking

- Example: Heatwave by blocking in 2010
- Eastern Europe: late June to late July
- Western Russia: late July to mid August
 - 38.2°C at Moscow on July 30 (15°C higher than climatology)
 - Heavy rainfall and floods over Pakistan
- Hot summer also over Japan

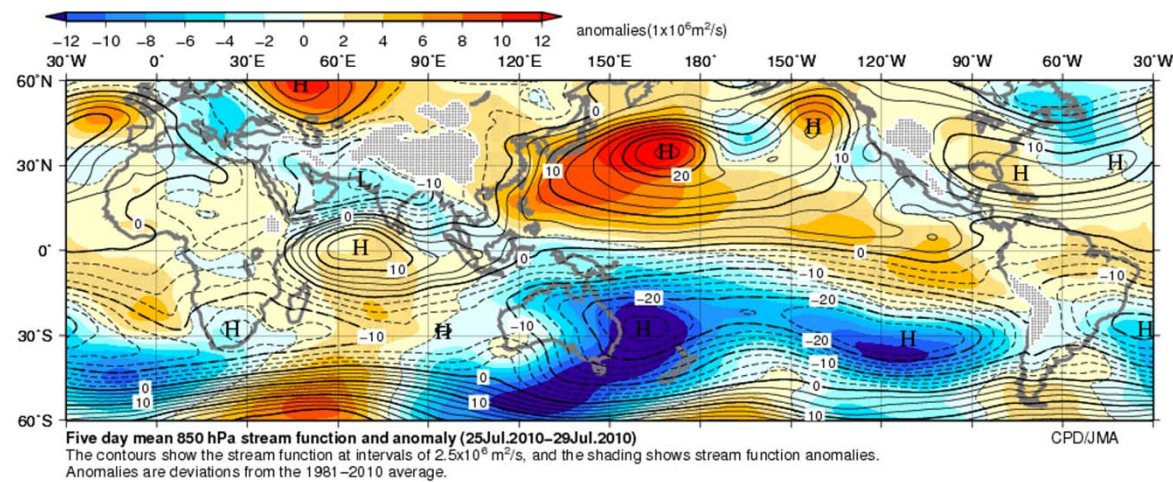


Heavy rainfall and floods over Pakistan

OLRa



PSI850a

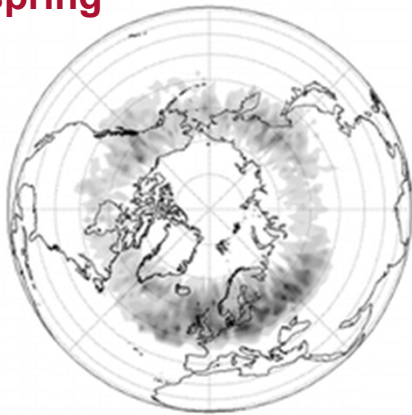


Blocking Climatology

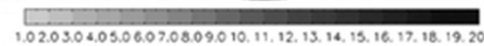
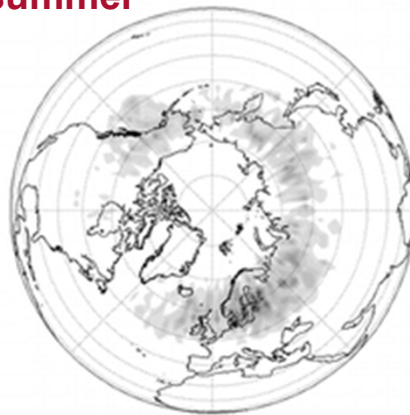
- Blocking events occur over Atlantic to Europe, and Russia to US
- Sometimes it continues over 30 days

Location

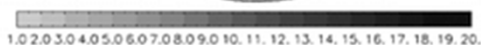
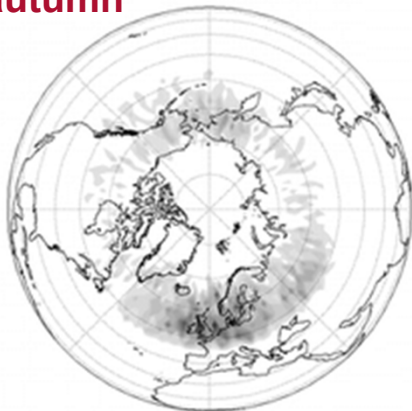
a **spring**



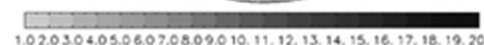
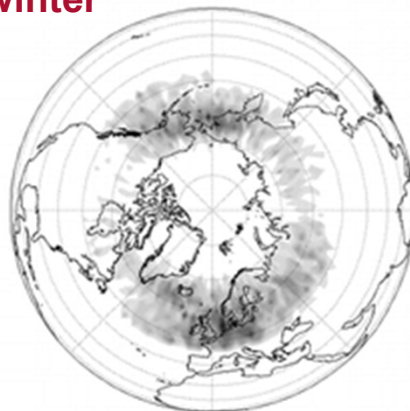
b **summer**



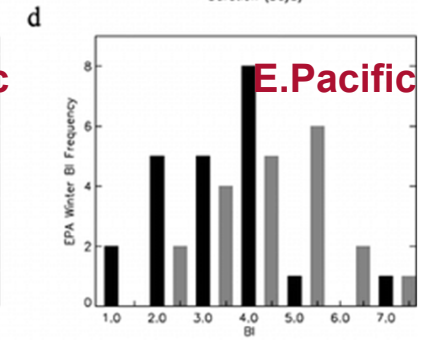
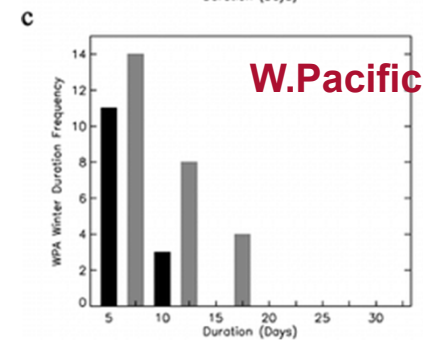
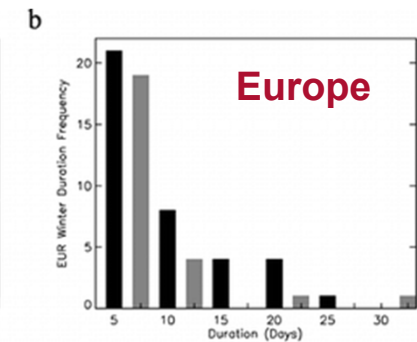
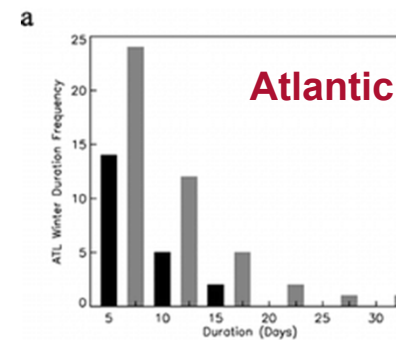
c **autumn**



d **winter**



Duration



(Barriopedro et al. 2006)

■ Examples of Quasi-stationary Rossby waves: 2005/2

Rossby waves:

are large scale (synoptic and planetary scale) waves in the atmosphere and ocean.

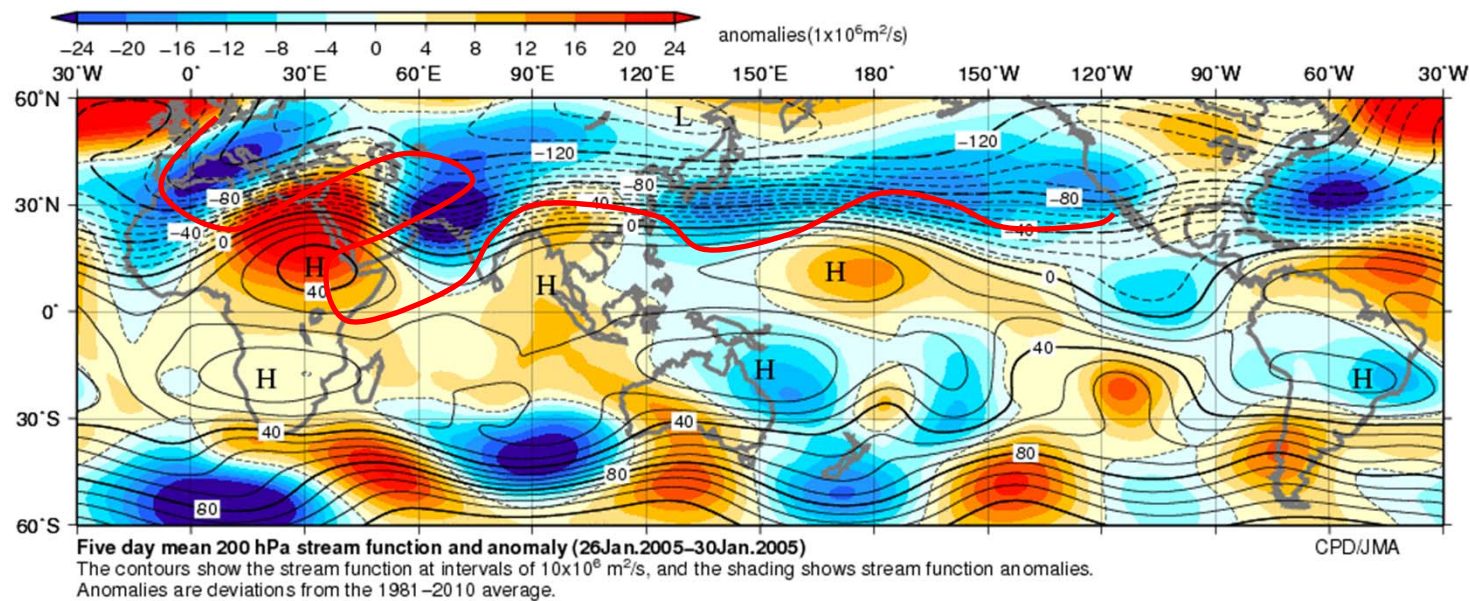
obey the conservation law of potential vorticity.

are dispersive and propagate westward (longer wave is faster).

are stationary if phase speed is the same as westerly wind which advect the waves.

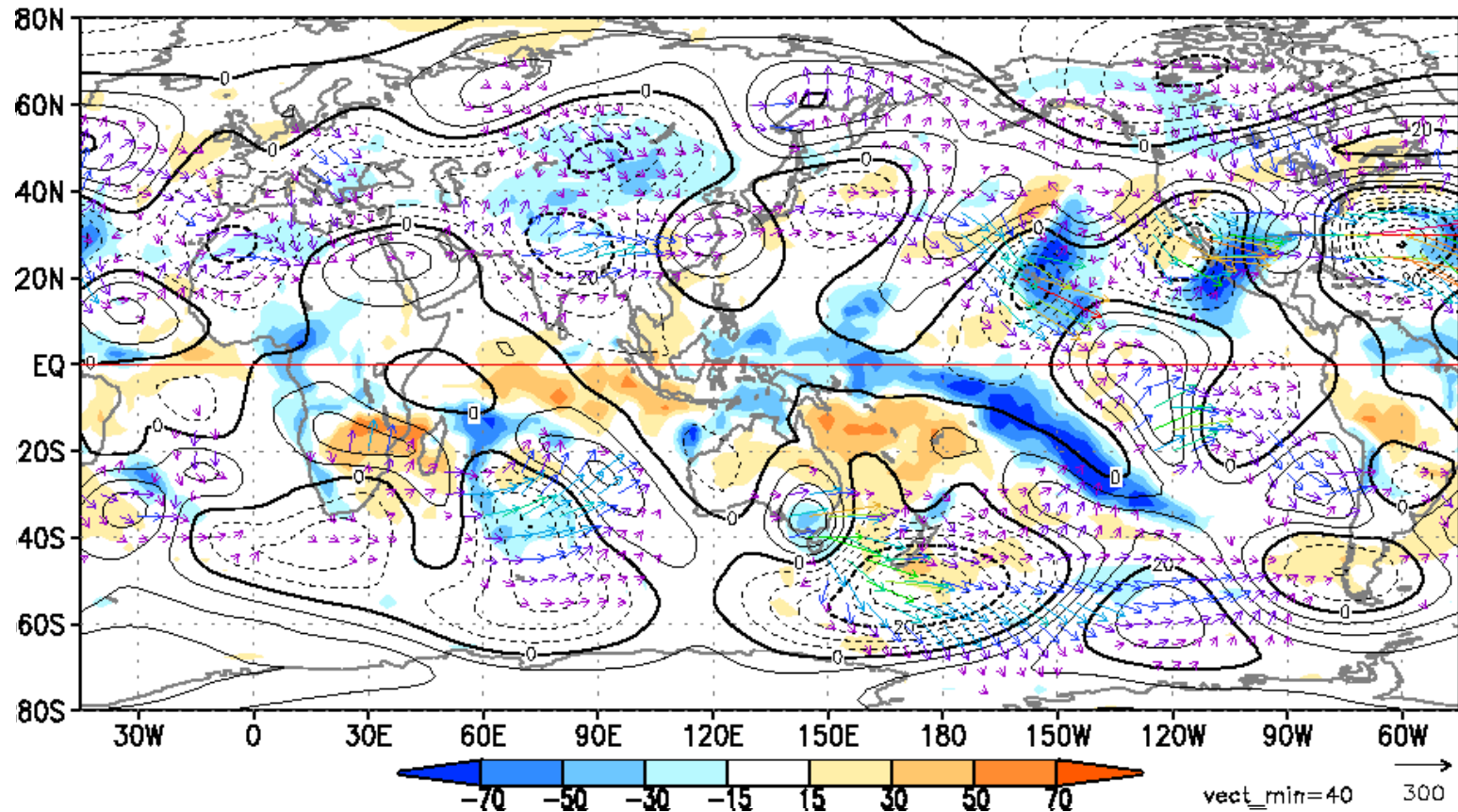
Group velocity of stationary Rossby wave packet is eastward.

Stationary Rossby wave packet tends to propagate trapped by Jet streams.

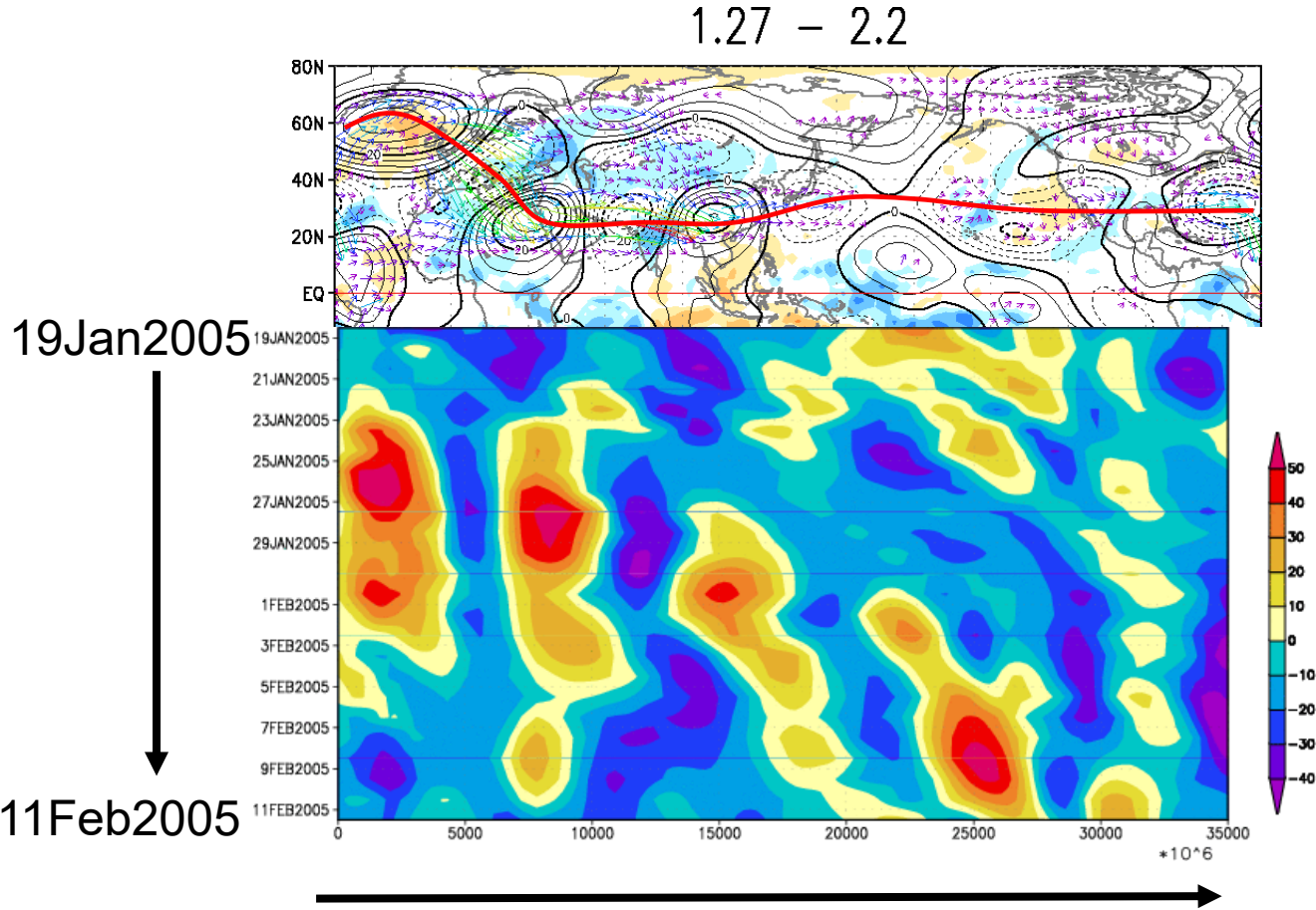


■ Blocking over the North Atlantic and Rossby wave trains along the Asian jet

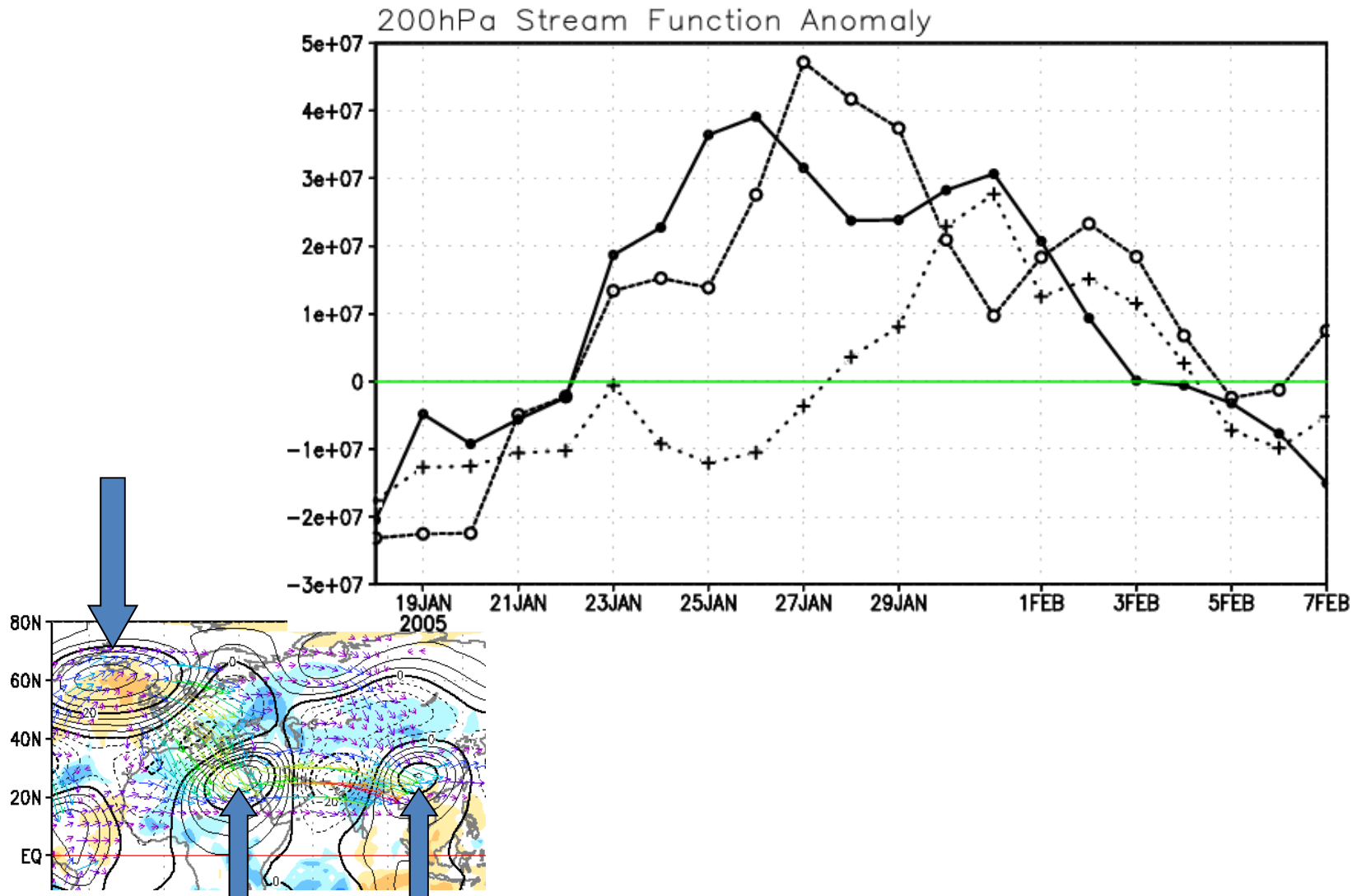
5-day mean stream function anomalies at 200hPa 2005.1.18-
2.2 - 2.6



Time cross section of stream function anomalies at 200hPa
x-axis : distance along the red line from a base point
(60W,60N)

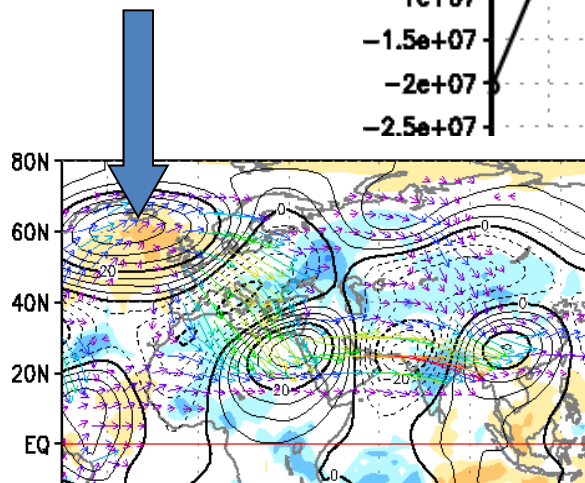
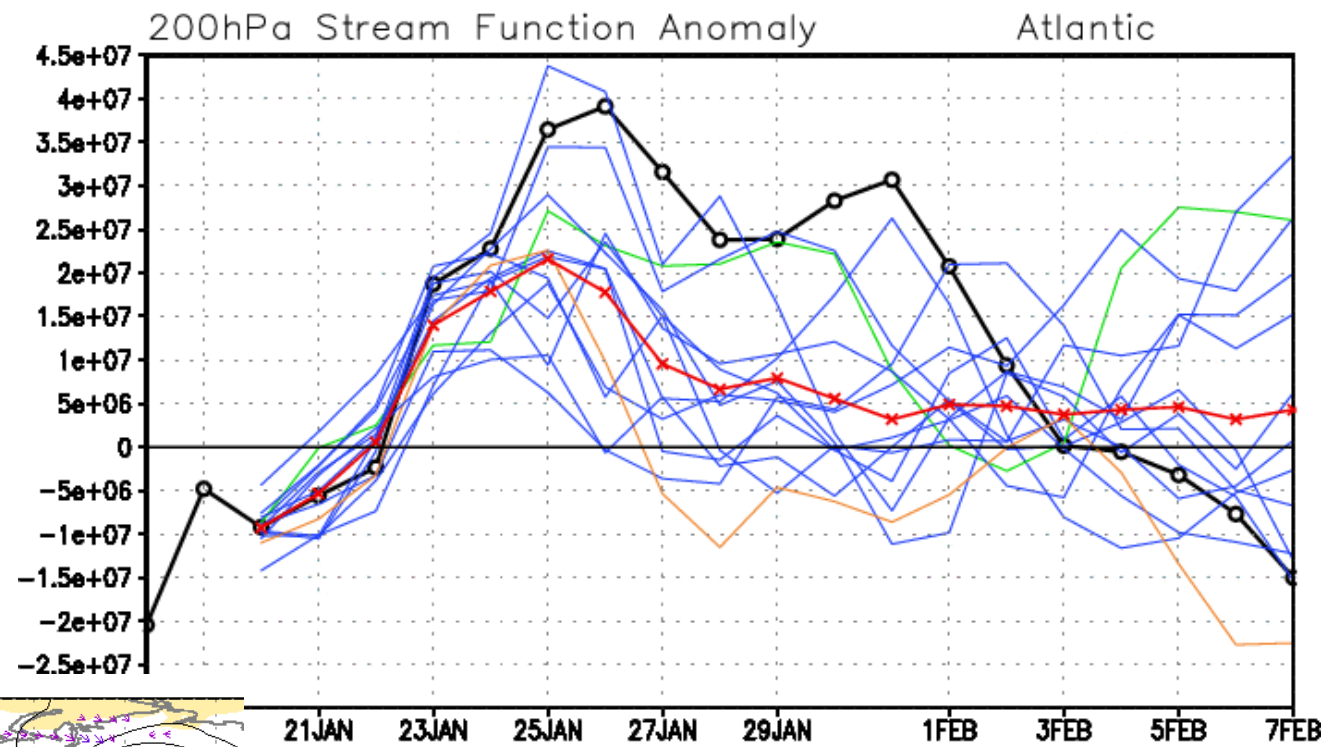


■ Decay of Blocking due to Rossby wave radiation



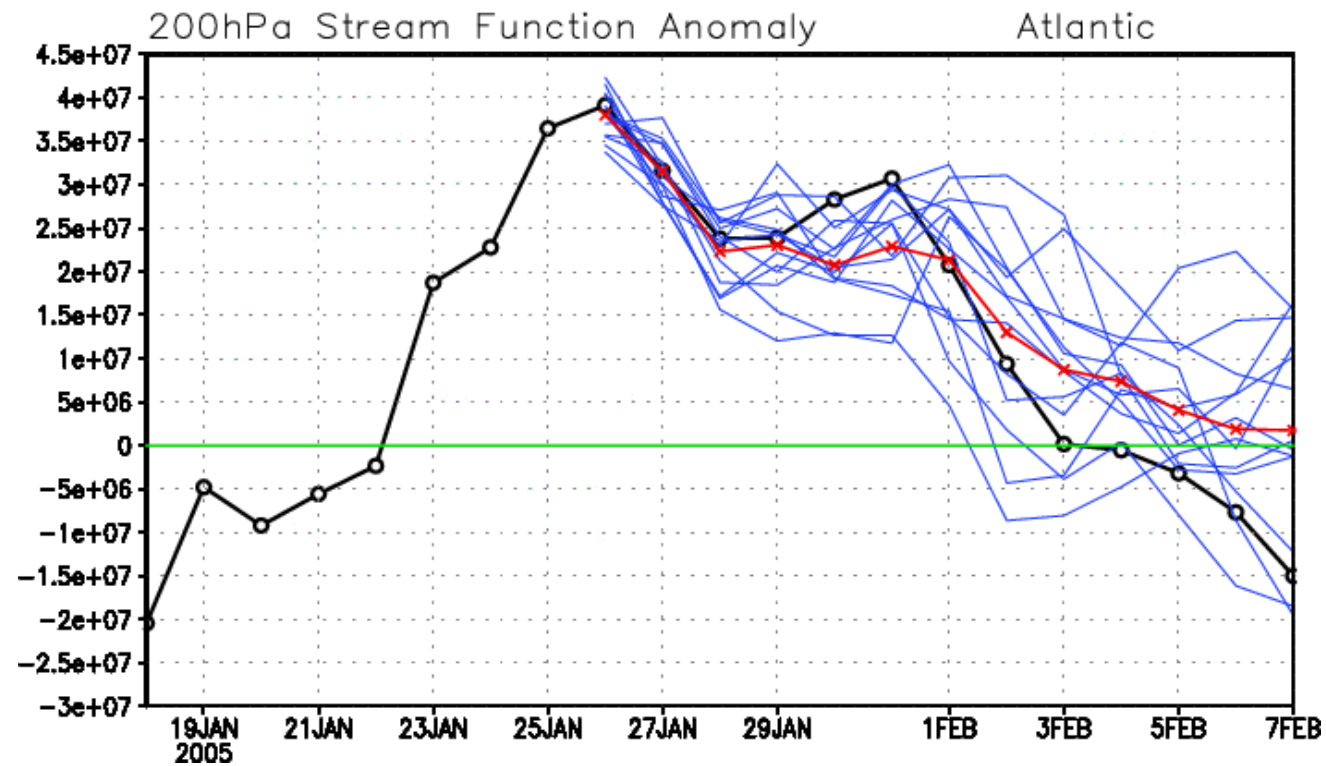
■ Prediction of development of Blocking

Initial : 20th JAN 2005



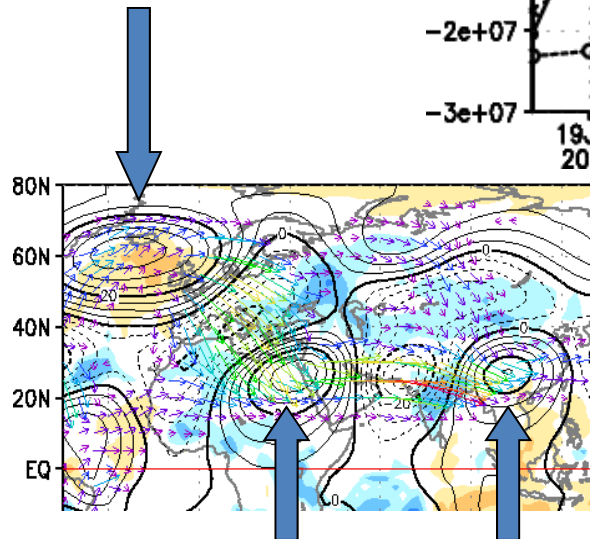
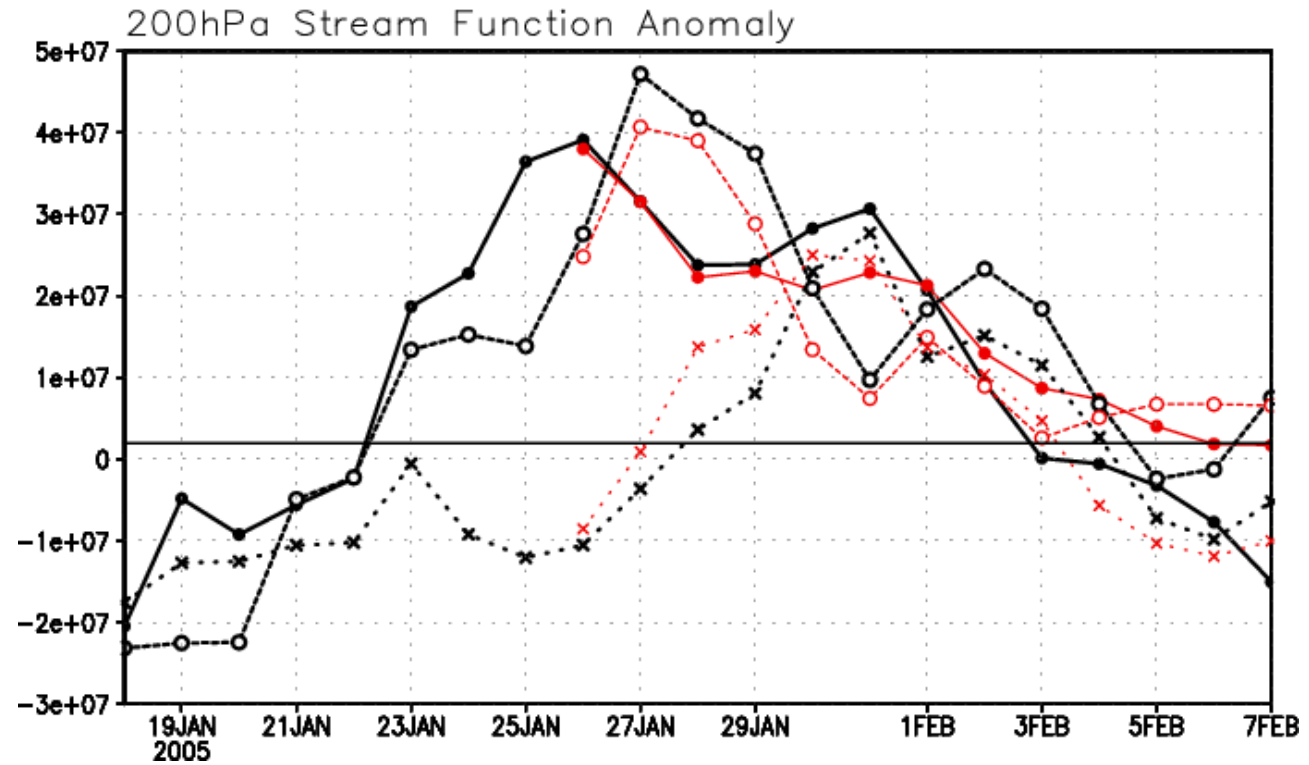
■ Prediction of decay of Blocking

Initial : 26th JAN 2005

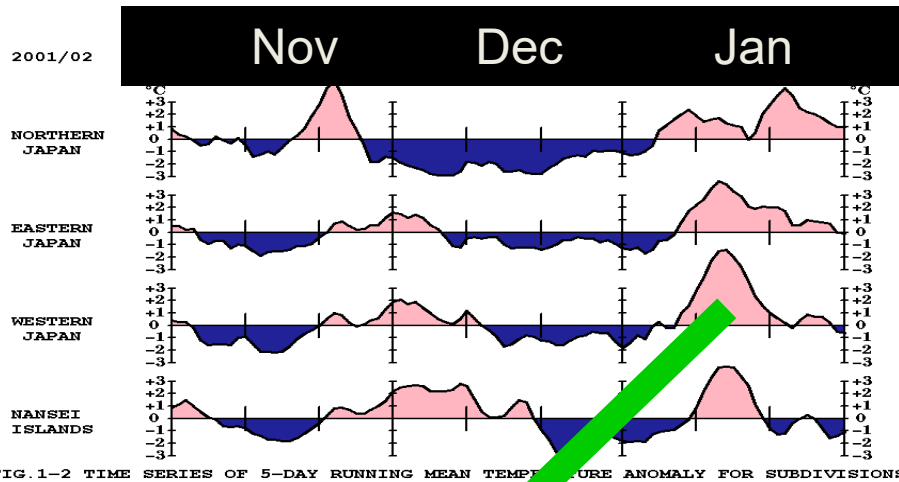


■ Prediction of decay of Blocking due to Rossby wave radiation

Initial : 26th JAN 2005

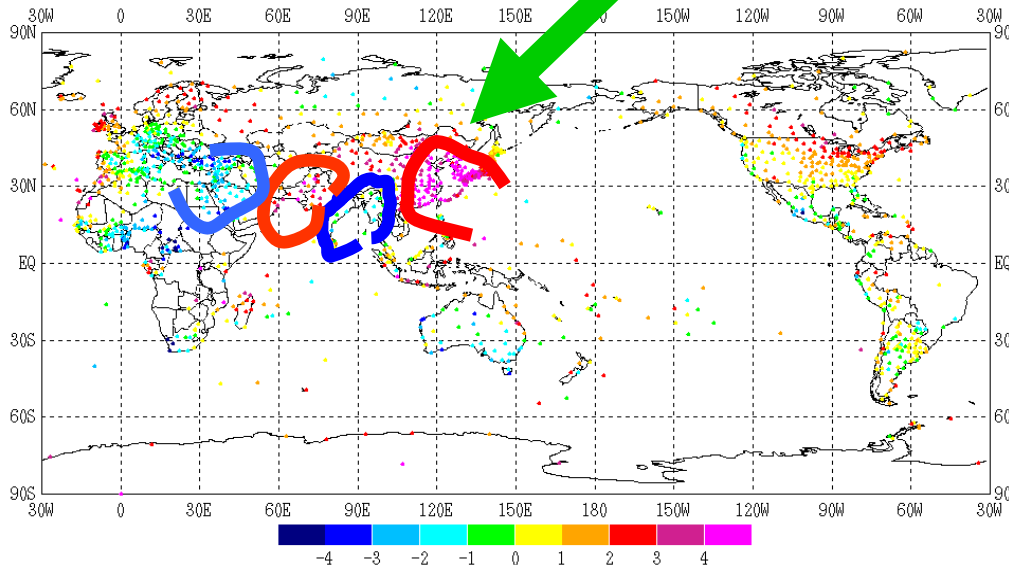


Examples of Quasi-stationary Rossby waves: 2002/1



Time sequences of temperature anomalies in Japan (5 day running mean)

2001.11-2002.2

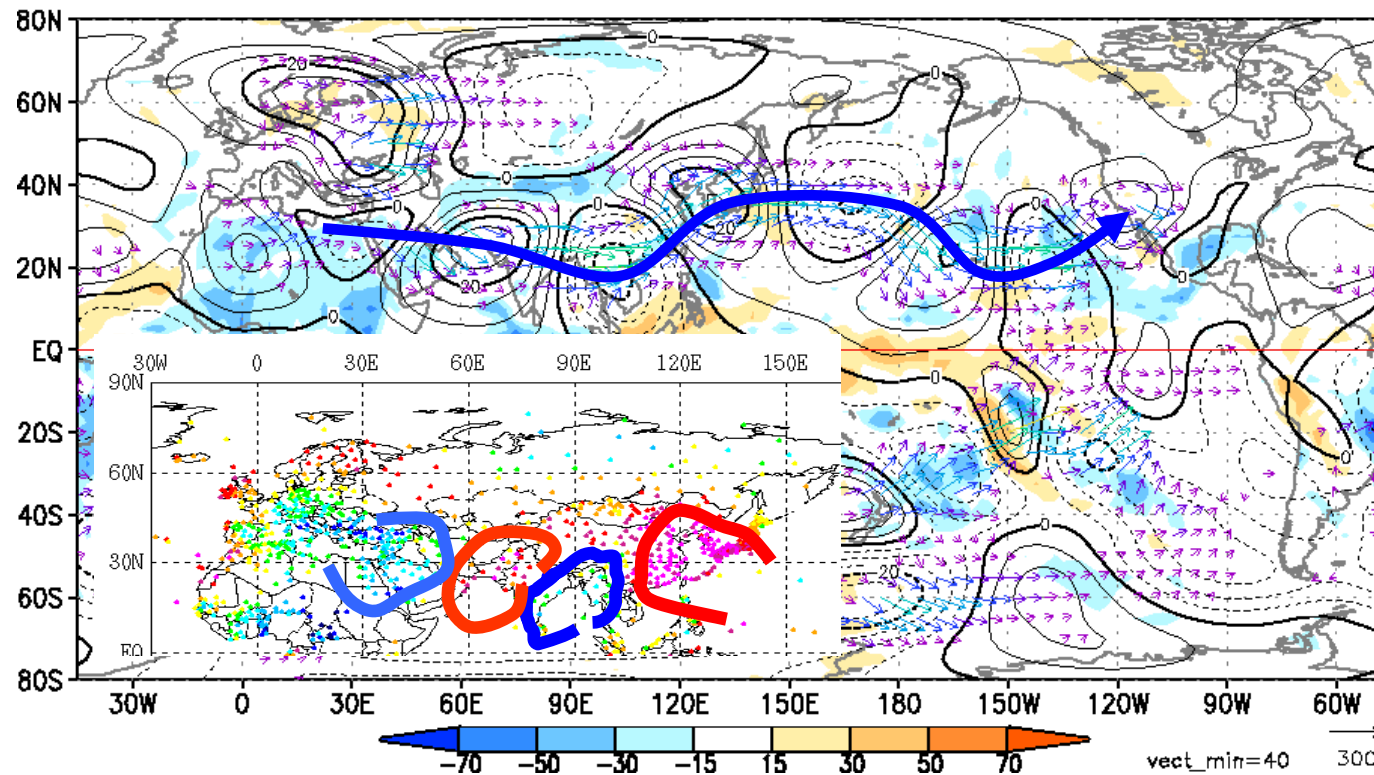


Observed normalized temperature anomalies

2002.1.11-15

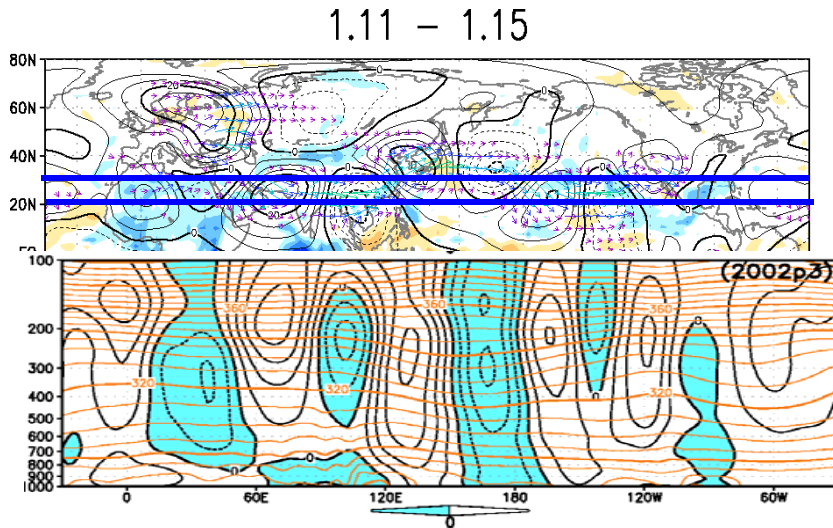
Wave train along the Asian jet

1.11 – 1.15



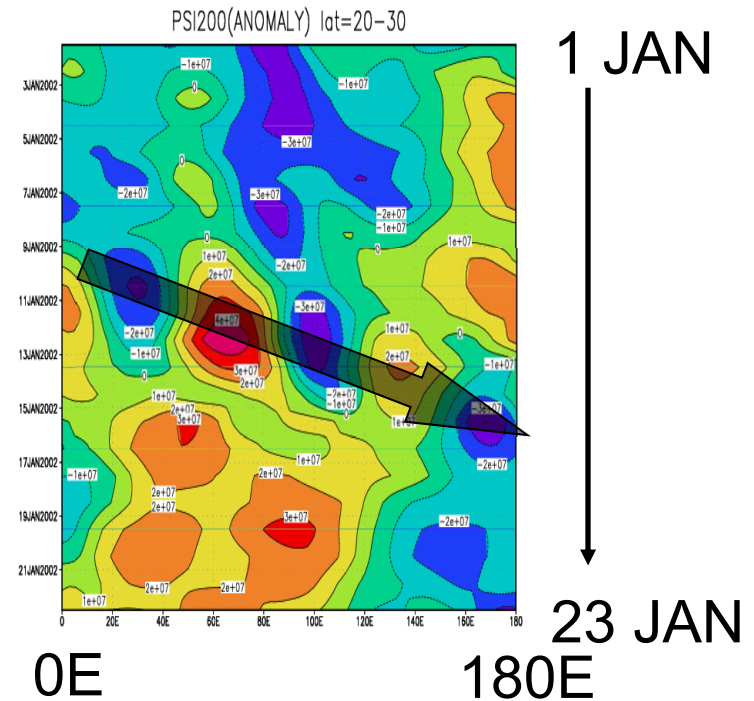
Observed 5-day mean stream function anomalies at 200hPa (contours) 2002.1.11-1.15

Structure of the wave train



Observed Longitude-height cross section of 20N-30N mean stream function anomalies

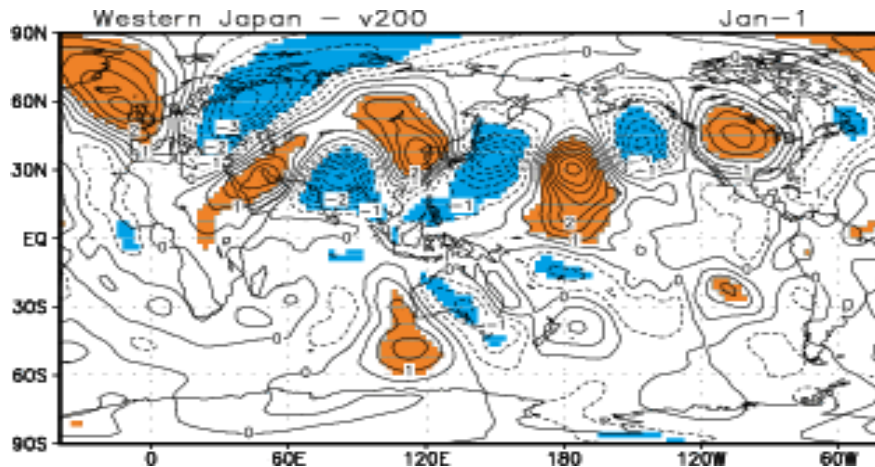
2002.1.11-1.15



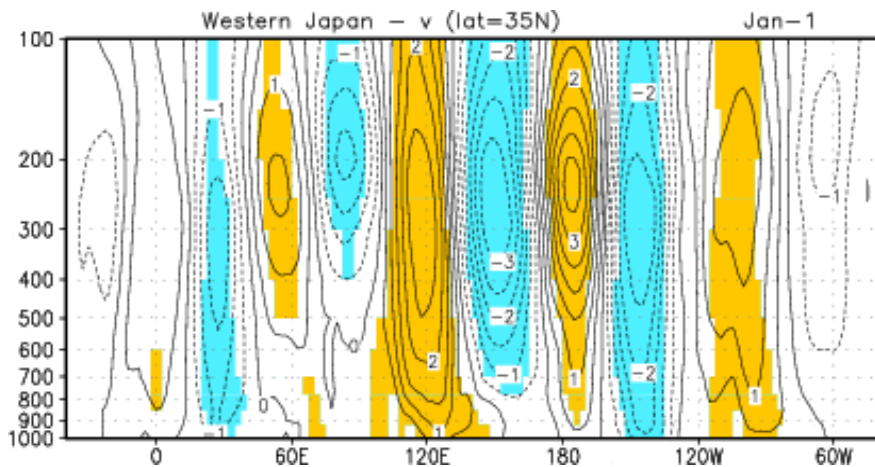
Observed Longitude-time cross section of 20N-30N mean stream function anomalies at 200hPa
2002.1.1-1.23

Equivalent barotropic stationary Rossby wave. Wave length: 70° Group velocity 30° /day

■ Statistical relationship between 10-day mean temperature in western Japan and wave trains along the Asian jet

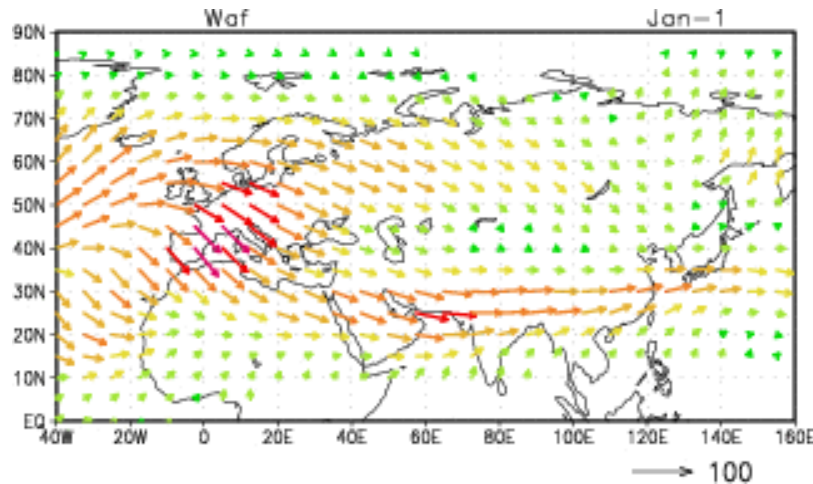


Regression of meridional wind v at 200hPa on 10-day mean temperature in western Japan . 1 Jan.-10 Jan.

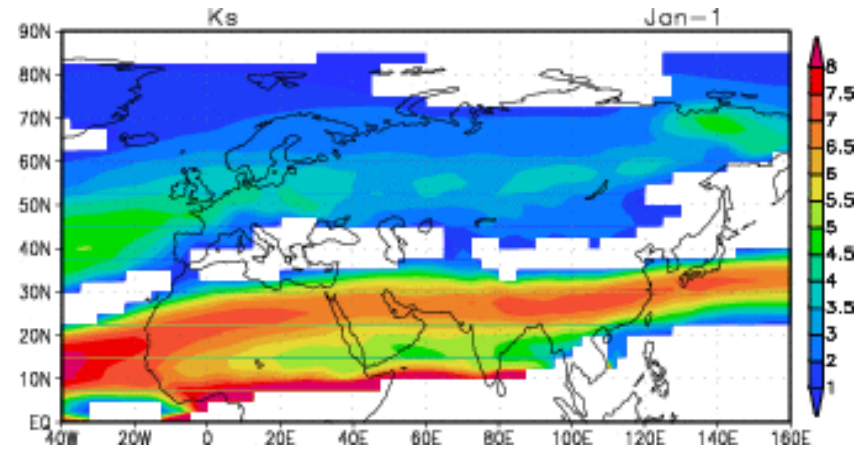


Longitude-height cross section of regression of meridional wind v at 35N

■ Climatology of stationary Rossby wave packets propagation (1-10 JAN,1971-2000)



Wave activity flux (Takaya and Nakamura,2001,JAS,608-) at 200hPa

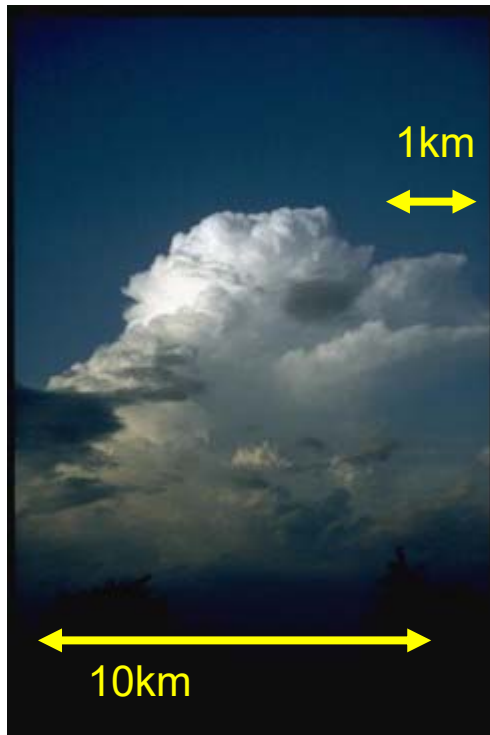


Stationary Rossby wave number Ks (Hoskins and Ambrizzi,1993,JAS,1661-) at 200hPa

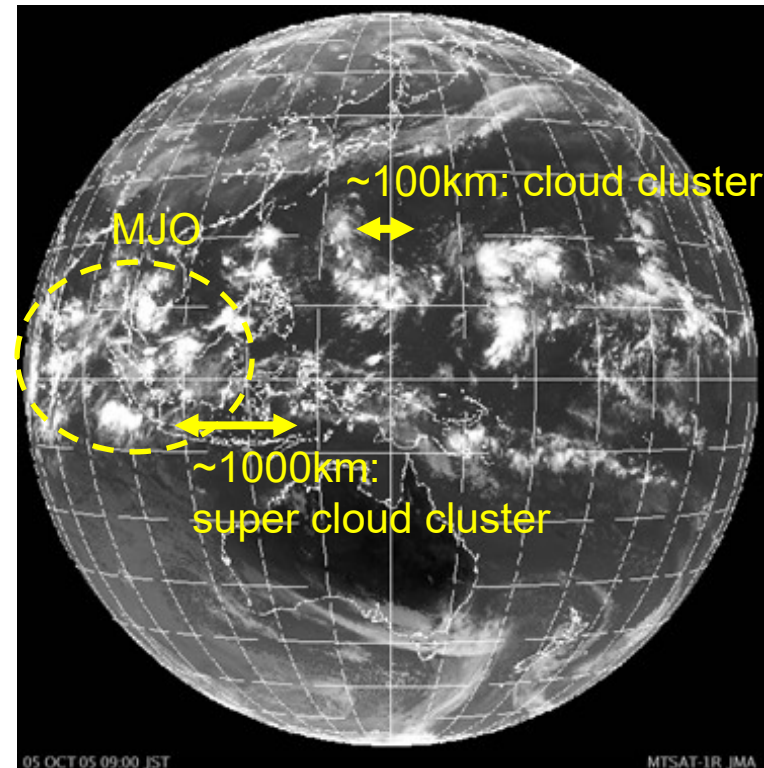
Source of Rossby wave train along the Asian jet ?

- Madden-Julian Oscillation (MJO) and equatorial waves

■ Multi-scale clouds in the tropics



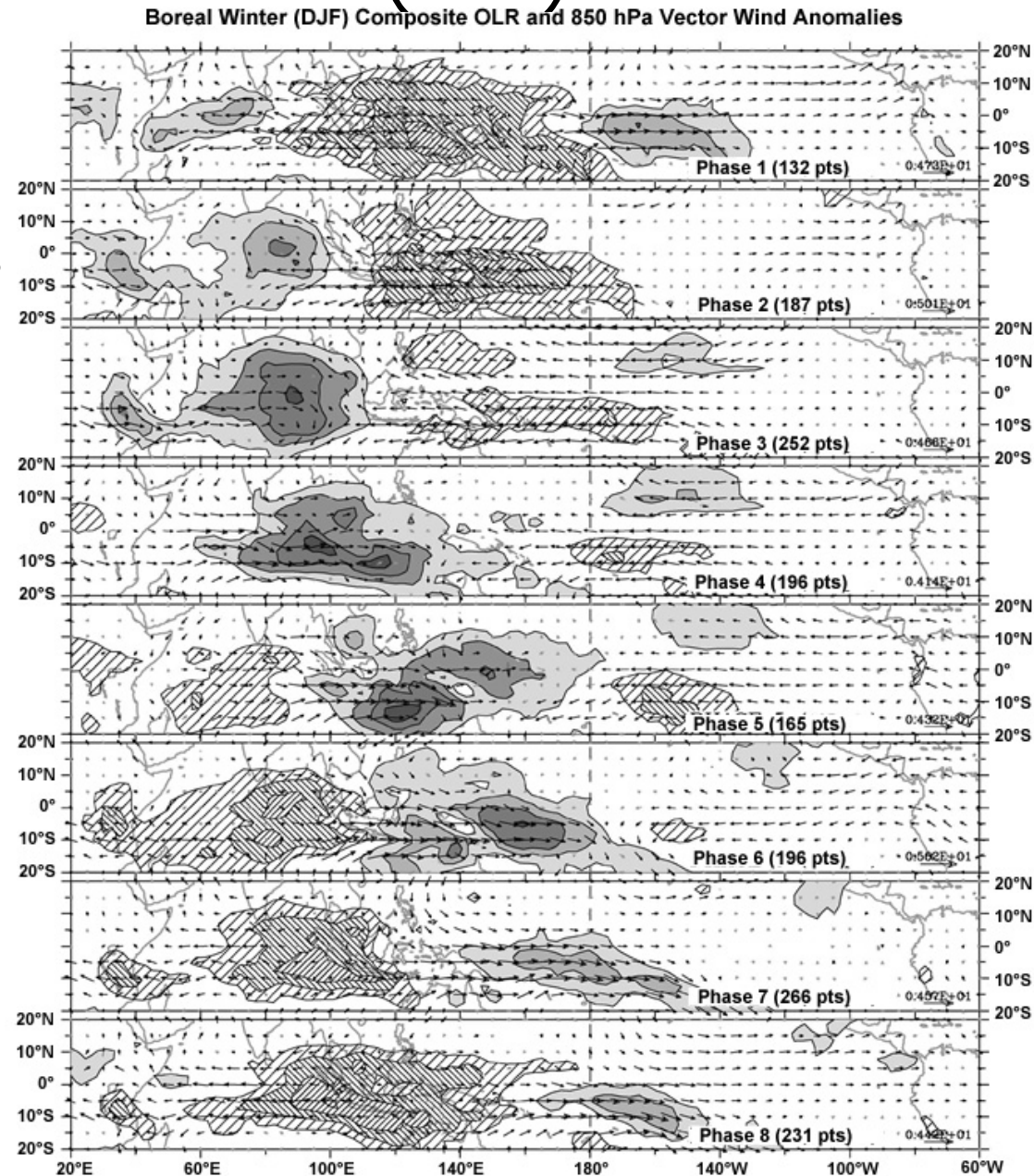
Outgoing Longwave Radiation (OLR) from
MTSAT JMA at 00 UTC Oct. 5, 2005



In the tropics, Heavy precipitation ->
Deep cloud -> Low cloud-top
temperature -> Low OLR

Madden-Julian Oscillation (MJO)

A broad area of active cloud and rainfall propagates eastwards around the equator at intervals of between about 30 to 60 days.

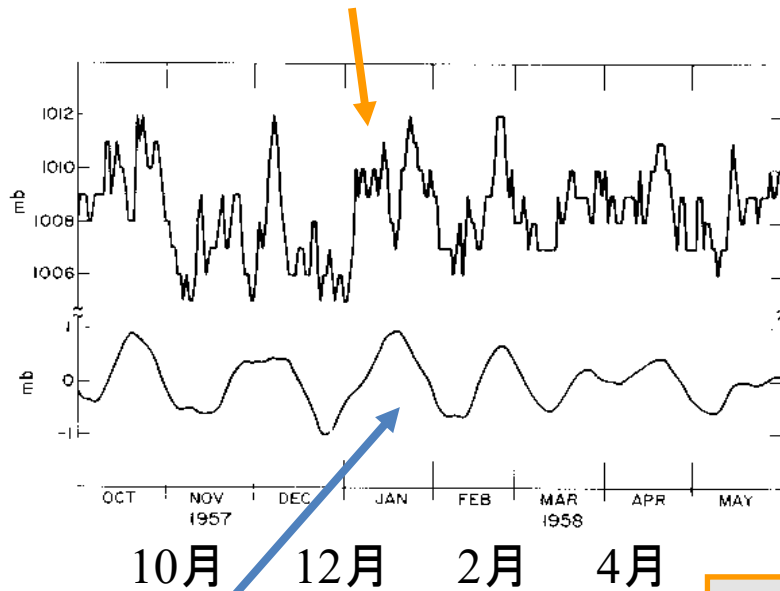


30-60 day Period

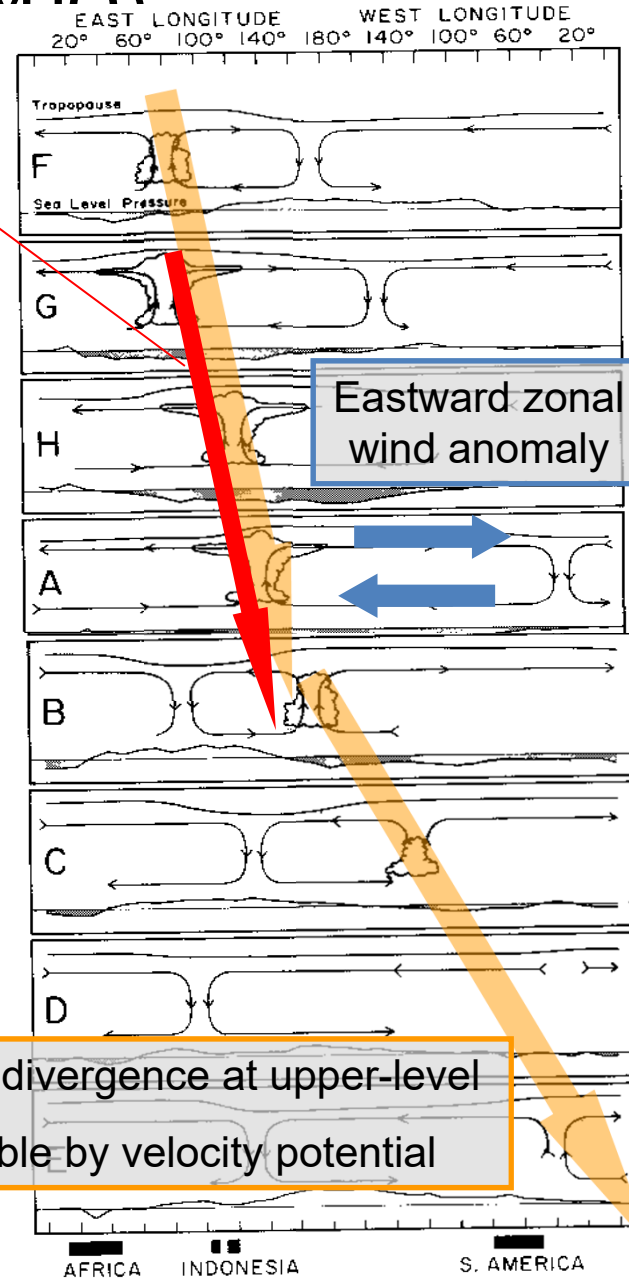
Madden-Julian Oscillation (MJO)

Eastward super cloud cluster detectable by OLR

Surface pressure at Canton Iceland (3S, 172W)



After applying band-pass filter around 45 days



Eastward zonal wind anomaly

Eastward divergence at upper-level detectable by velocity potential

30-60 day Period

AFRICA INDONESIA S. AMERICA
Madden and Julian (1972)

■ Schematic structure of MJO

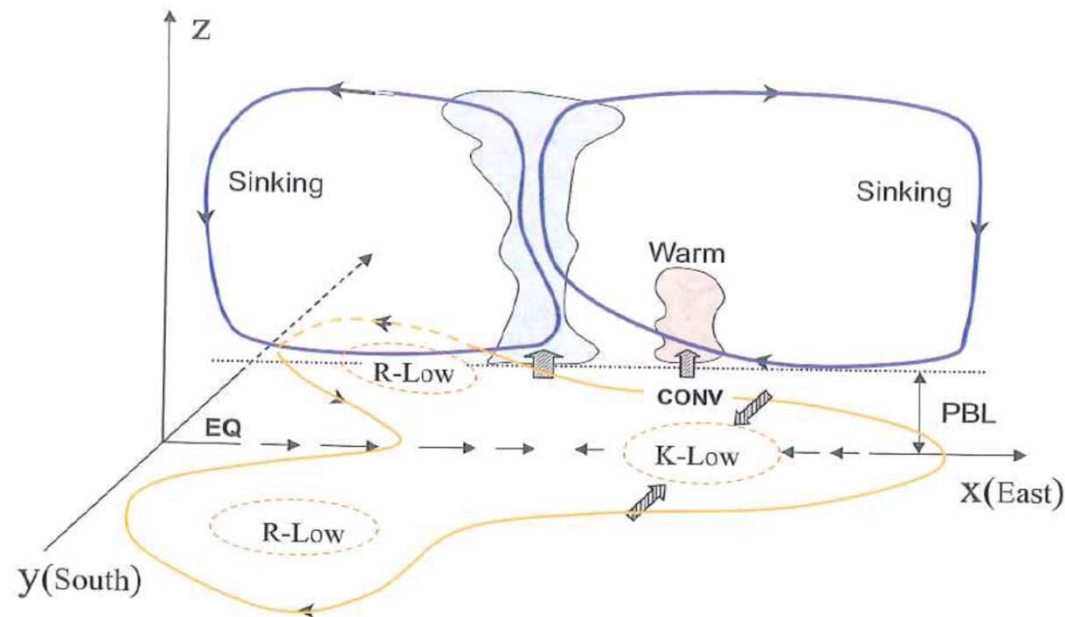
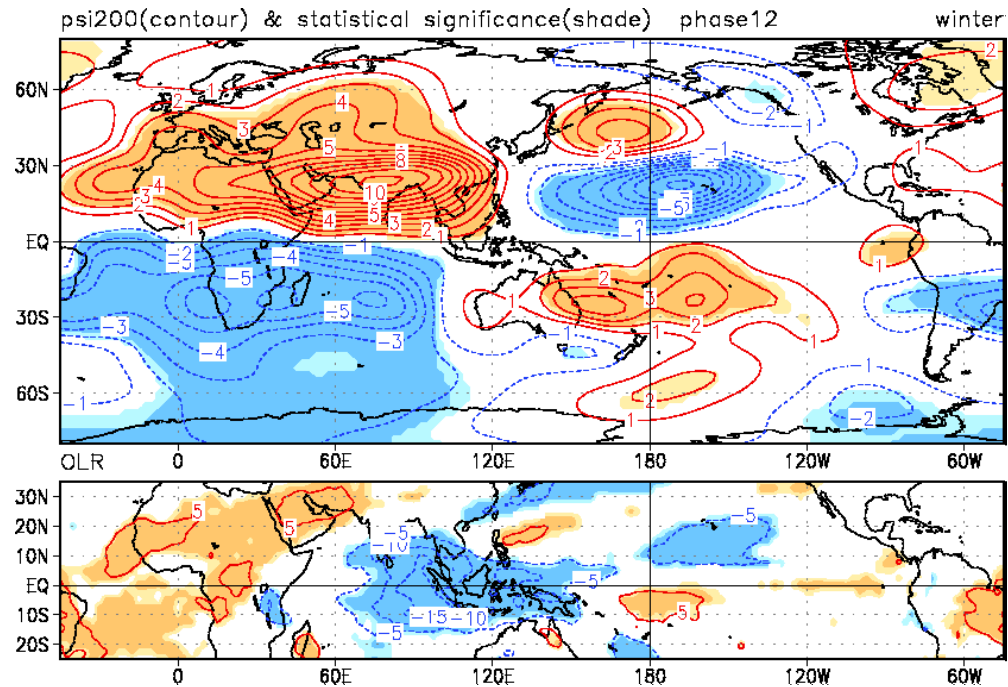


Figure 10.13. Schematic structure of the frictional CID mode, which is the counterpart of observed MJO mode. In the horizontal plane the “K-low” and “R-low” represents the low-pressure anomalies associated with the moist equatorial Kelvin and Rossby waves, respectively. Arrows indicate the wind directions. In the equatorial vertical plane the free-tropospheric wave circulation is highlighted. The wave-induced convergence is in phase with the major convection, whereas the frictional moisture convergence in the “K-low” region is ahead of the major convection due primarily to meridional wind convergence.

From Wang (2005)

Composition maps of stream function at 200hPa and OLR at each phase (1-12) of MJO in winter (DJF)



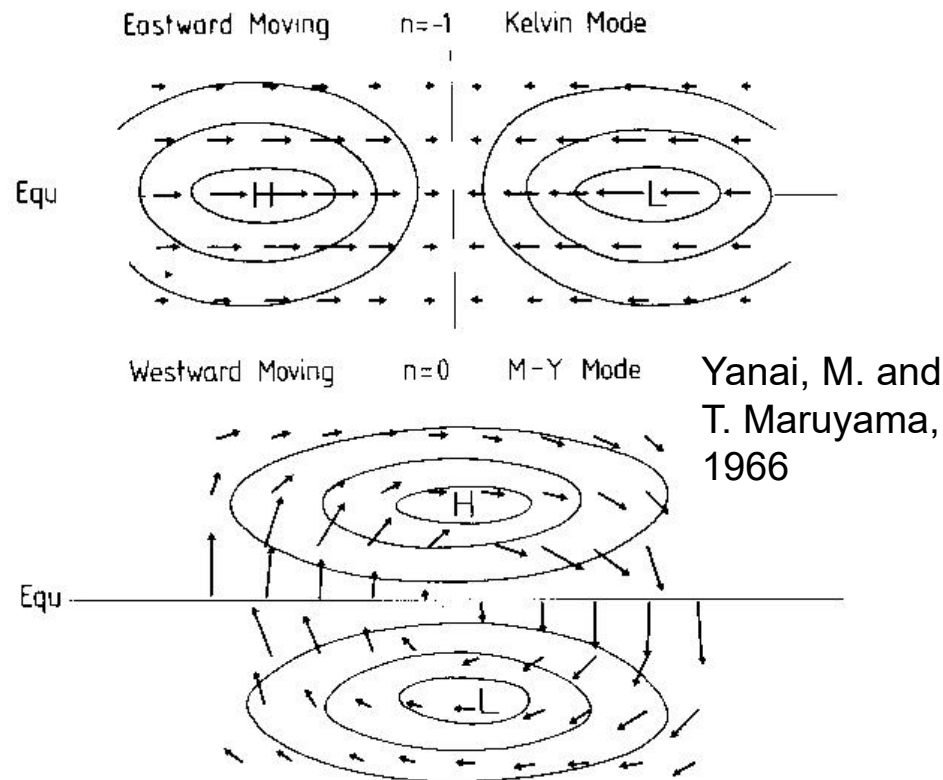
Stream
function at
200hPa

OLR

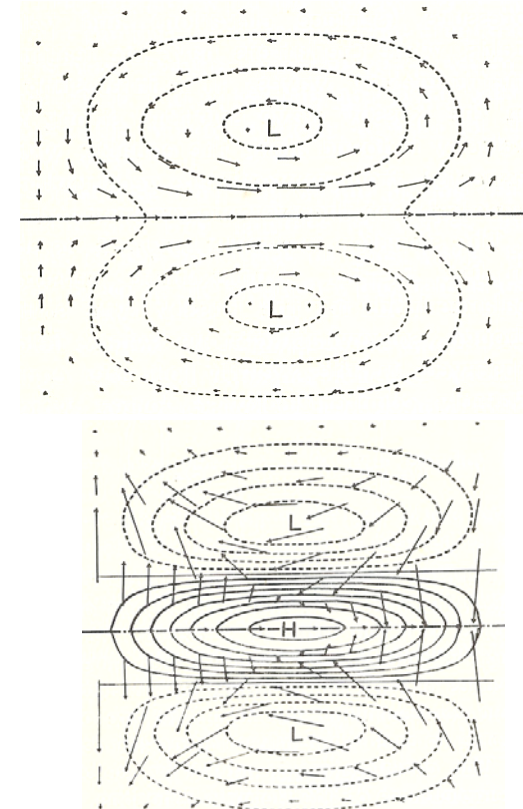
Endoh and Harada (2005)

Equatorial Waves

Kelvin wave



ER: Rossby wave ($n=1$)

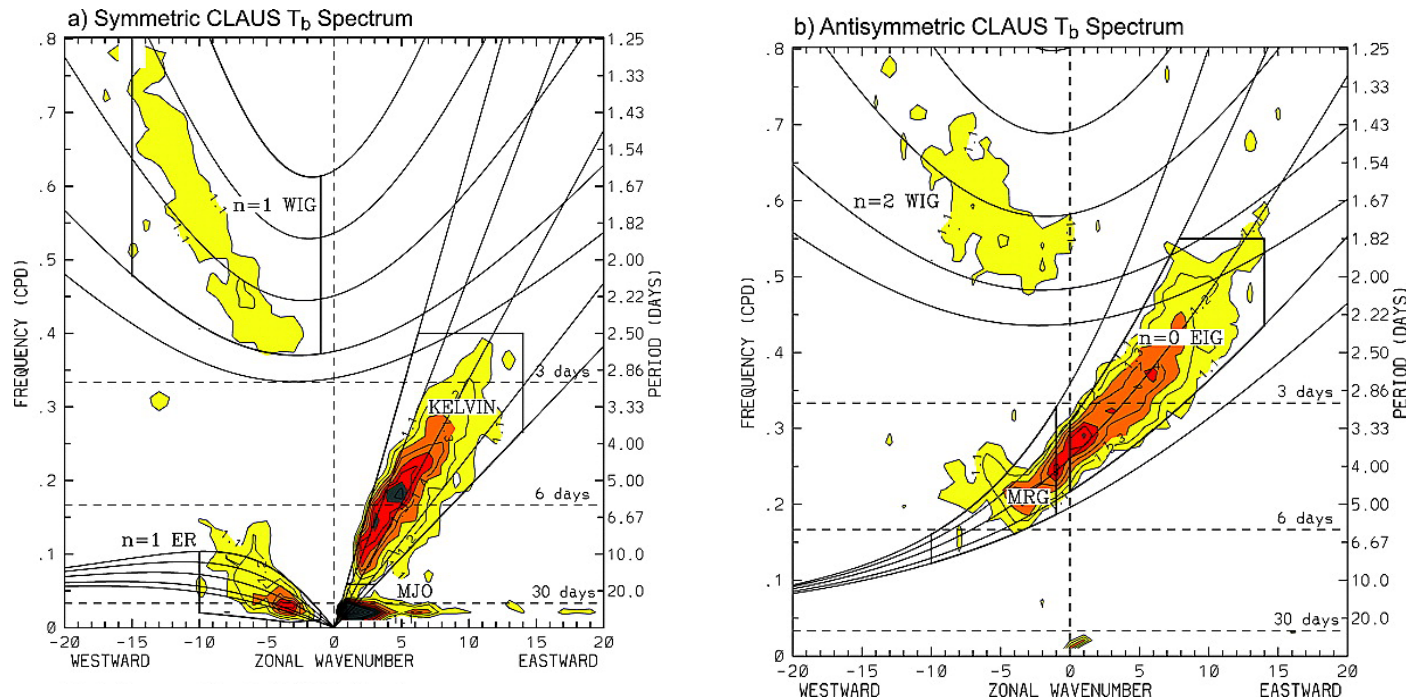


MRG : mixed Rossby-Gravity wave

EIG: eastward propagating inertio-gravity wave ($n=1$)

Convectively coupled equatorial waves

Wave number–frequency power spectrum of the (a) symmetric and (b) antisymmetric component of Cloud Archive User Services (CLAUS) T_b



Wave number–frequency power spectrum of the (a) symmetric and (b) antisymmetric component of Cloud Archive User Services (CLAUS) T_b for July 1983 to June 2005, summed from 15° N to 15° S, plotted as the ratio between raw T_b power and the power in a smoothed red noise background spectrum (see [WK99](#) for details). Contour interval is 0.1, and contours and shading begin at 1.1, where the signal is significant at greater than the 95% level. Dispersion curves for the Kelvin, $n = 1$ equatorial Rossby (ER), $n = 1$ and $n = 2$ westward inertio-gravity (WIG), $n = 0$ eastward inertio-gravity (EIG), and mixed Rossby-gravity (MRG) waves are plotted for equivalent depths of 8, 12, 25, 50, and 90 m. Heavy solid boxes represents regions of wave number–frequency filtering

Kiladis et. al.(2009)

Reviews of Geophysics

Volume 47, Issue 2, RG2003, 10 APR 2009 DOI: 10.1029/2008RG000266

<http://onlinelibrary.wiley.com/doi/10.1029/2008RG000266/full#rog1687-fig-0001>

Decomposition of the equatorial OLR anomalies

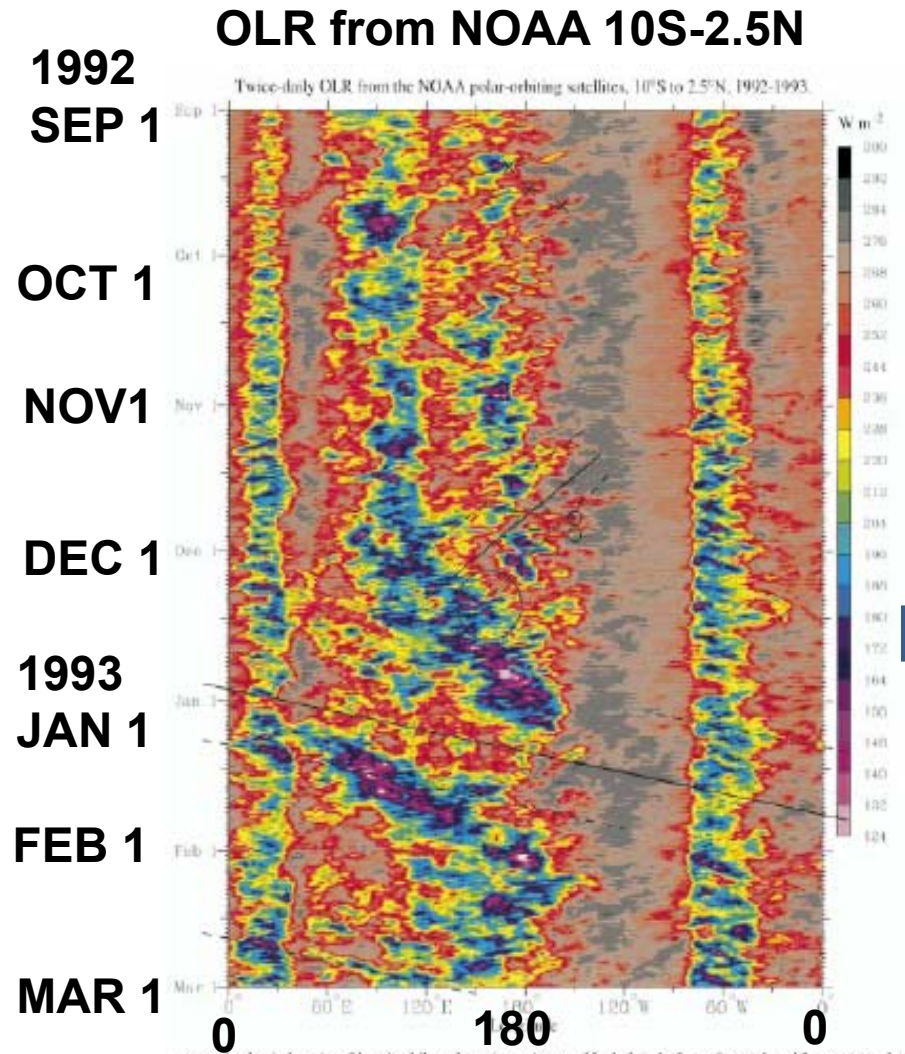
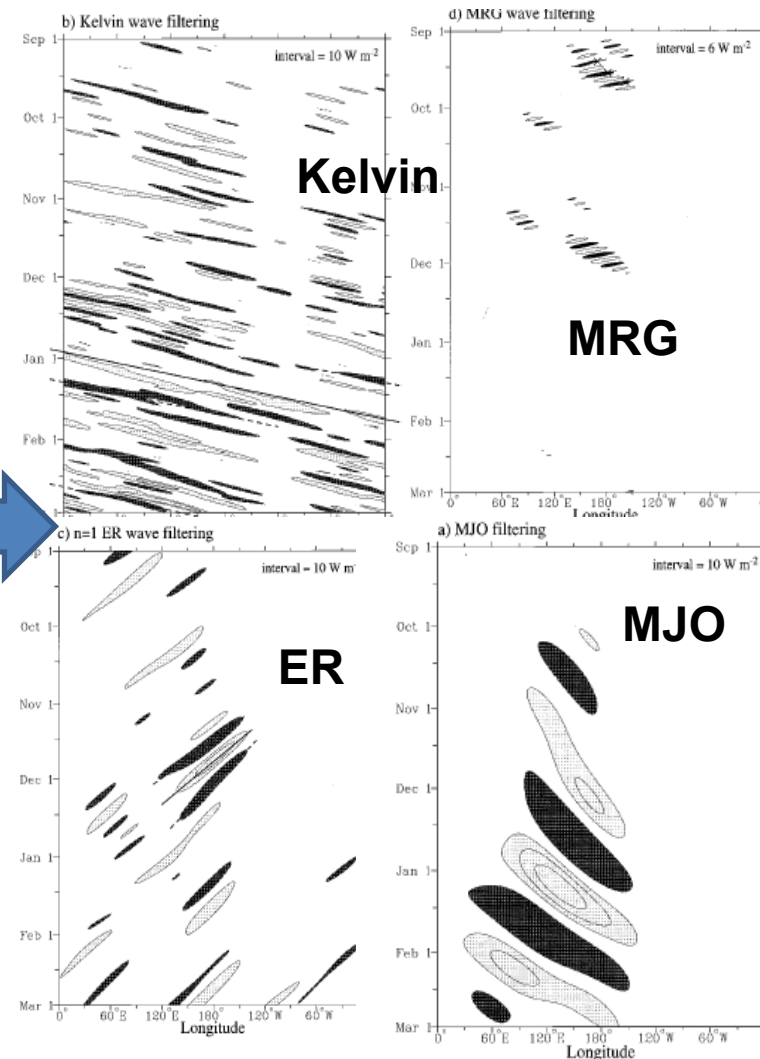


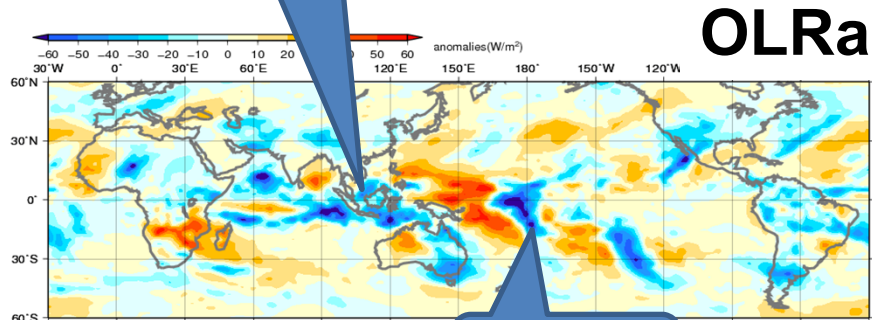
FIG. 8. Time-longitude section of the twice-daily total OLR ($W m^{-2}$) averaged for the latitudes from $10^{\circ}S$ to $2.5^{\circ}N$ and for 6 Z 1 September 1992 through 6 Z 1 March 1993. Values correspond to the color bar. Each time section consists of half nighttime and half daytime data from the polar-orbiting satellite (see text for details). Dark lines, circles, and crosses refer to respectively complexed equatorial wave disturbances, and wotch those of Fig. 9.

FIG. 9. (a) Time-longitude section of the OLR anomalies for the MJO-filtered band for the same 6-month sample period as Fig. 8, averaged for the latitudes from $10^{\circ}S$ to $2.5^{\circ}N$. The zero contour has been omitted. Light shading for positive anomalies and dark shading and dashed contours for negative anomalies. (b) Same as in panel a except for the Kelvin wave-filtered band. (c) The $n = 1$ ER wave-filtered band. (d) The MRG wave-filtered band.

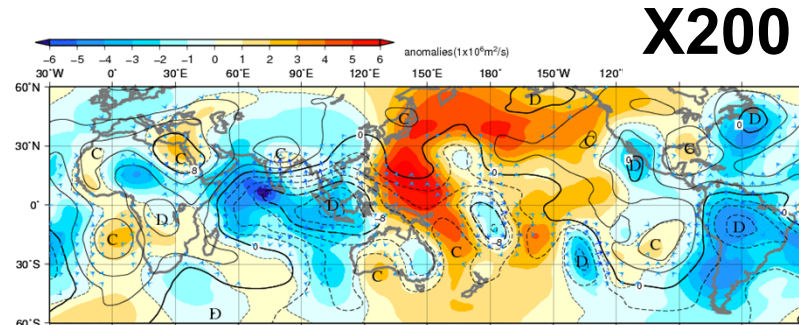


Dec 2 – Dec 6 in 1992

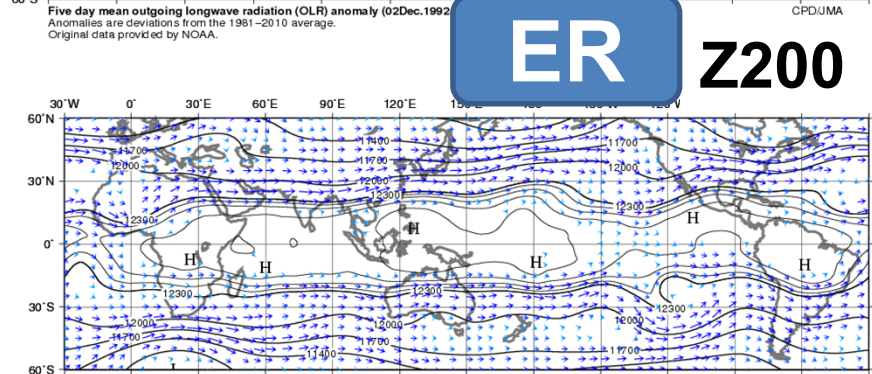
MJO



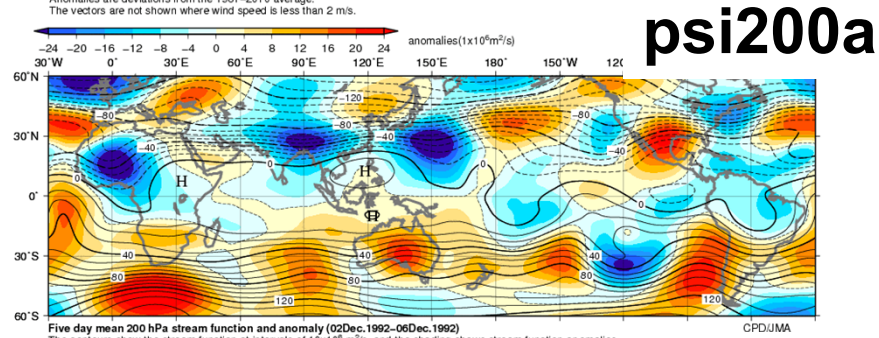
Five day mean outgoing longwave radiation (OLR) anomaly (02Dec.1992-06Dec.1992). Anomalies are deviations from the 1981-2010 average. Original data provided by NOAA.



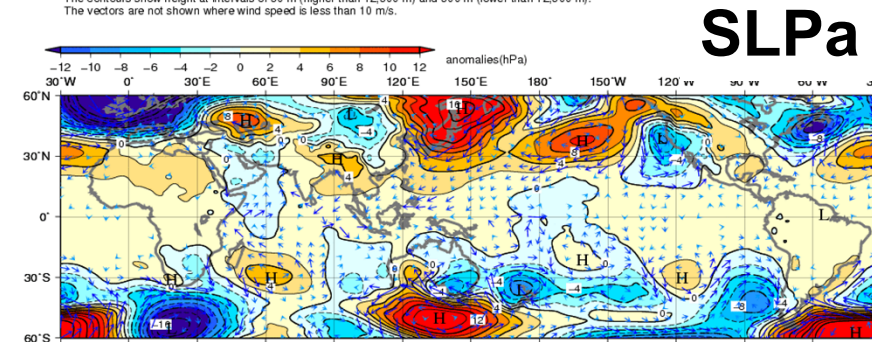
Five day mean 200 hPa velocity potential, divergent wind vector and velocity potential anomaly (02Dec.1992-06Dec.1992). The contours show the velocity potential at intervals of 2×10^6 m²/s, and the shading shows velocity potential anomalies. Anomalies are deviations from the 1981-2010 average. The vectors are not shown where wind speed is less than 2 m/s.



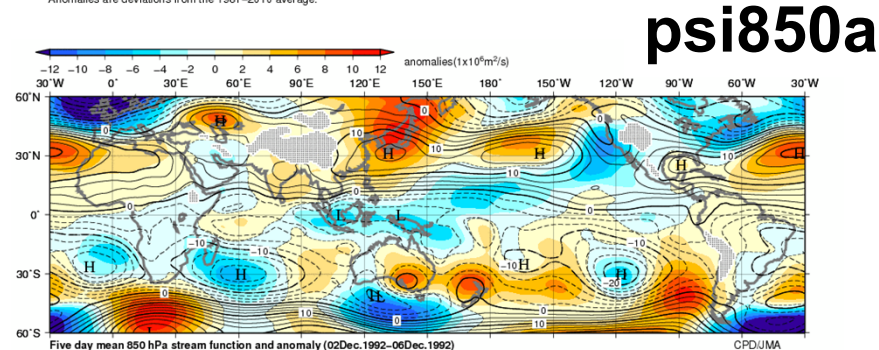
Five day mean 200 hPa height and wind speed vector (02Dec.1992-06Dec.1992). The contours show height at intervals of 30 m (higher than 12,300 m) and 300 m (lower than 12,300 m). The vectors are not shown where wind speed is less than 10 m/s.



Five day mean 200 hPa stream function and anomaly (02Dec.1992-06Dec.1992). The contours show the stream function at intervals of 10×10^6 m²/s, and the shading shows stream function anomalies. Anomalies are deviations from the 1981-2010 average.

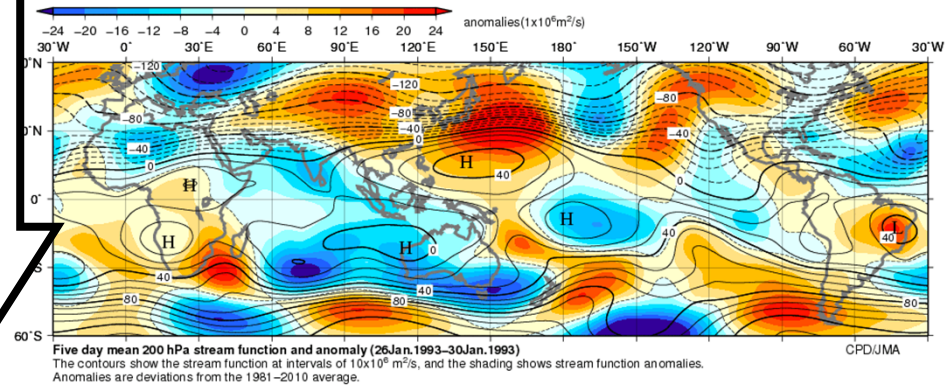
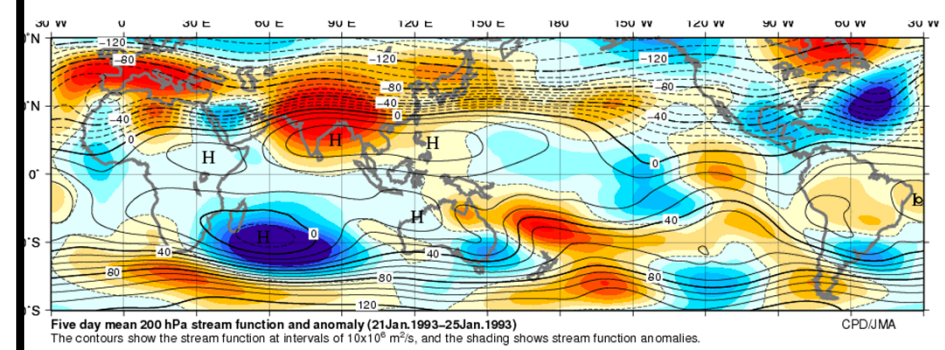
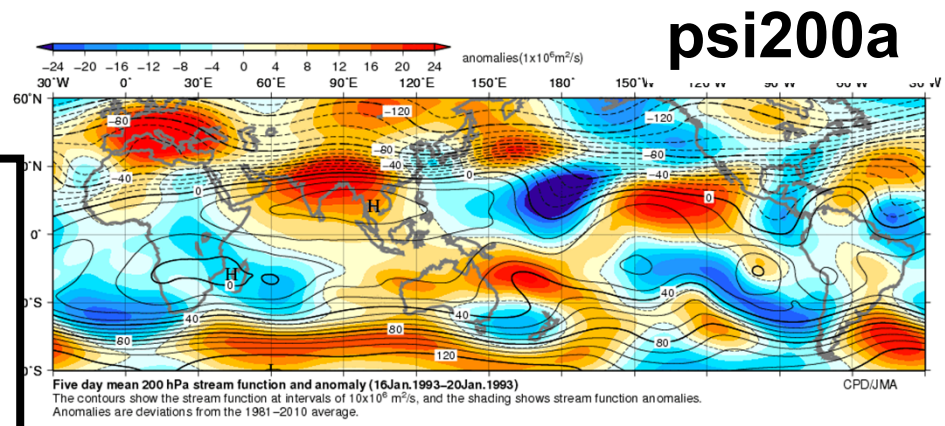
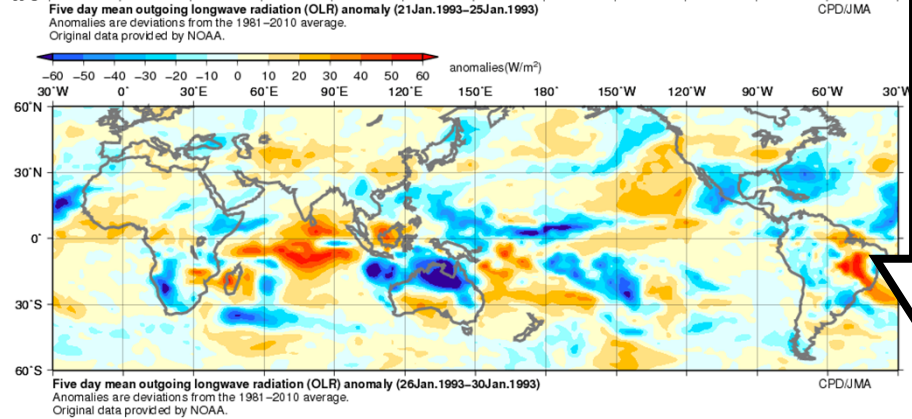
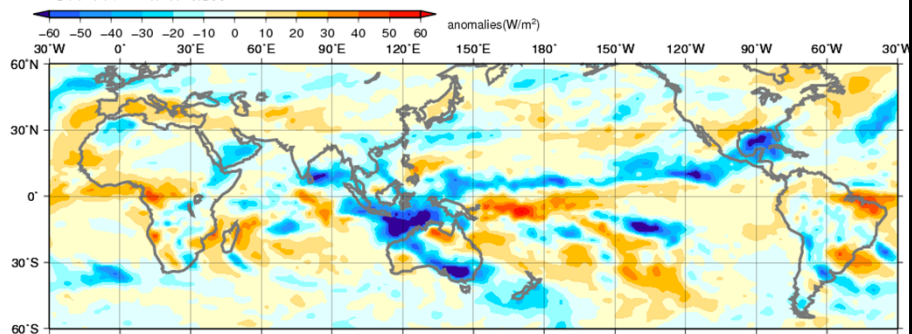
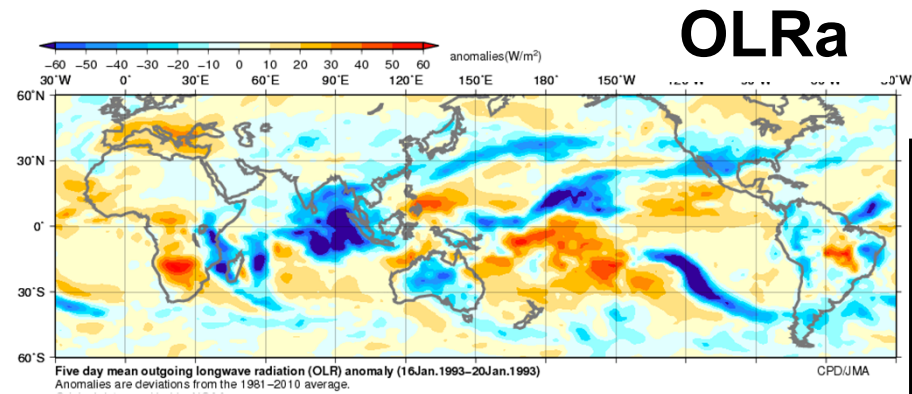


Five day mean sea level pressure anomaly and surface wind vector anomaly (02Dec.1992-06Dec.1992). The contours show sea level pressure anomalies at intervals of 2 hPa. Anomalies are deviations from the 1981-2010 average. The vectors are not shown where wind speed is less than 1 m/s.

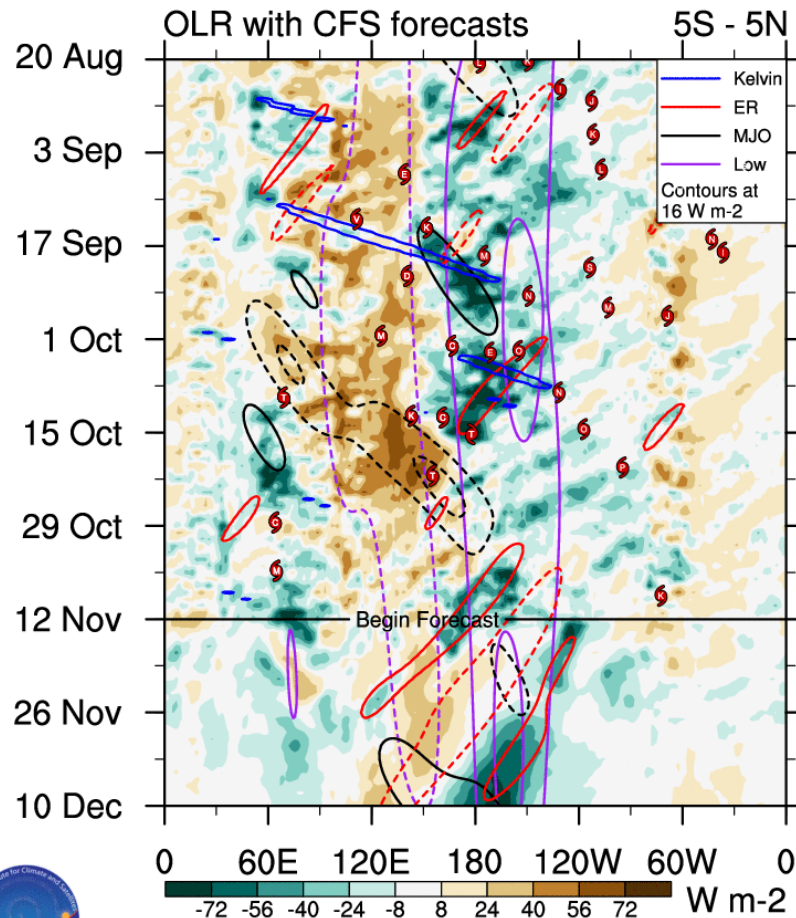


Five day mean 850 hPa stream function and anomaly (02Dec.1992-06Dec.1992). The contours show the stream function at intervals of 2.5×10^6 m²/s, and the shading shows stream function anomalies. Anomalies are deviations from the 1981-2010 average.

MJO during Jan 16-30 in 1993



Decomposition of the equatorial OLR anomalies

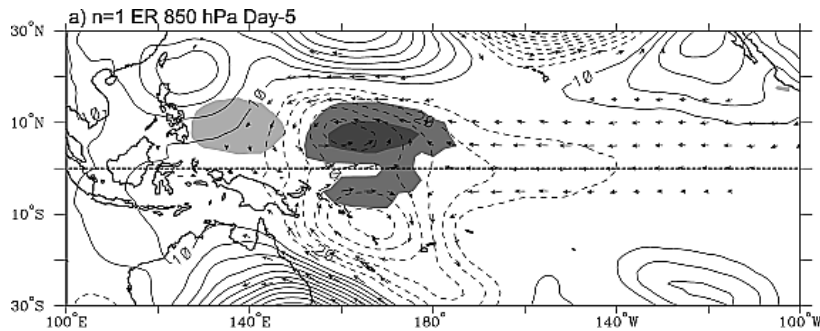


monitor.cicsnc.org/mjo

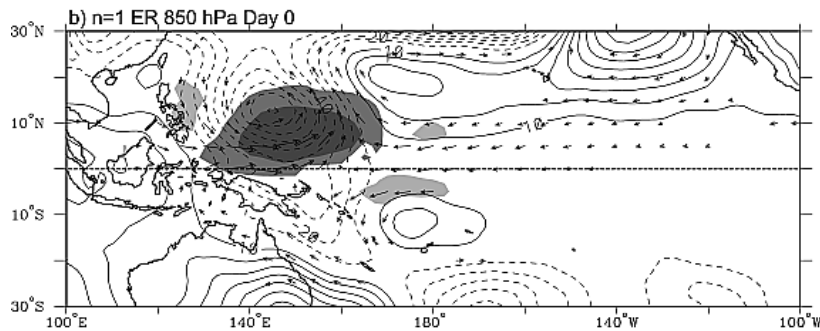
Carl Schreck (cjschrec@ncsu.edu)

<https://monitor.cicsnc.org/mjo/v2/images/spectra.png>

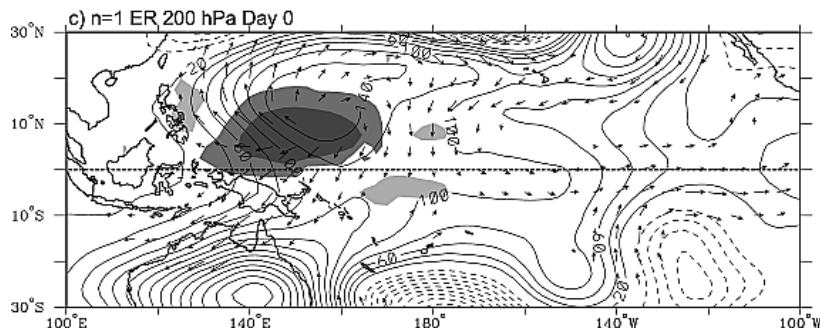
Equatorial Rossby wave



850hPa day= -5



850hPa day= 0



200hPa day= 0

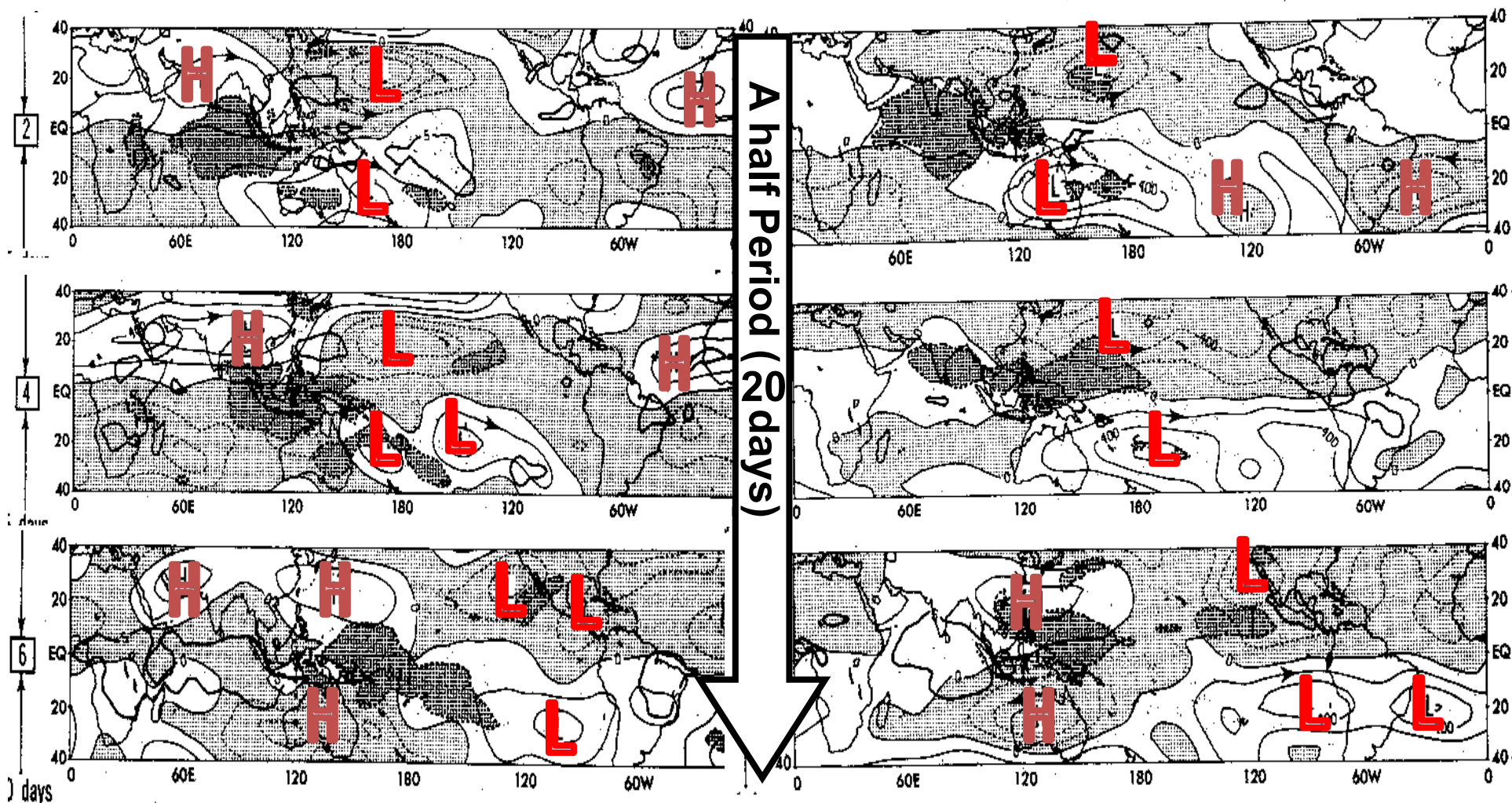
Maps of **anomalous T_b (shading), geopotential height (contours), and wind (vectors)** associated with a -20 K perturbation in $n = 1$ ER wave T_b at the base point 7.5° N, 152.0° E, for (a) day -5 at 850 hPa, (b) day 0 at 850 hPa, and (c) day 0 at 200 hPa. The contour interval is 10 m in Figures 17a and 17b and 20 m in Figure 17c, with negative contours dashed. Dark (light) shading is for negative (positive) T_b perturbations of ± 10 K and 3 K. T_b and wind vectors are locally significant at the 95% level, with the largest vectors around 2 m s^{-1} .

Kiladis et. al.(2009)

Statistics for 250 hPa stream-function and OLR composites at phases of MJO

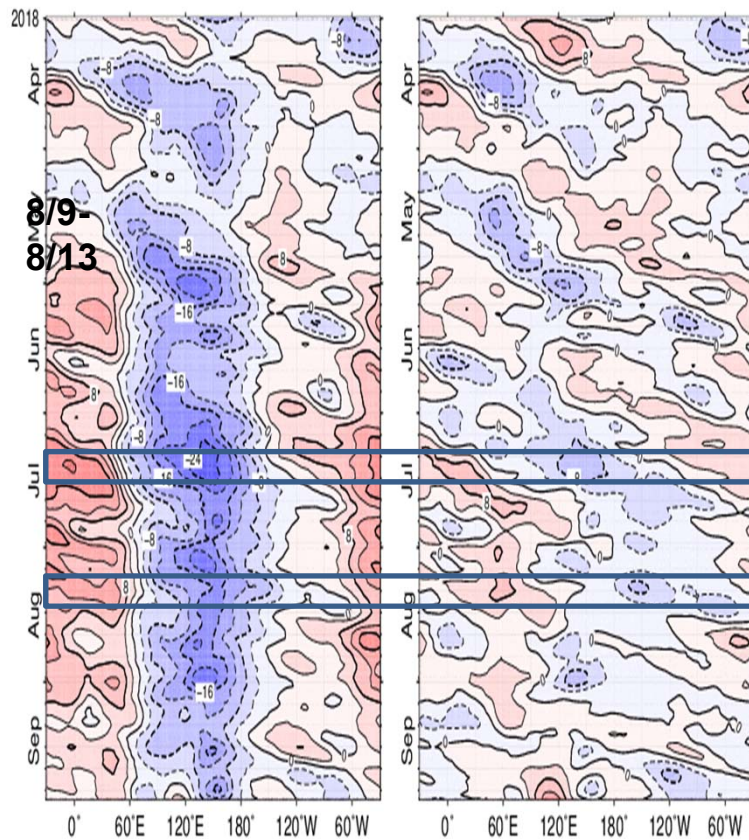
Northern winter

Northern summer



■ According to the statistics in the previous slide, MJO-related OLR anomaly migrates northward in NH summer

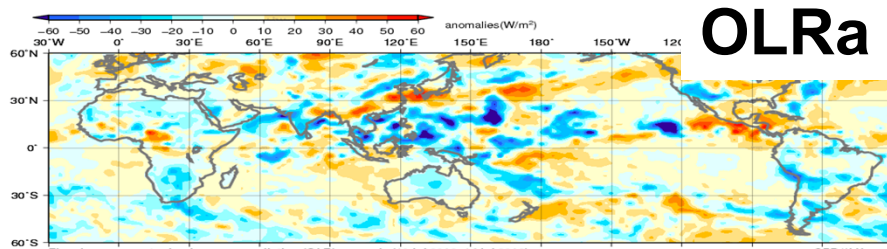
How about NH summer in 2018
X200 & X200anomaly



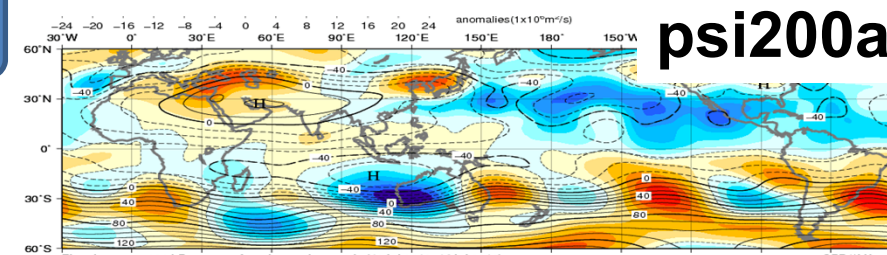
Time-longitude cross section of five day running mean (left) 200 hPa velocity potential and (right) anomaly around the equator averaged between 5°S and 5°N. The contour interval is 4×10^6 m²/s. Anomalies are deviations from the 1981–2010 average.

7/10-7/14

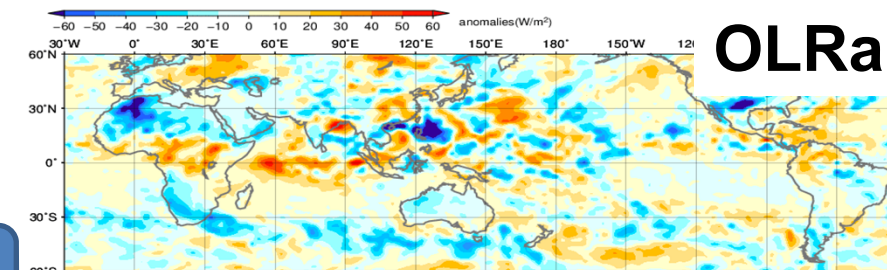
8/9-8/13



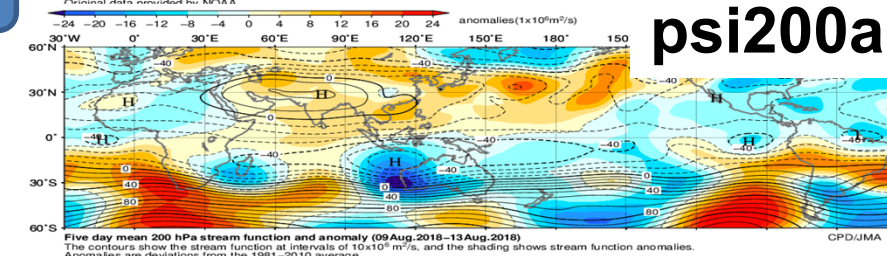
Five day mean outgoing longwave radiation (OLR) anomaly (10 Jul. 2018–14 Jul. 2018). Anomalies are deviations from the 1981–2010 average. Original data provided by NOAA. CPD/JMA



Five day mean 200 hPa stream function and anomaly (10 Jul. 2018–14 Jul. 2018). The contours show the stream function at intervals of 1×10^6 m²/s, and the shading shows stream function anomalies. Anomalies are deviations from the 1981–2010 average. CPD/JMA



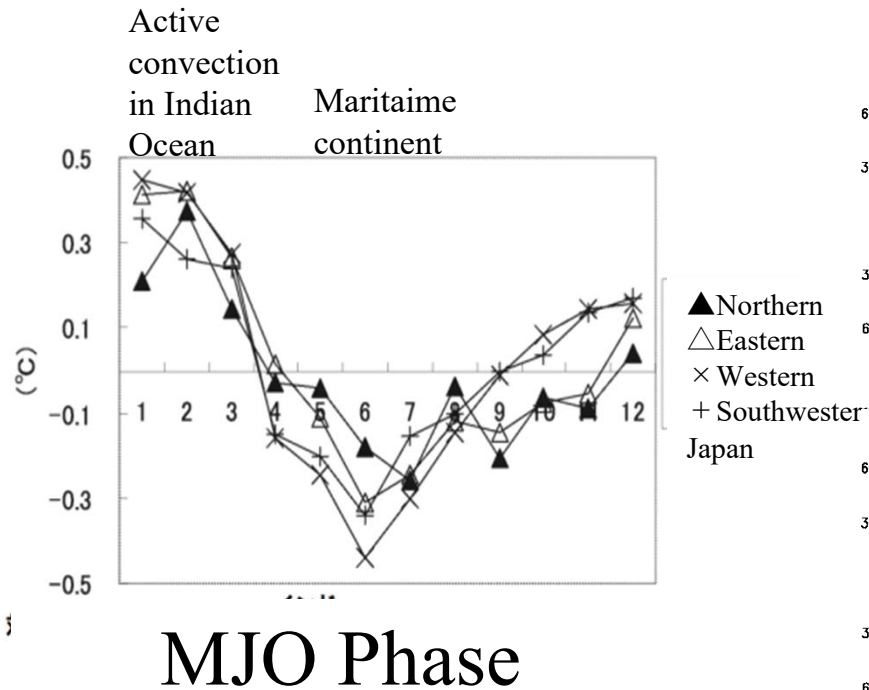
Five day mean outgoing longwave radiation (OLR) anomaly (09 Aug. 2018–13 Aug. 2018). Anomalies are deviations from the 1981–2010 average. Original data provided by NOAA. CPD/JMA



Five day mean 200 hPa stream function and anomaly (09 Aug. 2018–13 Aug. 2018). The contours show the stream function at intervals of 1×10^6 m²/s, and the shading shows stream function anomalies. Anomalies are deviations from the 1981–2010 average. CPD/JMA

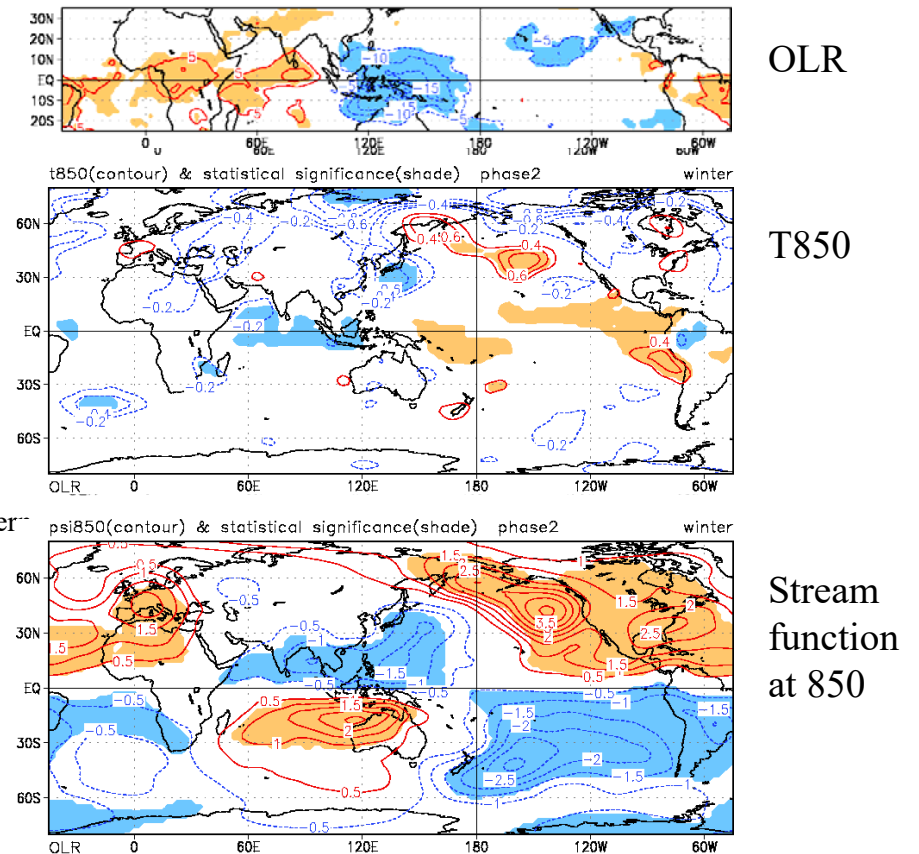
Impact of MJO (Example for Japan)

DJF Temperature Anomaly over Japan



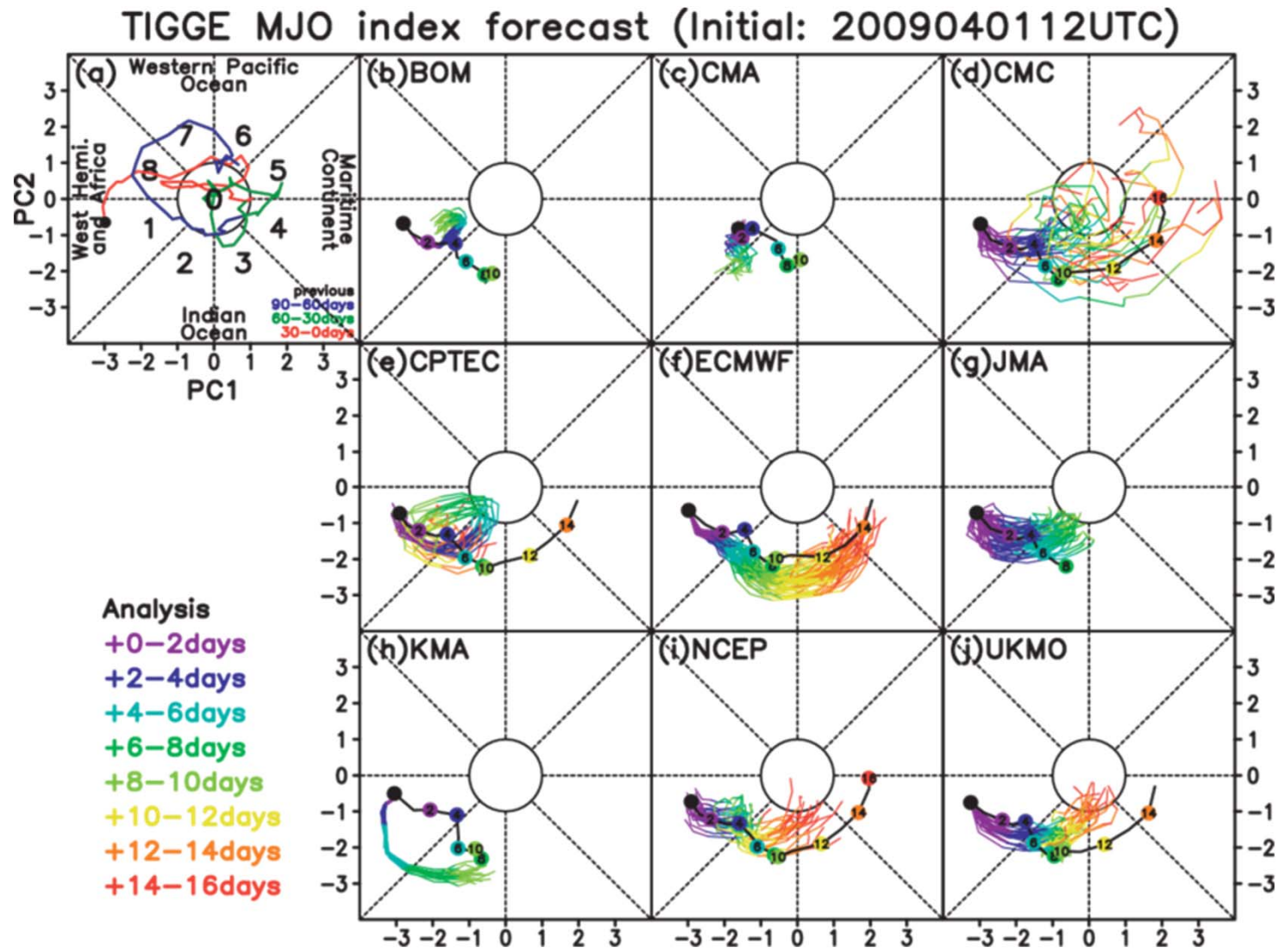
Endo and Harada (2008)

Composition maps of MJO in DJF

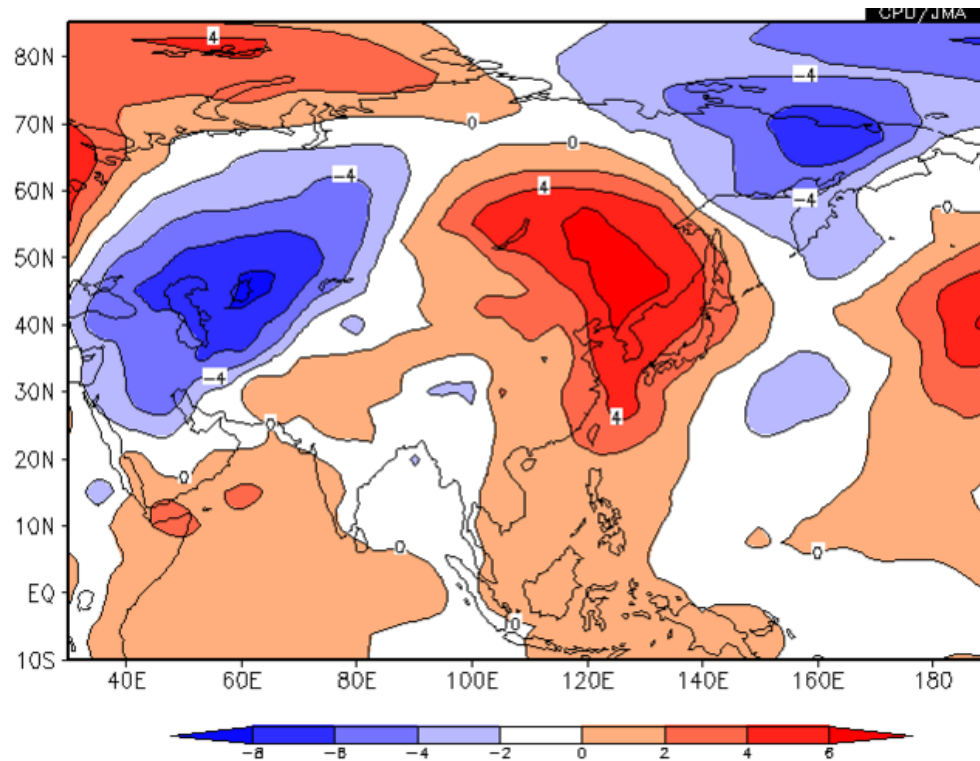


Endoh and Harada (2005)

- MJO predictability is not so much.



- Example: extreme event caused by Rossby waves and MJO
- Extreme warm event in early Nov. 2011

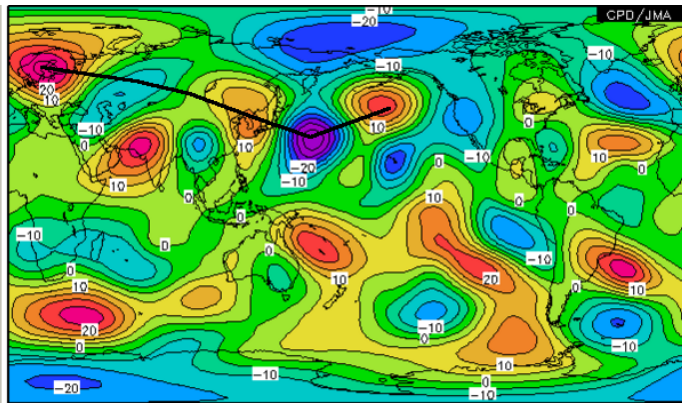


Western Japan experienced the warmest first ten days of Nov. since 1961.

10 day mean temperature anomalies at 850hPa in 1-10th Nov. 2011

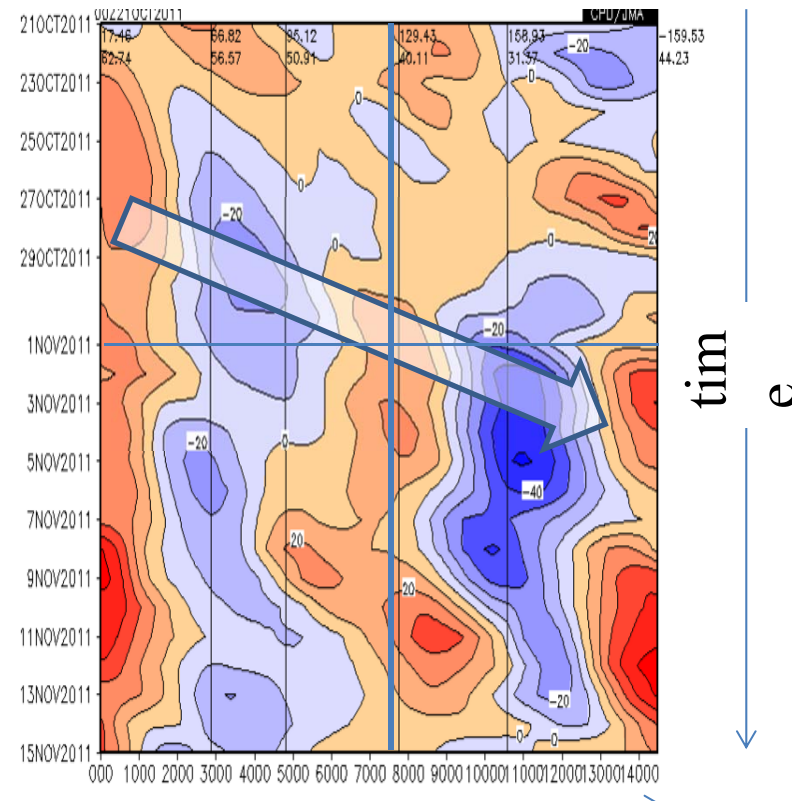
■ Propagation of Stationary Rossby wave packet along the Polar front jet

10 day mean Stream function anomalies at 200hPa, 2011.11.1-10



Wave length \doteq 8000km
Group velocity \doteq 25m/s

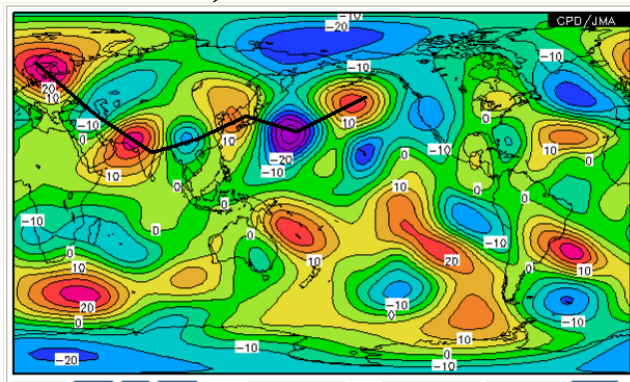
Stream function anomalies at 200hPa along the black line in the right figure, 2011/10/25-11/15



Distance from blocking high in Northern Europe (km)

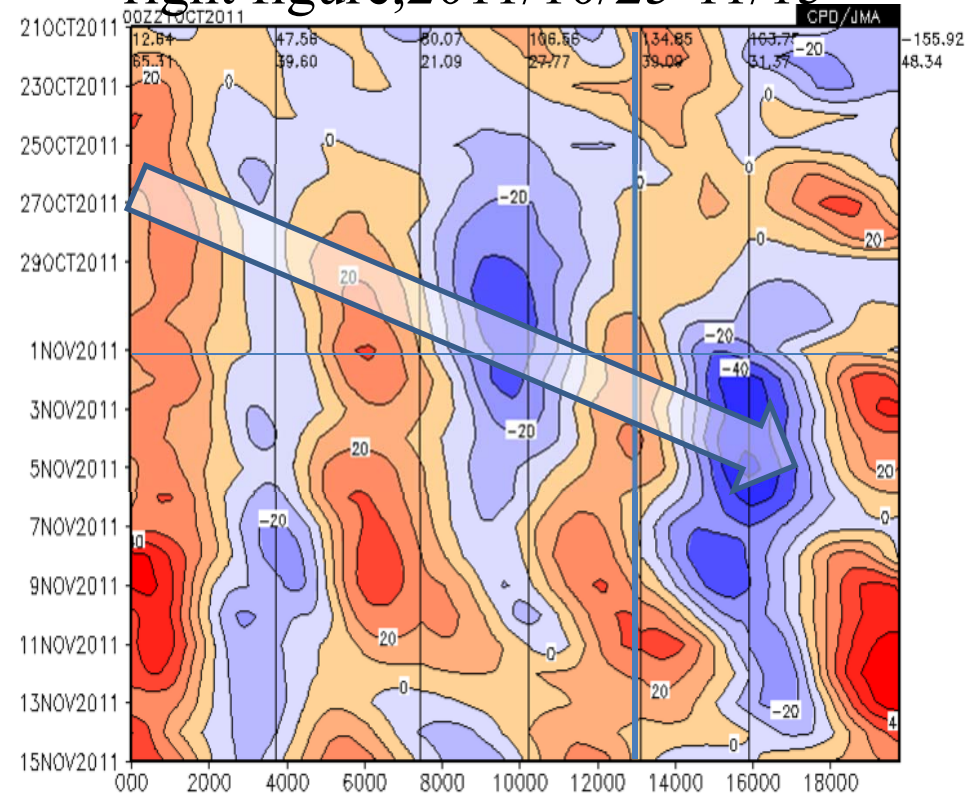
■ Propagation of Stationary Rossby wave packet along the Sub tropical jet

10 day mean Stream function anomalies at 200hPa, 2011.11.1-10



Wave length \doteq 6000km
 Group velocity \doteq 25m/s
 Enhanced near Pakistan in the end of Oct.

Stream function anomalies at 200hPa along the black line in the right figure, 2011/10/25-11/15

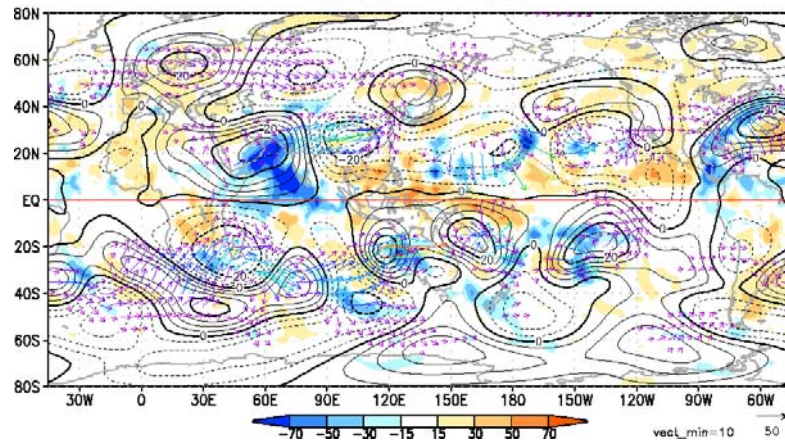


Distance from blocking high in Northern Europe(km)

■ Enhancement of the Rossby wave packet by convection over east north Indian Ocean in the end of Oct. 2011

Stream function and OLR anomalies

10.28 - 11.1



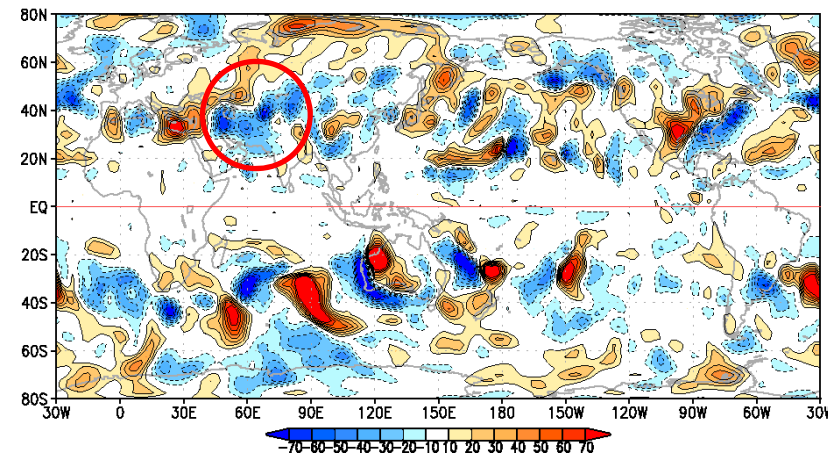
Contour : 5day mean Stream function anomalies at 200hPa

Shade : 5day mean OLR anomalies

Arrows : Wave activity flux (Takaya and Nakamura, 2000) at 200hPa

Rossby wave source anomalies

10.28 - 11.1



Shade: Rossby wave source anomalies at 200hPa. 10^{-6} /s /day

■ Origin of active convection over western Indian Ocean

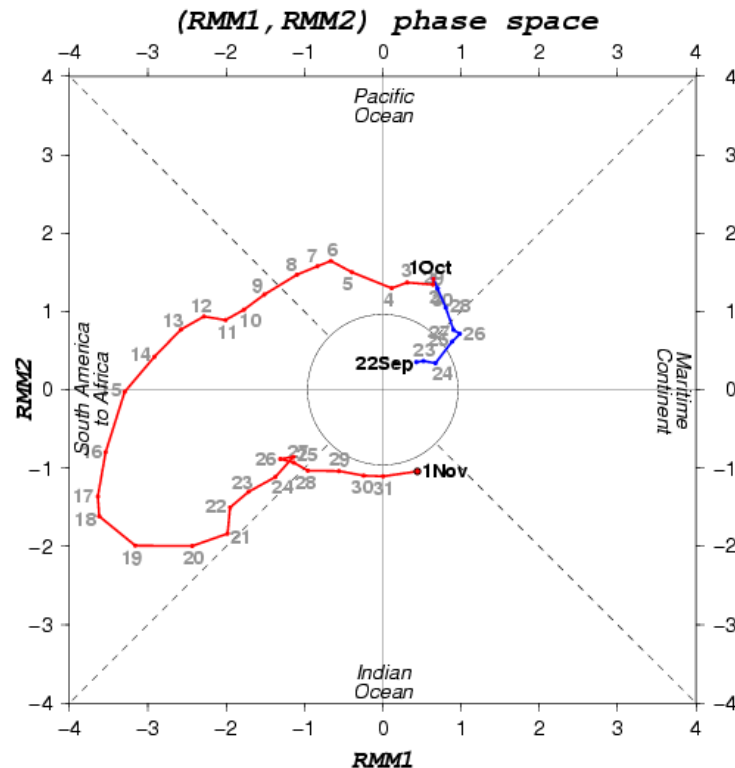


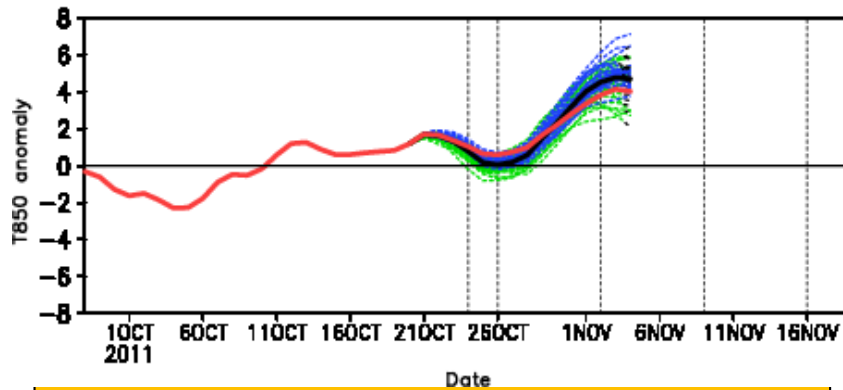
Fig. MJO phase monitor based on multivariate EOF analysis (OLR+U200+U850.) Data period for the normal is from 1981 to 2010. Seasonal, interannual and ENSO variations were subtracted from the tropical variations (Wheeler and Hendon, 2004). JRA-55 is used for the atmospheric data. OLR data are provided by NOAA. NINO.3 index was used for calculating ENSO variation instead of COBE-SST because of the difficulty to extract ENSO variation. Each figures show the last 40 days trajectory from the final day of each month.

<http://ds.data.jma.go.jp/tcc/tcc/products/clisys/mjo/monitor.html>

- Strong MJO (at peak, the second strongest since 1979) propagated from the Atlantic to the Indian Ocean in the end of Oct.
- The MJO weakened over Indian Ocean
- So, active convection over western Indian Ocean is triggered by the MJO.

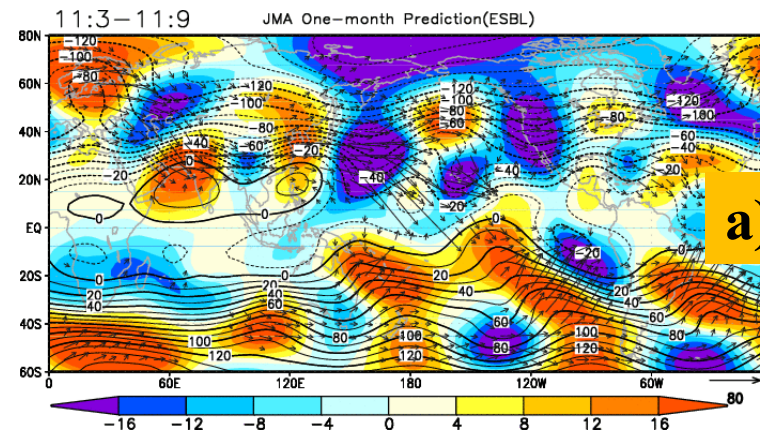
■ Could we predict the event? Initial: 2011.10.24

7day mean temperature anomaly at 850hPa in Western Japan.
 Red: Obs. Others:FCST

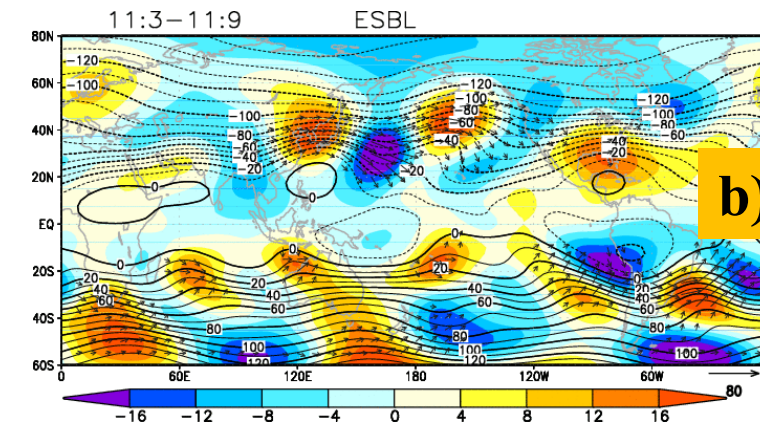


• The event was well predicted from 2011.10.24 initial (Rossby wave packets along PFJ and STJ which was enhanced by MJO related convection, and extremely high Temperature)

7day day mean Stream function anomalies and wave activity flux at 200hPa from 11/3-11/9 .



a) OBS



b) FCST

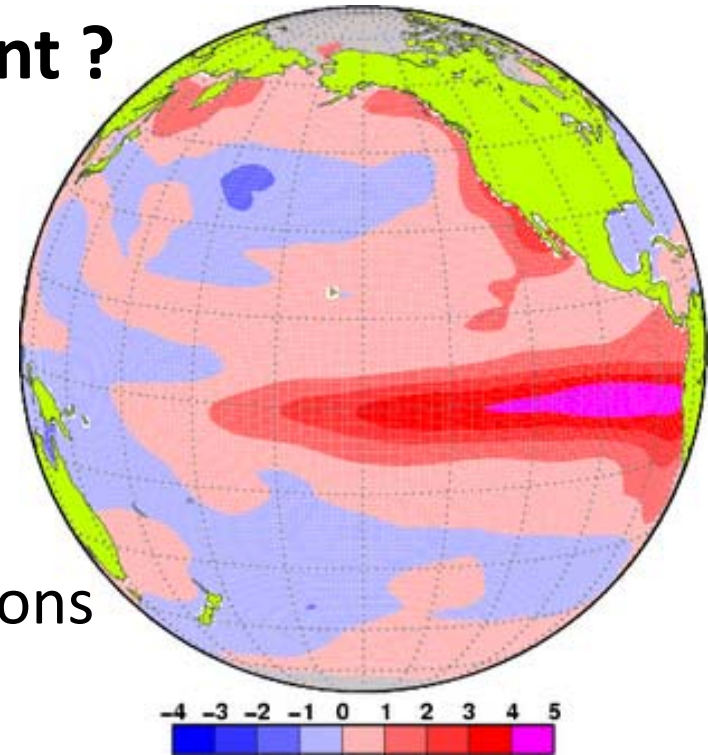
■ 2.3 Interannual Variability

ENSO, El Niño Modoki, IOD

■ El Niño and Southern Oscillation (ENSO)

Why is El Niño/La Niña important ?

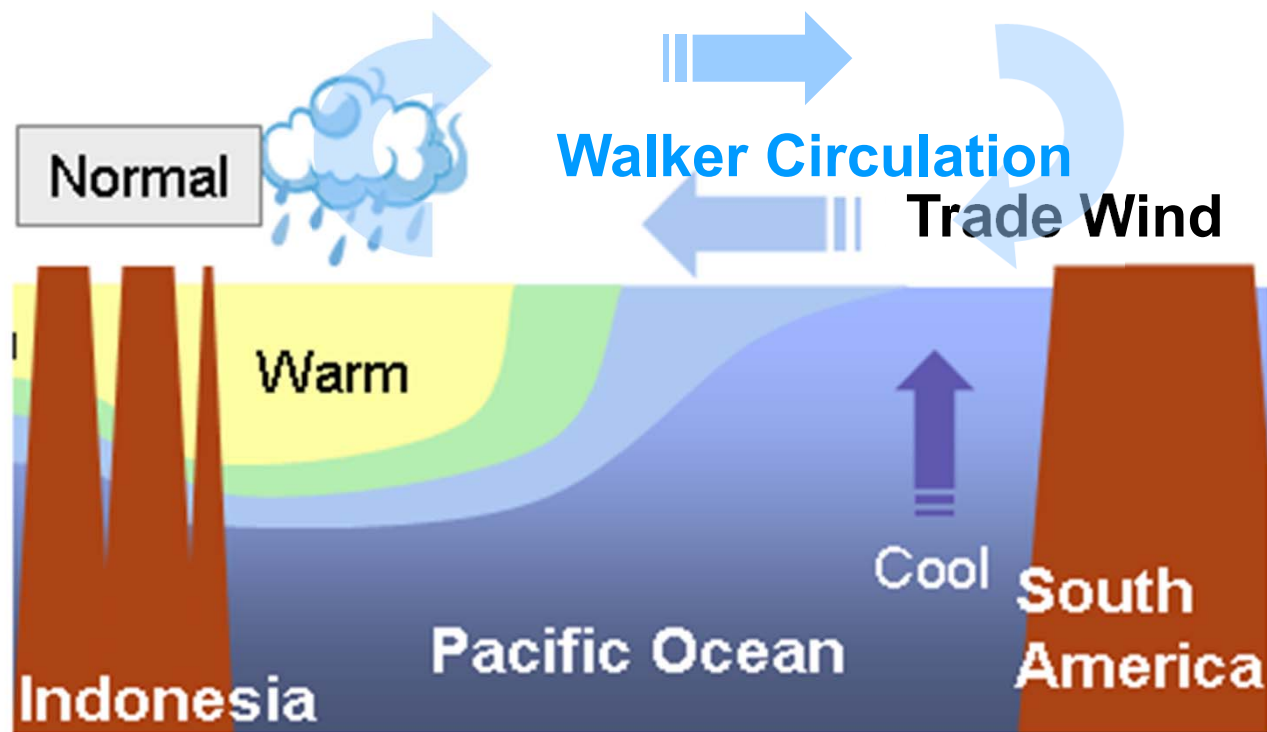
1. Predominant inter-annual climate variability
2. Big Impact on the world climate
3. Predictable with one or two seasons lead time



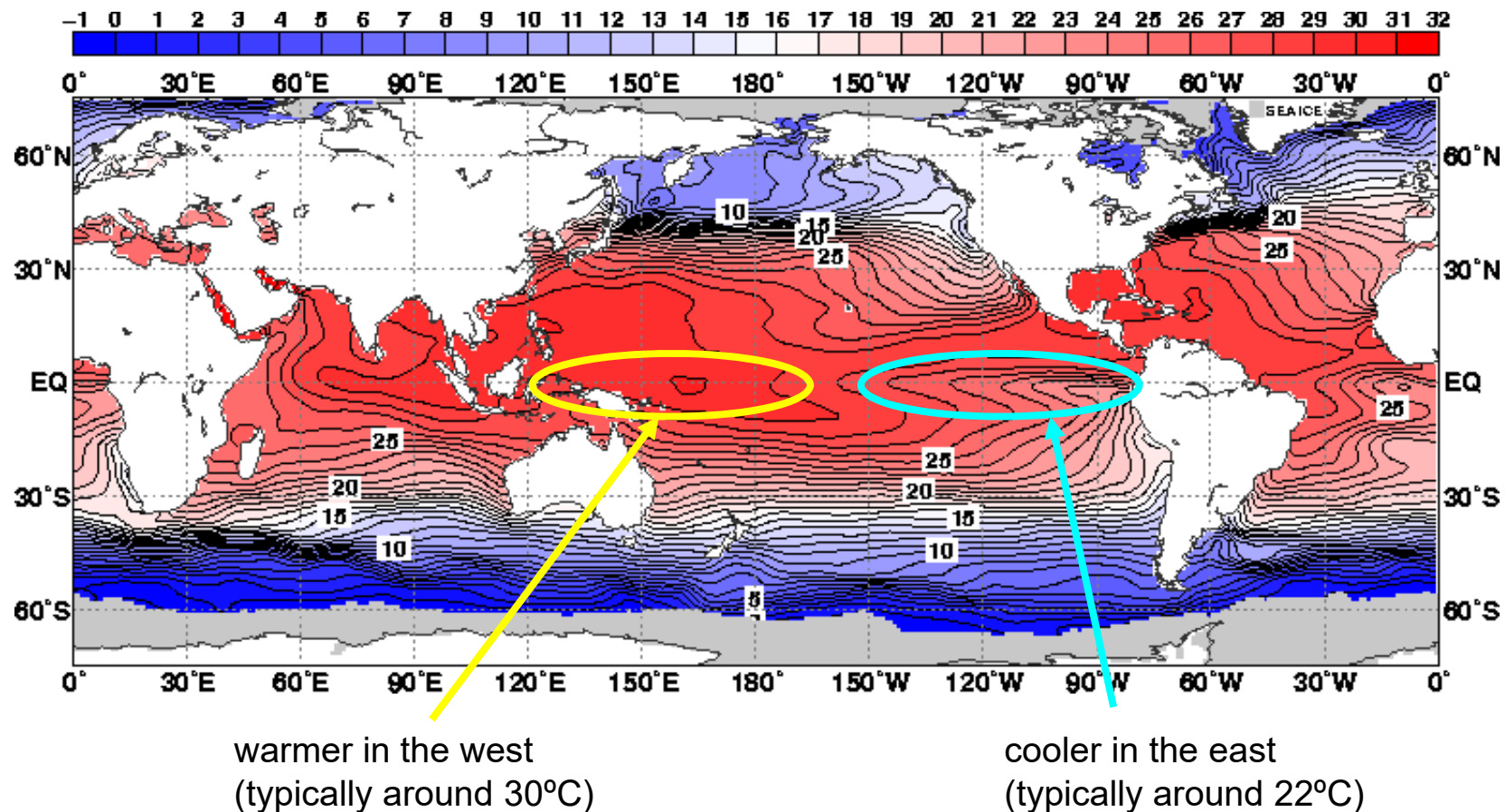
The prediction of El Niño or La Niña is a base of our long range forecast. First, we check the ENSO conditions and then discuss our long range forecast.

■ Normal condition in the equatorial Pacific Ocean

Trade wind, a persistent easterly atmospheric flow blowing over the equatorial Pacific Ocean, sustains warmer-western, cooler-eastern sea surface condition.

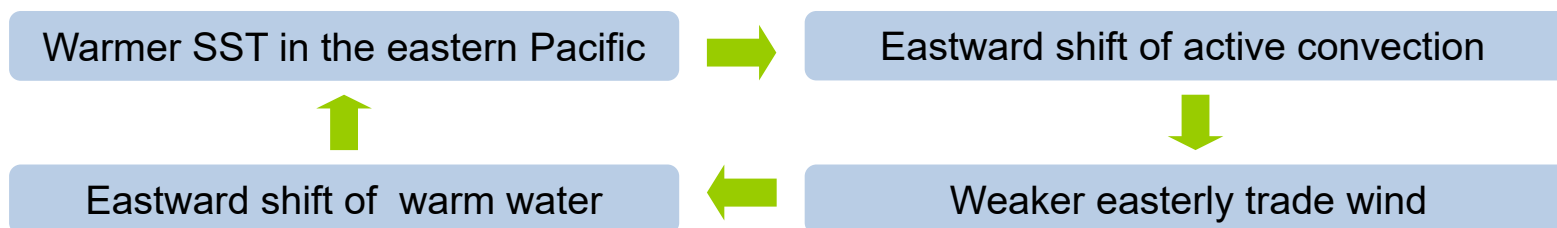
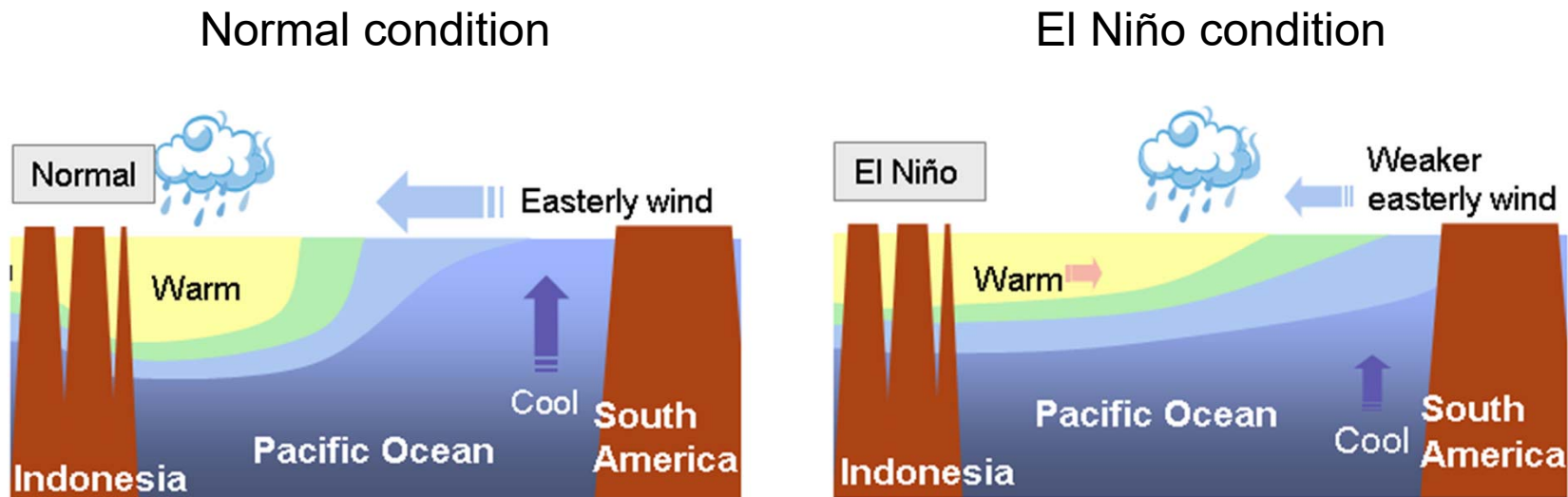


Sea surface temperature (SST)



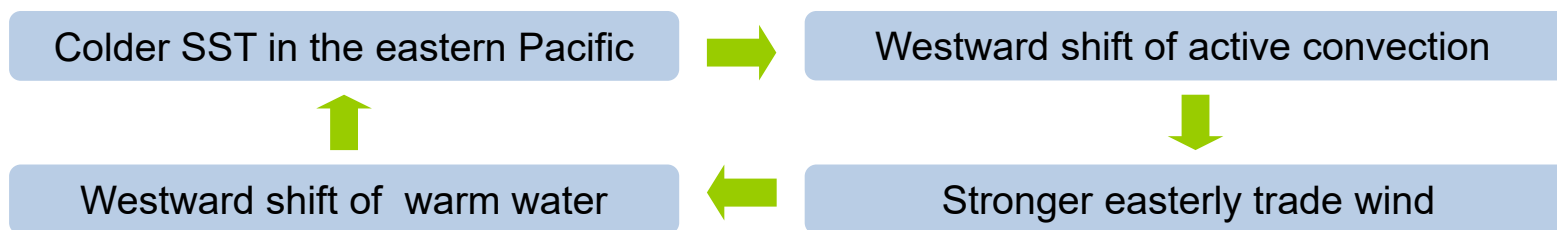
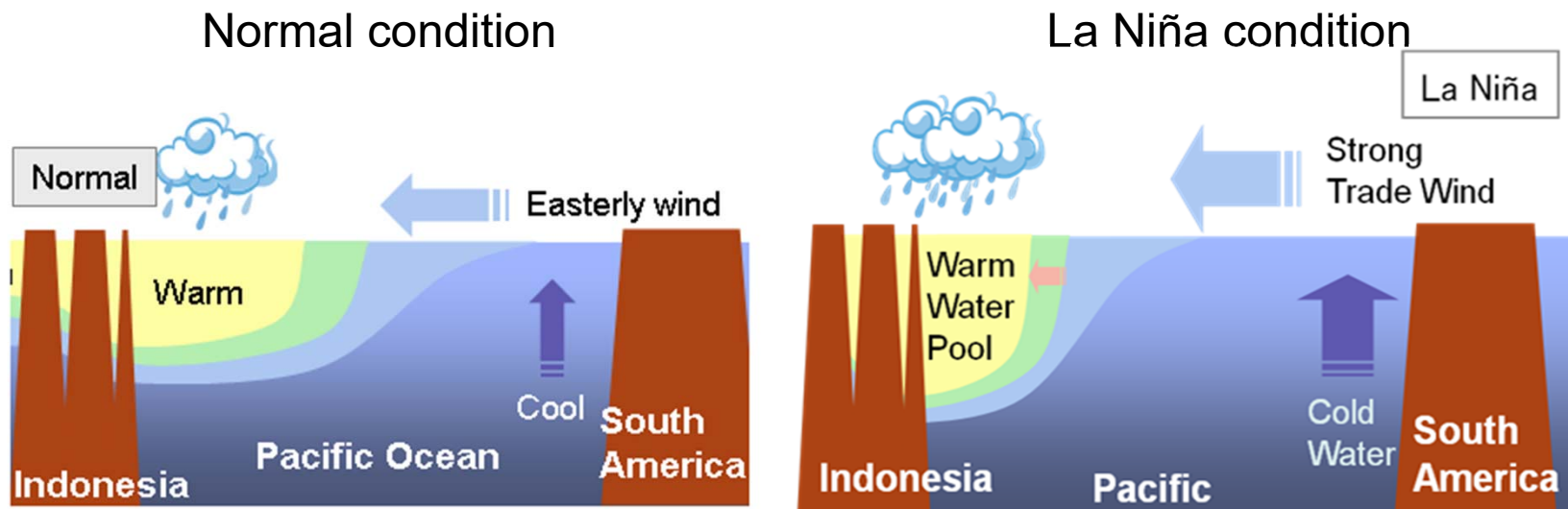
1-month mean sea surface temperature observed in July 2005 when the conditions in the equatorial Pacific Ocean stayed close to normal.

Atmosphere-ocean interaction during El Niño



El Niño + Southern Oscillation = ENSO

■ Atmosphere-ocean interaction during La Niña



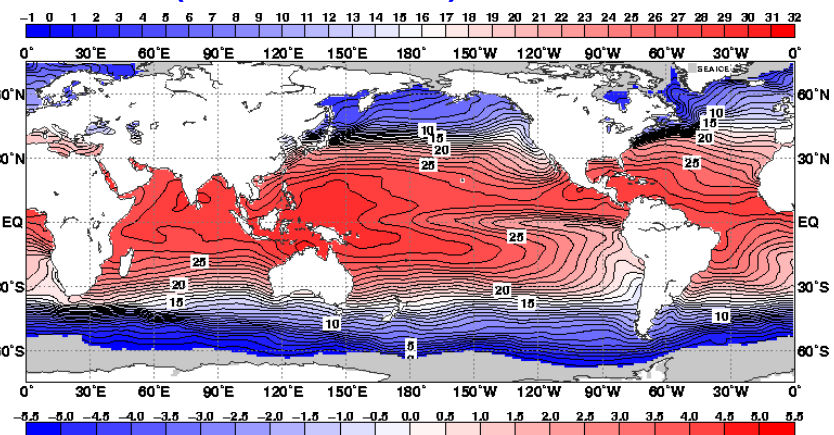
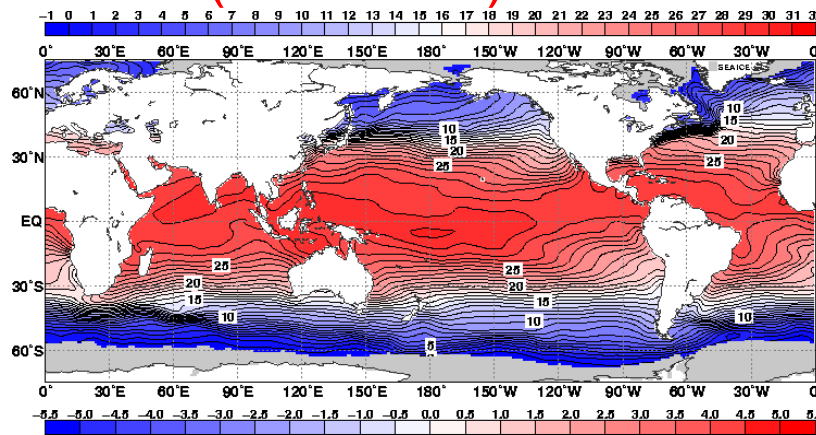
■ “El Niño”(“La Niña”) refers to:

A large-scale ocean climate phenomenon linked to a periodic rise (fall) in sea surface temperatures across the central to east equatorial Pacific

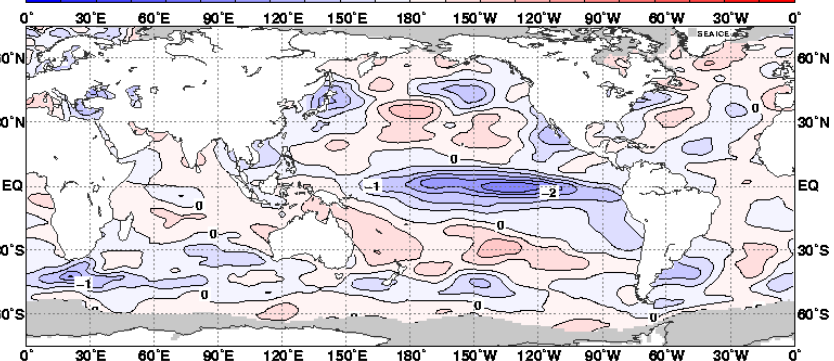
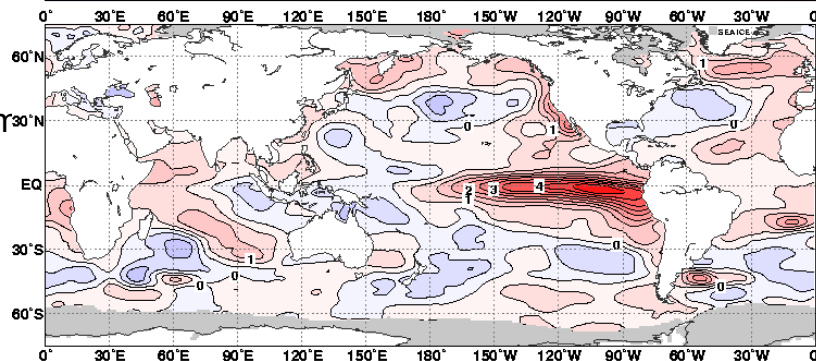
El Niño (NOV1997)

La Niña (NOV1988)

sea surface temperature

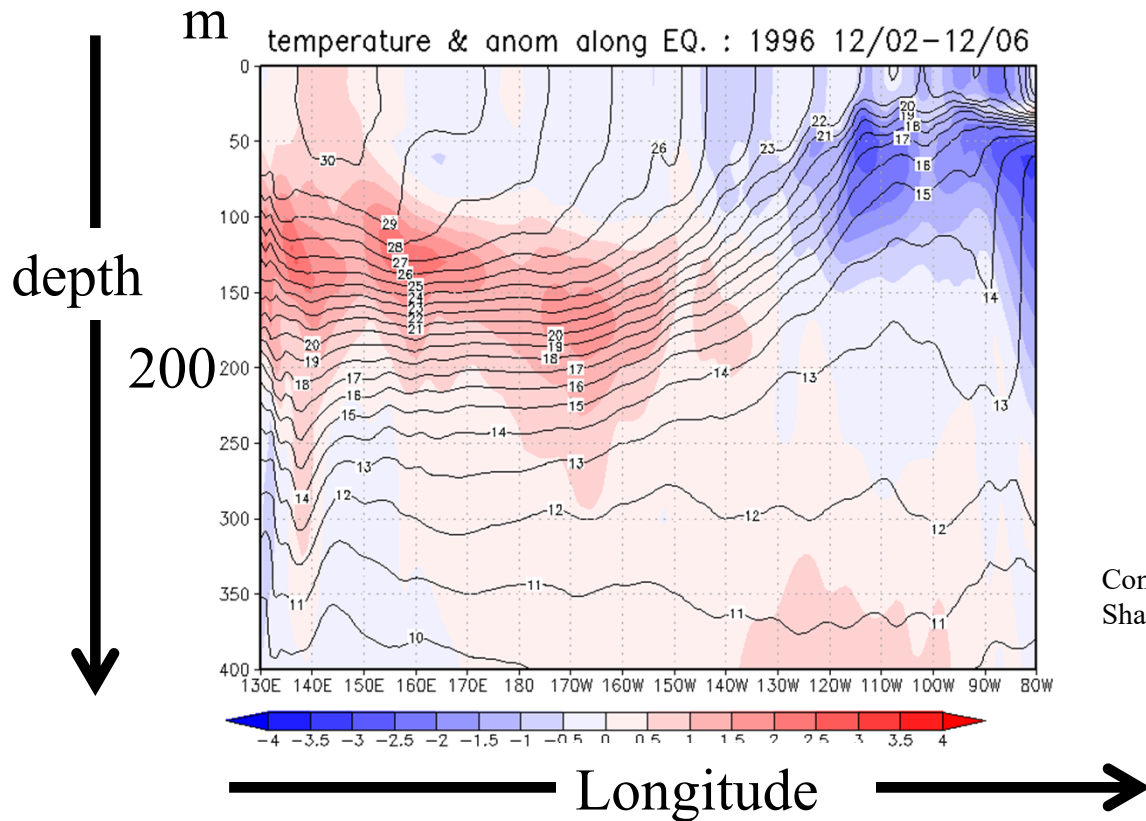


departure from normal

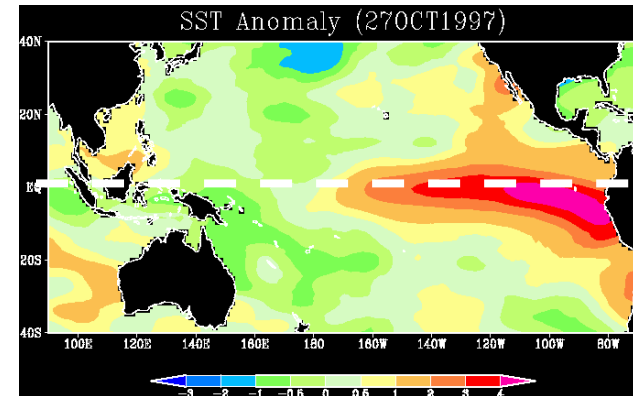


Look deep into the sea

Subsurface temperatures in the equatorial Pacific in 1996/12-98/12

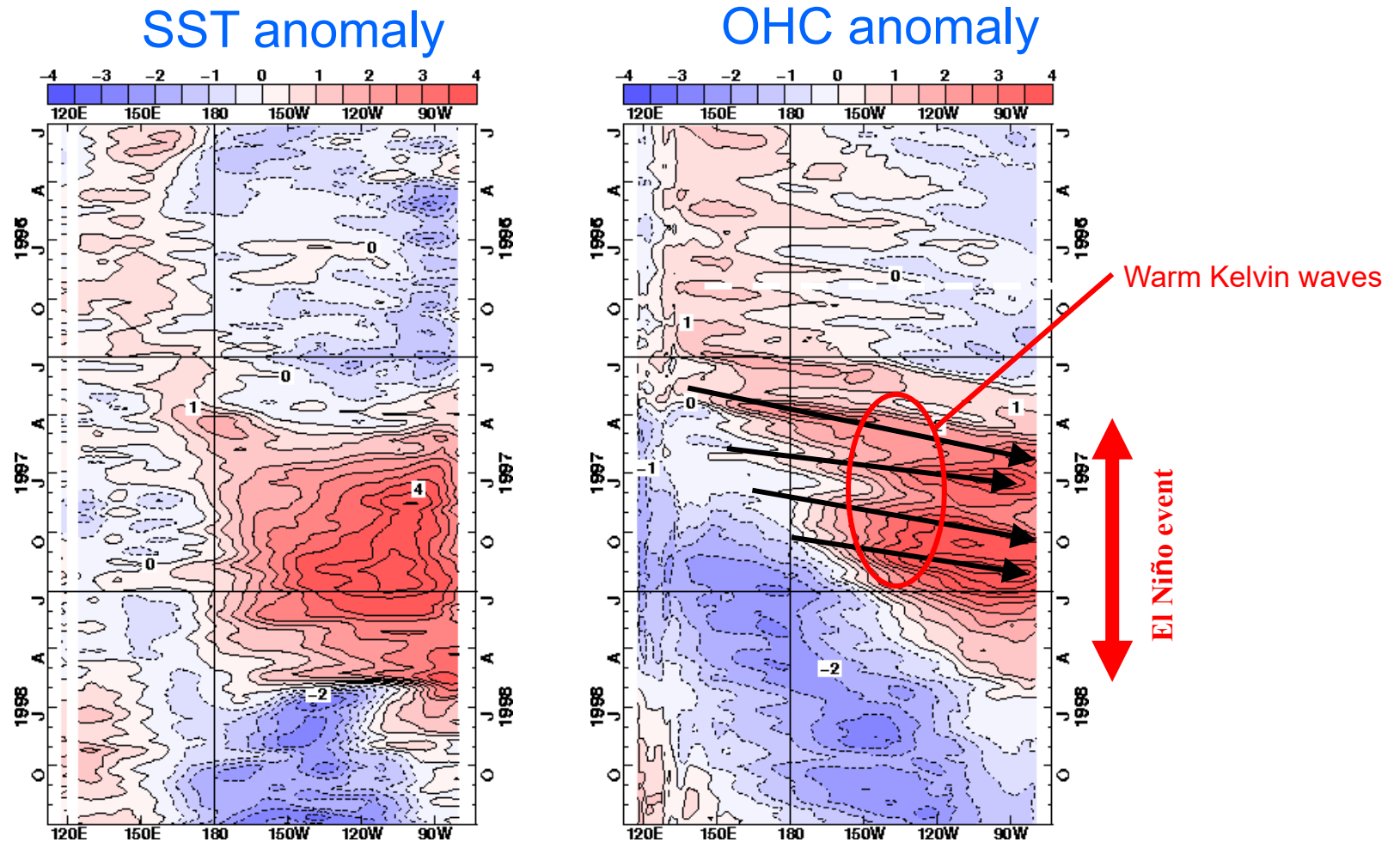


SST anomaly in 27OCT1997



Contour: sea temperature (°C)
Shade: anomaly (°C)

1997/98 El Niño development and decay – hovmoeller plots



OHCs are defined as vertically averaged temperatures of top 300m.

■ ENSO is huge heat variation in the climate system

	Atmosphere	Ocean
Density	1.2-1.3kgm ⁻³	10 ³ kgm ⁻³ : atom. X 800
Mass(per 1 m ²)	(Top ~ Surface) 10 ⁴ kgm ⁻²	(Surface ~10m depth) 10 ⁴ kgm ⁻² : Mass of the atmosphere is the same as that of ocean with 10m depth
Specific heat	10 ³ Jkg ⁻¹ K ⁻¹	4 × 10 ³ Jkg ⁻¹ K ⁻¹ : atom. X 4
Heat capacity (per 1 m ²)	(Top ~ Surface) 10 ⁷ JK ⁻¹ m ⁻²	(Surface ~2.5m depth) 10 ⁷ JK ⁻¹ m ⁻² : Heat capacity of the atmosphere is the same as that of ocean with 2.5m depth

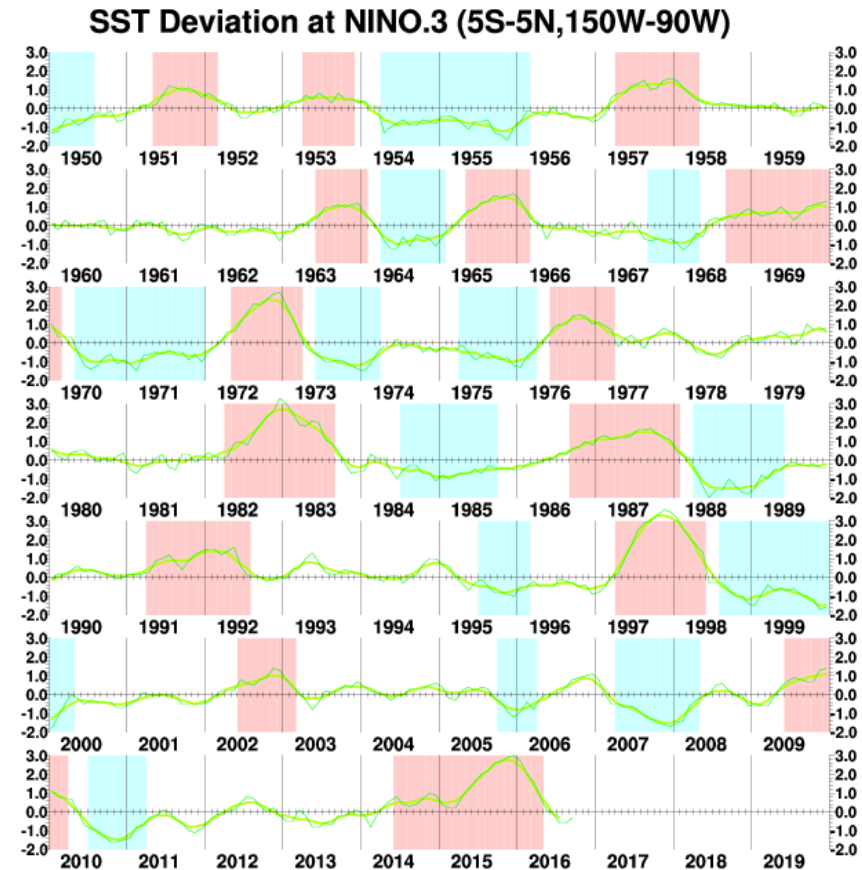
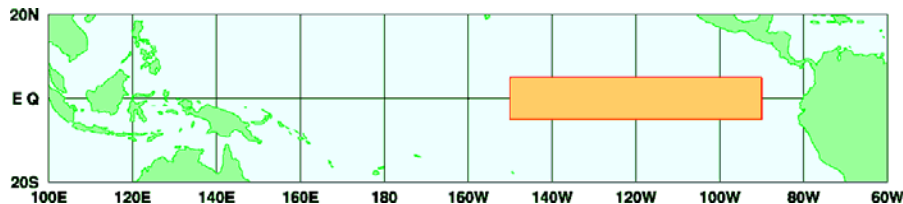
“1K in 250m depth ocean” is near equal to “100K in the atmosphere”

* from Gill 1982

Historical look at SST variations

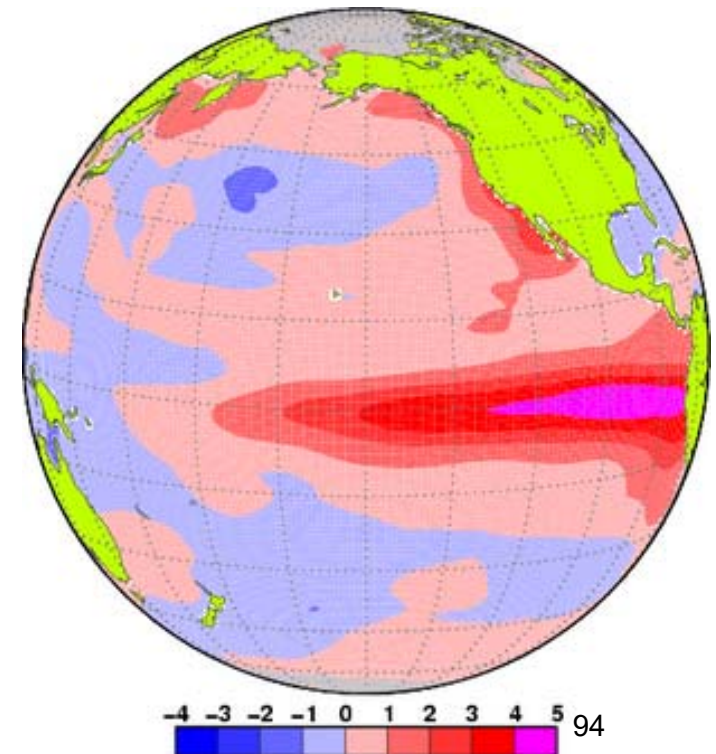
5-month running mean SST departures from normal in the JMA's El Niño monitoring region for 1950-2016

red: El Niño period
blue: La Niña period





■ El Niño and La Niña impact on the world climate



■ El Niño and La Niña impact on the world climate

Walker Circulation along the equator during El Niño (lower panel) and La Niña (upper panel)

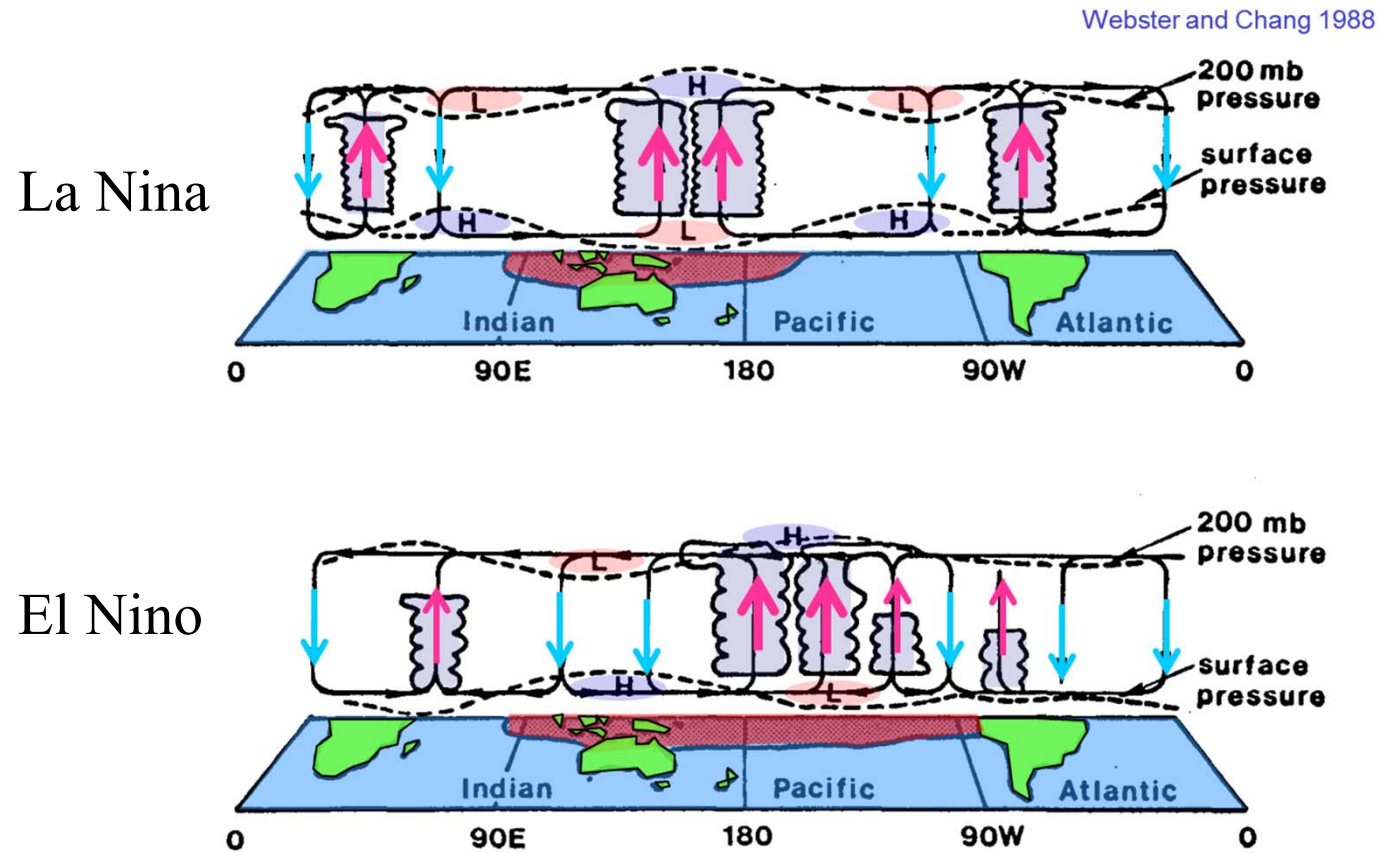
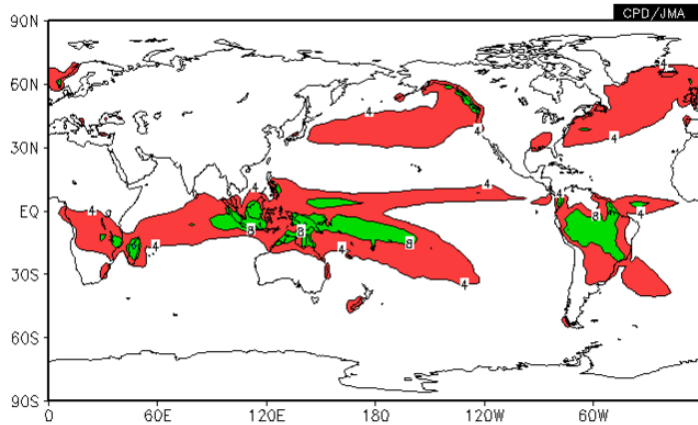
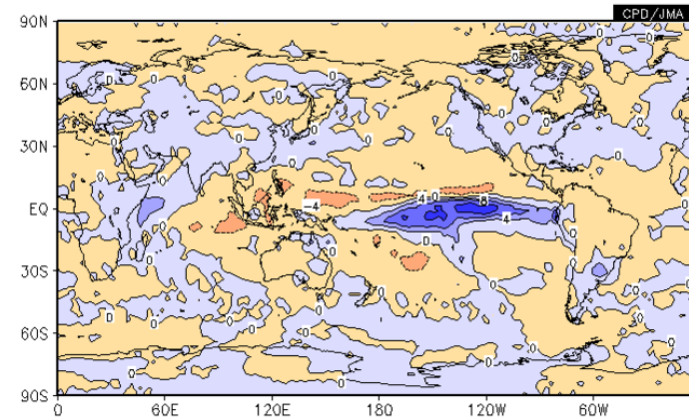
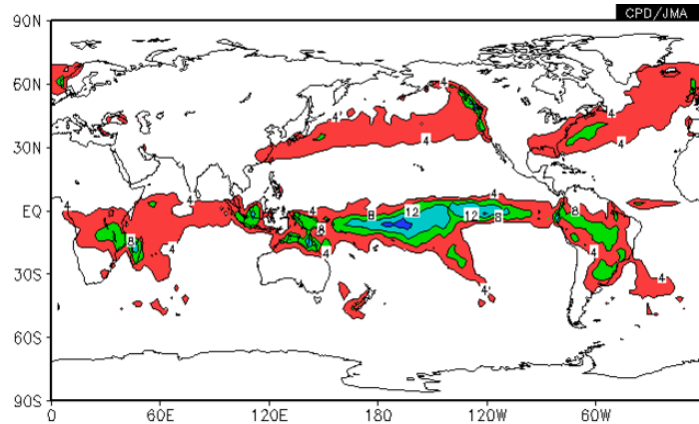


FIG. 1. Schematic view of the Walker Circulation along the equator during El Niño (lower panel) and La Niña (upper panel) periods that occur at the extremes of the Southern Oscillation. The shaded areas indicate sea surface temperatures warmer than 27°C and the dashed lines show relative horizontal pressure variations in the lower and upper troposphere. (From Webster, 1983)

■ Precipitation in 1997/98 winter(DJF)

Upper : 1997/98, lower : normal

Anomalies in 1997/98



Atmospheric heating by condensation

Latent heat

$$: 2.5 \times 10^6 \text{Jkg}^{-1}$$

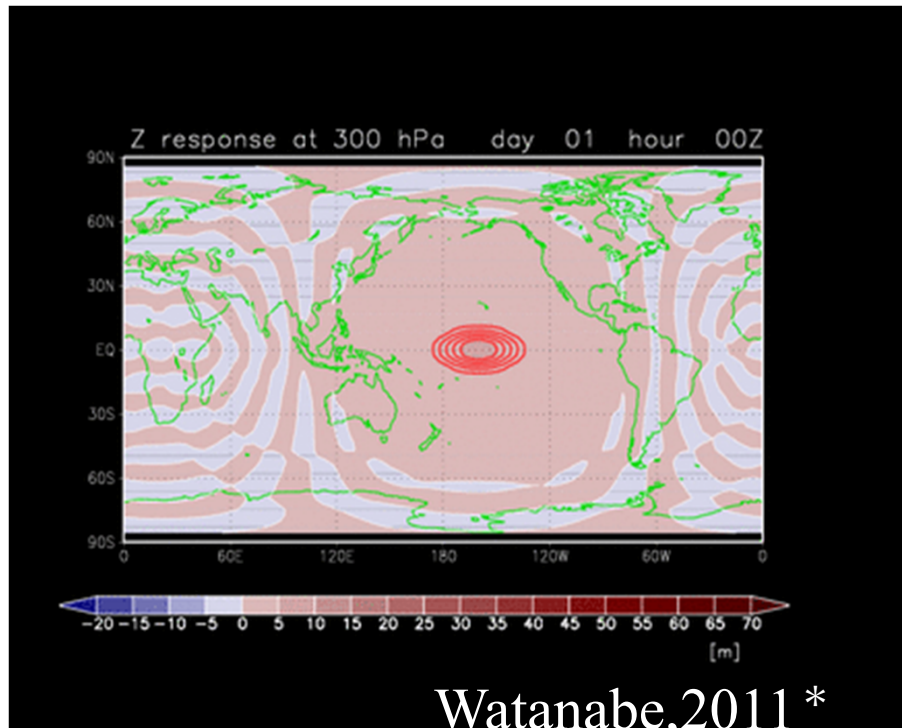
Heat capacity of the atmosphere (per 1m^2)

$$: 10^7 \text{JK}^{-1}\text{m}^{-2}$$

→

4kg/day(=4mm/day) condensation heats the atmosphere
1K/day

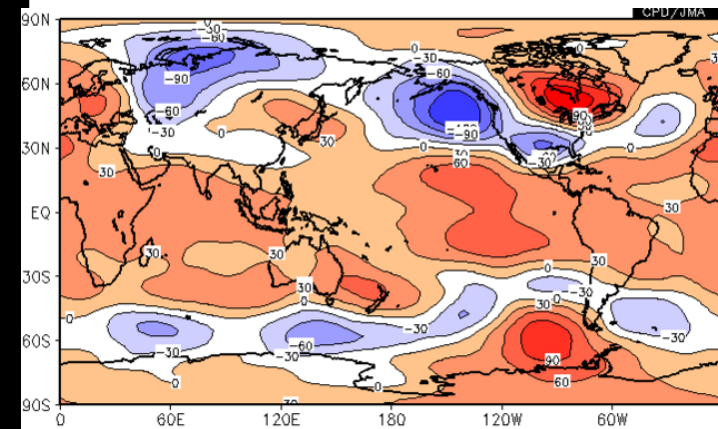
Global atmospheric response to condensation heating in the central equatorial Pacific



LBM simulation of response to condensation heating in the central equatorial Pacific.

Geopotential height at 300hPa

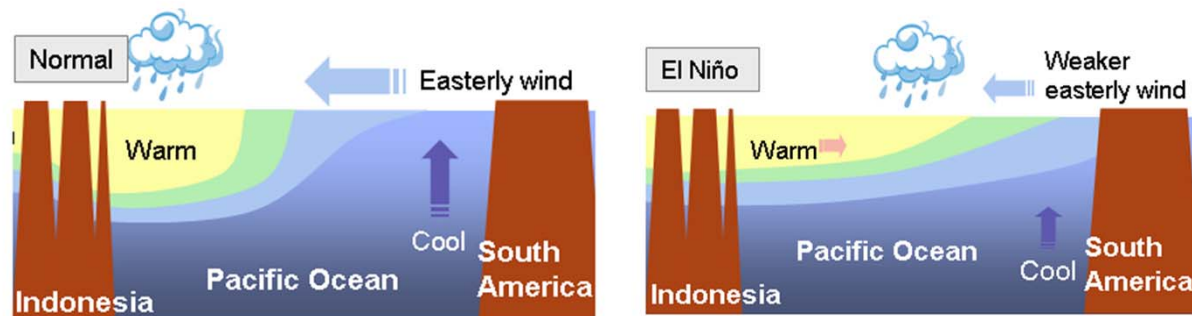
* from his presentation in "Twelfth Joint Meeting for the Seasonal Prediction of the East Asian Winter Monsoon"



Geopotential height anomalies at 300hPa in 1997/98 winter (DJF).

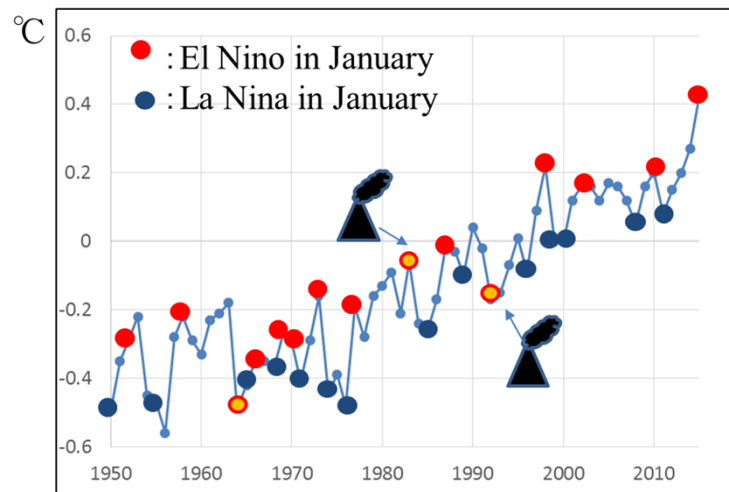
Localized condensation heating in the tropics force stationary Rossby waves which propagate to the mid-high latitudes.

■ Impact of ENSO on Global average surface temperature



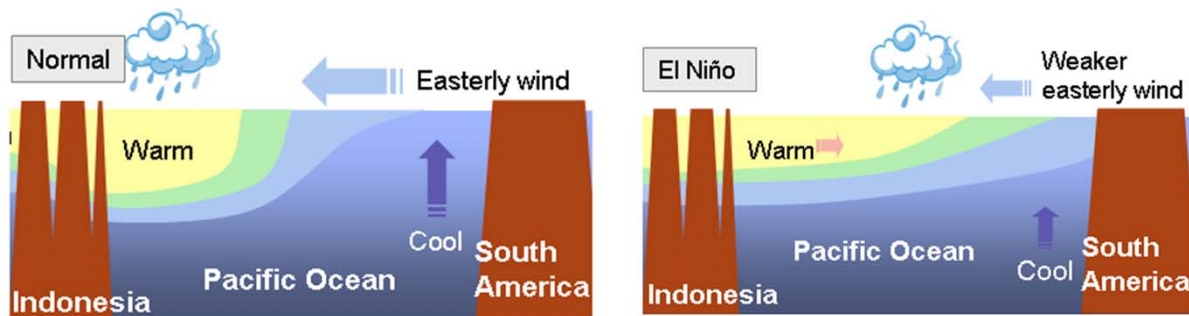
Sub-surface sea temperature in the equatorial Pacific is warmer than normal during El Niño

Global average surface temperature anomalies (1950-2015)



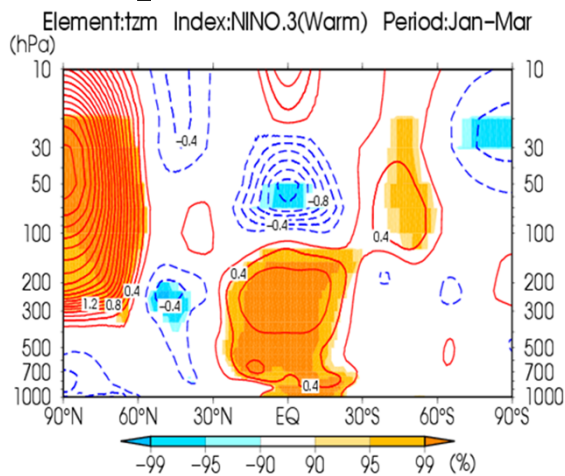
Global average monthly surface temperature tends to raise 0.09 °C per Niño3.4 with three months lag (Trenberth, 2002).

Impact of ENSO on zonal average temperature and circulation

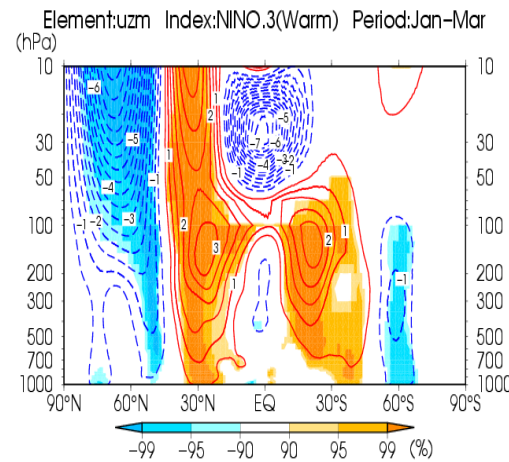


Sub-surface sea temperature in the equatorial Pacific is warmer than normal during El Niño

Temperature in JFM



Zonal Wind in JFM



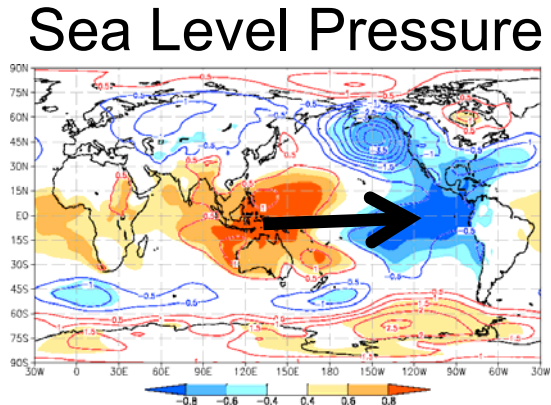
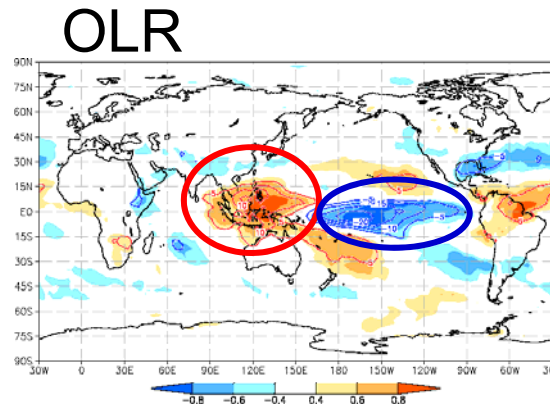
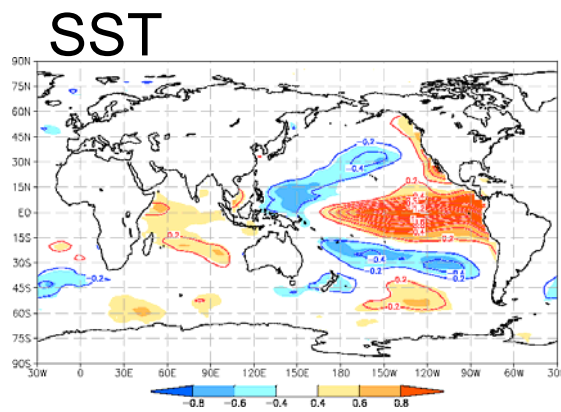
Temperature is higher in the tropics in the troposphere during El Niño.

Temperature gradient between the tropics and mid-latitudes is greater during El Niño

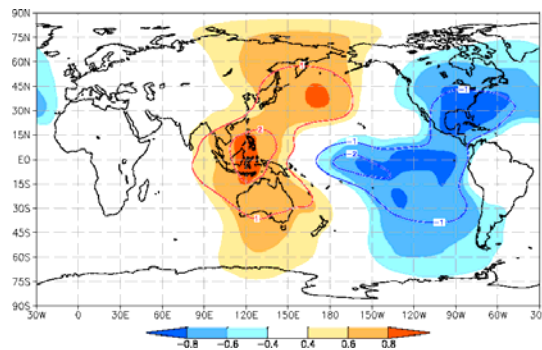
Zonal wind in the sub-tropics is stronger during El Niño

Composite maps in El Niño years

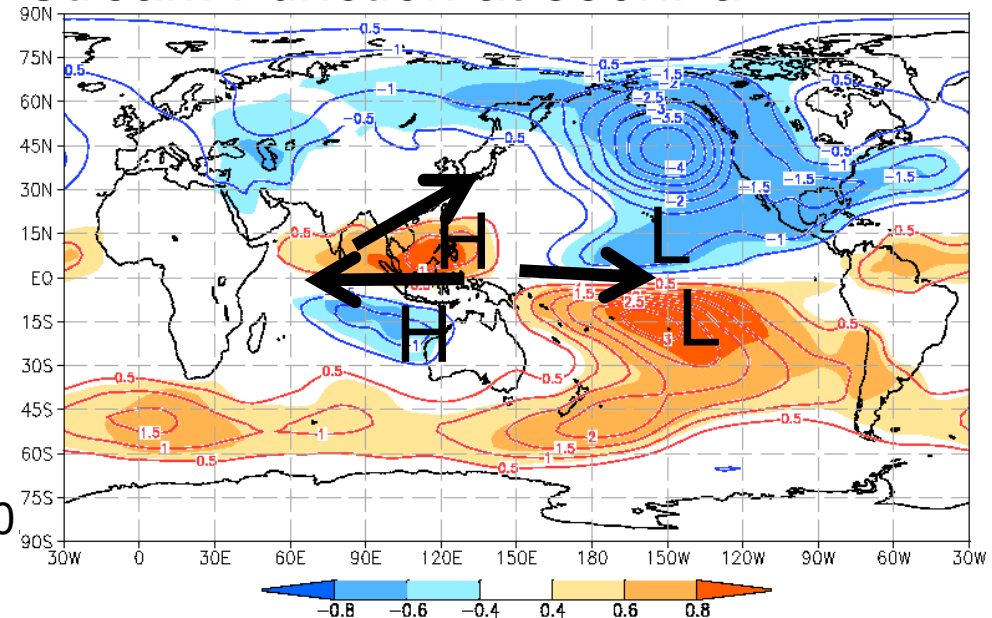
Statistical relationship between NINO.3 and atmospheric circulation fields in DJF



Velocity Potential at 200hPa



Stream Function at 850hPa



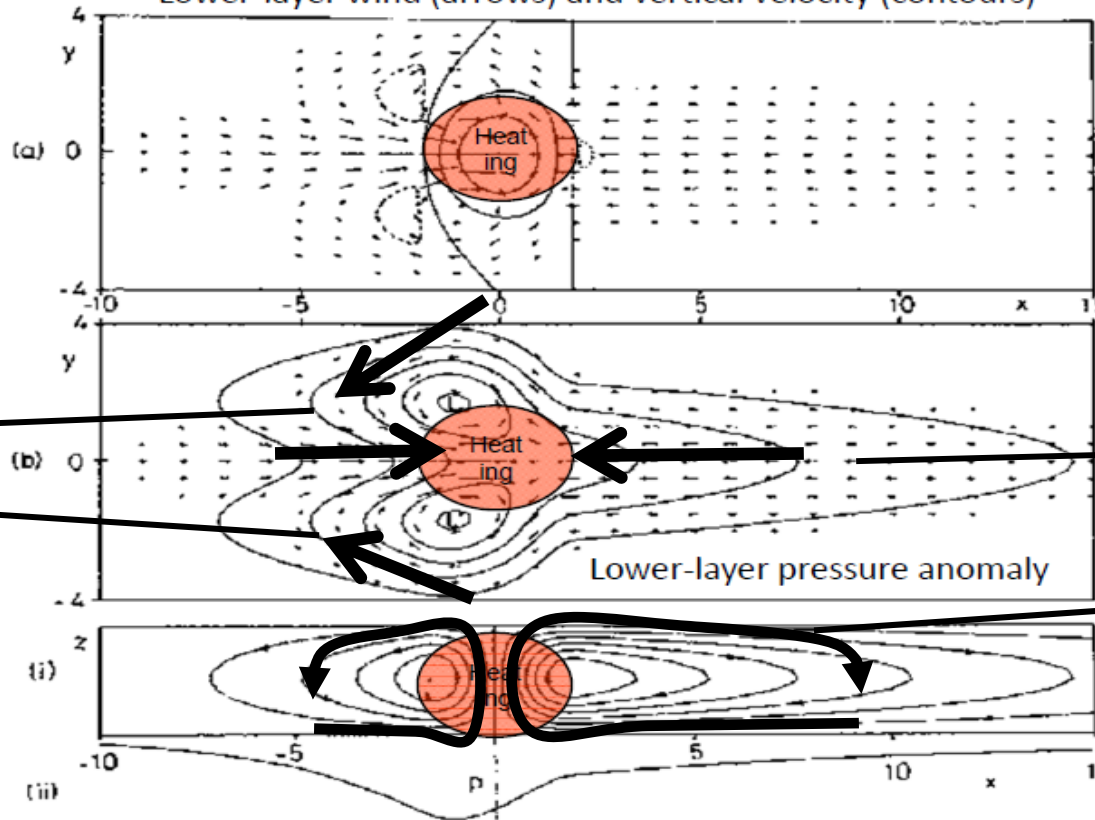
Contours show atmospheric circulation anomalies when normalized NINO.3 is +1.0
 Shadings show correlation coefficients.

Some simple solutions for heat-induced tropical circulation

Quarterly Journal of the Royal Meteorological Society
Volume 106, Issue 449, July 1980, Pages: 447–462, A. E. Gill

Symmetric Heating Anomaly about the equator

Lower-layer wind (arrows) and vertical velocity (contours)



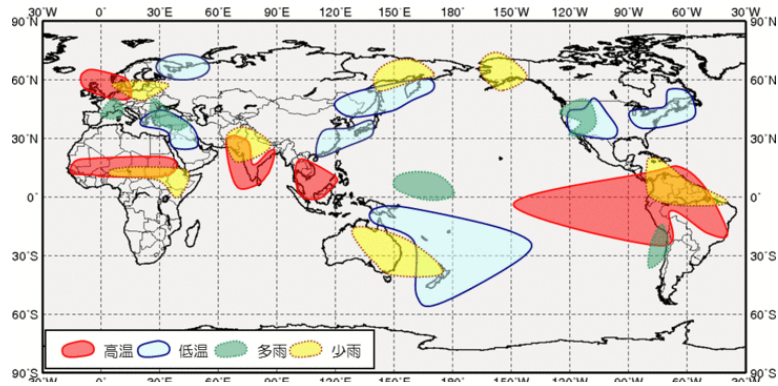
Rossby wave

Kelvin wave
Walker circulation
Vertical-longitudinal circulation

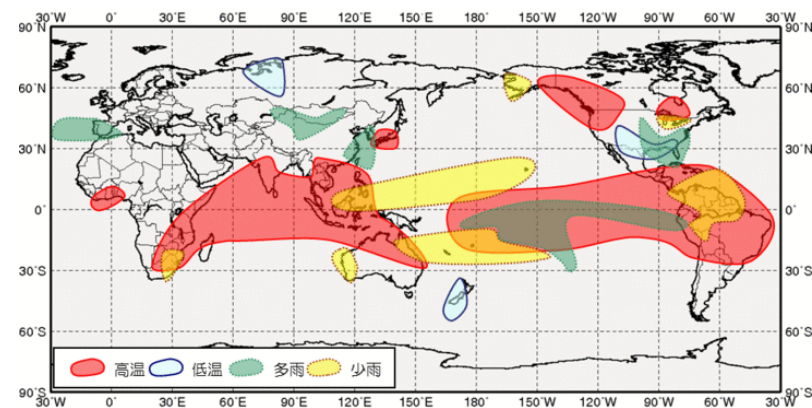
Climate tendencies during El Nino/La Nina



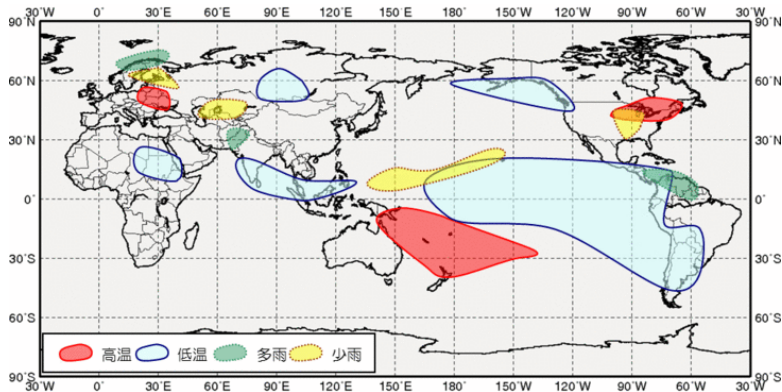
EL in boreal summer



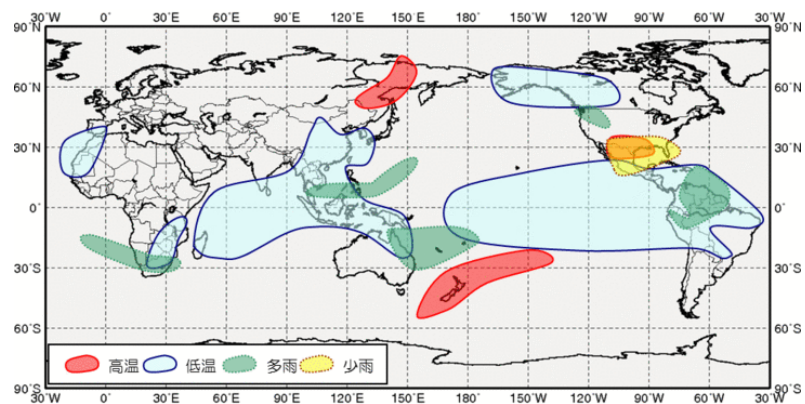
EL in boreal winter



LA in boreal summer



LA in boreal winter



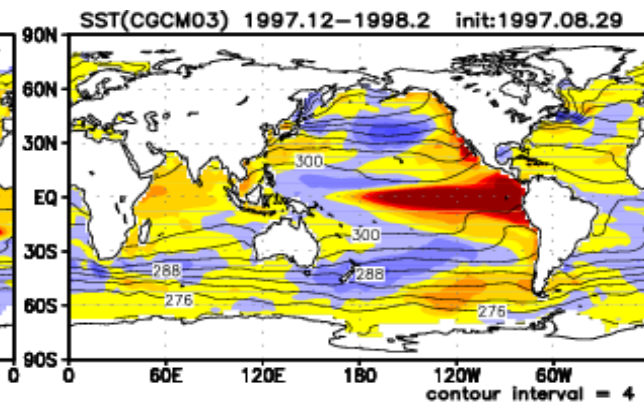
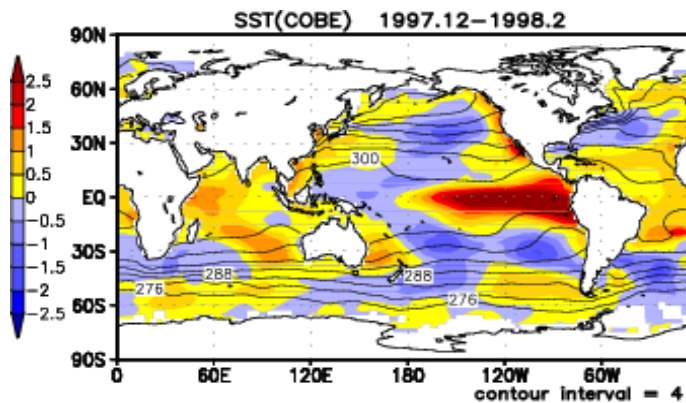
The maps show the regions where climate tendencies observed during El Niño/La Niña episodes are statistically significant in boreal summer/winter.

■ Example of ENSO prediction

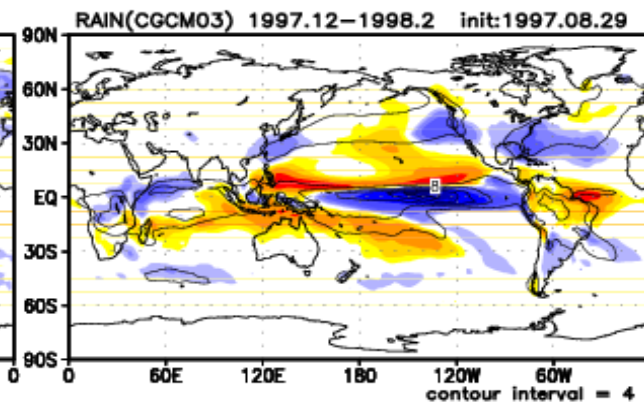
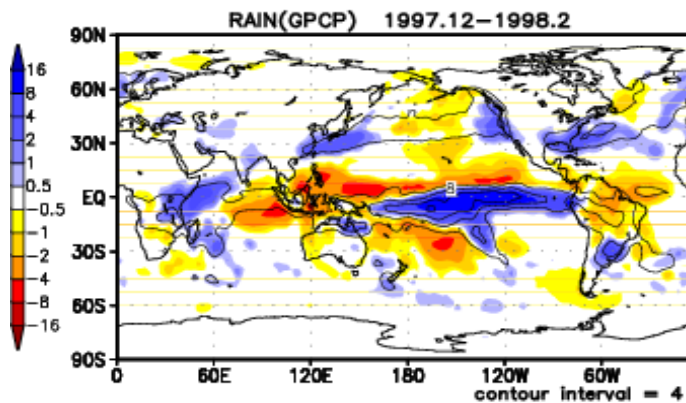
Initial :1997.8.29, Valid time : 1997.12~1998.2

OBS.

Prediction



Contour : SST
Shade:
SST anomaly



Contour :
Precipitation
Shade:
Precipitation
anomaly

■ Lingering impacts of ENSO through change in SST in Tropical Indian Ocean (TIO)

SST in TIO tends to raise associated with El Nino with one-season lag

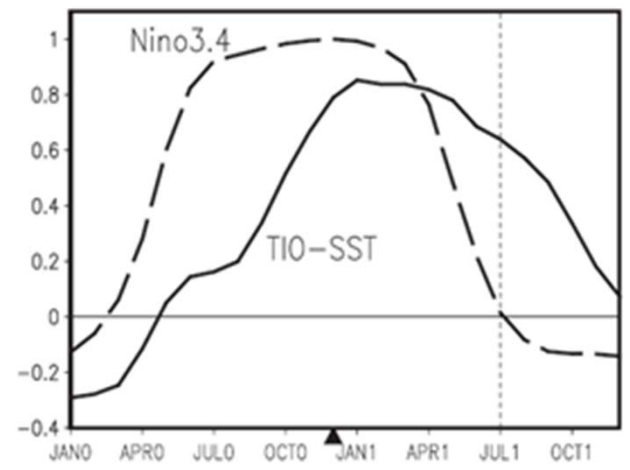
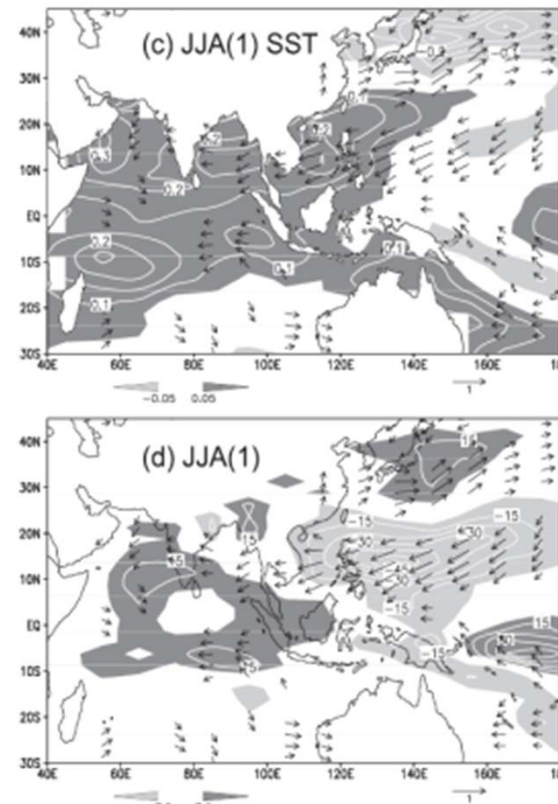


Fig. 1. Correlation of tropical Indian Ocean (40-100°E, 20°S-20°N) SST (solid) with the Nino3.4 (170°W-120°W, 5°S-5°N) SST index for Nov(0)-Dec(0)-Jan(1). Numerals in parentheses denote years relative to El Nino: 0 for its developing and 1 for decay year. The dashed curve is the Nino3.4 SST auto-correlation as a function of lag. The black triangle denotes Dec(0), the peak phase of ENSO.

Warm SST in TIO has impact on atmospheric circulation in Asia Pacific region in JJA



Precipitation anomaly (mm/month)

Xie et al.(2009)

■ El Niño Modoki & CP El Niño

Nature, 2009

The El Niño with a difference

Karumuri Ashok and Toshio Yamagata

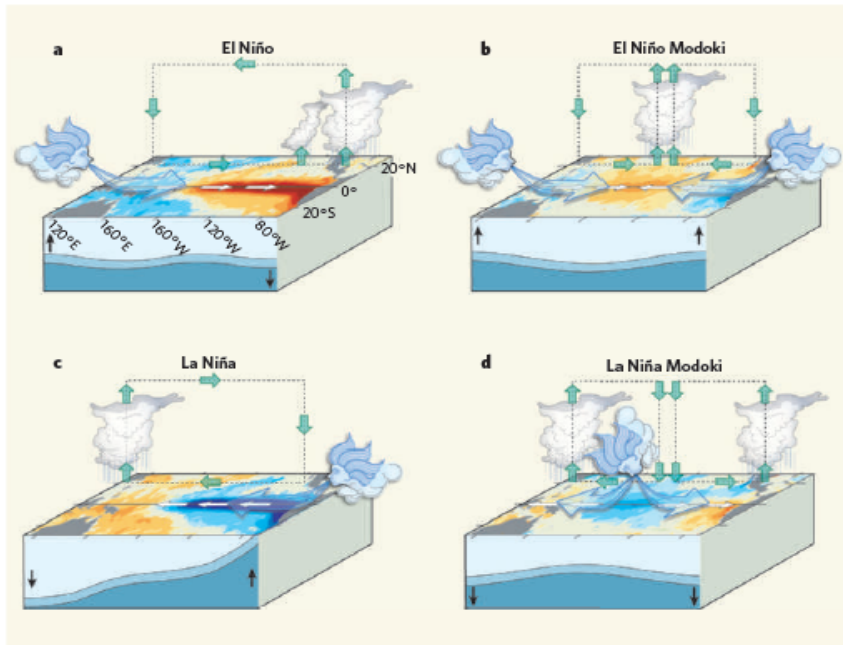


Figure 2 | Anomalous conditions in the tropical Pacific. a, An El Niño event is produced when the easterly winds weaken; sometimes, in the west, westerlies prevail. This condition is categorized by warmer than normal sea surface temperatures (SSTs) in the east of the ocean, and is associated with alterations in the thermocline and in the atmospheric circulation that make the east wetter and the west drier. b, An El Niño Modoki event is an anomalous condition of a distinctly different kind. The warmest SSTs occur in the central Pacific, flanked by colder waters to the east and west, and are associated with distinct patterns of atmospheric convection. c, d, The opposite (La Niña) phases of the El Niño and El Niño Modoki respectively. Yeh *et al.*³ argue that the increasing frequency of the Modoki condition is due to anthropogenic warming, and that these events in the central Pacific will occur more frequently if global warming increases.

Nature, 2009

El Niño in a changing climate

Sang-Wook Yeh¹, Jong-Seong Kug¹, Boris Dewitte², Min-Ho Kwon³, Ben P. Kirtman⁴ & Fei-Fei Jin

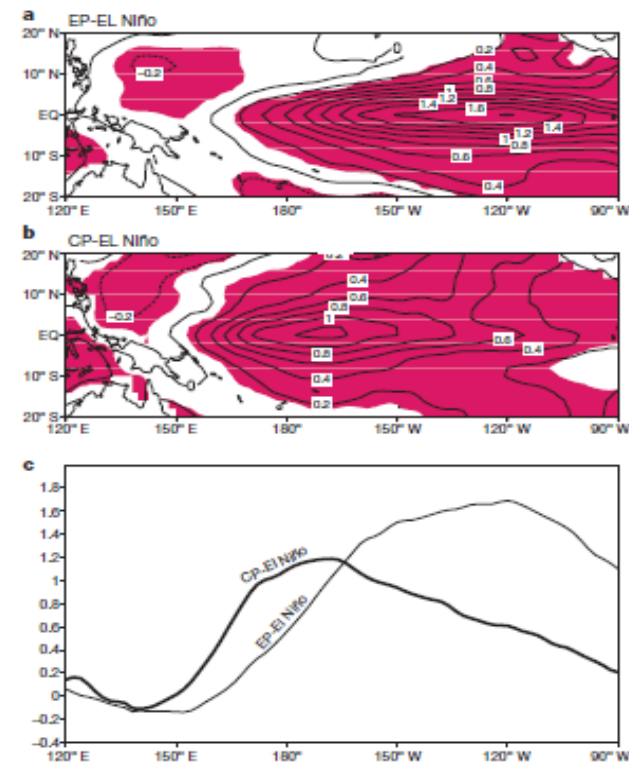
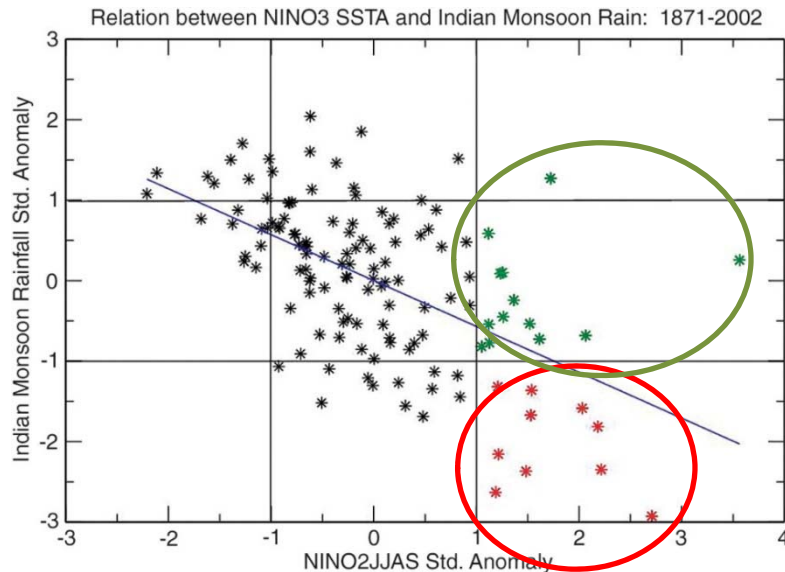


Figure 1 | Deviations of mean SST for the two characteristics of El Niño from the 1854–2006 climatology. a, The EP-El Niño; b, the CP-El Niño. The contour interval is 0.2 °C and shading denotes a statistical confidence at 95% confidence level based on a Student's *t*-test. c, The zonal structure for the composite EP-El Niño (thin line) and CP-El Niño (thick line) averaged over 2°N to 2°S.

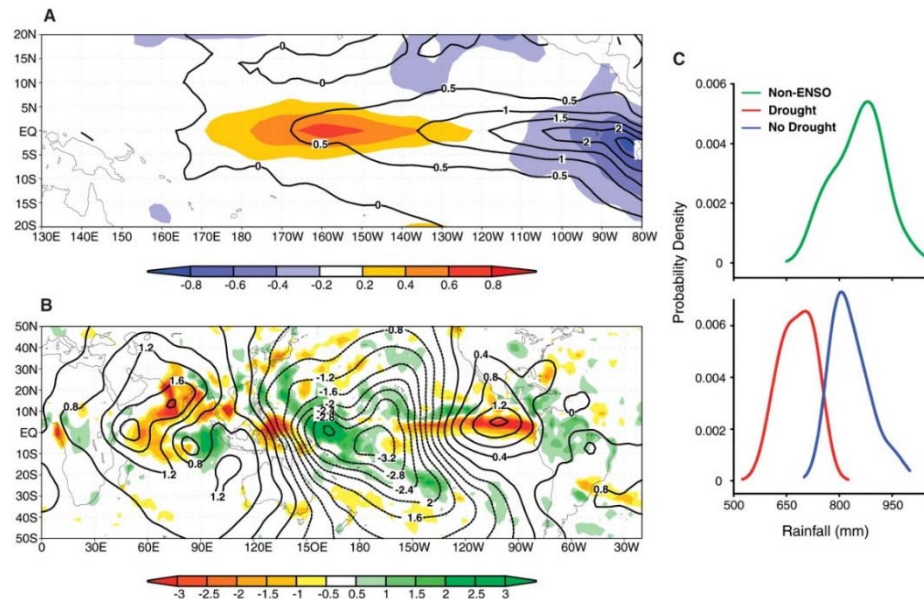
■ ENSO-Monsoon relation

Severe droughts in India have always been accompanied by El Niño events. SST anomalies in the central equatorial Pacific are more effective in focusing drought-producing subsidence over India.



Plot of standardized, all-India summer [June to September (JJAS)] monsoon rainfall and summer NINO3 anomaly index. Severe drought and drought-free years during El Niño events (standardized NINO3 anomalies > 1) are shown in red and green, respectively.

Kumar et al.(2006)



(A) Composite SST difference pattern between severe drought (shaded) and drought-free El Niño years. Composite SST anomaly patterns of drought-free years are shown as contours. (B) Composite difference pattern between severe drought and drought-free years of velocity potential (contours) and rainfall (shaded). (C) PDF of all-India summer monsoon rainfall from severe-drought (red curve) and drought-free (blue curve) years associated with El Niño occurrence and from the non-ENSO years (green curve). SST and velocity potential composite differences are based on 1950 to 2004, rainfall composites are based on 1979 to 2004, and PDFs are based on 1873 to 2004.

A dipole mode in the tropical Indian Ocean

N. H. Saji*, B. N. Goswami†, P. N. Vinayachandran* & T. Yamagata*‡

Saji et al., Nature 1999

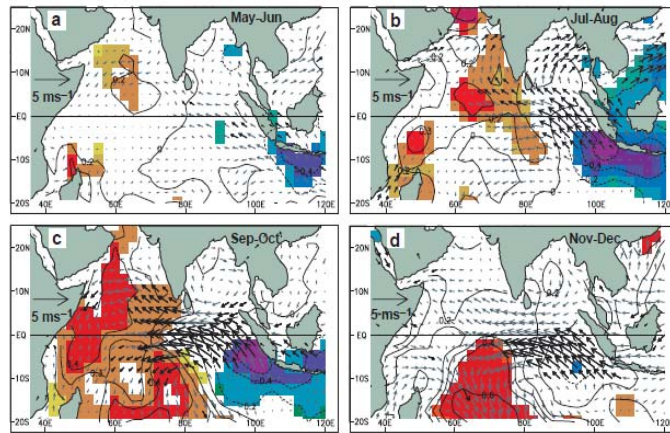


Figure 2 A composite dipole mode event. **a–d**, Evolution of composite SST and surface wind anomalies from May–June (**a**) to Nov–Dec (**d**). The statistical significance of the

analysed anomalies were estimated by the two-tailed *t*-test. Anomalies of SSTs and winds exceeding 90% significance are indicated by shading and bold arrows, respectively.

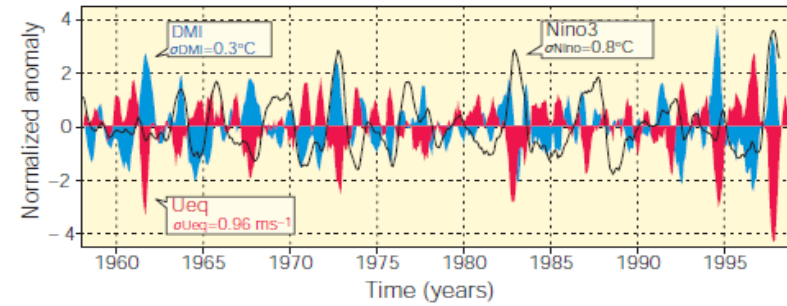


Figure 1 Dipole mode and El Niño events since 1958. Plotted in blue, the dipole mode index (DMI) exhibits a pattern of evolution distinctly different from that of the El Niño, which is represented by the Nino3 sea surface temperature (SST) anomalies (black line). On the other hand, equatorial zonal wind anomalies U_{eq} (plotted in red) coevolves with the DMI. All the three time series have been normalized by their respective standard deviations. We have removed variability with periods of 7 years or longer, based on harmonic analysis, from all the data sets used in this analysis. In addition, we have smoothed the time series using a 5-month running mean.

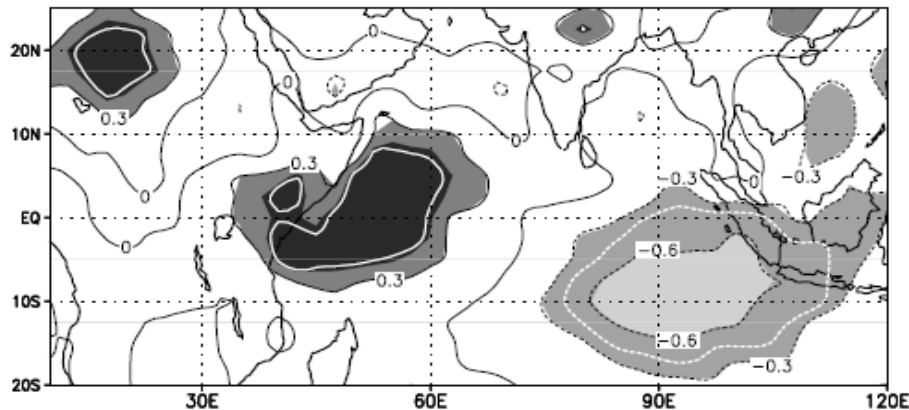


Figure 4 Rainfall shifts northwest of the OTCZ during dipole mode events. The map correlates the DMI and rainfall to illustrate these shifts. The areas within the white curve exceed the 90% level of confidence for non-zero correlation (using a two-tailed *t*-test).

Possible impacts of Indian Ocean Dipole mode events on global climate

N. H. Saji^{1,3,*}, T. Yamagata^{1,2}

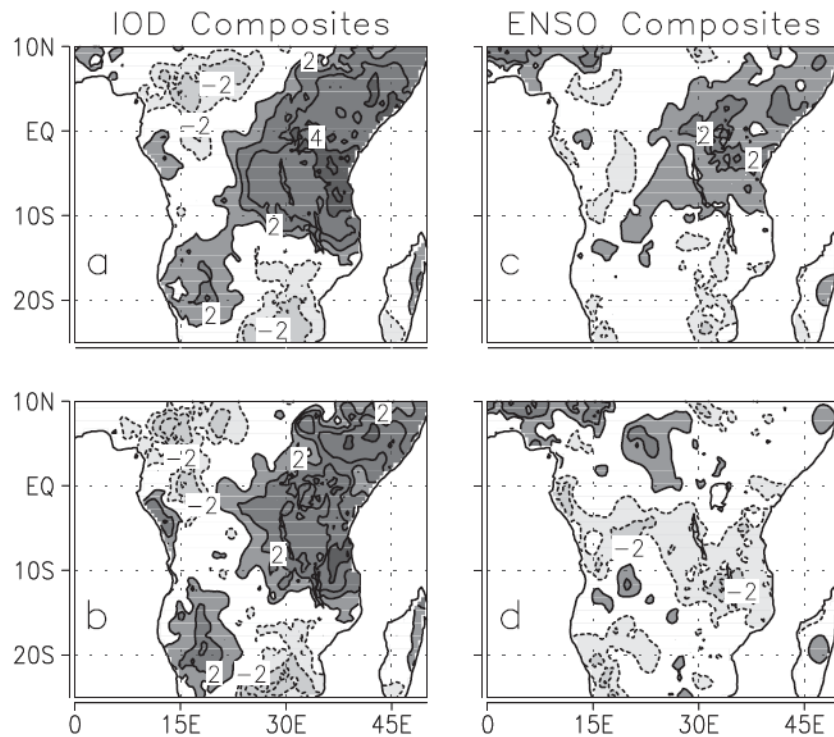


Fig. 1. Composite OND rain anomaly over Africa for (a) 19 IOD events, (b) 11 ENSO-independent IOD events, (c) 20 ENSO events and (d) 12 IOD-independent ENSO events. The composite anomaly was normalized by the standard deviation of rain during OND. Contours given at ± 1 , ± 2 , etc.

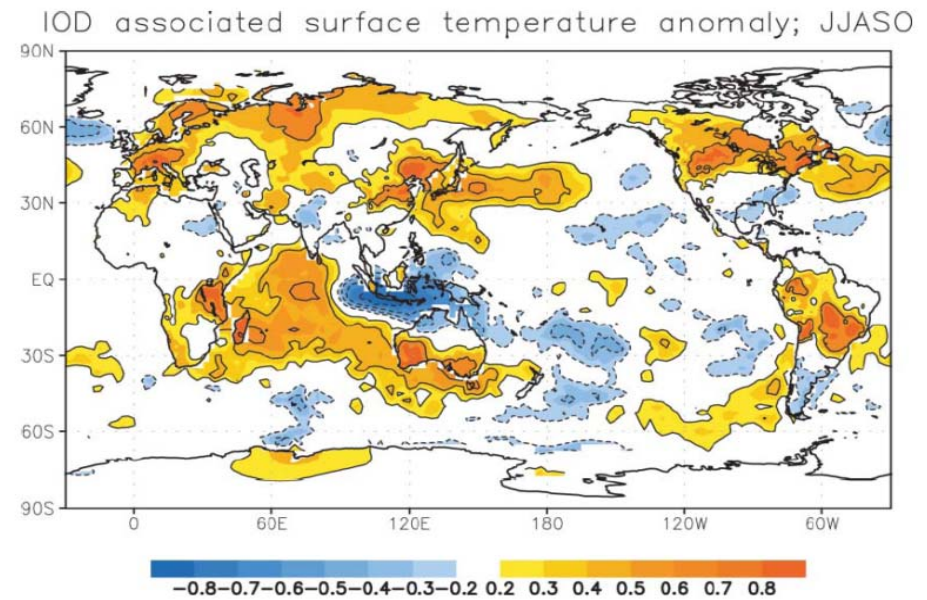
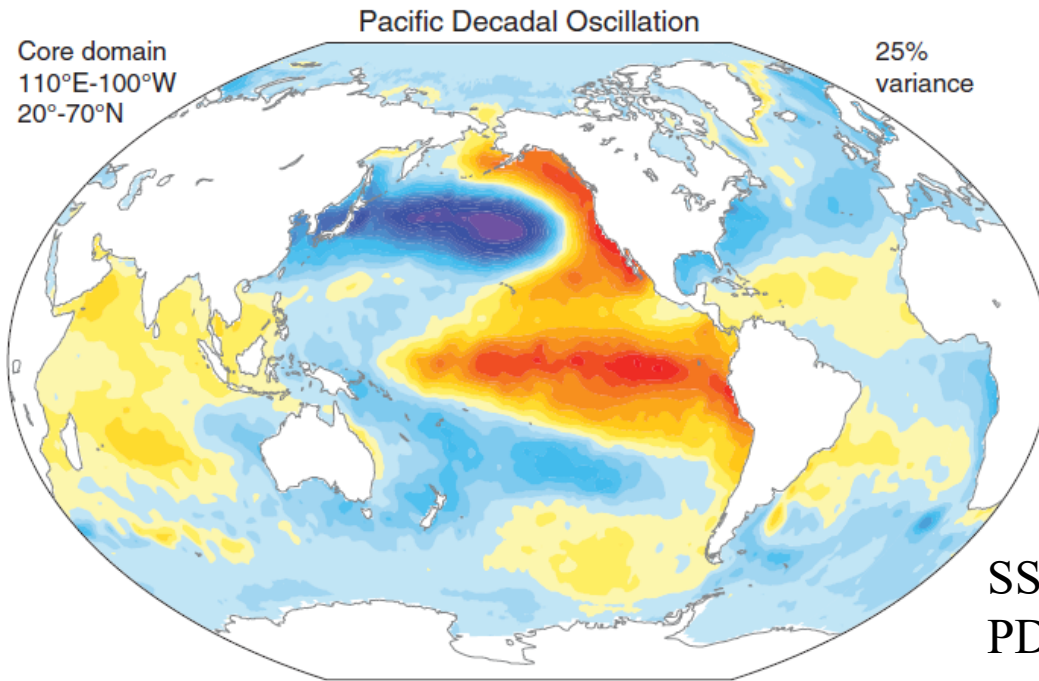


Fig. 21. Partial correlation of land and sea-surface temperature on DMI independent of Nino3 during JJASO

■ 2.4 Decadal Variability

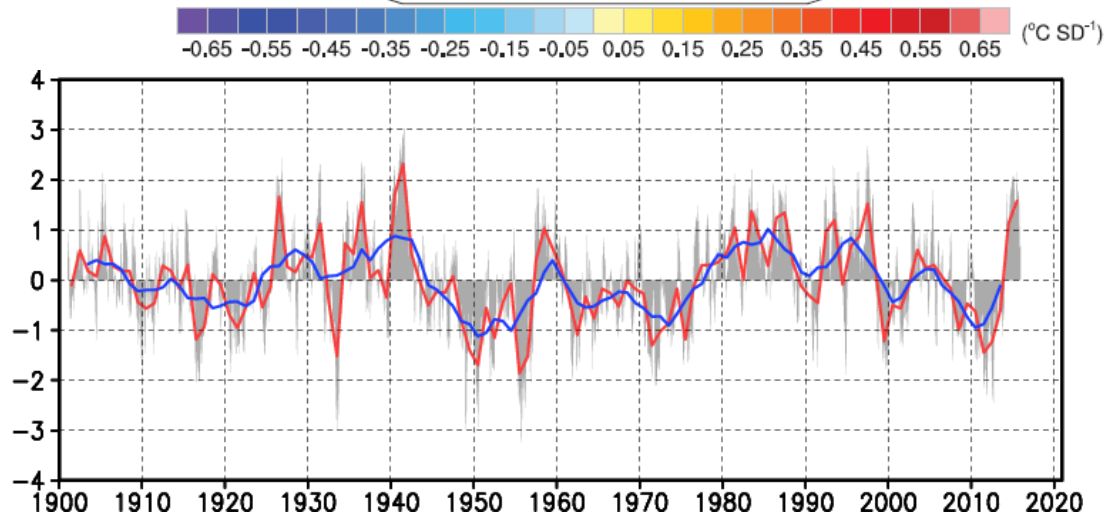
PDO, AMO, ENSO-Monsoon relation

■ Pacific Decadal Oscillation (PDO)



Trenberth and Fasullo (2013)

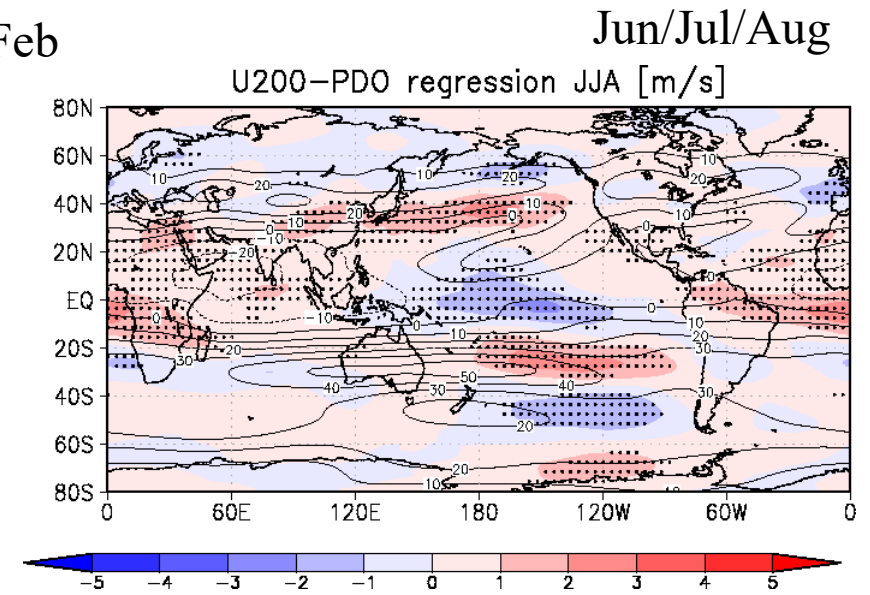
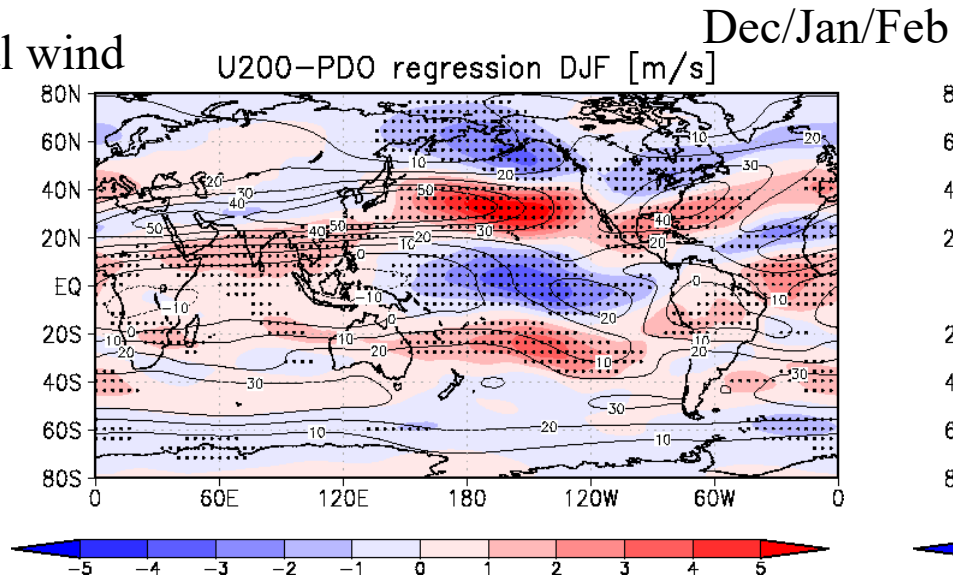
SST pattern regressed on PDO index



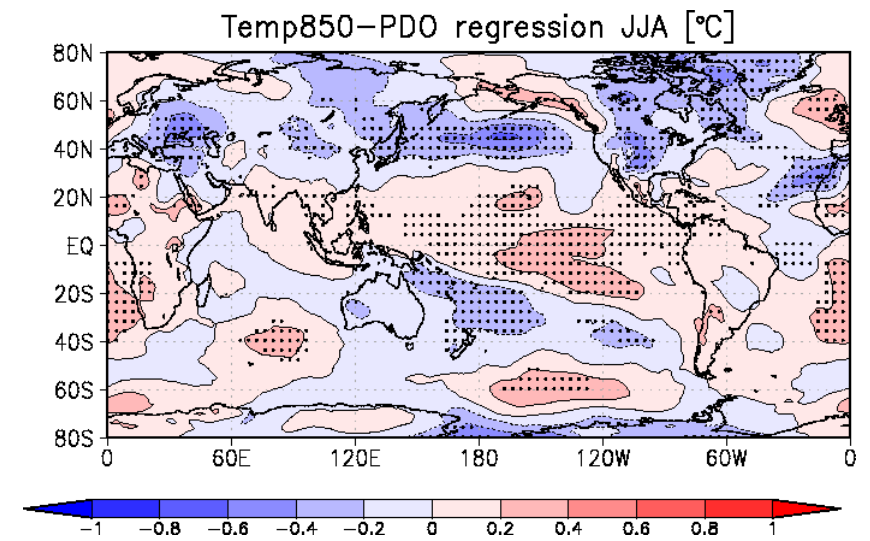
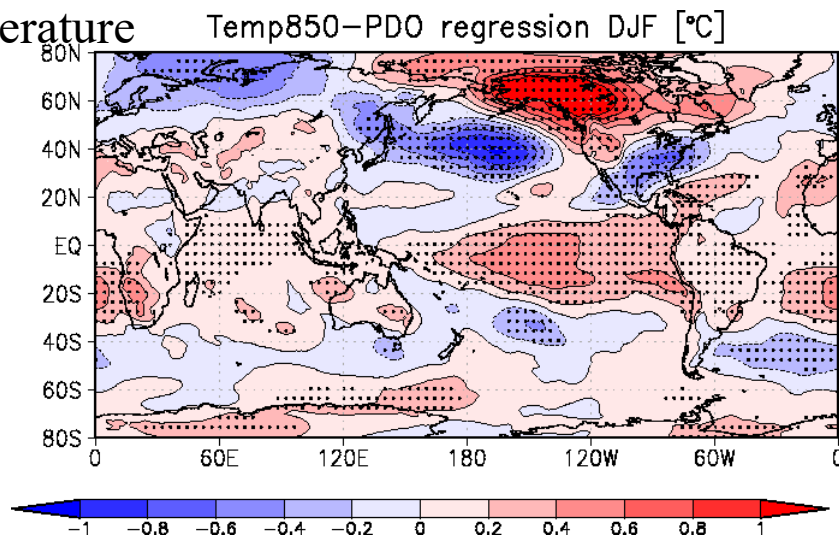
PDO index
(from JMA website)

■ PDO and local climate

Zonal wind

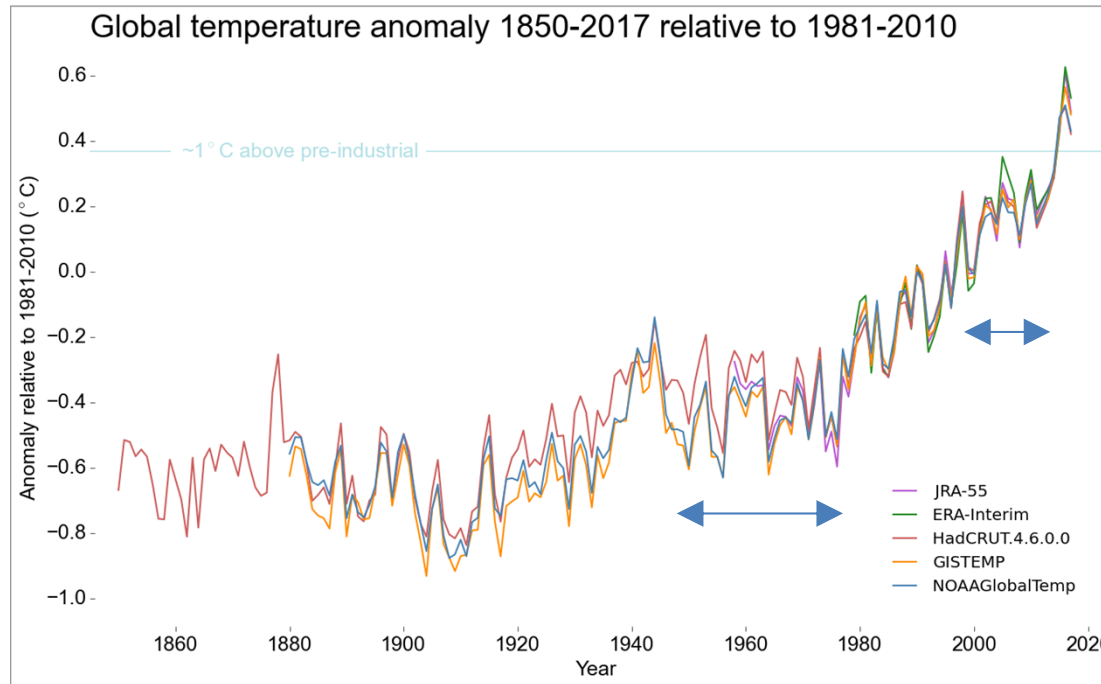


Temperature



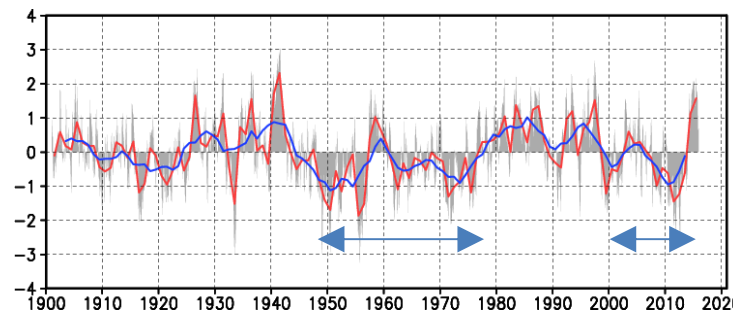
(from JMA website)

Global Warming Slowdown and PDO

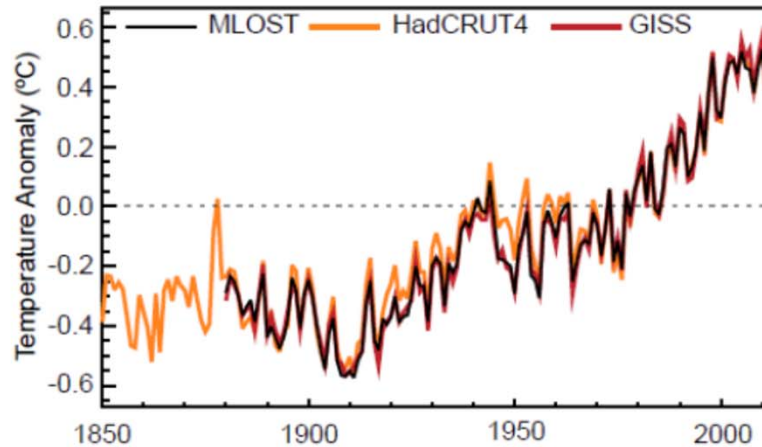


Phases of global warming slowdown (“hiatus”) correspond to the negative phase of PDO index

PDO index

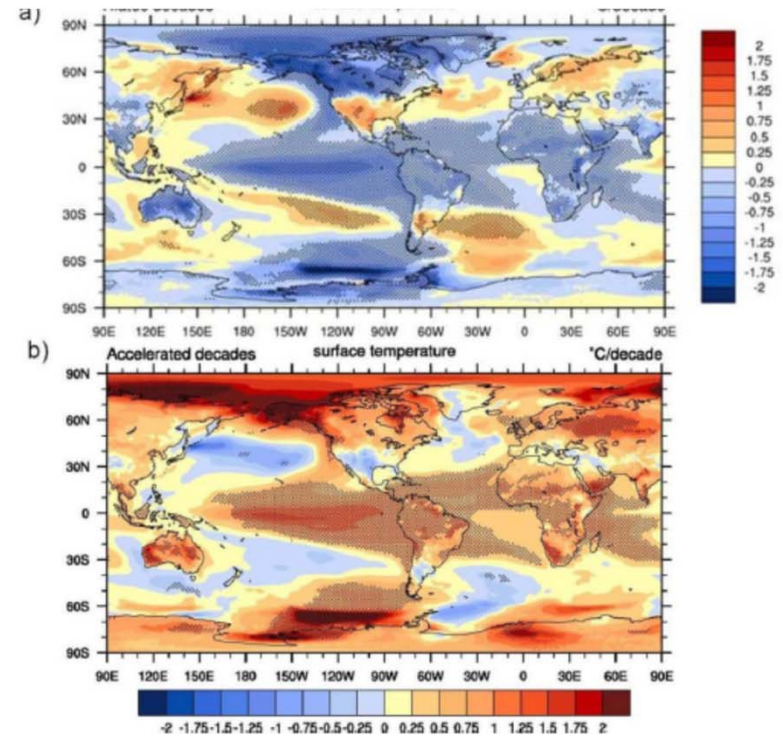


Global warming slowdown and PDO/IPO



Annual Global Mean Surface Temperature (GMST) anomalies relative to a 1961–1990 climatology from the latest version of the three combined Land-Surface Air Temperature (LSAT) and Sea Surface Temperature (SST) datasets (HadCRUT4, GISS and NCDC MLOST).

IPCC AR5 (2014)

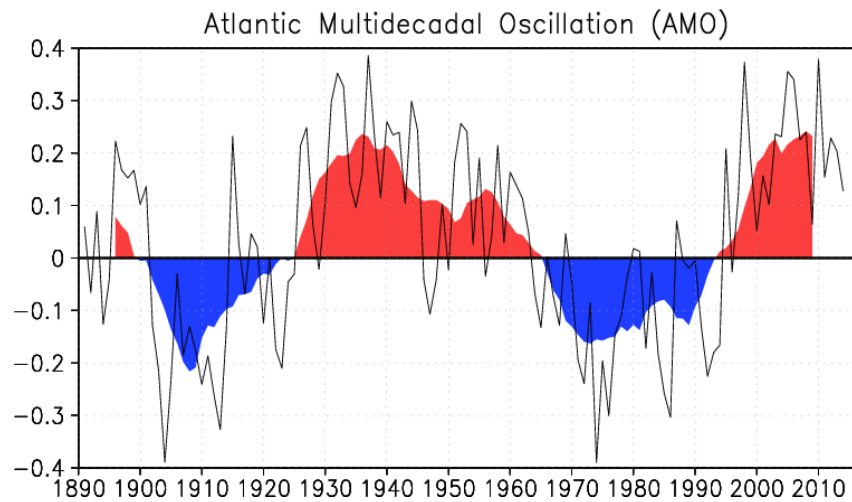


Five CCSM4 21st century simulations with RCP4.5 (uniform increase in GHGs, no volcanoes): Composites of decades with near-zero warming trend (hiatus decades) and decades with rapid global warming (accelerated warming decades) show opposite phases of the IPO in the Pacific (hiatus=linear trend of global T < -0.10K/decade; 8 hiatus decades Accelerated=linear trend of global T > +0.41K/decade; 7 accelerated warming decades)

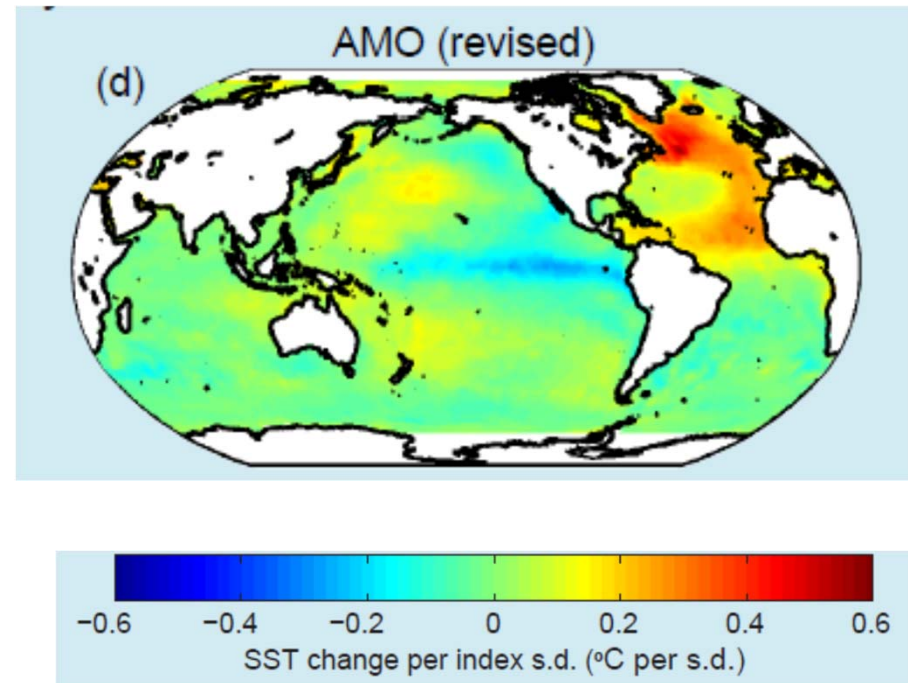
Meehl et al. (2013)

- IPO in positive phase → Accelerated warming decades
- IPO in negative phase → Hiatus decades

■ Atlantic Multidecadal Oscillation (AMO)



SST anomalies averaged in North Atlantic after removed linear trend. From JMA-HP



■ Decadal variability of ENSO/ Monsoon and their relationship

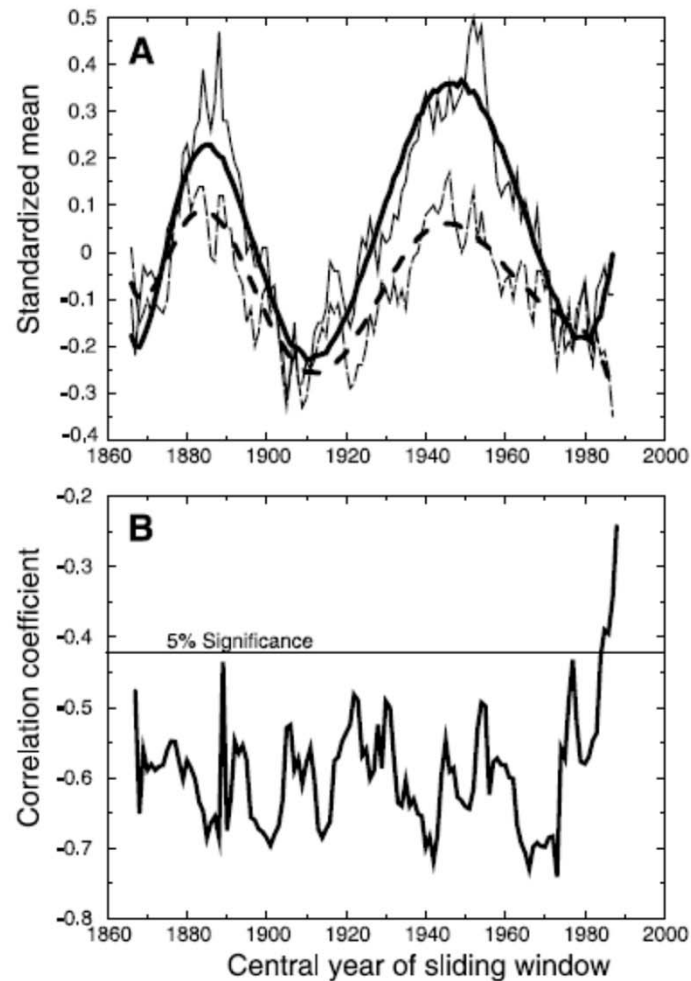


Fig. 1. (A) Shown are 21-year sliding standardized means of Indian summer monsoon rainfall (thin line) and June to August (JJA) NINO3 SST anomalies (thin dashed line) during 1856–1997. The corresponding solid lines represent the smoothed values (smoothing is done by fitting a polynomial). The sign of NINO3 SST is reversed to facilitate direct comparison. (B) Shown are 21-year sliding correlations between Indian summer monsoon rainfall and NINO3 SST anomalies (JJA) during 1856–1997. The horizontal line shows the 5% significance level.

On the Weakening Relationship Between the Indian Monsoon and ENSO

K. Krishna Kumar,^{1*} Balaji Rajagopalan,² Mark A. Cane² 1999

■ Outline of the lecture

1. Climate System (60 min. + α)

1.1 Introduction

1.2 Radiative Balance

1.3 Horizontal Radiative Imbalance and Circulations

1.4 Seasonal Change

1.5 Role of Orography on Climate

2. Climate Variability (90 min. + α)

2.1 Introduction

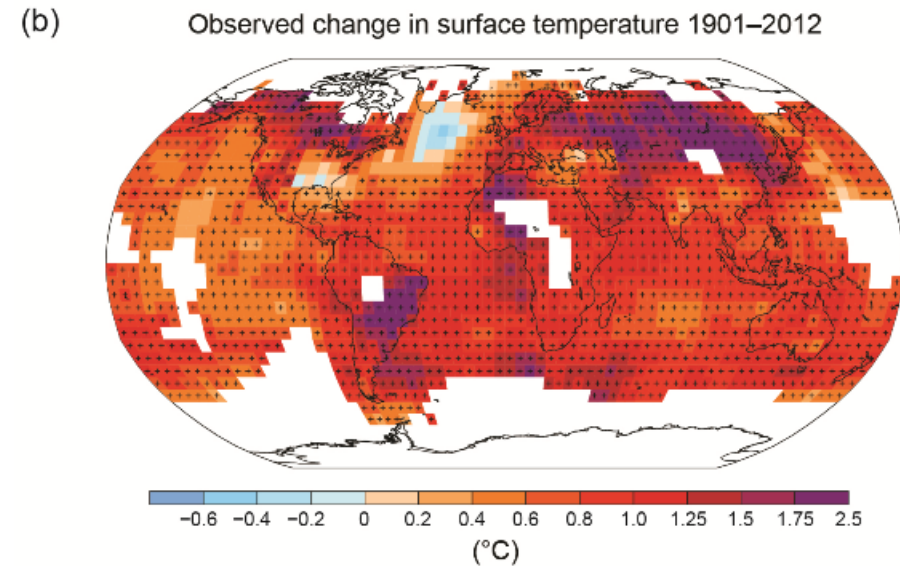
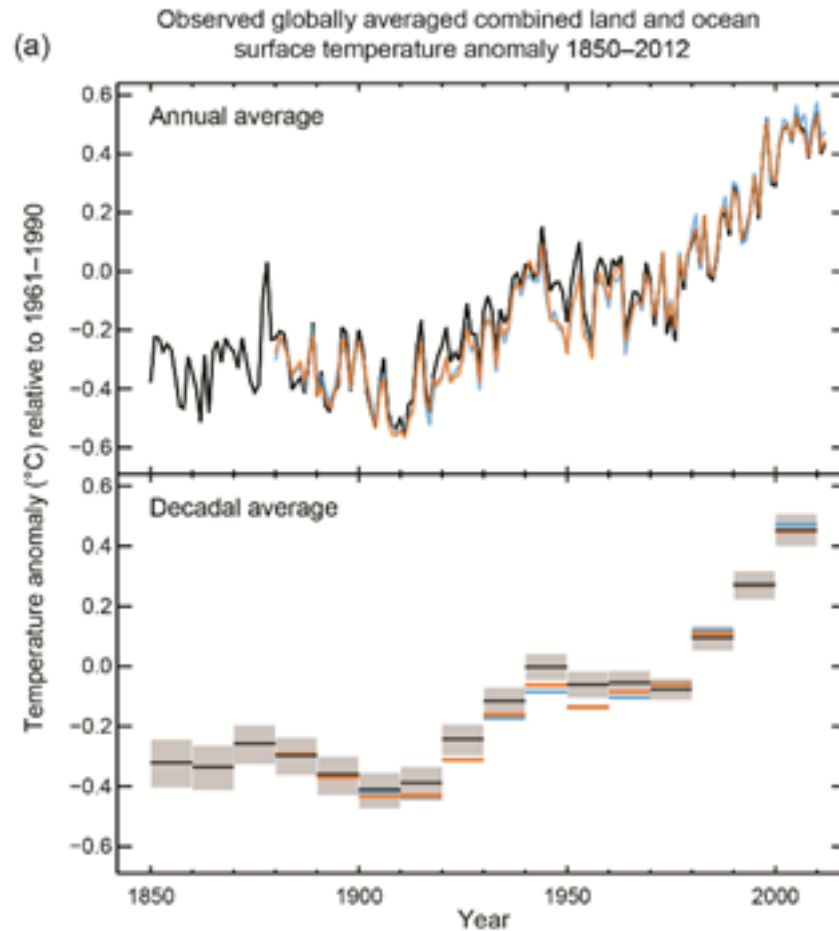
2.2 Intraseasonal Variability: Quasi-stationary Rossby wave, MJO and equatorial waves

2.3 Interannual Variability: ENSO, El Nino Modoki, IOD

2.4 Decadal Variability: PDO, ENSO-Monsoon relation

3. Climate change due to anthropogenic forcing (30 min. + α)

Global mean surface air temperature





2017 is set to be in top three hottest years, with record-breaking extreme weather

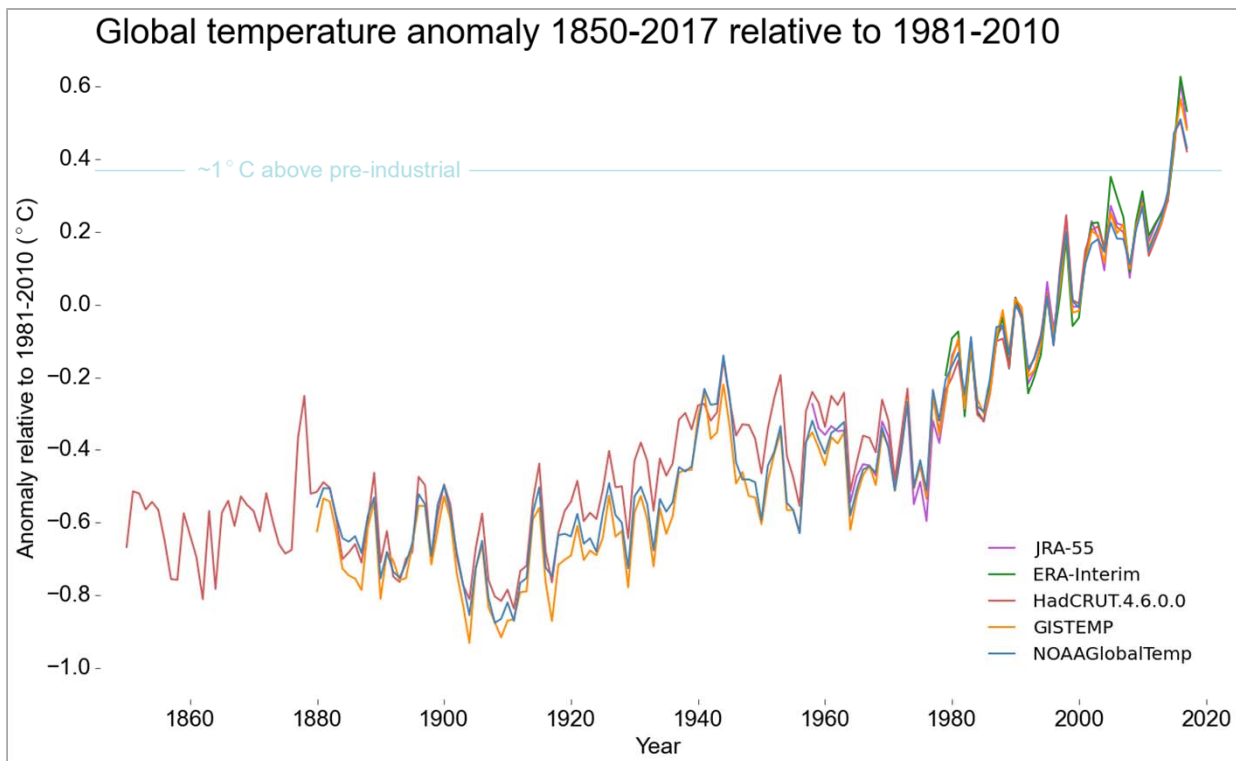
Tags: [Climate](#)

6

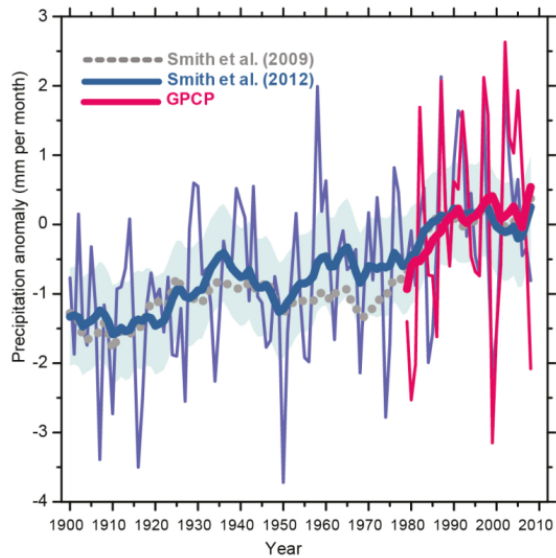
Published 6 November 2017

“The past three years have all been in the top three years in terms of temperature records. This is part of a long term warming trend,” said WMO Secretary-General Petteri Taalas.

Press Release Number: 06112017



Annual precipitation over land



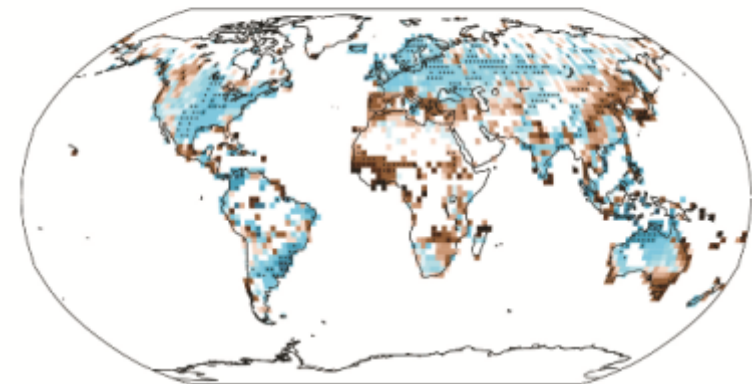
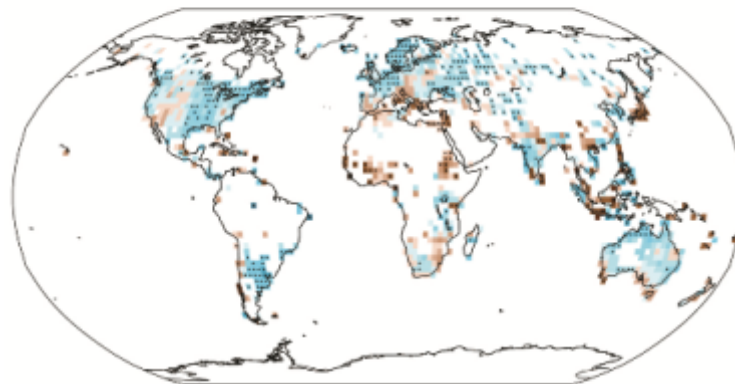
WGI_AR5_FigSPM-2

Observed change in annual precipitation over land

1901–2010

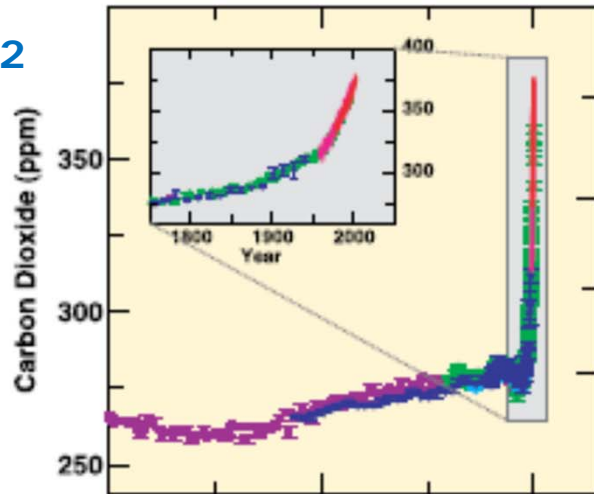
1951–2010

WGI_AR5_Fig3-7

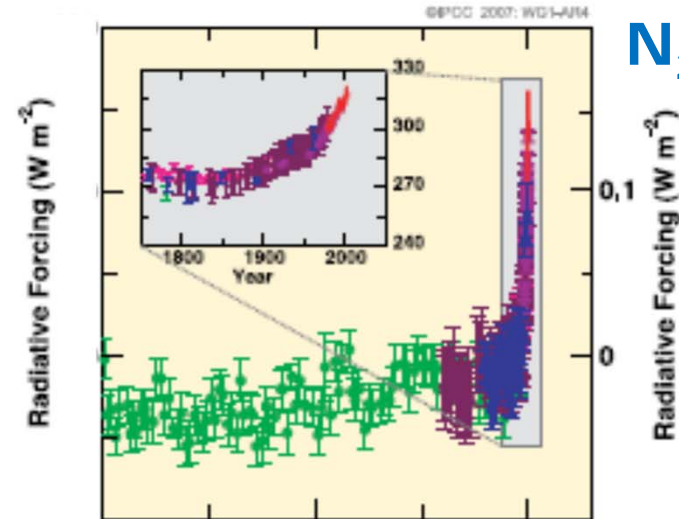


Changes in greenhouse gases

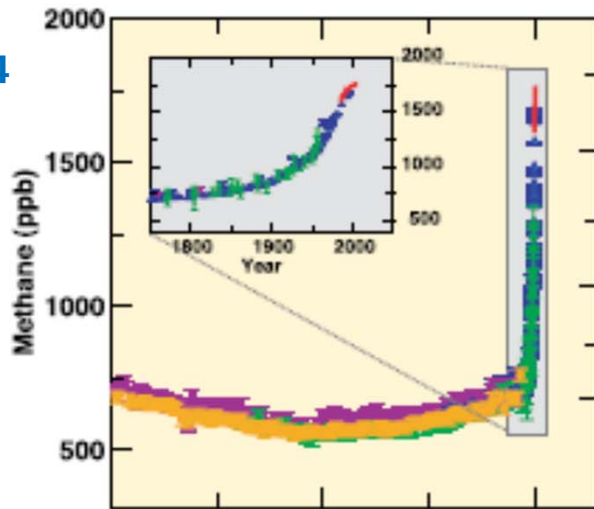
CO₂



N₂O



CH₄

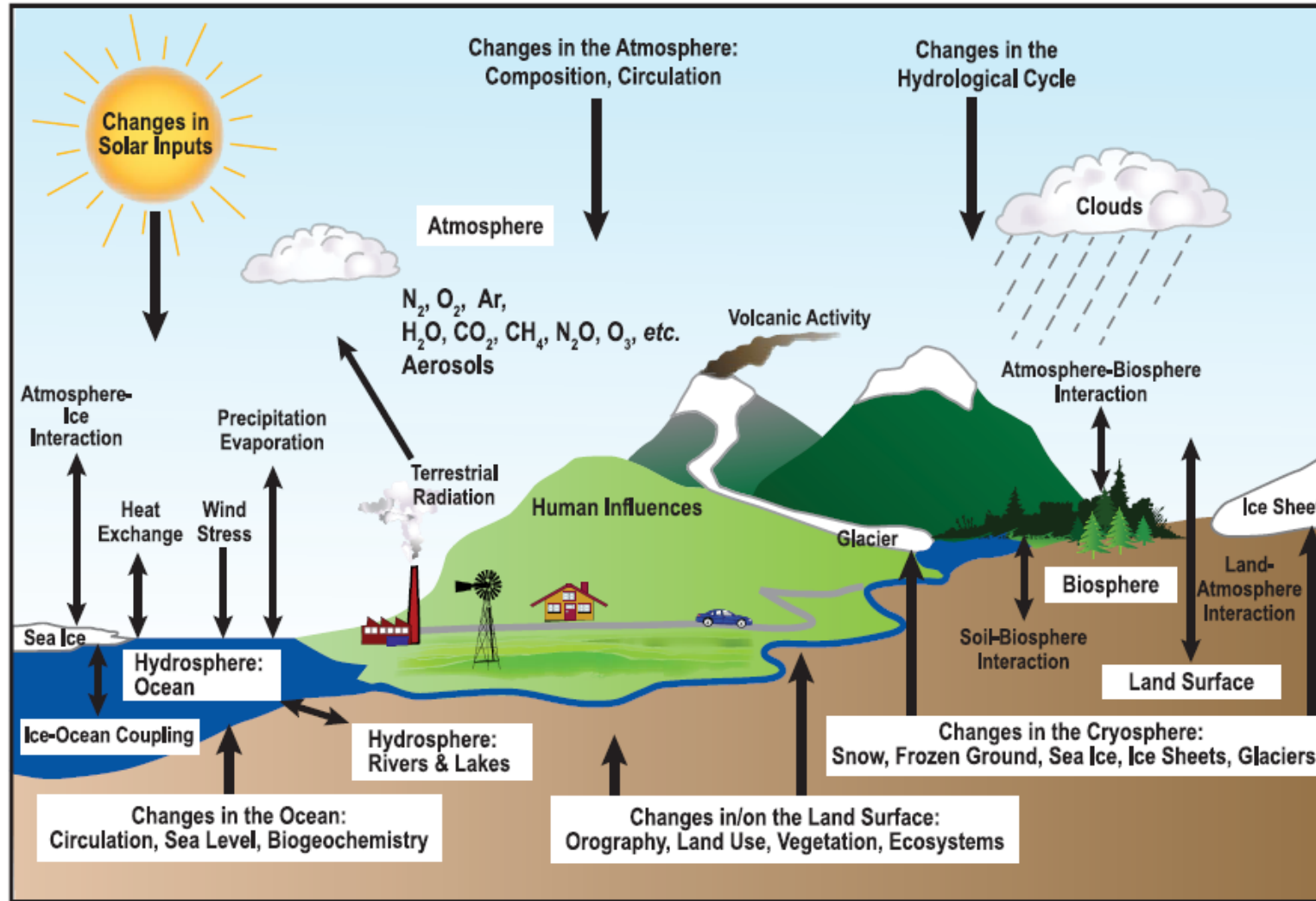


10000 5000 0
Year Before Present

(IPCC AR4)

10000 5000 0
Year Before Present

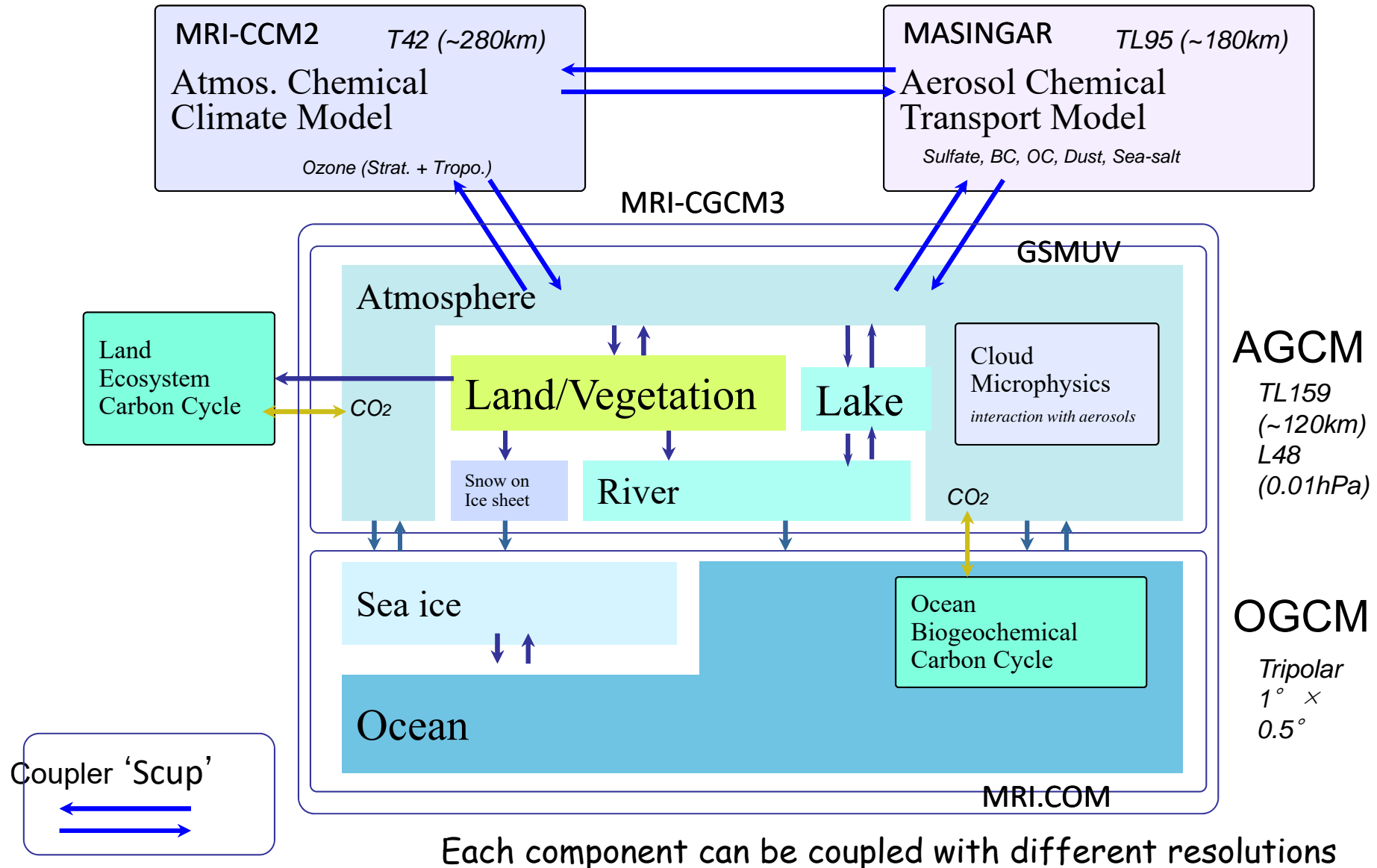
■ The climate system is complicated!



FAQ 1.2, Figure 1. Schematic view of the components of the climate system, their processes and interactions.

(IPCC AR4)

Example: MRI Earth System Model

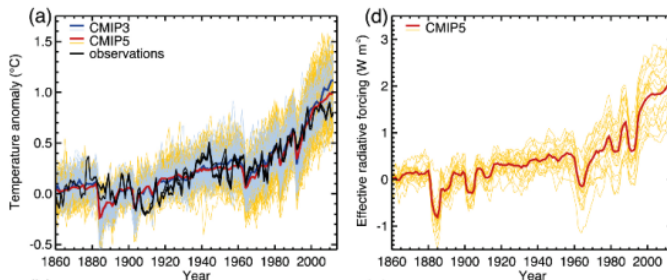


Historical Global Warming Experiments

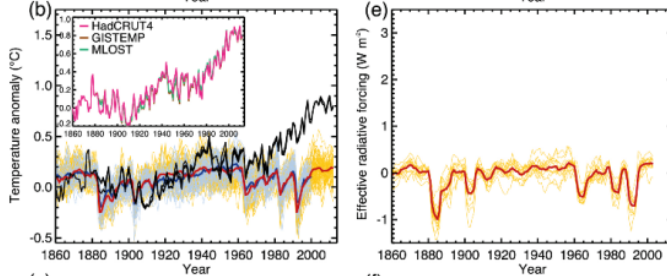
- Radiative forcing is the difference between insolation (sunlight) absorbed by the Earth and energy radiated back to space.

Model Experiments

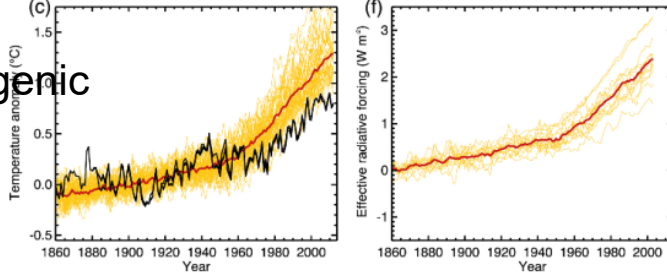
All forcing



Natural forcing only

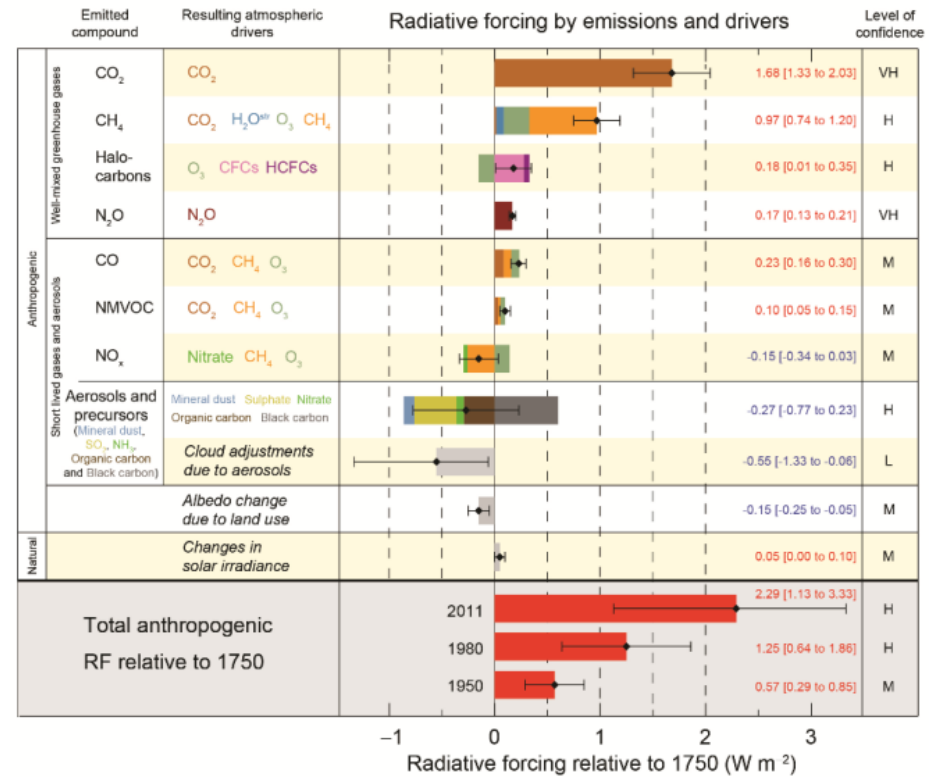


Anthropogenic forcing only



WGI_AR5_Fig10-1

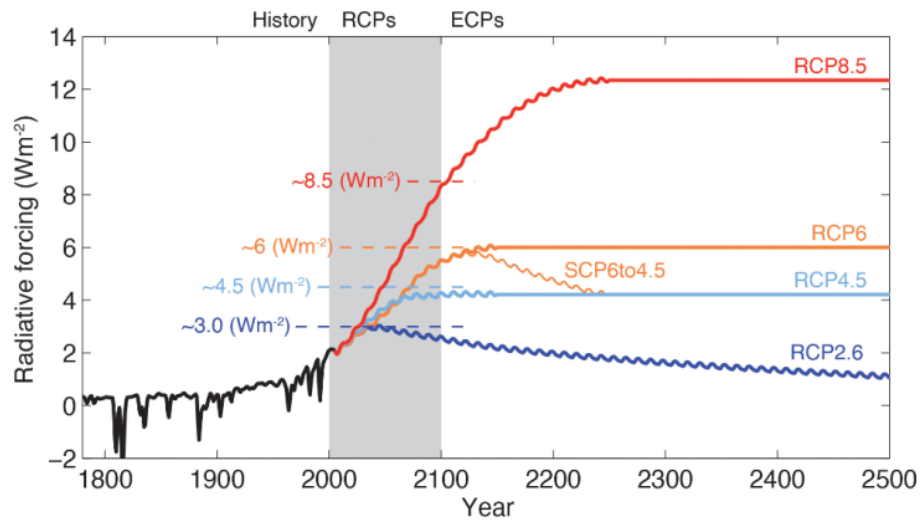
Radiative Forcing



WGI_AR5_FigSPM-5

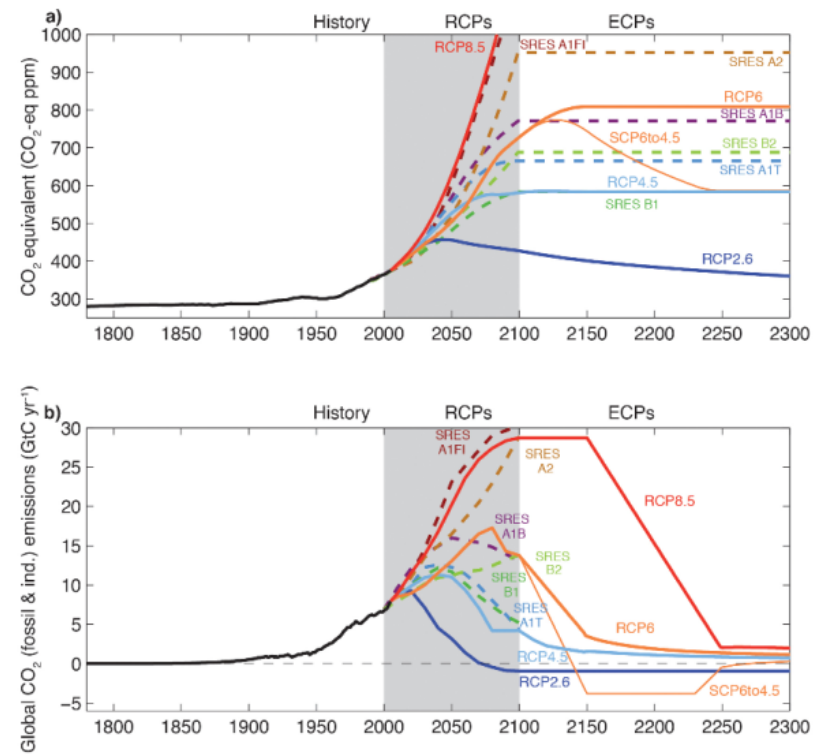
Future Scenarios

Radiative Forcing



WGI_AR5_FigBox11-1

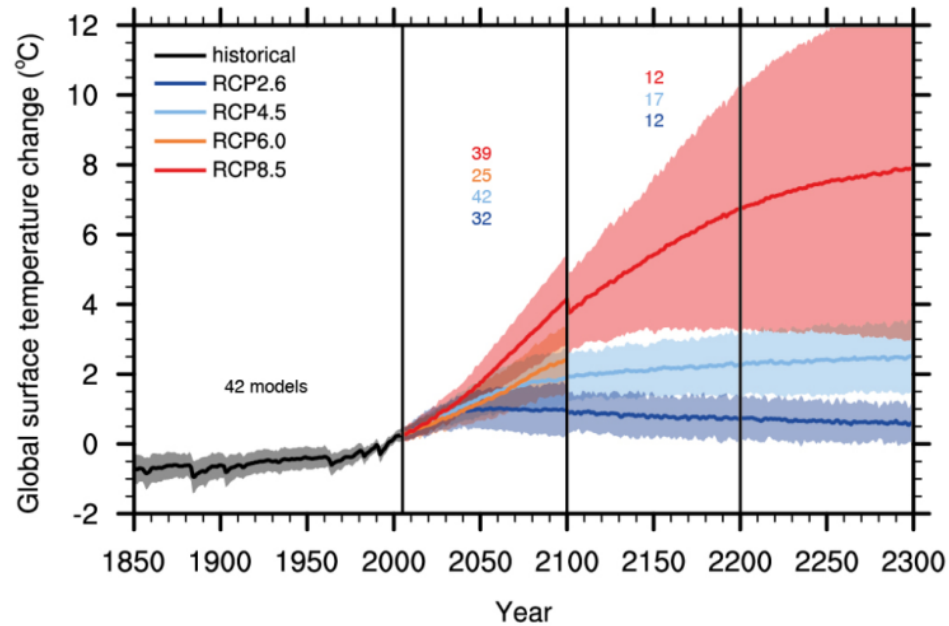
CO2 and Emission



WGI_AR5_FigBox1_1-3

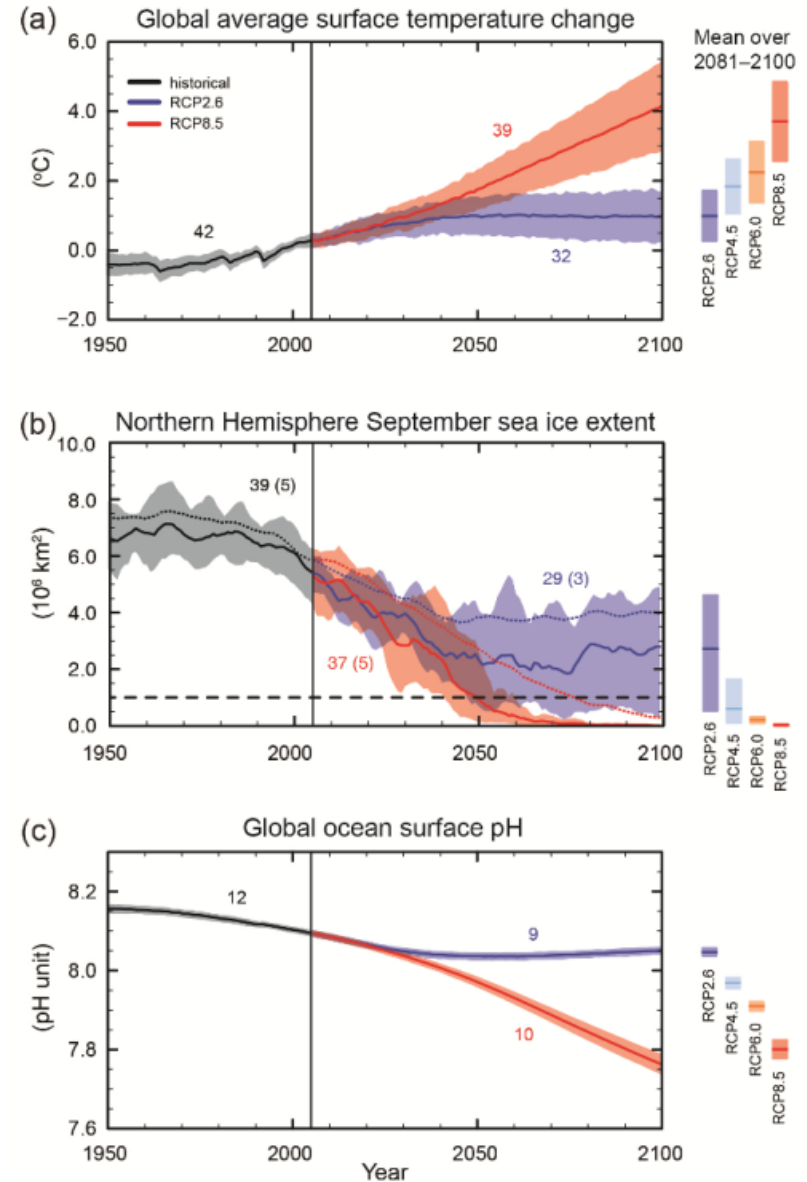
Future Projection

Surface temperature



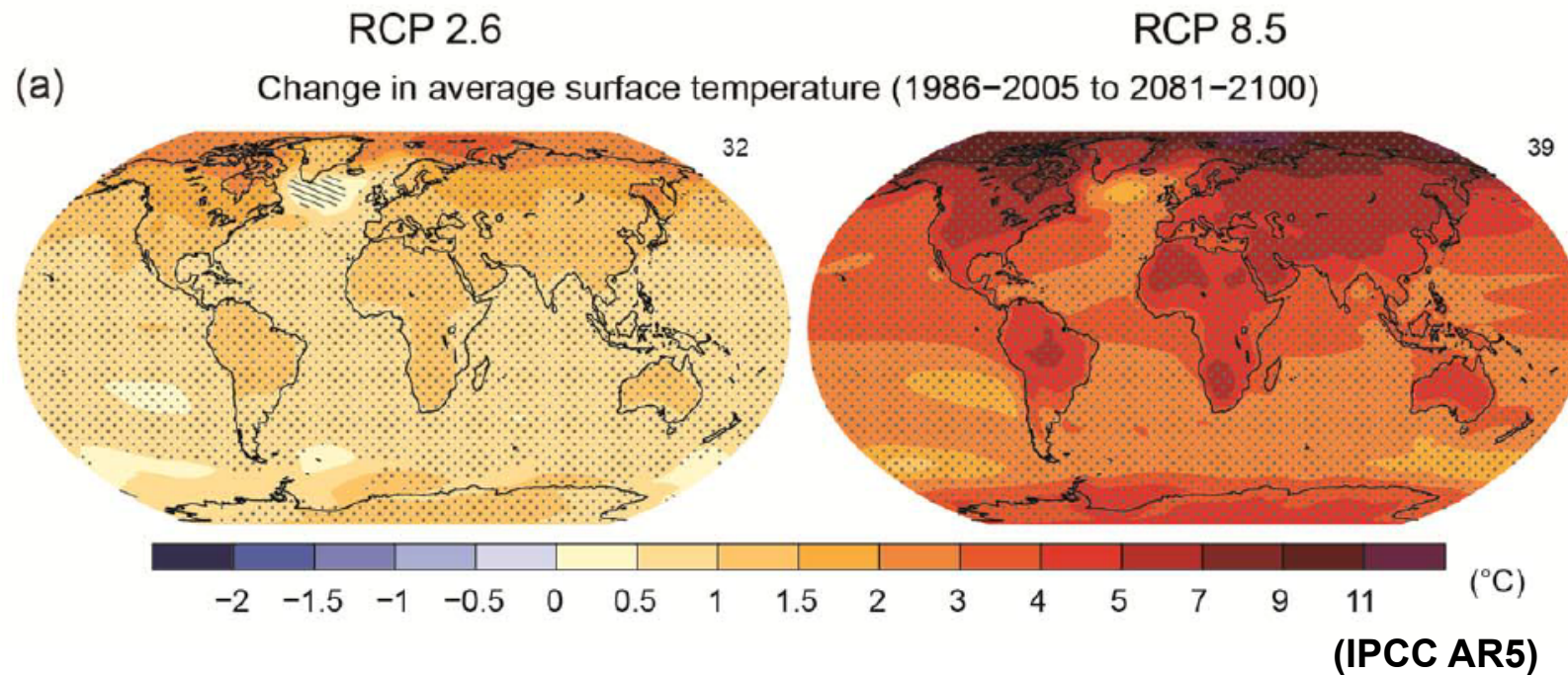
WGI_AR5_Fig12-5

WGI_AR5_FigSPM-7



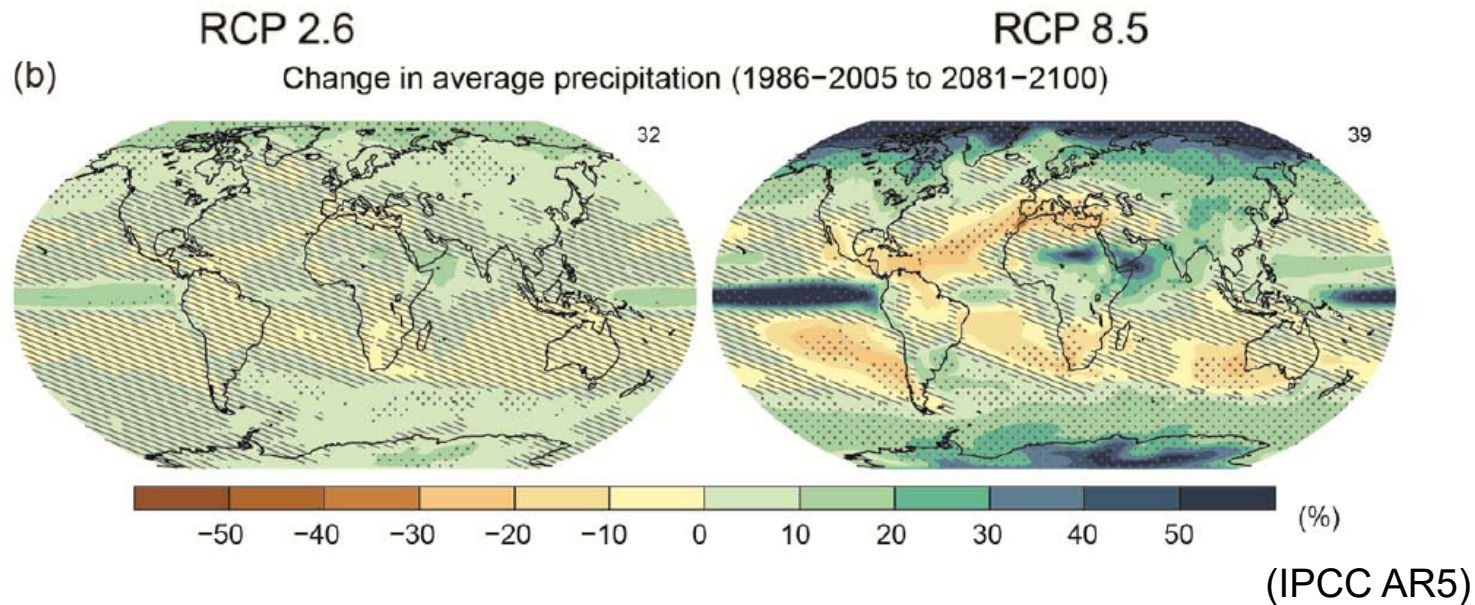
■ Map of Warming Projections for Late 21C

- Large difference depending on the regions
- Larger warming over lands and high-latitudes

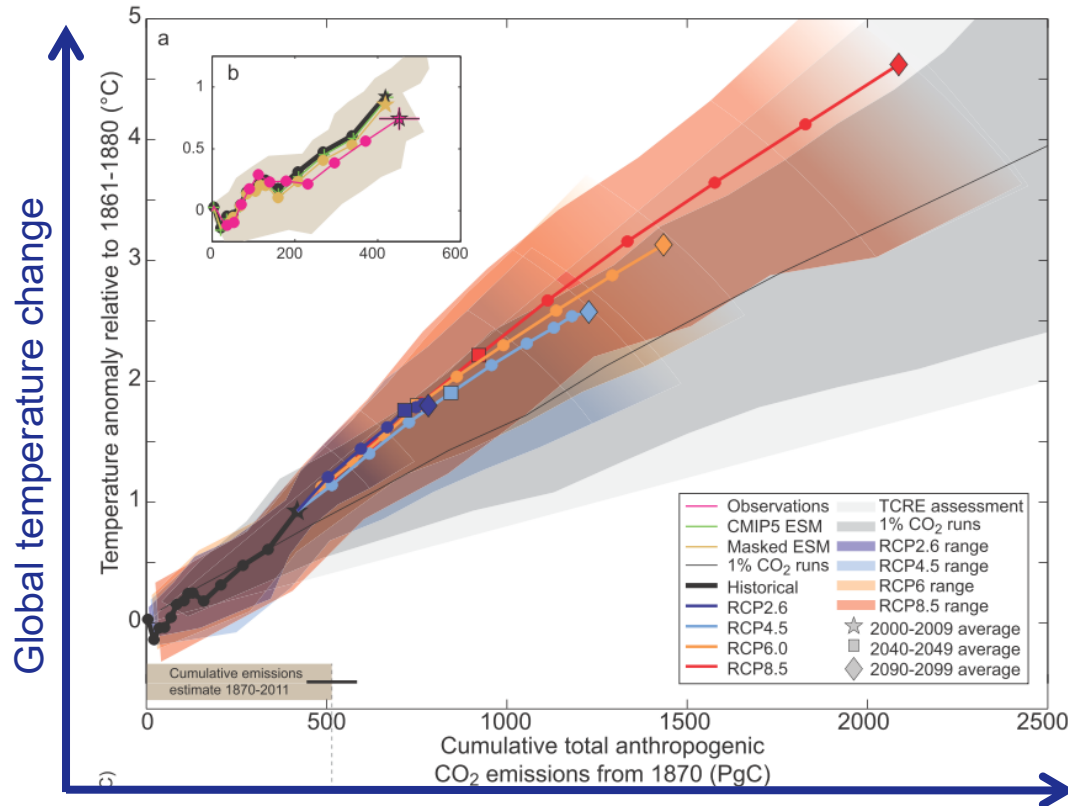


■ Precipitation Change

- Increase of precipitation near the currently rainy regions (“wet-get-wetter” effect)
- Both flood risk and drought risk should be considered



Temperature Change vs Cumulative CO2 Emission



Warming is proportional to total cumulative CO2 emissions

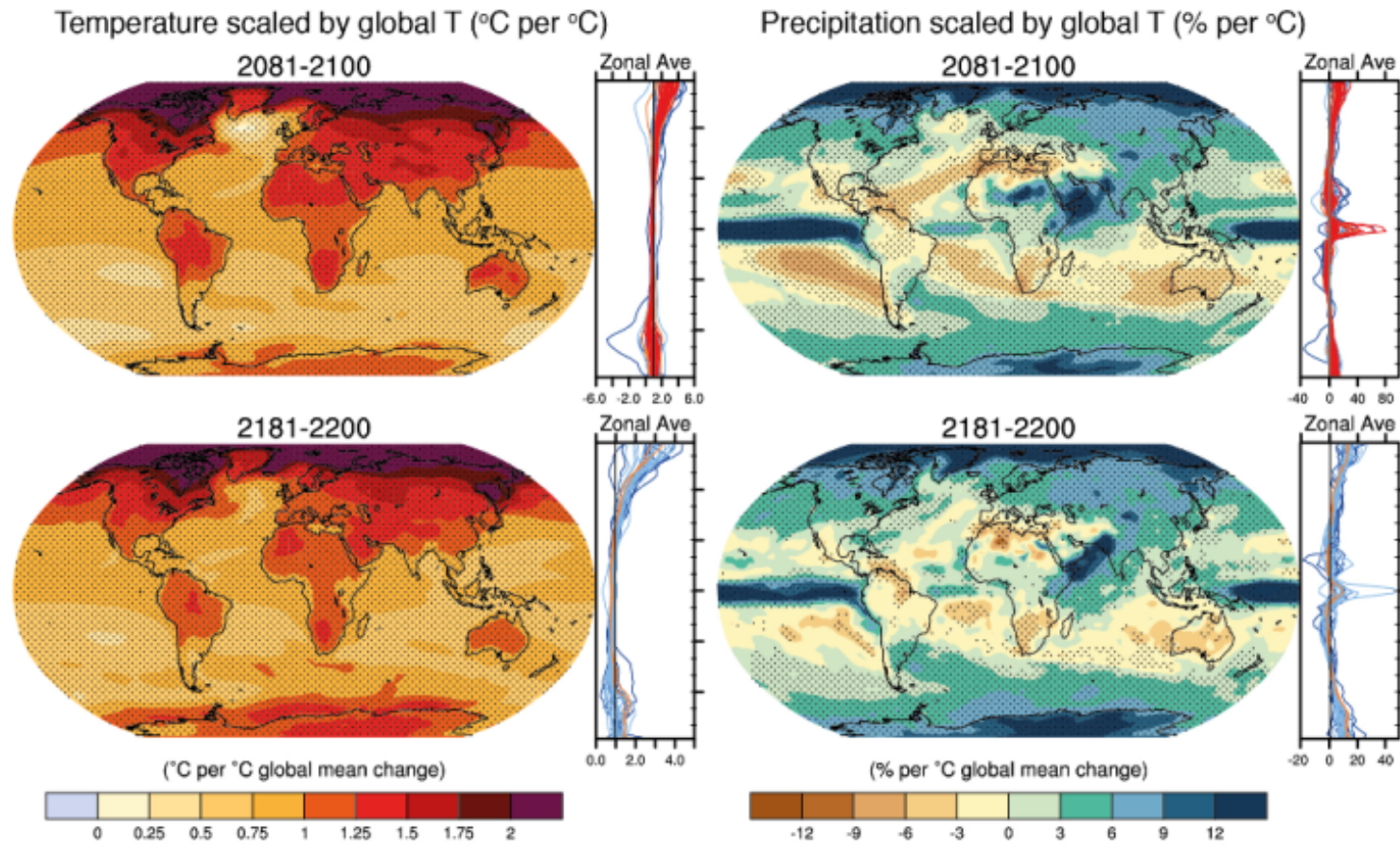


Warming continues even if emission is reduced.

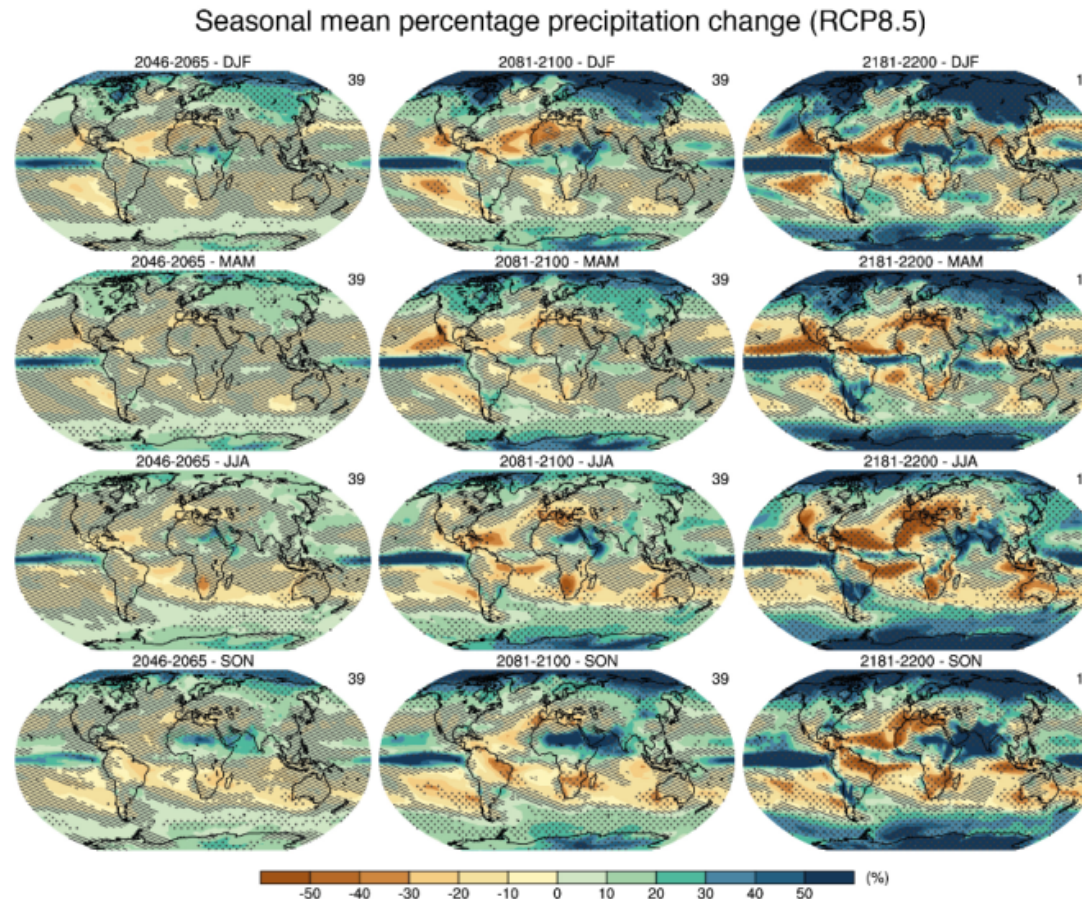
Zero emission is not enough to go back.

The total amount of anthropogenic CO₂ released in the atmosphere since pre-industrial (IPCC AR5)

■ Ts and Precipitation Changes



■ Seasonal Precipitation Change

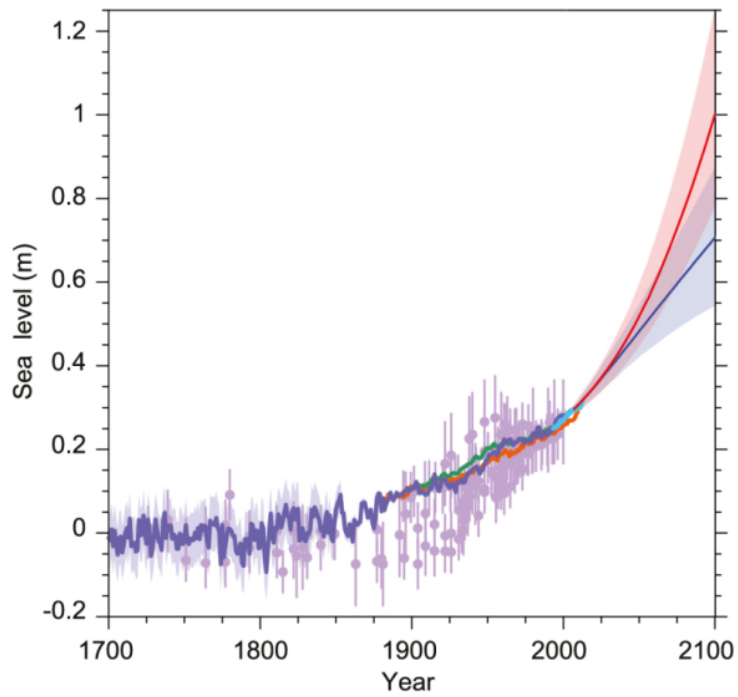


WGI_AR5_Fig12-22

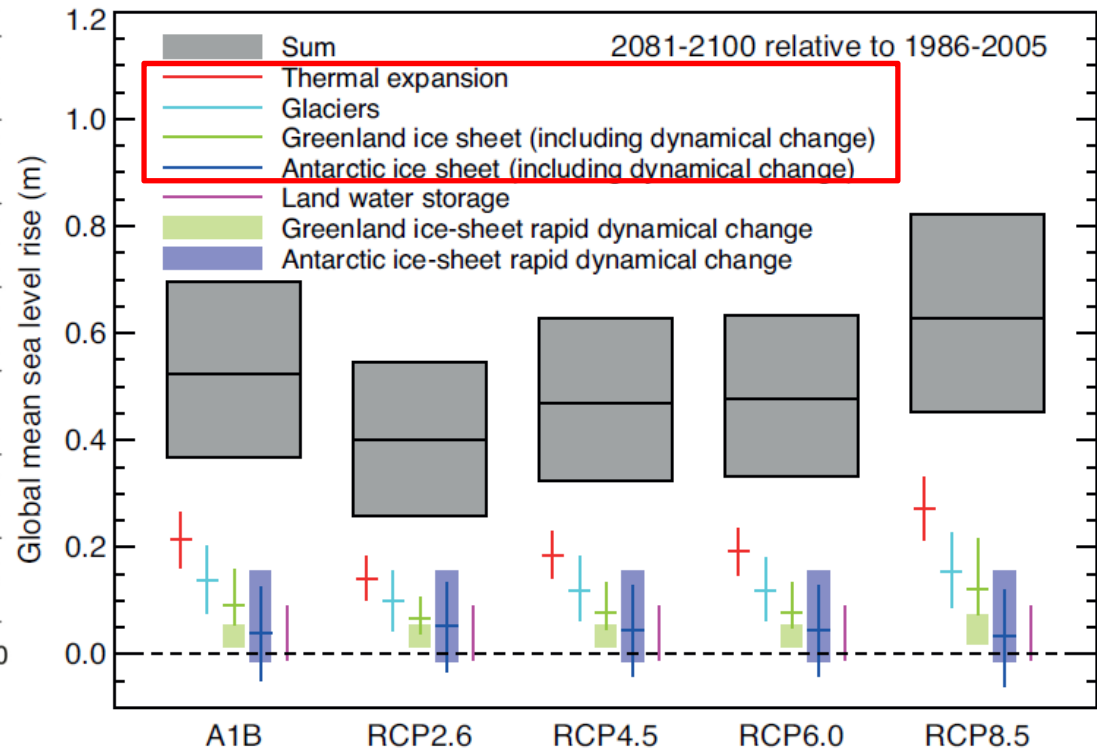
Figure 12.22 | Multi-model CMIP5 average percentage change in seasonal mean precipitation relative to the reference period 1986–2005 averaged over the periods 2045–2065, 2081–2100 and 2181–2200 under the RCP8.5 forcing scenario. Hatching indicates regions where the multi-model mean change is less than one standard deviation of internal variability. Stippling indicates regions where the multi-model mean change is greater than two standard deviations of internal variability and where at least 90% of models agree on the sign of change (see Box 12.1).

■ Sea Level Rise

Sea level rise comes from thermal expansion, as well as retreating glaciers and ice sheet



WGI_AR5_Fig13-27



WGI_AR5_Fig13-10

■ Five-day Precipitation amount and Dry days

WGI_AR5_Fig12-26

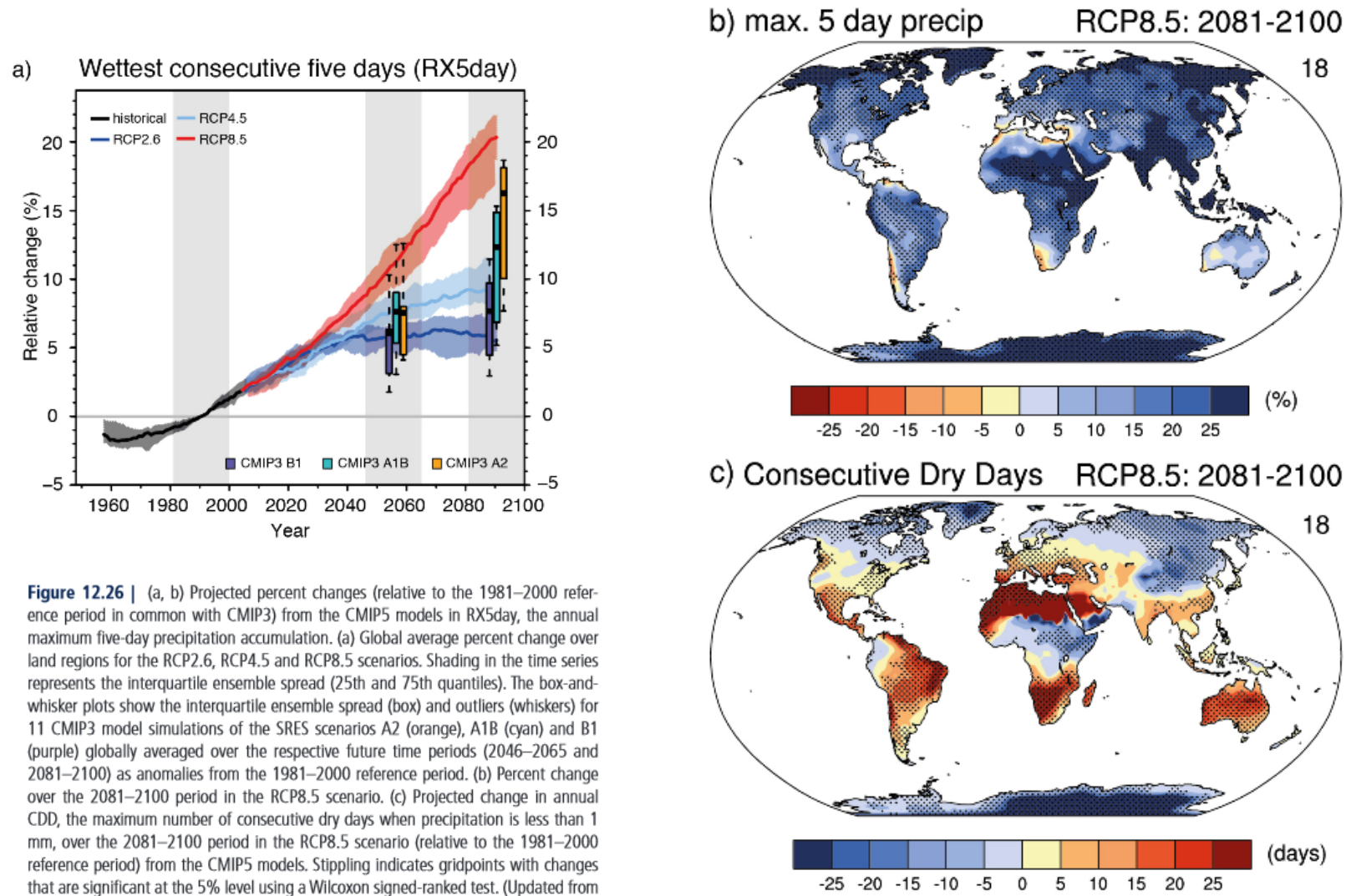
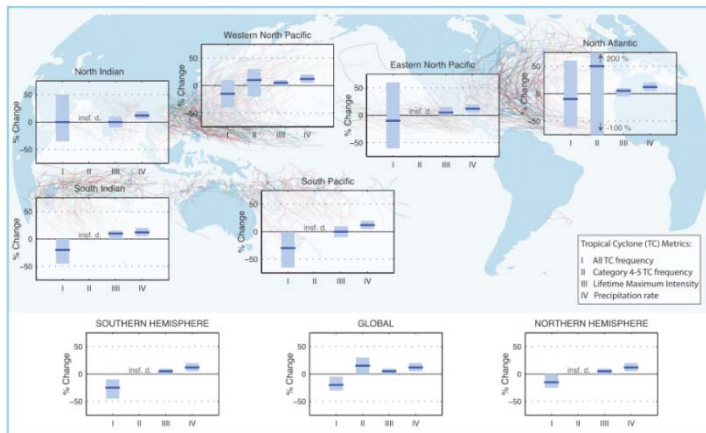


Figure 12.26 | (a, b) Projected percent changes (relative to the 1981–2000 reference period in common with CMIP3) from the CMIP5 models in RX5day, the annual maximum five-day precipitation accumulation. (a) Global average percent change over land regions for the RCP2.6, RCP4.5 and RCP8.5 scenarios. Shading in the time series represents the interquartile ensemble spread (25th and 75th quantiles). The box-and-whisker plots show the interquartile ensemble spread (box) and outliers (whiskers) for 11 CMIP3 model simulations of the SRES scenarios A2 (orange), A1B (cyan) and B1 (purple) globally averaged over the respective future time periods (2046–2065 and 2081–2100) as anomalies from the 1981–2000 reference period. (b) Percent change over the 2081–2100 period in the RCP8.5 scenario. (c) Projected change in annual CDD, the maximum number of consecutive dry days when precipitation is less than 1 mm, over the 2081–2100 period in the RCP8.5 scenario (relative to the 1981–2000 reference period) from the CMIP5 models. Stippling indicates gridpoints with changes that are significant at the 5% level using a Wilcoxon signed-ranked test. (Updated from Sillmann et al. (2013), excluding the FGOALS-s2 model)

Changes in Regional Climate and Extreme Events

- Changes in high-impact weather events are the direct risk to people.
- However, regional characteristics of the changes cannot be directly simulated by CMIP5 global climate models.



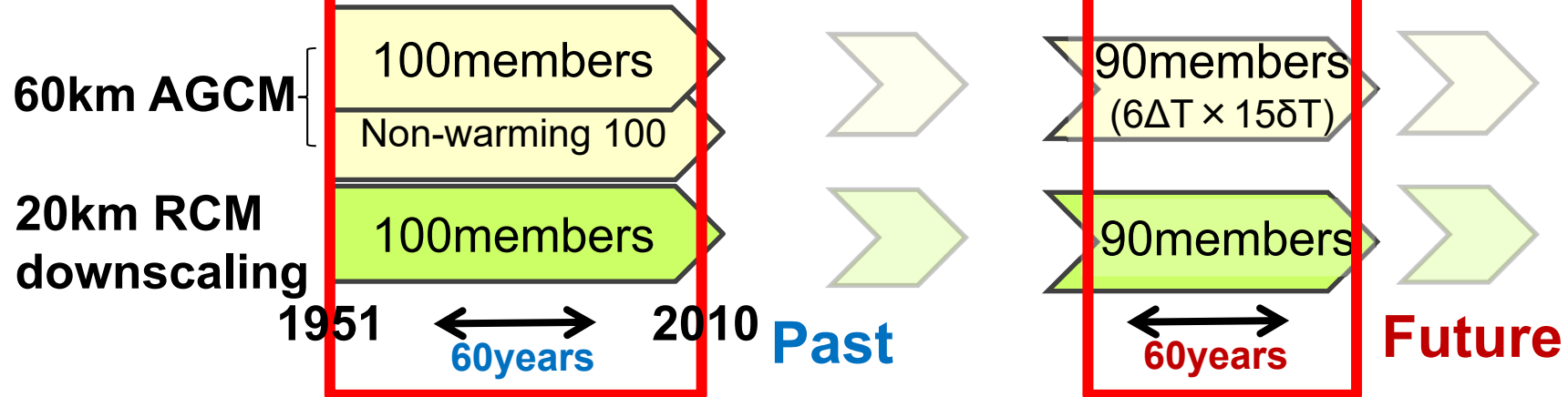
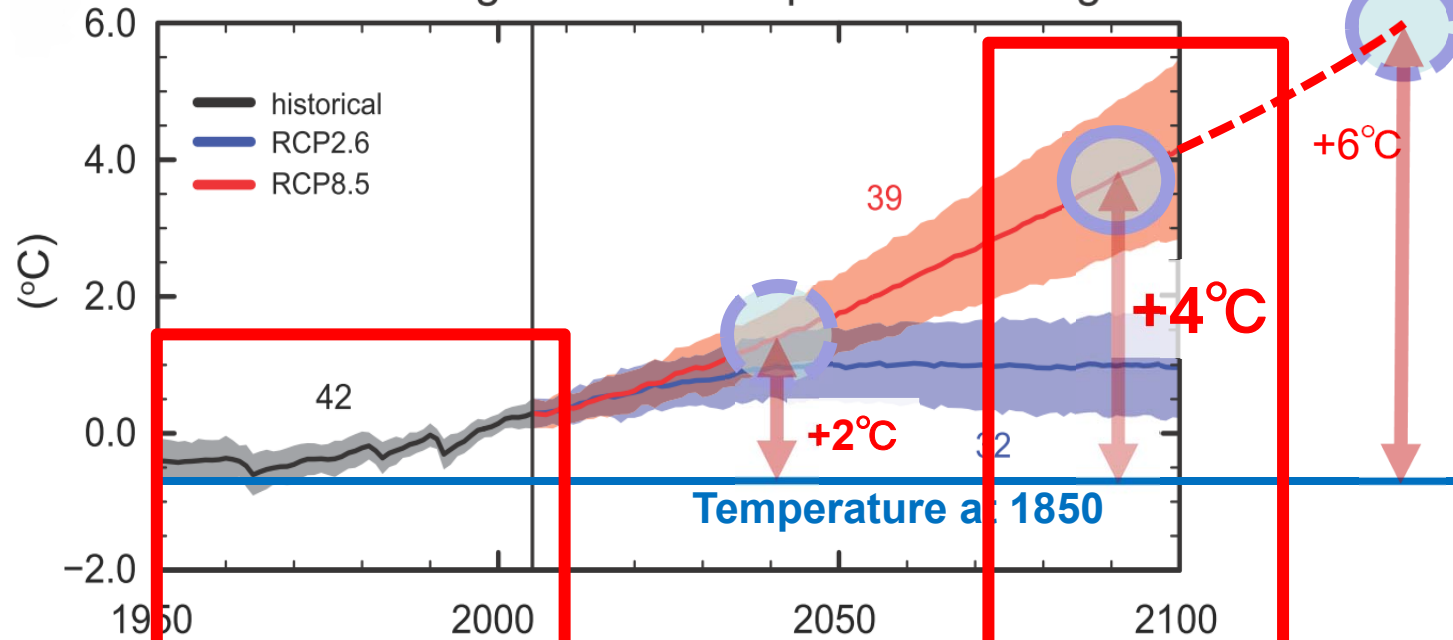
Phenomenon and direction of trend	Likelihood of further changes	
		Late 21st century
Warmer and/or fewer cold days and nights over most land areas	{11.3}	Virtually certain Virtually certain Virtually certain
Warmer and/or more frequent hot days and nights over most land areas	{11.3}	Virtually certain Virtually certain Virtually certain
Warm spells/heat waves. Frequency and/or duration increases over most land areas	{11.3}	Very likely Very likely Very likely
Heavy precipitation events. Increase in the frequency, intensity, and/or amount of heavy precipitation	{11.3}	Very likely over most of the mid-latitude land masses and over wet tropical regions Likely over many areas Very likely over most land areas
Increases in intensity and/or duration of drought	{11.3}	Likely (medium confidence) on a regional to global scale ^b Medium confidence in some regions Likely ^e
Increases in intense tropical cyclone activity	{11.3}	More likely than not in the Western North Pacific and North Atlantic ^c More likely than not in some basins Likely
Increased incidence and/or magnitude of extreme high sea level	{13.7}	Very likely ^f Very likely ^m Likely

(IPCC AR5)



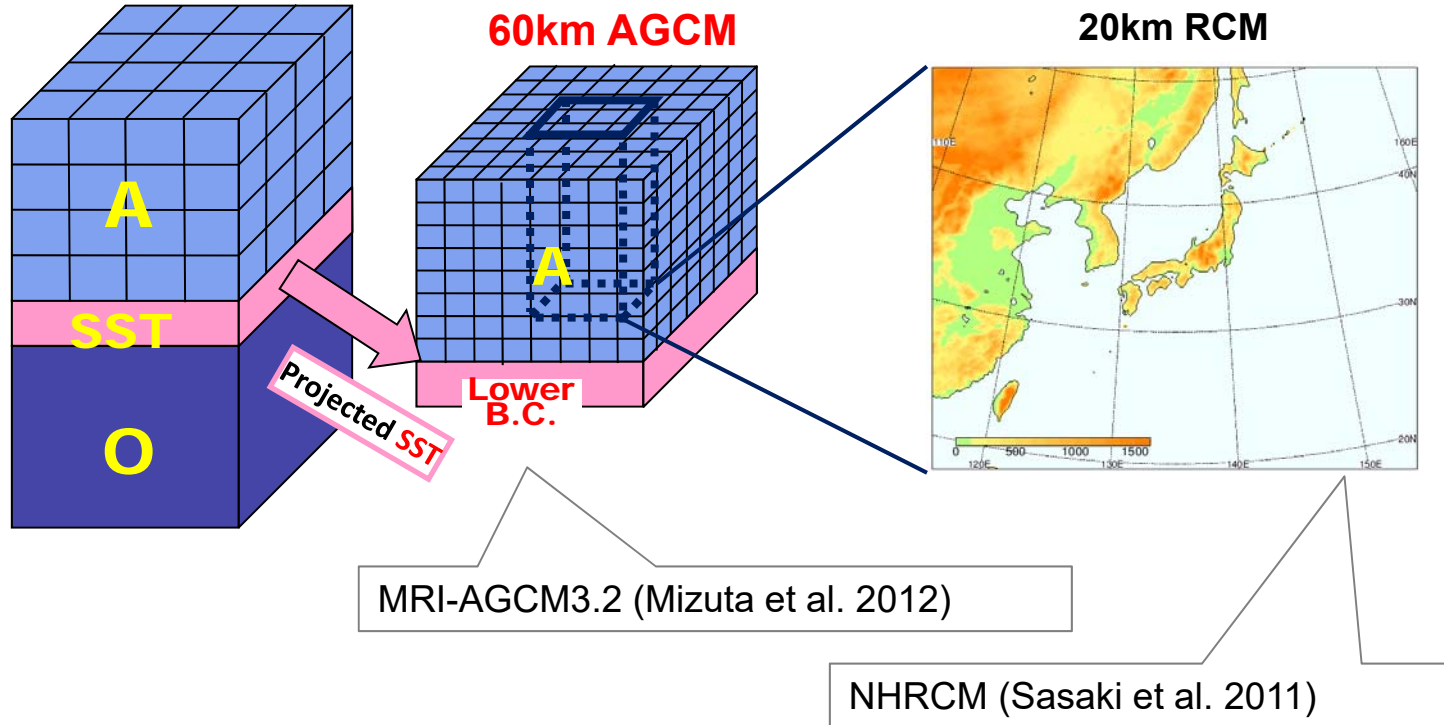
d4PDF:
database for Policy Decision
making for Future climate change

Global average surface temperature change



■ 60km AGCM + 20km RCM

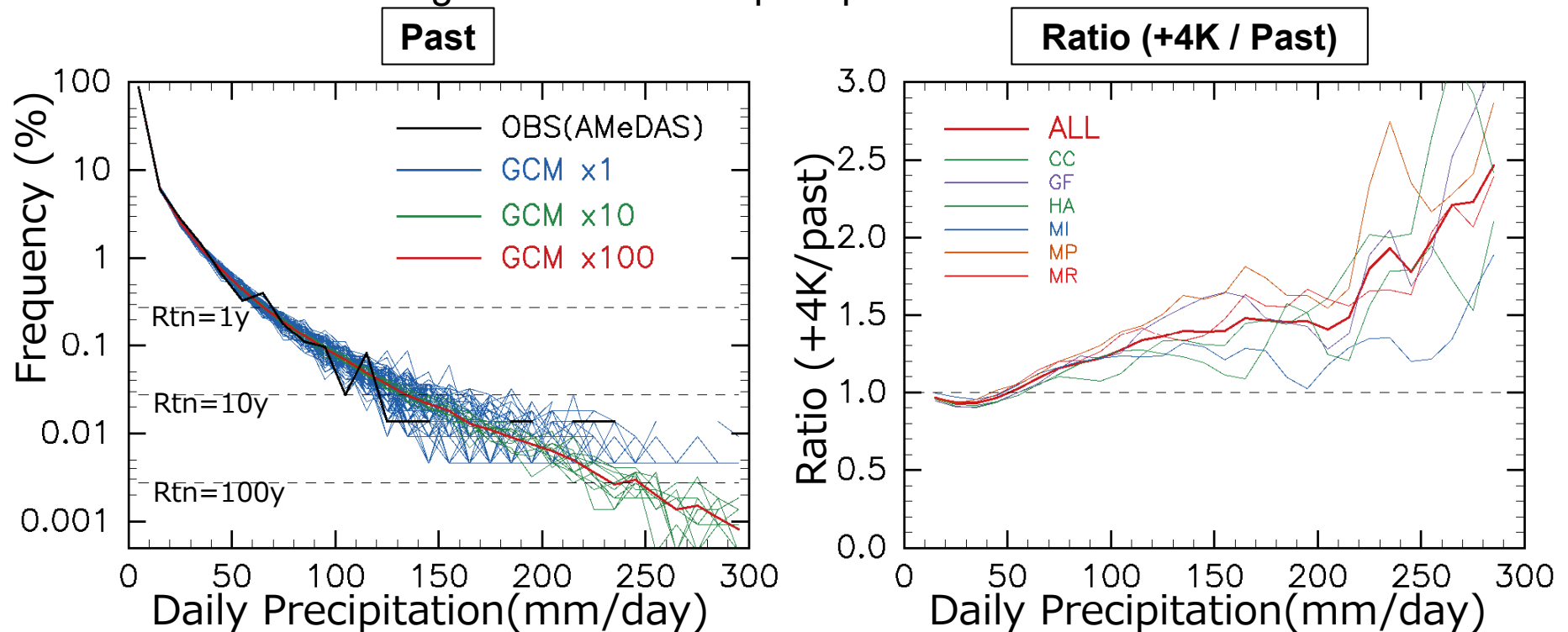
CMIP Climate Models



- 60km AGCM is:
 - lowest resolution capable of simulating tropical cyclones
 - highest possible resolution for large ensembles at the latest super computer

■ Benefits from high-res large ensemble

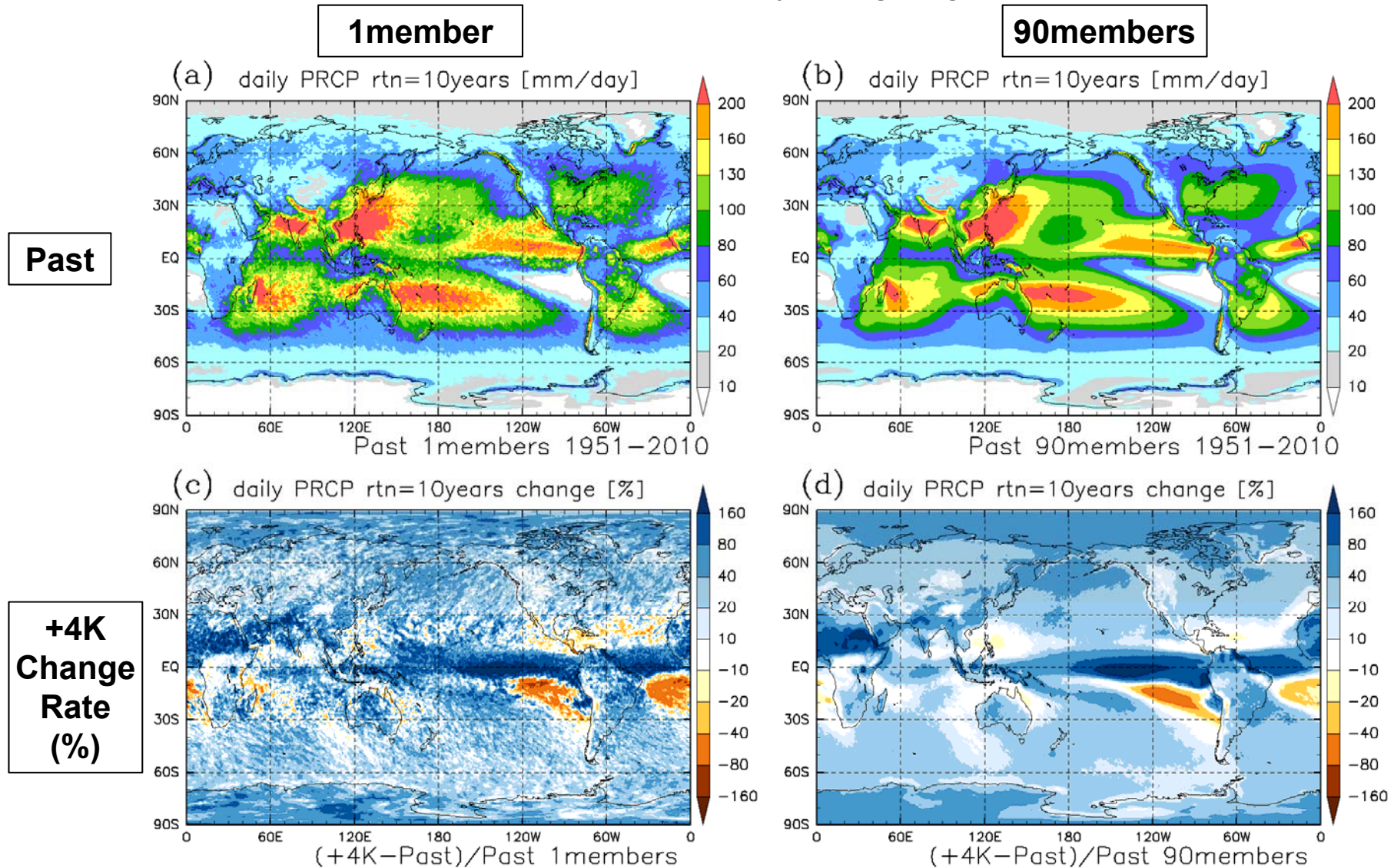
- Frequency distribution of daily precipitation at Tokyo
 - Ensemble spread between members (**Blue**) is large in rare events
 - Observation (**Black**) is inside the ensemble spread without any bias corrections
 - Results from the total 100 members (**Red**) shows reasonable frequencies of extremes as low as 0.003%(=once in 100 years)
 - Increase is larger in the heavier precipitation rate



(Mizuta et al. 2017)

10-year return value of daily precipitation

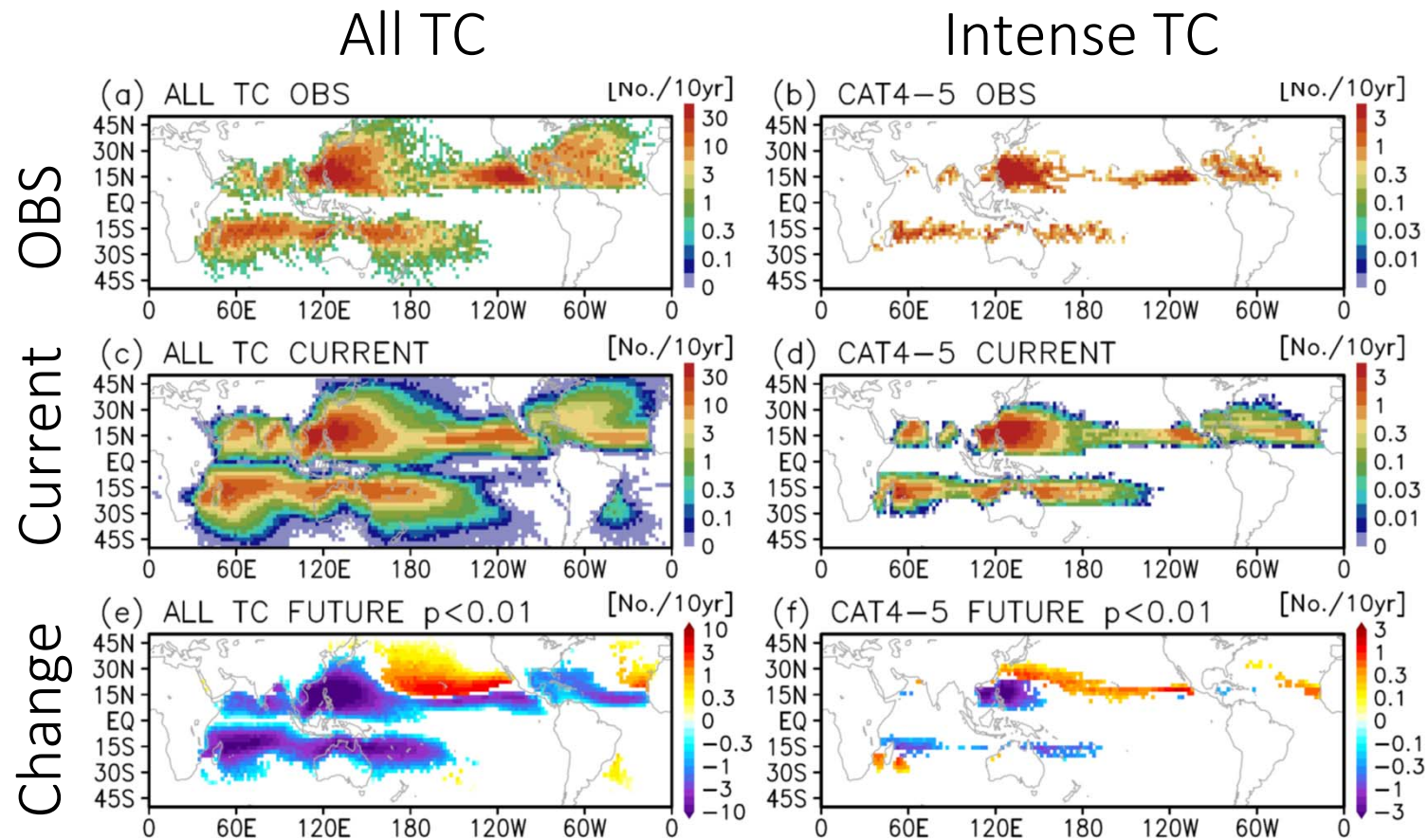
Clear and smooth picture can be obtained by using large ensembles



(Mizuta et al. 2017)

■ Tropical Cyclone Frequencies

- Similar, but smoother distribution compared with the observation
- After the bias correction for the 60km model, Category 4-5 increases on N. W. side of Pacific and Atlantic, as well as eastern side.



(Yoshida et al. 2017)

Future Change in Tropical Cyclones

Projection of the Change in Future Weather Extremes Using Super-High-Resolution Atmospheric Models

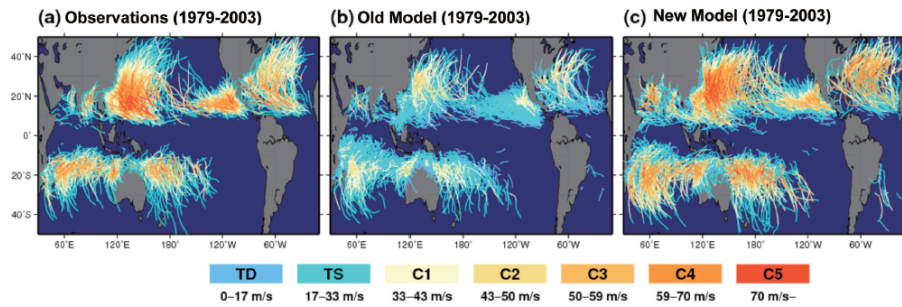


Figure 1. Global distribution of tropical cyclones for (a) observations, (b) the present-day simulation using the old model, and (c) using the new model. Tropical cyclone track

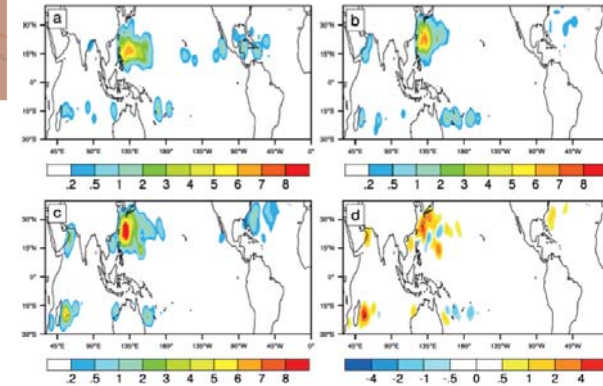


Figure 2. Tropical cyclone frequency of Category 5 storms for (a) observations (1979–2003), (b) present-day simulation by the new model (1979–2003), (c) future simulation, and (d) future changes. Unit is number per 25 years.

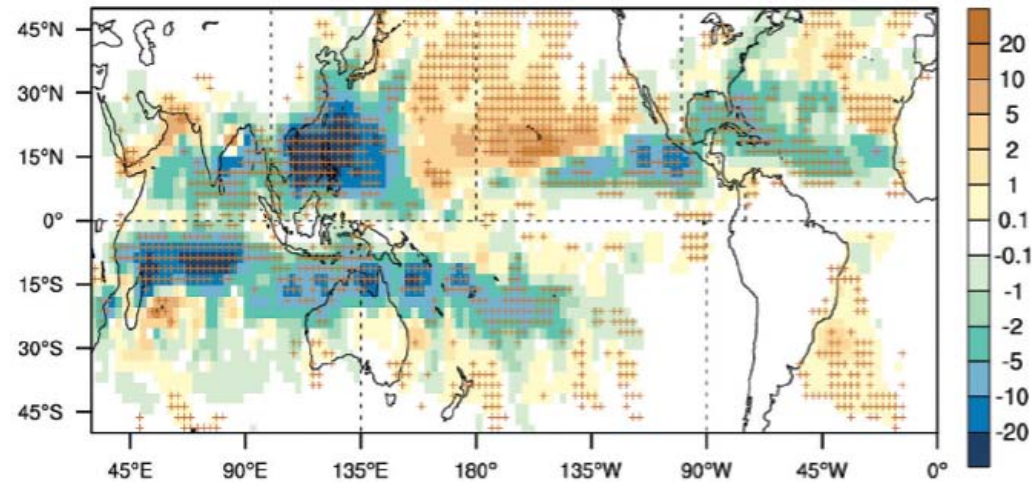
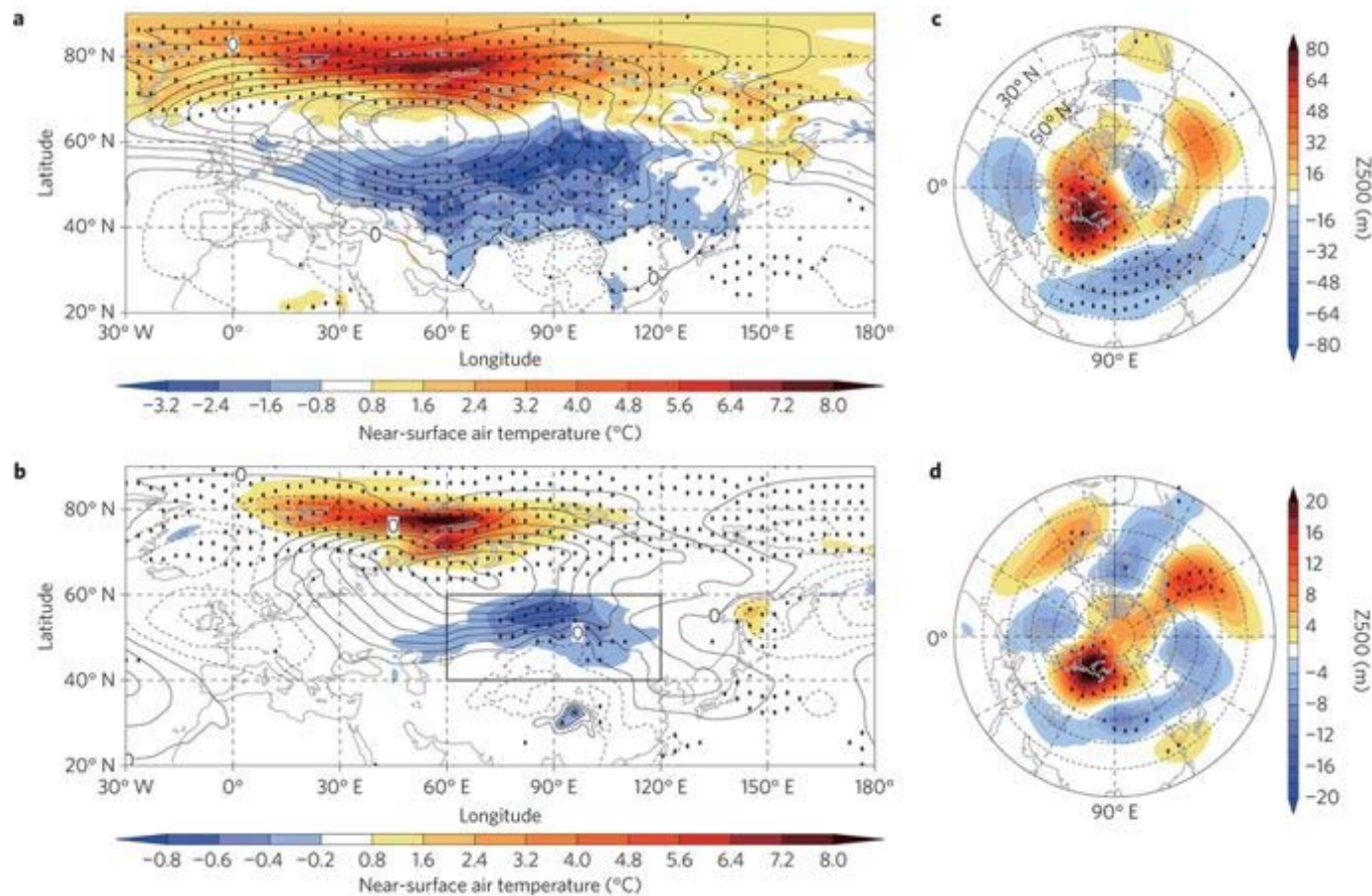


Figure 3. Ensemble mean future changes in tropical cyclone frequency. Unit is number per 25 years. Cross marks indicate that more than 10 experiments out of 12 experiments project the same sign.

■ Observed (upper figs.) and simulated (lower figs.) change in winter SAT and atmospheric circulation associated with sea-ice retreat in the Barents–Kara region (Mori et al. 2014, Nature Geoscience)



■ Concluding remarks

- The global climate system consists of atmosphere including its composition and circulation, the ocean, hydrosphere, land surface, biosphere, snow and ice, solar and volcanic activities.
- These components interact on various spatial and temporal scales through the exchanges of heat, momentum, radiation, water and other materials.
- Climate variability refers to variations in the mean state and other statistics of the climate on all spatial and temporal scales beyond that of individual weather events.
- Climate variability may be due to natural internal processes within the climate system (internal variability), or to variations in natural or anthropogenic external forcing.
- Experts of climate services must learn climate system, causes, impacts, and predictability of climate variability in various spatial and temporal scales.

■ Concluding remarks (+)

- Unusual weather and climate are attributed to unusual atmospheric flows, storms and convective disturbance. Diagnostic analysis shows that those disturbances are often related to atmospheric intrinsic waves and phenomena.
- However, atmospheric environment is maintained and influenced by other elements consisting of the climate system. Unusual and steady convective activity is sometimes connected to long-term SST anomalies related to ocean variability.
- Radiative processes including longwave absorption by greenhouse gases and shortwave reflection by snow, ice, clouds and aerosols determine the local Earth's ground temperature. The distribution of ground temperature is influential to vertical and horizontal atmospheric and oceanic stabilities, the amount of water vapor and the speed of water cycle. Then, those can affect atmospheric and oceanic flows, the features of storms and convections and eventually our daily lives. Therefore, we need to continue careful watches and diagnostics for global and local climate systems .